38th International Gemmological Conference

Athens - Greece
October 2025

Cover Photo Credits

Upper photo: View of Athens and Acropolis. Photo by: Constantinos Kollias, unsplash.

Bottom photo: A ring and bracelet both uncovered during excavations in the northern regions of Greece and are dated to the Roman period. The ring is set with a sapphire weighing approximately 12.4 carats, found to be most likely from Sri Lanka (inv. no. ΜΘ 16274). The bracelet features an emerald of approximately 6.7 carats, found to be most likely of Egyptian origin (inv. no. ΜΘ 15321). Photos by M. Nikopoulou, © Archaeological Museum of Thessaloniki, Hellenic Ministry of Culture and Sports.

38th International Gemmological Conference October 2025 Athens, Greece

Dear Colleagues,

It is with great pleasure and pride that we welcome you to the 38th International Gemmological Conference (IGC), set against the timeless backdrop of Athens, Greece; a city where culture meets science.

Greece, long recognized as a lighthouse of knowledge, philosophy, and scientific thought, offers an inspiring setting for this prestigious event. The intellectual heritage of Ancient Greece is deeply embedded in the foundations of modern science.

Among the earliest voices in the study of minerals and gems was Theophrastus, the philosopher and naturalist who, around 315 BCE, penned the seminal work "On Stones" (*"Περί Λίθων"*). His insights remind us that gemmology, though a modern science, has ancient roots. Also significant is the influence of Alexander III of Macedon, better known as Alexander the Great, whose conquests carved vast pathways across continents. Along these ancient routes flowed not only ideas and cultures, but also gems carried from distant lands, traded, and admired. During this time, the appreciation of many gems grew, transcending political borders and enduring through the ages.

Beyond its historical legacy, Greece's geology continues to fascinate scientists. From the ancient mines of Lavrio, to the volcanic landscapes of Santorini Island, and the spectacular rock formations of Meteora, the country offers geological sites that are as unique as they are significant. As part of this year's IGC, participants will have the opportunity to visit several of these remarkable locations, deepening both scientific insight and cultural connection.

May your time in Greece be both intellectually stimulating and personally enriching. We look forward to the exchange of knowledge, ideas, and discoveries that will continue to shape the future of gemmology.

On behalf of the Organizing Committee,

Prof. Dr. Stefanos Karampelas

The 38th IGC will take place at the Athens Chamber of Commerce and Industry (ACCI), located in downtown Athens (photo by: Andrea Leopardi, unsplash)

The Temple of Poseidon is situated on Cape Sounion, near Lavrion, and is about a one-hour drive from downtown Athens (photo by: Christina Gottardi, unsplash)

Organization of the 38th International Gemmological Conference

Organizing Committee
Prof. Dr. Stefanos Karampelas
(University of Thessaloniki - LFG)
Giorgos Spyromilios (IGLcert)
Dr. Maria Nikopoulou (University of Thessaloniki)
Aurélien Delaunay (LFG)
Dr. Jayshree Panjikar (IGC Executive Secretary)

Excursions
Prof. Dr. Stefanos Karampelas
Travelgate
Dr. Maria Nikopoulou

Guest Programme
Prof. Dr. Stefanos Karampelas
Travelgate
Dr. Anastasia Rousaki

Homepage
Dr. Laurent Cartier
Prof. Dr. Stefanos Karampelas

Proceedings
Pascaline Minella
Dr. Laurent Cartier
Prof. Dr. Stefanos Karampelas

Abstract Review Board
Prof. Dr. Emmanuel Fritsch
Dr. Ulrich Henn
Dr. Michael Krzemnicki
Dr. Karl Schmetzer
Dr. Hanco Zwaan

Special thanks to Mrs. Yasmine Cailliot and Mrs. Clémence Brahmy-Marty for their invaluable assistance with the accounting, as well as UBJOP and LFG for general support.

Sponsors

SCHOOL OF GEOLOGY
A.U.TH.

FACULTY OF SCIENCES
ARISTOTLE UNIVERSITY OF THESSALONIKI

100 YEARS AUTH
ARISTOTLE UNIVERSITY OF THESSALONIKI
KNOWLEDGE INNOVATION CULTURE

IGLcert
INDEPENDENT GEMOLOGICAL LABORATORY
Real Value to Real Gems

C. DUNAIGRE
Consulting GmbH

THE GEM MUSEUM
SINGAPORE

RENISHAW

HELLENIC REPUBLIC
ATHENS CHAMBER OF COMMERCE & INDUSTRY

LFG
PARIS
Laboratoire Français de Gemmologie

International Gemmological Conference

History of the IGC

The International Gemmological Conference (IGC) owes much of its origin to BIBOA (Bureau International pour la Bijouterie, Orfèvrene, Argenterie), the International Jewellery and Gemstone Federation, the first Congress of which in 1926 recommended and defined use of the term cultured pearl.

Experts from various European gem testing laboratories were invited to attend a series of expert meetings that aimed to formulate the policies of BIBOA. In 1936, at the fifth conference of experts, collaboration among laboratories was acclaimed by traders and they encouraged Laboratory Directors to meet each other at a technical conference from which all commercial delegates would be excluded.

Technical meetings were held annually, and in 1951 a Technical Conference was held in Idar Oberstein to prepare for the next London Congress in 1952. Those attending the 1951 conference included Mr B.W. Anderson, Mr G. Göbel, Dr E. Gübelin, Mr F. Wolf, Mr A. Bonebakker, Mr H. Tillander, Mr A. Strondahl, and Mr O. Dragstead. It has been suggested that the future framework of the IGC was established at this meeting in Idar Oberstein.

The London Congress saw the restructuring of BIBOA in which Gemmological Associations were replaced by National Federal Committees, and BIBOA evolved into BIBOAH – the forerunner of CIBJO, now known as The World Jewellery Confederation.

A Technical Conference met at Lugano from 23rd to 25th October 1952 at the initiative of Prof. K. Schlossmacher and Dr. E. Gübelin. Also present at this conference were Messrs B.W. Anderson, A. Bonebakker, O. Dragstead, G. Göbel, K. Siess and H. Tillander. At this historic meeting Dr E. Gübelin proposed creation of a "Committee of an International Gemmological Association" that would consist of one member per country; this member being the Director of a Gem Testing Laboratory, or a gemmologist of the calibre who could attend that meeting. This was agreed to, and this meeting was later considered to be the inaugural meeting of the IGC.

The first meeting of the IGC in Lugano was followed by subsequent meetings in Amsterdam, The Netherlands (1953), Copenhagen, Denmark (1954), London, UK (1955), Munich, Germany (1956), Oslo, Norway (1957), Paris, France (1958), Milano, Italy (1960), Helsinki, Finland (1962), Vienna, Austria (1964); Barcelona, Spain (1966); Stockholm, Sweden (1968); Brussels, Belgium (1970); Vitznau, Switzerland (1972); Washington D. C., USA (1975), The Hague, The Netherlands (1977), Idar Oberstein, Germany (1979), Kashiko-Jima, Japan (1981), Beruwela, Sri Lanka (1983); Sydney, Australia (1985); Rio de Janeiro, Brazil (1987), Tremezzo, Italy (1989); Stellenboch (1991), Paris, France (1993); Bangkok, Thailand (1995); Idar Oberstein, Germany (1997); Goa, India (1999); Madrid, Spain (2001), Wuhan, China (2004); Moscow, Russia (2007); Arusha, Tanzania (2009), Interlaken, Switzerland (2011); Hanoi, Vietnam, (2013); Vilnius, Lithuania (2015); Windhoek, Namibia (2017); Nantes, France (2019); Tokyo, Japan (2023).

Over the history of the IGC, that now in its fourth decade, it can therefore be seen that the International Gemmological Conference is the longest surviving gemmological conference to remain largely in its original format. Over its history, have been invited to participate in IGC meetings gemmologists from over 40 countries or areas – including Australia, Austria, Bahrain, Belgium, Brazil, Canada, China, Czech Republic, Denmark, Dubai (UAE), England, Finland, France, Greece, Germany, Greenland, Hong Kong, Israel, India, Italy, Japan, Kenya, Korea, Liechtenstein, Lithuania, Namibia, the Netherlands, Norway, Russia, Singapore,

South Africa, Spain, Sri Lanka, Switzerland, Sweden, Tanzania, Thailand, U.S.A., Vietnam and Zimbabwe.

During the 20th IGC, which was held in Sydney, Australia, the members present elected nine members to Honorary Members status. The first Honorary Members of the IGC were Oliver Chalmers (Australia), Prof. A. Chikayama (Japan), and Mr R. Crowningshield (U.S.A), Mr. O. Dragsted (Sweden), Prof. E. Gübelin (Switzerland), Mr. R. T. Liddicoat (U.S.A), Mr. M. Masso (Spain), Dr. F. H. Pough (U.S. A) and Dr. J. M. Saul (Kenya).

In Italy, the IGC logo was designed by Roberto Sambonet, made in gold by Roberto Cusi, and offered to the conference delegates during the Tremezzo 1989 edition.

In Italy, in 1989, the following rules were agreed for future meetings of the IGC:

1. The prime objective was to be the exchange of gemmological experiences.
2. Gemmology was to be the platform for all topics and was to be regarded as the principal theme.
3. It was decided that attendance at all further Conferences should be by invitation that would be determined where necessary by the Conference Secretary and the Executive Committee.
4. All delegates were to be encouraged to present papers; but this would not be mandatory.
5. All delegates must have a publishing record and all papers at IGC meetings must presented in English, both when written or spoken.
6. The Conference must keep foremost in mind the prime objectives and avoid dilution/confusion of this objective which, if not maintained, could result in a blank organization without true status or credibility.
7. Peripheral commercial activity must be kept to a minimum, and there should be no blatant sponsorship of any kind.

These rules, combined with the original concepts, have been kept as the basis for all conferences since. Any invitation is specific to the person invited and is not transferable.
Rules/Standard Operating Procedures of the IGC as of the 2019 revision

Introduction

Over the years, the Rules/Standard Operating Procedures for the IGC have evolved. These were last published in the Proceedings of the 35th IGC 2017 (Windhoek, Namibia). The following Rules and Procedures have been revised in 2018 and 2019 by the Executive Committee of the IGC and agreed for future meetings.

I. General rules

1. The prime objective is the exchange of gemmological experiences. Gemmology is to be regarded as the principal theme.
2. Attendance at the IGC is by invitation only (see Categories of Membership following).
3. All Members (delegates and observers) are encouraged to present a paper or poster. To receive further invitations, it is mandatory for observers to present a paper or poster, at least at their second attendance at the conference.
4. All Members (delegates and observers) must have a publishing record. All papers at IGC meetings must be presented in English, both written and spoken.
5. The Conference must keep foremost in mind the prime objective and avoid dilution or confusion of this objective, which if not maintained could result in the loss of status or credibility.
6. Peripheral commercial activity must be kept to a minimum, and there should be no blatant sponsorship of any kind.

These rules, combined with the original concepts, have been kept as the basis for all conferences since. Any invitation is specific to the person invited and is not transferable.

Membership

Honorary Members are senior members of the IGC who are elected by Delegates at the Business Meeting following each IGC, following nomination by the Executive Committee. Delegates are those who are elected from Observers who have established eligibility by presenting worthwhile presentations (either lectures and/or posters) at three IGC meetings. Following recommendation by the Executive Committee, new Delegates shall be elected by majority vote of Delegates at the Business Meeting following each IGC.

Observers are those who are invited to attend an IGC meeting by majority vote of the Executive Committee. Invitations shall be given only to internationally recognized gemmologists who have published in the gemmological field.

Applications for Observer status, which shall be supported by a pertinent CV and list of publications, should be submitted to the Executive Committee for consideration. An invitation will then be offered by the Secretary of the IGC.

Executive Committee (Execo)
The day-to-day administration and decision making of the IGC shall be overseen by an Executive Committee that meets formally at IGC meetings, and between meetings conducts the routine business of the IGC electronically by email. New members of the Executive Committee are chosen from among IGC Delegates. Following nomination, new members of the Executive Committee shall be elected by majority vote of Delegates at the Business Meeting that follows each IGC.

From time to time, the Executive Committee shall elect a Secretary, who will be responsible for detailed administration, especially activities related to invitations to the conference, and the distribution of decisions of the Executive Committee to Honorary Members and Delegates.

Written minutes shall be kept for all meetings of the Executive Committee and approved by the Executive Committee. After a Conference, written minutes of the General Business Meeting shall be distributed by email to all Members to inform everyone, including those not present, about decisions and further activities.

The Executive Committee elects a Chairman of the Abstract Review Committee, who organizes the handling and review process of the Abstracts. Delegates and Observers shall submit the title and a three-page extended abstract of a paper proposed for presentation at an IGC meeting to the Abstract Review Committee for approval.

II. Meetings of the IGC

IGC meetings should be held every two years in a host country approved by Honorary Members and Delegates.

IGC meetings should be timed so as not to clash with other meetings (e.g. IMA meetings) that Delegates are likely to attend.

A country wishing to host an IGC meeting shall submit a proposal first to the Executive Committee, and then present it formally to Delegates. The decision to accept or reject a proposal to host an IGC meeting will be made by majority vote of Honorary Members and Delegates present at the IGC Business Meeting, or electronically if an IGC meeting is not being held at the time a decision needs to be made.

Countries hosting IGC meetings shall establish their own administrative structures to ensure the efficient planning and operation of the Conference. Costs involved in hosting the Conference shall be met by registration fees paid by Honorary Members, Delegates and Observers attending the meeting, and financial sponsorship from private, institutional and government sources.

Day-to-day administration shall be the responsibility of a Conference Organizer, who is either an Honorary Member or a Delegate. The Conference Organizer is chosen at a Business Meeting following recommendation by the Executive Committee. The Conference Organizer may appoint a Conference Secretary and further members of a Committee as needed.

General responsibilities of the Conference Organizer of each IGC include:
Planning and implementation of
- pre-conference activities
- post-conference activities
- the formal IGC conference
- associated cultural activities and events
- entertainment program for registered Guests of Members
- all finances
- receipt and compilation of abstracts of papers after acceptance by the abstract review committee

- publication of Proceedings of the IGC conference
- implementation of poster presentations
- coordination with the Execo, and updates on progress of arrangements for members

Obtaining the necessary government permissions and other political requirements, including organisation of formalities required for different foreign visitors in the host country, e.g. visas, special permissions etc.

The Conference Organizer is responsible for informing Honorary Members, Delegates and Observers of the prospective dates of the next IGC at least 10 months in advance.

Attendance at IGC meetings of Delegates and Observers from countries other than the host country shall be restricted to a maximum of five registrations per country. This restriction does not include Honorary Members.
Local Guests are gemmologists who may be invited by the Conference Organizer to attend an IGC meeting held in the country in which they are resident.

Each IGC shall consist of a minimum of:

1. Two to three day pre- and post-conference study excursions to areas and facilities of gemmological interest.
2. A one-day session, prior to the IGC at which previously nominated Delegates and/or Observers will be invited to give presentations to gemmologist members of the host country
3. A three to five-day professional conference to consist of:
   - Formal papers of 15 minutes duration, followed by 5 minutes of questions and answers; and,
   - Poster presentations that shall be scheduled independently so that adequate time is allowed for each poster to be presented by its authors and then have its content available for discussion.
4. A Business Meeting for Honorary Members, Delegates and Observers that traditionally follows closure of the IGC professional conference to exchange opinions on further directions of IGC, and to decide the location for further IGC meetings. Only Honorary Members and Delegates are allowed to vote at the Business Meeting.

International Gemmological Conference Executive Committee

The IGC Executive Committee

Dr. Ahmadjan Abduriyim
Prof. Dr. Emmanuel Fritsch
Dr. Anette Juul-Nielsen
Dr. Michael Krzemnicki
Dr. Jayshree Panjikar
Dr. Karl Schmetzer
Mr. Thye Sun Tay
Mrs. Willow Wight
Dr. Gamini Zoysa
Dr. J. C. Hanco Zwaan

IGC 2025 programme

17 - 19 October 2025	Pre-conference tour (Central and Northern Greece)
20 - 24 October 2025	Conference, Athens Chamber of Commerce and Industry (ACCI)
24 - 27 October 2025	Post-conference tour (Santorini Island)

Monday 20 October

8:30 - 9:30	Registration at ACCI (6th floor)
9:30 - 9:45	IGC Opening (Greek representatives)
9:45 - 10:00	IGC history (Dr. Jayshree Panjikar - IGC Executive secretary)
10:00 - 10:45	Coffee Break - Outside Conference Room Area

Open Session: Gemmology and Greece

10:45 - 11:10	P. Voudouris, S. Karampelas, V. Melfos: Gems in Greece: Geology, mineralogy and crystallizing environment
11:10 - 11:25	M. Nikopoulou, S. Karampelas, E. Tsangaraki, L. Papadopoulou, C. Katsifas, I. Nazlis, V. Melfos, N. Kantiranis: Gems in Hellenistic and Roman Jewellery of Northern Greece: An investigation from the Collections of the Archaeological Museum of Thessaloniki, Greece
11:25 - 11:40	A. Sergoulopoulos: Gemmological education in Greece
11:40 - 12:00	A. Krikos, I. Papadopoulos: Glyptography in Greece
12:00 - 13:30	Lunch Break - Outside Conference Room Area Executive Committee meeting

Session 1: History and Museums - *Chairperson: Karen Fox*

13:30 - 13:50	E. Gaillou, G.A. Farfan G.A., U.F.S. D'Haenens-Johansson, S. Persaud, R.C. Feather II , W.H. Towbin, D.C. Jones: Studying renowned fancy color diamonds in museum collections: The case of the Winston Red
13:50 - 14:10	K. Schmetzer: History of Garnet Mining and Cutting in the Austro-Hungarian Monarchy
14:10 - 14:30	M.-L. Cassius-Duranton, V. Pardieu, S. Karampelas: Historic Emeralds and their Geographic Origin: A Retrospective Study
14:30 - 14:50	S. Karampelas, E. Gaillou, A. Herreweghe, U. Hennebois, F. Maouche, R. Bolzoni, S. Riou, Q. Dartois, B. M. S. Beuve, C. Gliksman, T. Magalhaes, V. Demetz, A. Delaunay: Study of "amethysts" from the French Crown Jewels
14:50 - 15:10	B. Shirdam, Y. Mingxing, A. H. Shen, H. F. Nashli: Cross-Cultural Provenance and Characterization of Turquoise Artefacts: A Multi-Analytical Non-Destructive Study of Reshui Tomb Cluster, China (744 AD) and Tepeh Zagheh, Iran (5200–4200 BCE)
15:10 - 15:40	Coffee Break - Outside Conference Room Area

Session 2: Pearls and Amber - *Chairperson: Dr. Michael Krzemnicki*

15:40 - 16:00	Y. Li, Q. Su: Unravelling the luminescence spectrum of novel ceramic nucleus cultured pearl and the cause of its strong luster
16:00 - 16:20	N. R. Hansen: Modern Cultivation of Freshwater Pearls in China: Advances in Materials, Technique
16:20 - 16:40	A. Costanzo, A. Klikowicz-Kosior, M. Kosior: Amber and its treatments: A New Baltic Amber Classification Chart
16:40 - 17:00	T. N. Thet, T. S. Tay, L. Soe, L. Cheyenne, H. Y. Loke: Amber from the Thanbaya Gaing Coal Mine, Minbu Township, Magwe Region, Myanmar
17:00 - 17:20	N. Renfro: A Photo Survey of Inclusions in Fossiliferous Amber
19:30	Cocktail at the restaurant of Benaki Museum of Greek culture

Tuesday 21 October

Session 3: Gemmology 1 - *Chairperson: Dr. Ahmadjan Abduriyim*

9:30 - 9:50	M. Vigier, H. Evans, G.R. Rossman, S. Jobic, E. Fritsch: Fe-Ti charge transfers: A comprehensive review and its applications to minerals and gems
9:50 - 10:10	C. Wang, A.H. Shen: Recent Progress on the Formation Mechanism of Copper Nanoparticle in Oregon Sunstone
10:10 - 10:30	U. Henn: Application of Fibre Optics Reflectance Spectroscopy (FORS) for the determination of mineral pigments in jasper
10:30 - 11:00	Coffee Break - Outside Conference Room Area

Session 4: Gemmology 2 - *Chairperson: Dr. Karl Schmetzer*

11:00 - 11:20	C. Schwarzinger, S. Ulatowski, G. R. Rossman: Zoisite and its many colors
11:20 - 11:40	L. Gilles-Guéry: Pink-orange gem quality euclase from Bahia, Brazil
11:40 - 12:00	K. E. Fox, A.M. McDonald, C. Yakymcuk: On the nature of blue rose quartz
12:00 - 12:20	M. F. Hügi, M.S. Krzemnicki, M. Wälle: Gem-quality pink fluorite from Planggenstock, Switzerland: chemical and physical properties and a comparison with pink fluorites from other localities)
12:20 - 13:20	Lunch Break - Outside Conference Room Area Executive Committee meeting

Session 5: Gemmology 3 - *Chairperson: Dr. Pornsawat Wathanakul*

13:20 - 13:40	A.Y. Shelementyeva, Y.B. Shelementyev, O.V. Yarapova: Typomorphic features of tourmalines of the Malkhan pegmatite field from the Irkutyanka vein
13:40 - 14:00	J. M. Saul: Colored gemstones of metamorphic origin: Progress report in understanding how they crystallize at depth in East Africa, the Hindu Kush, Pamir Mountains, and the Middle-Urals Ring Structure
14:00 - 14:20	J. Panjikar, A. Panjikar: Hessonite garnet from Angul district of Odisha, India
14:20 - 14:40	D. Gravier, A. Delaunay, J. Boemo, J.-M. Arlabosse, E. Fritsch, S. Karampelas: Hurlbutite from Myanmar
14:40 - 15:00	G. Choudhary: A convincing glass imitation of larimar (pectolite)
15:00 - 15:30	Coffee Break - Outside Conference Room Area

Session 6: Gemmology 4 - *Chairperson: Prof. Dr. Stefanos Karampelas*

15:30 - 15:50	S.F. McClure: Bertrandite in Emeralds
15:50 - 16:10	R.A. Schultz-Güttler, A.R. Borotti, I.P. Marques, A. L. S. Pestilho: Found, Lost, and Found Again: The Geological and Gemological Significance of the Salininha Emerald Deposit, Brazil
16:10 - 16:30	T. Sripoonjan, M. Seneewong-Na-Ayutthaya, S. Saengdech, S. Singbamroong, A. Fanka: Automated Data Processing of Raman Spectra for Supporting Spinel Origin Determination
16:30 - 16:50	G. Zoysa, D. Schwarz, A. Kleismantas: Spinel from Sri Lanka - An update
16:50 - 17:10	B. Laurs: The Importance and Methodology of Undertaking a Literature Search for Gemmological Research and Article Publishing
17:10 - 17:30	J.Garcia-Toloza, R. J. David, O. Cristian, C. C. Julio: An approach to understanding the factors in the emerald enhancement clarity grading system used at CDTECGemlab
19:30	Folk night - Acropol Restaurant

Wednesday 22 October

8:00-19:00	Excursion to the Lavrion Mines and Cape Sounion
14:30	Group photo in front of the Mineralogical Museum of Lavrion
Free evening	

Thursday 23 October

Session 7: Corundum 1 - *Chairperson: Dr. Ulrich Henn*

9:30 - 9:50	B. Chauviré, M. Corre, M. Curti, C. Gautheron, S. Figowy, L. Pinsault: Noble gas in corundum: interests in gemology
9:50 - 10:10	A. Abduryim, F. L. Sutherland, T. Coldham, E. Belousova: Gem zircon and sapphire age dating and application of origin determination: A study from New England sapphire fields, New South Wales, Australia
10:10 - 10:30	M. Seneewong-Na-Ayutthaya, B. Wanthanachaisaeng, T. Leelawatanasuk, W. Atichat, S. Saengdech, P. Kamkaew, T. Sripoonjan: Geographic Origin Determination of Natural Yellow Sapphires: The Preliminary Study
10:30 - 11:00	Coffee Break - Outside Conference Room Area

Session 8: Corundum 2 - *Chairperson: Dr. Jayshree Panjikar*

11:00 - 11:20	V. Pardieu: Rubies from Greenland
11:20 - 11:40	M. Furuya: Blue sapphire from Malacacheta of Minus Gerais, Brazil
11:40 - 12:00	S. Singbamroong, T. Sripoonjan, M. Seneewong Na Ayutthaya, P. Piantumdee, T. Sutipanya, K. Hussein, N. Ahmed: Gemological Characteristics of New Transparent Brown Sapphire)
12:00 - 13:00	Lunch Break - Outside Conference Room Area Executive Committee meeting

Session 9: Corundum 3 - *Chairperson: Shane Mcclure*

13:00 - 13:20 M.S. Krzemnicki, W. Zhou, P. Lefèvre, M. Wälle, H.A.O. Wang: HFSE-enriched sapphires of gem quality: A combined FTIR and trace element study and implications for heat treatment detection
13:20 - 13:40 E.B. Hughes, R. Perkins: Low Temperature Heat Treatment of Madagascar Sapphire
13:40 - 14:00 H.A.O. Wang, M. Wälle, V. Hutanu, X. Li, M. S. Krzemnicki: Effects of Gamma Irradiation on Corundum: Towards a Potential Detection Method
14:00 - 14:20 S. Promwongnan, W. Atichat, C. Suphan, W. Chongraktrakul, V. Pisutha-Arnond: Challenges in the Detection of Ruby and Sapphire Treatment in the Thai Market
14:20 - 14:40 S. Kennedy: Padparadscha sapphires and heat treatment
14:40 - 15:10 Coffee Break - Outside Conference Room Area

Session 10: Jade - *Chairperson: Thye Sun Tay*

15:10 - 15:30 S.-I (Edward) Liu, K.-Y. (Angela) Man, M. Seneewong-Na-Ayutthaya, B. Wanthanachaisaeng: Advancing Fei Cui Origin Authentication: A comparison of green Fei Cui from Myanmar, Guatemala, Italy and Russia
15:30 - 15:50 E. Su: Color Genesis Analysis and Characteristics for Origin Identification of Purple Jadeite
15:50 - 16:10 M. Seneewong-Na-Ayutthaya, B. Wanthanachaisaeng, T. Lhuaamporn, W. Suwanmanee, W. Atichat, T. Leelawatanasuk: Dyed purple Fei Cui (Lavender jade) from Mandalay's jade market, Myanmar
19:30 Gala Dinner – Attikos Restaurant

Friday 24 October

9:00 - 9:30 Coffee – Outside Conference Room Area

Session 11: Diamonds - *Chairperson: Prof. Dr. Emmanuel Fritsch*

9:30 - 9:50 T. Hainschwang: Pink to Red and Violet Diamonds from the Argyle Mine, Australia: Properties, Color Origin and Latest Research Results
9:50 - 10:10 M. Bouman, J. Zarupski: Shining light on “480 nm band” diamonds: Gemmological characteristics of an unusual group of diamonds with yellow and red luminescence
10:10 - 10:30 K. Emori, H. Kitawaki, M. Hisanaga, M. Yamamoto: Identification of melee size synthetic coloured diamond for jewellery
10:30 - 10:50 Y. Shelementyev, G. Kriulina, O. Yarapova1, V. Vins, A. Stolyarevich: Nitrogen aggregates in yellow HPHT and CVD synthetic diamonds
10:50 - 11:10 H. Y. Loke, L. C. H. Timothy, H. Nyunt, T. N. Thet, S. Linda, T. S. Tay: Diamonds from Than Lwin River near Mong Hsu, Myanmar
11:10 - 11:30 S. Sakkaravej, T. Lhuaamporn, P. Lomthong, W. Atichat, P. Wathanakul: Morphologies and Surface Features of Diamond Samples from Southern Thailand
11:30 - 12:30 Lunch Break - Outside Conference Room Area
Executive Committee meeting
12:30 - 13:30 Announcements for IGC 2027 - Closing IGC 2025

38th International Gemmological Conference
Pre-conference tour
Central and Northern Greece

The Meteora complex offers a remarkable landscape of geological and archaeological significance
(photo by: Lorenzo Spolet, unsplash)

Thessaloniki is Greece's second-largest city, located by the sea and known for its rich cultural heritage
(Photo https://commons.wikimedia.org/wiki/File:Thessaloniki_Aristotelous_Square_02.jpg)

38th International Gemmological Conference
Post-conference tour
Santorini Island

Santorini Island was formed by a volcanic eruption, creating unique geological phenomena and stunning views (photo by: Dimitris Kiriakakis, unsplash)

Thanks to its unique geology, Santorini Island offers breathtaking views (photo by: Gontran Isnard, unsplash)

38th International Gemmological Conference
Accompanying persons

The historic neighborhood of Plaka in Athens is within walking distance of the IGC 2025 conference venue.
(photo by: Olivier Legrand, unsplash)

The Theater of Epidaurus was built in the 4th century BCE
(photo by: Jeroen Van Nierop, unsplash)

Gems in Greece: Geology, mineralogy and crystallizing environment

Panagiotis Voudouris[1*], Stefanos Karampelas[2,3], Vasilios Melfos[2]

[1] Faculty of Geology & Geoenvironment, National and Kapodistrian Universtiy of Athens, 15784 Athens, Greece

[2] School of Geology, Aristotle University of Thessaloniki, 54124, Thessaloniki, Greece

[3] LFG (Laboratoire Français de Gemmologie), 30 rue de la Victoire, 75009, Paris, France.

[*] voudouris@geol.uoa.gr

Keywords gems; corundum; beryl; garnet; silica gems; Greece

In the accretionary Hellenides Orogen, gems occur in various rock types of mainly four tectonometamorphic units, the Rhodope- and the Attico-Cycladic massifs, the Pelagonian zone, and the Phyllites-Quartzites of Crete Island (Fig. 1). In crystalline rocks, two groups of gems are distinguished, those formed during regional metamorphism and those associated with late alpine-type fissures (Voudouris *et al*. 2019 a,b). The first group includes Mn-bearing silicates (Mn-andalusite, spessartine, Mn-grossular, Mn-clinozoisite, Mn-zoisite and orange-colored Fe-Mn-kyanite; Fig. 2a-d) hosted in gneisses and marbles in both Thassos and Paros Islands (Rhodope- and Attico-Cycladic massifs respectively), as well as corundum in Xanthi-Drama areas/Rhodope massif and Naxos-Ikaria Islands (Attico-Cycladic massif).

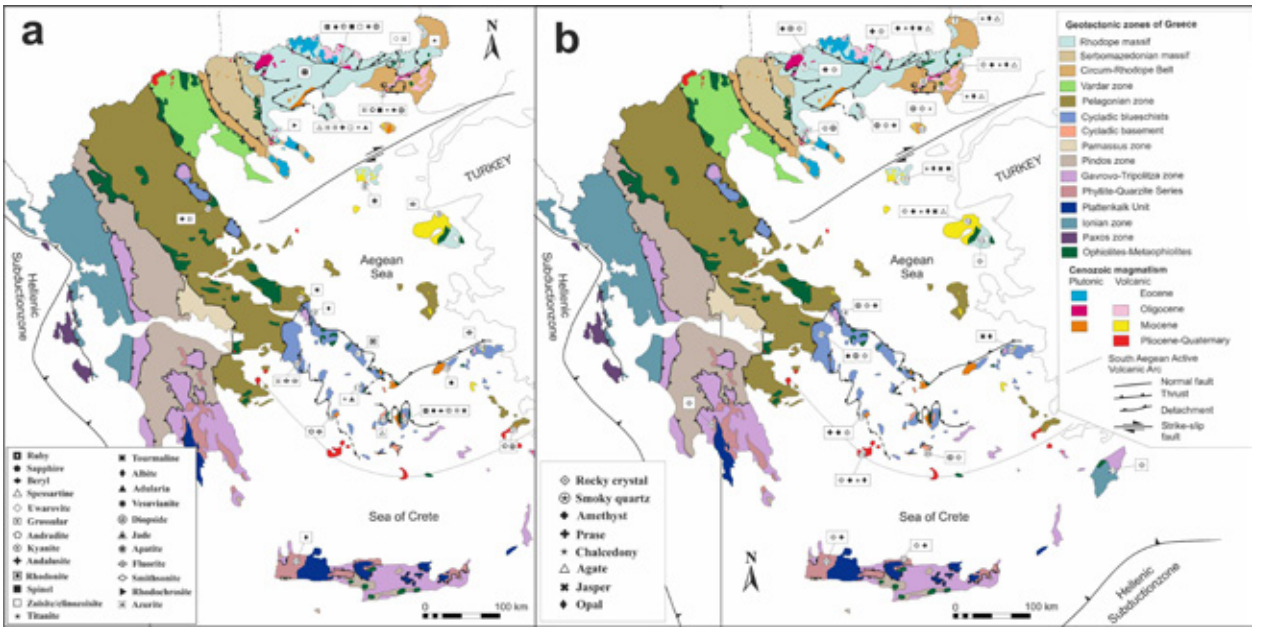

Figure 1. (a) Occurrences of various gemstones in metamorphic and igneous rocks of Greece: 1&2 Evros, 3. Maronia/Rhodopi, 4. Kimmeria/Xanthi, 5. Paranesti/Drama, 6. Trikorfo/Thassos, 7. Olympiada/Chalkidiki, 8. Limnos Island, 9. Lesvos Island, 10. Larissa, 11&12 Evia Island, 13. Andros Island, 14. Samos Island, 15. Ikaria Island, 16. Lavrion/Attica, 17. Syros Island, 18. Serifos Island, 19. Paros Island, 20. Kinidaros/Naxos Island, 21. Kos Island, 22. Crete Island; (b) Occurrences of gem silica varieties in metamorphic and igneous rocks of Greece: 1-3. Evros 4. Sapes/Rhodopi, 5. Xanthi, 6&7. Drama, 8. Trikorfo/Thassos, 9. Stratoni-Olympiada/Chalkidiki, 10. Samothraki island, 11. Limnos Island, 12&12. Lesvos Island, 14. Evia Island, 15. Pentelikon Mt/Attika, 16. Samos Island, 17. Serifos Island, 18 Taygetos Mt. 19. Milos Island, 20. Ios Island, 21. Rhodes Island, 22&23. Crete Island. Modified after Voudouris *et al*. 2019a.

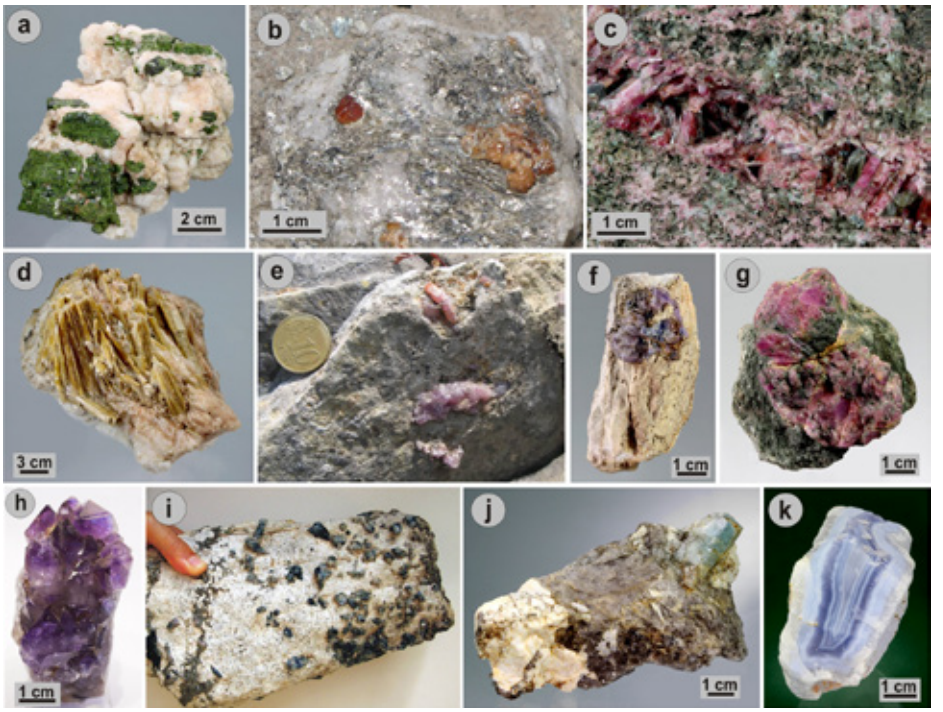

Figure 2. Photographs demonstrating various gem minerals from Greece. (a) Mn-rich andalusite from Trikorfo, Thassos Island; (b) spessartine crystals from Trikorfo; (c) Pink-red, Mn-bearing zoisite/clinozoisite from Trikorfo; (d) Orange kyanite at Trikorfo; (e,f) Pink to purple sapphires within Xanthi marbles; (g) Ruby within pargasite schist from Paranesti/Drama; (h) Amethyst from Dassoto, Drama; (i) Blue sapphires within desilicated pegmatite from Kinidaros, Naxos Island; (j) Aquamarine within pegmatite from Kinidaros, Naxos Island; (k) Blue agate from Aetochori, Evros. Photographs a,d,f,g,h,j,k are courtesy of Berthold Ottens.

In the Xanthi-Drama area, corundum mineralization (sapphires and rubies) occurs within marbles and eclogitic amphibolites within the Nestos suture zone (Fig. 2e-g). In the Attico-Cycladic massif, blue sapphires are found within marble-hosted metabauxites (Ikaria and Naxos Island).

Metamorphic/metasomatic processes within a subduction channel, resulted in the formation of the jadeitite bodies at Syros Island and of garnet and vesuvianite in rodingite bodies at the Rhodope massif and the Pelagonian zone. Alpine-type fissures in Greece contain gem quartz (green quartz -prasiolite-, amethyst, smoky and colourless quartz; Fig. 2h), albite and titanite. Host lithologies are ortho- and paragneisses and metabasites in the Rhodope- (Drama, Thassos Island) and the Attico-Cycladic (Pentelikon Mt, Evia, Ios Islands) massifs, and metaquartzites (Crete Island).

The Tertiary magmatic-hydrothermal environments in Greece (granitoids, pegmatites, skarns and carbonate-replacement deposits, and volcanic rocks) may also provide gem material of several species (beryl, corundum, garnet, vesuvianite, diopside, epidote, fluorite, rhodochrosite, silica varieties). The Naxos pegmatites are prospective for aquamarine and blue, purple to pink coloured sapphires (Fig. 2i,j). Miarolitic cavities and quartz veins cross-cutting granitoids (Samothraki Island, Maronia and, Kimmeria) contain colourless and smoky quartz. The endo- and exoskarns of Kimmeria and Maronia (Rhodope massif), Serifos Island (Attico-Cycladic massif) and Kos Island, contain grossular-andradite garnets, vesuvianite, epidote, as well as prasiolite and amethyst crystals. Rhodochrosite and fluorite occur in the carbonate-replacement deposits of Olympias/Chalkidiki and Lavrion/Attika respectively. Gems associated with hydrothermally altered volcanic rocks include amethyst, chalcedony (Fig. 2k), opal, fossilized wood and fluorite in Sapes, Soufli areas (Rhodope massif), Lesvos, Limnos and Samos Islands (northeastern and central Aegean volcanic arc) and Milos Island (Attico-Cycladic massif-south Aegean volcanic arc). Finally, the supergene oxidation of the Lavrion/Attika carbonate-replacement deposit contains smithsonite in several colourations. Figure 3 represents a hypothetical schematic model, where gem occurrences in Greece are related to the various geological environments (regional metamorphic-metasomatic, alpine-type fissures, plutonic-subvolcanic intrusions and pegmatites, zones of contact metamorphism and peripheral volcanic rocks).

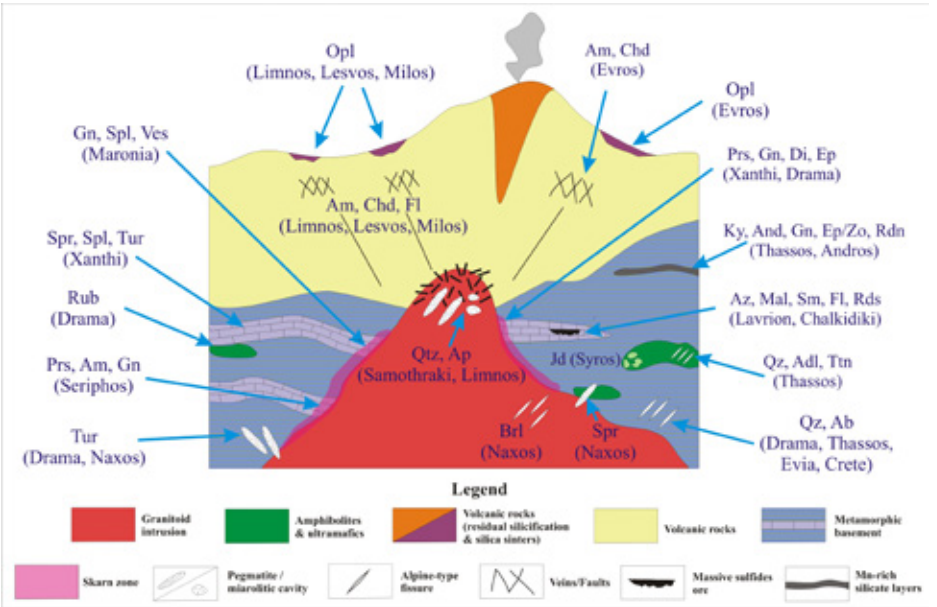

Figure 3. Hypothetical model presenting the various environments related to crystallization of gems in Greece. Abbreviations: Ab: Albite, Adl: Adularia; Am: Amethyst, And: Andalusite; Ap: Apatite; Az: Azurite; Brl: Beryl, Chd: Chalcedony, Di: Diopside, Epid: Epidote, Fl: Fluorite, Gn: Garnet, Jd: Jadeite; Ky: Kyanite; Prs: Prasiolite; Rdn: Rhodonite; Rds: Rhodochrosite; Sm: Smithsonite; Spr: Sapphire, Spl: Spinel; Ttn: Titanite; Tur: Tourmaline, Ves: Vesuvianite.

Greek corundum presents a variety of colour, with rough crystal sizes of up to 5 cm, transparent to translucent, having homogeneous colours (Fig. 4). Crystals of kyanite, green andalusite, garnet and red zoisite–clinozoisite from Trikorfo/Thassos, show vivid colours, and might be of gem quality. Finally, silica related gems can also be found (Fig. 4).

Figure 4. Various cut gems from Greece. Green Mn-andalusite from Thassos (2.2 cm length) in the left, dark green epidote from Kimmeria (1.3 cm) in the centre, ruby from Paranesti (4 cm) in the right of the photograph. The rest are silica related gems. Photo courtesy of Anastasios Tsinidis.

References:

- Voudouris, P., Mavrogonatos, C., Graham, I., Giuliani, G., Tarantola, A., Melfos, V., Karampelas, S., Katerinopoulos, A., Magganas, A. 2019a. Gemstones of Greece: Geology and Crystallizing Environments. Minerals, 9, 461.
- Voudouris, P., Mavrogonatos, C., Graham, I., Giuliani, G., Melfos, V., Karampelas, S., Karantoni, V., Wang, K., Tarantola, A., Zaw, K., Meffre, S., Klemme, S., Berndt, J., Heidrich, S., Zaccarini, F., Fallick, A., Tsortanidis, M., Lampridis, A. 2019b. Gem Corundum Deposits of Greece: Geology, Mineralogy and Genesis. Minerals, 9, 49.

Gems in Hellenistic and Roman Jewellery of Northern Greece: An investigation from the Collections of the Archaeological Museum of Thessaloniki, Greece

Maria Nikopoulou[1*], Stefanos Karampelas[1,2], Evangelia Tsangaraki[1], Lambrini Papadopoulou[1], Christos Katsifas[4], Ioannis Nazlis[4], Vasilios Melfos[1] and Nikolaos Kantiranis[1]

[1] Department of Mineralogy- Petrology-Economic Geology, School of Geology, Aristotle University of Thessaloniki, Thessaloniki, Greece.
[2] LFG (Laboratoire Français de Gemmologie), 30 rue de la Victoire, 75009, Paris, France.
[3] Archaeological Museum of Thessaloniki, Department of Ceramics, Metalwork and Minor Arts Collections, Thessaloniki, Greece.
[1] Archaeological Museum of Thessaloniki, Department of Conservation,
Chemical – Physical Analysis and Archaeometry, Thessaloniki, Greece.
*marthonik@geo.auth.gr

Keywords Hellenistic-Roman jewellery, Sapphire, Emeralds, Garnets, Chrome Chalcedony

This study presents the results of an interdisciplinary archaeogemological investigation focusing on gems embedded in Hellenistic and Roman jewellery from the collections of the Archaeological Museum of Thessaloniki (AMTh). Through a combination of non-destructive gemmological, spectroscopic and chemical analyses, a wide variety of gems – including a sapphire ring, emeralds, garnets and chalcedonies – were characterised and an attempt was made to determine their geographic – geological origin. This work is part of MN's PhD thesis conducted within the School of Geology at the Aristotle University of Thessaloniki, Greece. For security reasons, all experiments and analyses were carried out in the Archaeometry Laboratory of AMTh, using its equipment along with some portable instruments provided by the Laboratoire Français de Gemmologie (LFG).

Raman as well as photoluminescence (PL) spectroscopies were applied on all samples using a portable Raman spectrometer with a 532 nm laser excitation (GemmoRaman-532SG by MagiLABS). Vis-NIR spectra from 365 to 1000 nm were also acquired using a portable spectrometer (Gemmosphere by MagiLABS). Chemical analysis was contacted by EDXRF (micro-XRF, 1 mm, by Bruker, model: ARTAX 400) and for the observation of inclusions a Zeiss Stemmi, 500 was used.

In the collections of AMTh a rare Roman-period (3rd century CE) gold ring set (MΘ 16274) with a large (~12.4 ct) sapphire found in an unplundered marble sarcophagus in Thessaloniki was identified (Fig. 1a). Analytical results confirmed the natural origin of the sapphire without any indications of heat treatment, pointed to a metamorphic origin (Nikopoulou *et al*., 2023b), closely matching to Sri Lankan blue sapphires. The discovery of this elite jewel provides new insights into the rare use of sapphires in Roman-period luxury items and supports the existence of complex maritime and overland trade routes between South Asia and the Eastern Mediterranean during antiquity.

A group of 17 green-coloured gemstones which decorate 12 Roman-period jewellery (Fig. 1b) were identified as emeralds (ca. ~1.0 to 6.7 ct) and all of them presented similar spectroscopic and chemical characteristics. Under the microscope all emeralds presented growth tubes and/or prism-shaped multiphase inclusions without indications of treatments (Nikopoulou *et al*., 2024). Inclusion types along with the spectroscopic features and trace element concentrations strongly suggest an origin from the ancient emerald mines of Egypt (Nikopoulou *et al*., 2023a), highlighting their major role in the mining and trading of emeralds during the Roman era.

Figure 1. Representative macroscopic pictures of some of the studied gems from the Archaeological Museum of Thessaloniki. (a) ΜΘ 16274: Blue sapphire mounted in a gold ring (ca. 12.4 ct / 3rd century CE), (b) ΜΘ 15321: Emerald mounted in a gold bracelet (ca. 6.7 ct / 3rd – 4th century CE), (c) ΠΘ 76: Earrings with garnets (A: ca. 5.4 ct, B: ca. 3.7 ct / 3rd century BCE), (d) ΜΘ 11207: Pendant with chrome chalcedony (ca. 11.0 ct. / 1st century CE) © Archaeological Museum of Thessaloniki – Hellenic Ministry of Culture and Sports.

A large variety of 25 red garnet gems (ca. 0.6 to 16.7 ct) in 19 Hellenistic-Roman jewellery were also identified by Raman spectroscopy and micro-EDXRF analysis. These garnets (Fig. 1c) revealed three major compositional groups according to Thoresen & Schmetzer, 2013 and Gilg *et al*., 2024: (1) 17 garnets fall in the Cr-poor pyrope group (Cluster D), (2) 4 garnets fall in the Intermediate pyrope–almandine group (Cluster H), and (3) the rest 4 garnets belong in the Ca-rich almandine group (Cluster F) (Nikopoulou *et al*., 2025). These varieties are indicative of different geological sources, reflecting the diversity of garnet trade networks. The Cr-poor pyrope garnets (Cluster D) are associated with ultramafic and high-grade metamorphic rocks (e.g., Suimo in Portugal, Jos Plateau in Nigeria, Mount Carmel in Israel). The Intermediate pyrope–almandine garnets correspond to metamorphic rocks of granulite-amphibolite metamorphic phases which point to Sri Lankan sources, supporting the notion of gem importation from South Asia to the Mediterranean. Ca-rich almandine garnets, although their exact origin remains uncertain, suggest a source from metamorphic rocks with higher Ca content, such as amphibolites or biotite schists.

In the context of this study more than 40 gems composed of SiO_2 were identified, including varieties such as macrocrystalline quartz (e.g. rock crystal and amethyst), as well as microcrystalline forms like chalcedonies agates and jaspers. Among them there is a Roman gold pendant (ΜΘ 11207) decorated with a chrome chalcedony (ca. 11.0 ct, Fig. 1d) which further underlines the diversity of imported green materials during the Roman period, and it is possibly originating from deposits of Asia Minor (Hyrsl, 1999; Nikopoulou *et al*., 2024).

This study demonstrates the importance of interdisciplinary approaches combining archaeology, mineralogy, and gemmology, providing a clearer picture of the trading networks, socioeconomic dynamics and technological achieve-

ments of ancient civilizations. Similar studies have also been conducted focusing on the identification of gems from Hellenistic and Roman periods in collections from other museums, showing comparable results (Barone *et al*., 2016; Butini *et al*., 2018; Krzemnicki *et al*., 2019). The widespread presence of elite gems such as sapphires and emeralds, demonstrates both the technological adaptability of ancient artisans and the symbolic significance of gems in expressing wealth, status, and connections to global trade networks. Overall, the integration of advanced non-destructive analytical techniques has provided critical insights into the origin, selection, and distribution of gems in antiquity, underlining the pivotal role of ancient Macedonia in the broader context of economic, cultural, and technological exchanges across the Mediterranean and beyond in antiquity.

References:

- Barone, G., Mazzoleni, P., Raneri, S., Jehlička, J., Vandenabeele, P., Lottici, P. P., Lamagna, G., Manenti, A. M., & Bersani, D. (2016). Raman Investigation of Precious Jewelry Collections Preserved in Paolo Orsi Regional Museum (Siracusa, Sicily) Using Portable Equipment. Applied Spectroscopy, 70(9), 1420–1431.
- Butini, E., Butini, F., Angle, M., Cerino, P., De Angelis, A., Tomei, N., & Altamura, F. (2018). Archaeometric and gemmological analyses of a Roman imperial gold-and-sapphire jewel from Colonna (Rome, Italy). Measurement, 128, 160–169.
- Gilg, H. A., Then-Obłuska, J., & Dussubieux, L. (2024). Four millennia of garnet trade in Northeast Africa—chemical analysis of ancient and Late Antiquity beads from Lower Nubian sites. Archaeometry, 66(4).
- Hyrsl, J. (1999). Chrome chalcedony—a review. The Journal of Gemmology, 26(6), 364–370.
- Krzemnicki, M. S., Butini, F., Butini, E., & De Carolis, E. (2019). Gemmological Analysis of a Roman Sapphire Intaglio and Its Possible Origin. The Journal of Gemmology, 36(8), 710–724.
- Nikopoulou, M., Karampelas, S., Gaillou, E., Hennebois, U., Maouche, F., Herreweghe, A., Papadopoulou, L., Melfos, V., Kantiranis, N., Nectoux, D., & Delaunay, A. (2023a). Non-Destructive Study of Egyptian Emeralds Preserved in the Collection of the Museum of the Ecole des Mines. Minerals, 13(2), 158.
- Nikopoulou, M., Karampelas, S., Tsangaraki, E., Papadopoulou, L., Katsifas, C. S., Ioannis, N., Touloumtzidou, A., Melfos, V., & Kantiranis, N. (2023b). Study of a Third-Century CE Sapphire Gold Ring in the Archaeological Museum of Thessaloniki, Greece. The Journal of Gemmology, 38(8), 804–809.
- Nikopoulou, M., Karampelas, S., Tsangaraki, E., Papadopoulou, L., Katsifas, C., Nazlis, I., Touloumtzidou, A., Melfos, V., & Kantiranis, N. (2024). Study of green-coloured gems of the Roman period from the collections of the Archaeological Museum of Thessaloniki (Greece) and their possible geographic origin. Journal of Raman Spectroscopy, 55(12), 1341.
- Nikopoulou M., Karampelas S., Tsangaraki E., Papadopoulou L., Katsifas C., Nazlis I., Touloumtzidou A., Melfos V., and Kantiranis N., (2025). Study of Garnets in Hellenistic-Roman Jewellery from the Collections of the Archaeological Museum of Thessaloniki, Greece, Journal of Raman Spectroscopy [In Press].
- Thoresen, L., & Schmetzer, K. (2013). Greek, Etruscan and Roman garnets in the antiquities collection of the J. Paul Getty Museum. The Journal of Gemmology, 33(7), 201–222.

Studying renowned fancy color diamonds in museum collections: the case of the Winston Red

Eloïse Gaillou[1], Gabriela A. Farfan[2], Ulrika F. S. D'Haenens-Johansson[3], Stephanie Persaud[3], Russell C. Feather II[2], William Henry Towbin[3], Daniel C. Jones[3]

[1] Mines Paris, PSL University, Mineralogy Museum, 75006 Paris, France. eloise.gaillou@minesparis.psl.eu

[2] Department of Mineral Sciences, Smithsonian NMNH, Washington, D.C., USA

[3] Gemological Institute of America, New York, New Jersey, USA

Introduction

Museums are unique repositories of international treasures. They are also places of active research, even on the most valuable objects, such as famous and / or historic gemstones and jewels. As part of this approach and of its ongoing interest in unraveling the mysteries behind important diamonds, the Department of Mineral Sciences of the Smithsonian National Museum of Natural History (NMNH) teamed up with the Gemological Institute of America (GIA) and the director of the Mineralogy Museum of Paris School of Mines to investigate its newest and most exceptional acquisition: the 2.33ct Winston Red diamond (Figure 1). The stone was unveiled in a permanent exhibit on April 1, 2025, along with 40 Fancy color diamonds, that were part of a significant donation by Ronald Winston (son of famous jeweler Harry Winston) in December 2023. The study was conducted before the Winston Red went on exhibit, in June 2024. In order to organize for the most comprehensive study, a New York team of GIA set up a temporary gemological laboratory (for a week) in the Department of Mineral Sciences of Smithsonian Institution in Washington D.C. The main purpose of this study was to investigate the origin of the exceptional red color, and accumulate clues to better constrain its geological formation and geographic origin. This article will present the main results from this complete study, along with some behind-the-scenes pictures. In this abstract, only the main conclusions are presented.

Figure 1: Winston Red diamond, graded Fancy Red and weighing 2.33 ct. The old mine brilliant-cut stone measures 8.13 mm in the largest length.
Photo by Robert Weldon; courtesy of Ronald Winston.

History of the Winston Red

If the Winston Red is at this moment known because it is the largest pure red diamond on public display and the fifth largest diamond awarded the Fancy Red color grade, its history can be traced back to 1938. Back then, Jacques Cartier sold the stone to the Maharaja of Nawanagar, Digvijaysinhji, and suggested to set the red stone in a ring or "put in your big necklace between the green diamond and the pink diamond pendeloque [...]. The red diamond would take the place of the white triangular diamond.". The setting in the necklace was chosen. The "big necklace" was referring to the Ceremonial

Necklace of Nawanagar, best known for its cinematographic interpretation in the Ocean's 8 movie (2018): the "Toussaint Necklace" worn by actress Anne Hathaway.

By the early 1960s, the necklace was being dismantled and in 1988, Ronald Winston acquired the red diamond and nicknamed it the "Raj Red". The diamond's debut was at the Harry Winston salon of Tokyo in 1989 and worn in a ring by actress Brooke Shields. The "Raj Red" was donated by Ronald Winston in December 2023, alongside a collection of over 100 fancy color diamonds.

Main results and discussion

In order to study the Winston Red, a variety of equipment was used: optical imaging, FTIR absorption spectroscopy, visible and near infrared (Vis-NIR) spectroscopy, photoluminescence spectroscopy (PL), DiamondView Deep UV fluorescence imaging, all coming from the GIA, and scanning electron microscopy (SEM) equipped with cathodoluminescence imaging (CL) at the Smithsonian Institution.

The Winston Red was previously graded by GIA as a "Fancy Red" diamond, I2, weighing 2.33 ct, measuring 8.13 x 7.95 x 4.91 mm and being cut in an old mine brilliant cut.

First, it is important to note that red diamonds represent a specific saturation of the pink diamond grade (King *et al.*, 2002), we will therefore treat the red diamond as we would for other pink diamonds. The main features of optical observation of the Winston Red revealed a dense red color, heterogeneously distributed: three directions of red thin bands were observed. This color zoning is referred as graining, which has {111} orientation, and represents slip or glide bands created by plastic deformation (Figure 2).

FTIR spectroscopy helped classifying it as a type IaAB (A<B) diamond (Figure 3), with total nitrogen concentration visible by IR at 83 ± 8 ppm, with 76 ± 8 ppm B-centers and 7 ppm A-centers (i.e., 92% IaB). Vis-NIR analyses showed the 550 nm band, usually associated with the pink color and plastic deformation, as well as the nitrogen-related N3 (N_3V^0), H3 (N_2V^0), and H_4 ($N_4V_2^0$) defects.

PL spectroscopy using several laser wavelengths revealed the main following features: a broad band peaking at around 700 nm, possibly the 609 nm system, also visible in absorption, the 490.7nm peak (possibly related to plastic deformation; Collins & Woods, 1982), the H4, the H3, the 576 nm and the 668.7nm emission peaks. Other noticeable features are the 535.8, 654.9, 660.8 and 710 nm peaks. When viewed under the DiamondView, the Winston Red diamond displays a blue fluorescence with a color zoning due to growth features and emanating from the N3 center. After excitation under deep UV, the saturation of the red color decreased temporarily, a photochromic behavior known in pink diamonds in general (e.g., Fisher *et al.*, 2009; Byrne *et al.*, 2012). CL imaging revealed a "fish-scale" pattern related to a dislocation network, seen in low-nitrogen containing diamonds, including some pink diamonds (Gaillou *et al.*, 2010, 2012; Howell *et al.*, 2015).

All of these results show that the Winston Red belongs to the category of Group 1 pink diamonds, with a strong color saturation giving it its red hue (e.g. Gaillou *et al.*, 2010; Eaton-Magaña *et al.*, 2018). This helps narrow down the possible geographic origin of the diamond. Localities that can most likely be excluded are: Russia, Canada, South Africa, Tanzania (because they contain group 2 diamonds, those with discrete color lamellae instead of banding) and India (so far, only type IIa pinks have been reported) (Gaillou *et al.*, 2010, 2012; Howell *et al.*, 2015; Eaton-Magaña *et al.*, 2018). Recognized group 1 pink diamonds are known from Venezuela and from Argyle, but this later locality can also be excluded, as the Winston Red predates the opening of the Argyle mine in the 1980s. Non-classified red diamonds have been reported from Minas Gerais in Brazil, but no comprehensive studies have been done on pink to red diamonds from this locality. It is interesting to note that the 5.11 ct Moussaieff Red diamond cut from a 13.90 ct crystal recovered from an alluvial deposit in Noroeste de Minas, Minas Gerais, Brazil, in the mid-1990s (e.g., King *et al.*, 2002; King and Shigley, 2003). This leads us to conclude that the Winston Red diamond mostly comes from Venezuela or Brazil.

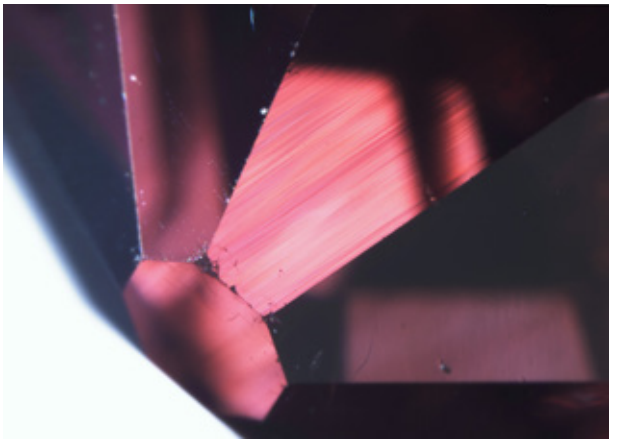

Figure 2: Pink color zoning observed in the Winston Red diamond. Here, only one direction of the banding is visible. Scale bar: 0.5 mm. © GIA / Smithsonian.

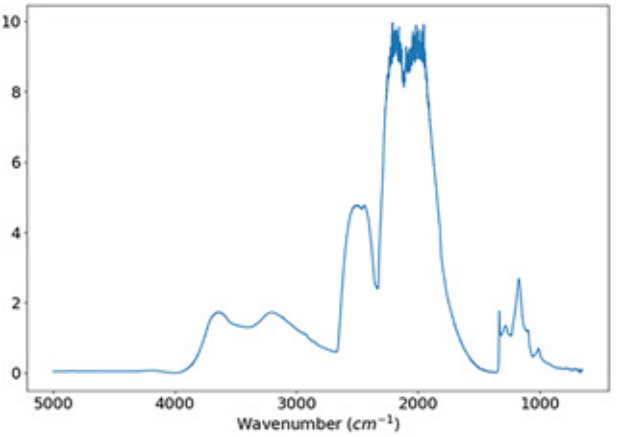

Figure 3: FTIR spectrum of the Winston Red diamond: Type IaA<B, with very small H at 3107 cm^{-1} and Amber Center AC1 at 4167 and 4839 cm^{-1}).

Conclusion

This study highlights the problem of establishing a geographic origin for diamonds, even if for pink to red diamonds, nitrogen content and aggregation along with color distribution help narrow the possibilities down. It will hopefully encourage institutions and private parties having pink to red diamonds of known origin to scientifically investigate their collection in order to help understanding the pink diamond story. Conducting such studies on a world-record red diamond also demonstrates that such experiments are safe to be conducted on valuable stones. In the meantime, the team has enjoyed being able to work on such an astonishing stone, which is now on public display for everyone to enjoy.

References:

- Byrne K.S., Anstie J.D., Chapman J.G., Luiten A.N., 2012. Optically reversible photochromism in natural pink diamond. Diamond and Related Materials, 30, 31–36.
- Collins A.T., Woods G.S.,1982. Cathodoluminescence from "giant" platelets, and of the 2.526 eV vibronic system, in type Ia diamonds. Philosophical Magazine B, 45 (4), 385–397.
- Eaton-Magaña S., Ardon T., Smit K.V., Breeding C.M., Shigley J.E., 2018. Natural-color pink, purple, red, and brown diamonds: Band of many colors. Gems & Gemology, 54 (4), 352–377.
- Fisher D., 2009. Brown diamonds and high pressure high temperature treatment. Lithos, 112S, 619–624.
- Gaillou E., Post J.E., Bassim N.D., Zaitsev A.M., Rose T., Fries M.D., Stroud R.M., Steele A., Butler J.E., 2010. Spectroscopic and microscopic characterizations of color lamellae in natural pink diamonds. Diamond and Related Materials, 19 (10), 1207–1220.
- Gaillou E., Post J.E., Rose T., Butler J.E., 2012. Cathodoluminescence of natural, plastically deformed pink diamonds. Microscopy and Microanalysis, 18 (6), 1292–1302.
- Howell D., Fisher D., Piazolo S., Griffin W.L., Sibley S.J., 2015. Pink color in type I diamonds: Is deformation twinning the cause? American Mineralogist, 100 (7), 1518–1527.
- King J.M., Shigley J.E., Guhin S.S., Gelb T.H., Hall M., 2002. Characterization and grading of natural-color pink diamonds. Gems & Gemology, 38 (2), 128–147.
- King J.M., Shigley J.E. (2003) An important exhibition of seven rare gem diamonds. G&G, Vol. 39, No. 2, pp. 136–143, http://dx.doi.org/10.5741/GEMS.39.2.136

History of Garnet Mining and Cutting in the Austro-Hungarian Monarchy

Karl Schmetzer
Petershausen, Germany; SchmetzerKarl@hotmail.com

Bohemian garnets, i.e., chromium-bearing pyropes, are found in several jewellery pieces from the Migration Period (circa 400 to 600 A.D.), and only a small number of jewels containing Bohemian garnets remain from the period of the Middle Ages thereafter (until 1500 A.D.). The exact locations from which these garnets were mined remain unknown, and it was Agricola who first mentioned specific occurrences for Bohemian garnets in his treatise from 1546. According to present knowledge, three areas in the former Bohemian kingdom, now in the Czech Republic, became important sources for rough garnets of gemstone quality, i.e., the Central Bohemian Highlands, the Podkrkonoší area, and the Kolin region (Figure 1). The most important location in the Central Bohemian Highlands supplying chromium-bearing pyropes for several centuries covered an area of approximately 70 km^2 (Figure 2). Production in the 19th and 20th centuries in these three different areas in Bohemia went up and down, yet even within the last few decades, discrete localities within these areas have seen mining activity using modern equipment.

Early cutting of gem materials in the Breisgau region, especially in Freiburg and the small town of Waldkirch north of Freiburg, dates back to the late 14th or early 15th century. The city of Freiburg belonged to territory controlled by the Austrian dukes since 1368, and the kingdom of Bohemia was then ruled from 1526 onwards by the Habsburg dynasty. Thus, when Bohemia became part of the Archduchy of Austria controlled by the Habsburgs, an industry for gemstone cutting had already been established in the Breisgau area for more than 100 years. It has been suggested that this was the main reason why cutting of Bohemian garnets in large quantities started in the Breisgau region, given that the mining sites and an area experienced in cutting of gem materials were then ruled by the same dynasty.

Figure 1: Administrative regions in the Czech Republic and location of the most important historical areas which supplied garnets of gem quality: 1) the Central Bohemian Highlands, northwest of Prague, 2) the Podkrkonoší area northeast of Prague, and 3) the Kolin region southeast of Prague.

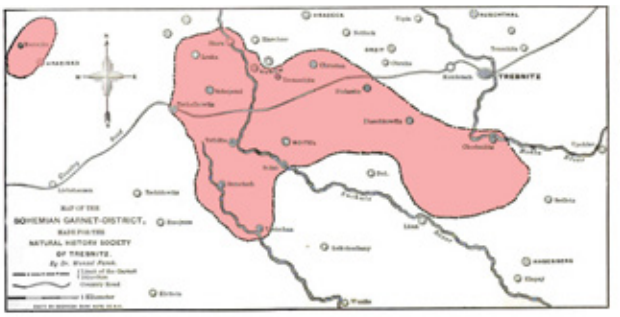

Figure 2: Map of the Bohemian garnet district in the Central Bohemian Highlands; after Kunz (1893).

Nonetheless, the start of garnet cutting in Freiburg and Waldkirch is not precisely dated. Garnet is first mentioned as a cutting material in a document from 1544 describing various rules and laws governing the gemstone cutting industry in both Freiburg and Waldkirch. The techniques applied for cutting the Bohemian garnet grains of small sizes, generally below 8 mm, on large rotating sandstone wheels (Figure 3), and for drilling the mostly small rough garnet grains were kept secret. Such secrecy, in turn, established what functioned largely as a monopoly for the Breisgau area until the mid of the 18th century, notwithstanding the fact that the mining areas in Bohemia were at a distance of more than 500 km from the Breisgau region.

The only notable exception to this monopoly was found in the Imperial City of Nuremberg, where Claudius vom Creutz devised a technique for cutting of Bohemian garnets and setting the rose cut gemstones on glass substrates, e.g., engraved glass goblets and glass beakers (Figure 4), by means of low melting-point lead glass fixation layers. Creutz and several of his successors received imperial privileges, comparable to modern patents, in 1591, 1653, and 1714. Starting around 1750, various garnet cutters from Freiburg or Waldkirch moved to Bohemia, together with their families. As a consequence, the requisite technical knowledge for garnet cutting and drilling was transferred from the Breisgau region to Bohemia. The result was a progressive decrease in the number of gem cutters in Breisgau and, conversely, a continuous increase in the gem cutting industry in Bohemia, with more than 3000 gem cutters working there during the second half of the 19th century. Gem cutting in Freiburg ceased completely before 1800, and in the 19th century, the garnet cutting industry in the Breisgau area only survived in the city of Waldkirch, where two new companies were founded.

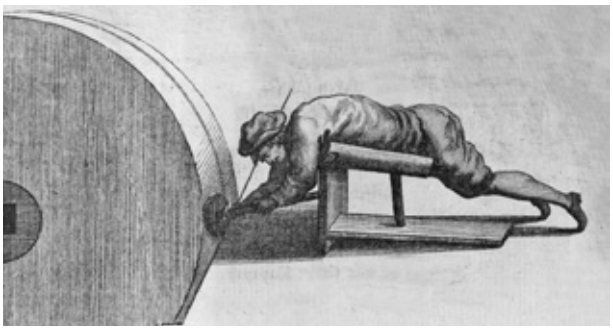

Fig. 3: Cutting of gem materials on large sandstone wheels with the gem cutter lying prone in front of the wheel; from Collini (1777).

Figure 4: Lid of a goblet from the collection of the Bavarian National Museum in Munich, embellished with red Bohemian garnets; height of the lid 8.3 cm. Courtesy of Bavarian National Museum Munich, photo by Bastian Krack.

Gemstone mining in the Ziller Valley in Northern Tyrol and cutting of these gemstones in Salzburg was initiated in 1782 by Ignaz Hirtz, who came from the Breisgau area. Hirtz cooperated with Peter Kreidl from the Ziller Valley for supply of the rough garnets, the latter of whose business was subsequently taken over by his sons Andrä and Jakob Kreidl, also born in the Ziller Valley. The cutting business for garnets in Salzburg remained small, and the supply of rough material surpassed the local cutting capacity. Hence, garnets from the Ziller Valley were exported to other cutting centers in Austria and Bohemia. The first garnets from the Ziller Valley arrived in the Bohemian cutting factories around 1800 or shortly thereafter.

During the late 1820s and early 1830s, the Kreidl brothers Andrä and Jakob established a monopoly for garnet mining in the Ziller Valley. Thus, when Joseph Hofer, also born in the Ziller Valley, became interested in garnet mining in the early 1830s, he found the main areas of interest, especially on the Roßrücken mountain, in the hands of the Kreidl family. Chemically the garnets from Roßrücken and other localities in the Ziller Valley were almandines (Figure 5). Searching for new promising locations for gem quality garnets, Hofer first moved to Southern Tyrol and later, in 1852, to the area around Radenthein in Carinthia, where he also found almandines of gem quality.

The Kreidl family mined garnets until 1904 in the Ziller Valley. The Hofer family operations, in turn, continued until forced to stop all activities during World War I, but they resumed on a very small scale after the war, before finally ceasing in the 1920s. Both the Hofer and Kreidl families sold their garnets as garnets from the Ziller Valley, disregarding their true origin, and after cutting, all faceted stones, whether pyropes from Bohemia or almandines from Tyrol and Carinthia, were characterized as "Bohemian garnets" in the trade.

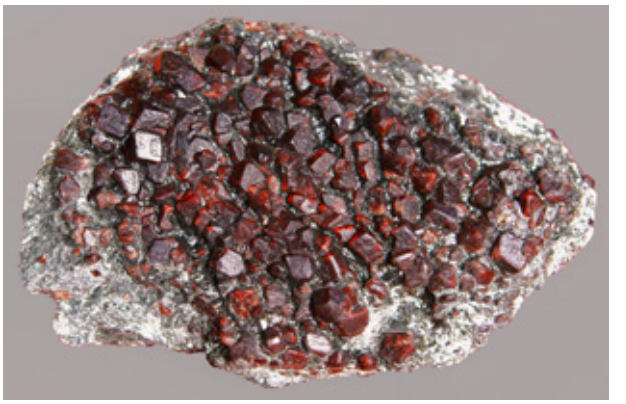

Figure 5: gem quality transparent almandines from the Ziller Valley in northern Tyrol, location of the most prominent garnets mined in Austria in the 19th century.
Photo courtesy of Walter Ungerank.

References:

- Agricola, G., 1546. De ortu & causis subterraneorum. Lib. V.
- Collini, C.A., 1777. Tagebuch einer Reise welches verschiedene mineralogische Beobachtungen besonders über die Agate und den Basalt enthält; nebst einer Beschreibung der Verarbeitung der Agate, 377-427.
- Kunz, G.F., 1893. Bohemian garnets. Transactions of the American Institute of Mining Engineers 21, 241-250.

Historic Emeralds and their Geographic Origin: A Retrospective Study

Marie-Laure Cassius-Duranton[1*], Vincent Pardieu[2], Stefanos Karampelas[3,4]

[1] L'ECOLE School of Jewelry Arts, Paris, France

[2] VP Consulting WLL, Manama, Bahrain

[3] School of Geology, Aristotle University of Thessaloniki, 54124, Thessaloniki, Greece

[4] LFG (Laboratoire Français de Gemmologie), 30 rue de la Victoire, 75009, Paris, France

[*] marie-laure.cassius-duranton@vancleefarpels.com

Keywords: Emerald, Silk Roads, History of Gemstones, Egypt, Pakistan

When it comes to the geographic origin of gems, curiously enough, historians sometimes put forward provenance without any documentary or scientific proof. This methodological weakness can lead to erroneous conclusions.

Figure 1: Catherine de Medici's 16th century pendant, enameled gold, diamonds, emeralds (BnF Collection No. 56.336). Photo by Serge Oboukhoff; courtesy of the Museum of the National Library of France

The history of a gem can sometimes be retraced thanks to archives. Moreover, to be certain of a gem's geographical origin, it is necessary to resort to scientific analysis. Indeed, even if historical documents mention an origin, this is often confused with a trading location, and only advanced technological methods can provide results that allow us to put forward hypotheses consistent with certain geographic origin.

A recent interdisciplinary study of a 16th century pendant on display at the Museum of the National Library of France in Paris, that has been linked to Catherine de' Medici, Queen of France from 1547 to 1559 (fig. 1), has called into question the geographic origin of the two emeralds that adorn it, that one historian claimed were Colombian without documentation or scientific proof. The microscopic, spectroscopic, and chemical data collected in this study indicate that these two emeralds are from Pakistan, specifically Swat Valley, challenging the previous assumption. In particular, the relatively high iron and chromium, the relatively low vanadium, and the detectable rubidium measured with EDXRF, as well as the low to medium absorption features in the visible range due to iron, can be observed in emeralds from this region. The inclusions observed in the studied samples have been observed in those from Swat Valley (Guo *et al*., 2020; Cornuz, 2021).The presence of emeralds from Pakistan in this 16th century European pendant provides strong evidence of the existence of trade routes between Asia and Europe during this time period and probably before, as gemstones are commonly reused (Panczer *et al*., 2025).

The Swat Valley emerald deposits are generally cited as having been discovered in 1958 (Gübelin, 1982). However, a Gallo-Roman earring preserved in the National Museum

of Natural History in Paris, discovered in Miribel, France, in 1997 (fig. 2), was found to have an oxygen isotope composition corresponding to emeralds from Swat Valley (Giuliani *et al*., 2000; Schwarz and Giuliani, 2002). Studying these samples using non-destructive methods, as used for Catherine de' Medici's pendant, may be useful in order to confirm (or affirm) those findings. Additionally, a thirteenth-century reliquary crown conserved in the Diocesan Museum in Namur (Belgium) appears to contain emeralds from Pakistan based solely on chemistry (Bruni *et al*., 2021).

Just because some emerald deposits were discovered in Colombia during the 16th century does not mean that all emeralds on the market at the time were of Colombian origin. If we compare with written sources, even if some authors allude to the new emeralds "from Peru", such as Georgius Agricola in De natura fossilium (1546) and Garcia de Orta in his Coloquios dos simples e drogas medicinais da India (1563), it is above all from Anselmus Boethius de Boodt, in his Gemmarum et lapidum historia (1609) that the new emeralds, qualified as 'Occidental', are described in comparison with "Oriental" emeralds. It is also interesting to compare the results obtained thanks to gemological analysis with ancient sources, in particular lapidaries. These treatises describe the properties of gems according to classification criteria that differ from modern mineralogy, and the first difficulty encountered by the historian is translation. Few historians are able to read the original texts in ancient Greek, Latin, Sanskrit, Persian, etc... Historians are not philologists, and if they set out to study the global history of gems, they must be aware of the methodological pitfalls they are likely to encounter. Translators interpret, and the choices they make in translating gem names,

Figure 2: Gallo–Roman earring (excavated in Miribel, France), Gold, Emerald (Swat, Pakistan), 1st century CE, MNHN, Paris, Photo by François Farges.

colors and regions can be misleading. That's why it's also important to contextualize and compare precious objects and jewels that can be dated with certainty.

Before the discovery of Colombian emeralds, which indeed revolutionized the international emerald market, the main sources mentioned in lapidaries since Pliny the Elder were Egypt, Bactria and Scythia. For emeralds set in historic jewels that have been analyzed by teams of gemologists, the results in most cases point to Egyptian origins; while

Austrian sources have been suggested in some instances, these have never been conclusively confirmed through comprehensive studies (Giuliani *et al*., 2000; Aurisicchio *et al*., 2006; Gilg and Grundmann, 2022; Schmetzer, 2022; Cao *et al*. 2024). Egyptian deposits seem to have been the main source of emeralds traded worldwide for centuries, from Roman times to the Renaissance. If Egyptian deposits are a historical reality, why not Bactria and Scythia?

References:

- Agricola G., 1546, De natura fossilium, Basel
- Aurisicchio C. *et al*., « The Emerald and Gold Necklace from Oplontis, Vesuvian Area, Naples, Italy", in The Journal of Archaeological Science, Vol. 33, Issue 5, May 2006, p. 725-734.
- Boethius de Boodt A., 1609, Gemmarum et lapidum historia, Lyon
- Bruni Y., Hatert F., George P., Cambier H., Strivay D., 2021, "A gemmological study of the reliquary crown of Namur, Belgium", European Journal of Mineralogy, vol. 33, No. 2, pp. 221-232.
- Cao Y., Yang M., Luo Z. (2024) Late but precious: The dissemination and use of emerald in the Ming Dynasty in China. [in Chinese with English abstract], Journal of Gems & Gemmology, Vol. 26, No. 6, pp. 140–147.
- Cornuz L., 2021, The relationship between the geological context and the inclusions found into the emeralds of the Mingora district (Swat Valley, Pakistan). Mémoire de DU de Gemmologie, Université de Nantes.
- Da Orta G., 1563, Coloquios dos simples e drogas medicinais da India, Goa
- Gilg, H.A. & Grundmann, G., 2022, "Géologie et genèse des gisements d'émeraudes d'Egypte", in Giuliani, G. (ed), Émeraudes, Tout un Monde! Les Éditions Piat, Paris, pp. 153-158.
- Giuliani G., Chaussidon M., Schubnel H.-J., Rollion-Bard C., France-Lanord C., Giard D., Narvaez D., Rondeau B., 2000, "Oxygen isotopes and emerald trade routes since antiquity", Science, vol. 287, No. 5453, pp. 631-633.
- Gübelin, E., 1982, "Gemstones of Pakistan : emerald, ruby and spinel", Gems & Gemology, vol. 18, No. 2, pp. 123-139.
- Guo H., Yu X., Zheng Y., Sun Z., Ng M.F.-Y., 2020, "Inclusion and trace element characteristics of emeralds from Swat Valley, Pakistan". Gems & Gemology, Vol. 56, No. 3, pp. 336–355 (http://dx.doi.org/10.5741/GEMS.56.3.336)
- Panczer G., Fesquet R., Moshi L., Riondet G., Cassius-Duranton M.-L., Gilles-Guéry L., Delaunay A., Karampelas S., 2025. "Emeralds in Catherine de' Medici's Pendant: an Unexpected Geographic Origin", Gems & Gemology, vol. 61, No.1, Spring 2025, pp. 44-56 (https://www.gia.edu/doc/spring-2025-catherine-de-medici-emerald-pendant.pdf).
- Schmetzer K., "History of Emerald Mining in the Habachtal Deposit of Austria, Part I", Gems & Gemology, Vol. 57, No. 4, Winter 2022, pp. 338-371.
- Schwarz D., Giuliani G., "Emeralds from Asia: Pakistan, Afghanistan and India: Historically significant deposits?", in Giuliani G., Jarnot M., Neumeier G., Ottaway T., Sinkankas J., Staebler G. (eds), Emerald: The most valuable beryl: The most precious gemstone, Lapis International, East Hampton, pp. 60-63.

Study of "amethysts" from the French Crown Jewels

Stefanos Karampelas[1,2*], Eloïse Gaillou[3*], Annabelle Herreweghe[2], Ugo Hennebois[2], Farida Maouche[3], Romain Bolzoni[3], Steven Riou[2], Quentin Dartois[2], Bérengère Meslin Sainte Beuve[2], Christelle Gliksman[2], Thiala Magalhaes[2], Valentine Demetz[2], Aurélien Delaunay[2]

[1] School of Geology, Aristotle University of Thessaloniki, 54124, Thessaloniki, Greece

[2] LFG (Laboratoire Français de Gemmologie), 30 rue de la Victoire, 75009, Paris, France

[3] Mines Paris - PSL, PSL Research University, Musée de Minéralogie, 60 boulevard Saint-Michel, 75006 Paris, France

[*] skarampelas@geo.auth.gr; s.karampelas@lfg.paris; eloise.gaillou@minesparis.psl.eu

Keywords French Crown jewels; historic amethysts; non-destructive methods

The French Crown Jewels have a long and tumultuous history. Established in 1530 by King Francis I, a royal decree declared them a national treasure meant to be enriched over time. They survived the upheaval of the French Revolution, only to be dispersed after the fall of the Empire. In 1887, under the French Third Republic, the collection -then comprising 77,486 gems- was mostly sold off in lots of loose stones. The remaining few jewels of the last empresses were sold as is, and the symbols of the monarchy and the empire (the coronation crown and two swords) got dismantled before being dispersed in lots of gemstones. But three French institutions inherited a few individual gems and a few lots. Among those, a suite of "Siberian amethysts" (as listed in the historic documents) that were once in a "parure" (ornament) made by French Jeweler Nitot in 1810, for the Empress Marie-Louise, the second wife of Napoléon the First, which got attributed to the Paris School of Mines (referred as "School" in the rest of the text). Since 1887, the 177 amethysts were kept by this French Institution. For the past few years, the Mineralogy Museum of Paris School of Mines (cited as Mineralogy Museum at the rest of the text) has displayed over one hundred of those amethysts in its permanent collection, along with some emeralds and "Brazilian rubies" (pink topaz) that were also part of the same national treasure.

Figure 1. Amethysts from the French Crown Jewels ranging from 0.10 to 77.42 ct. Photo: Mineralogy Museum, Mines Paris – PSL / E. Gaillou.

This national treasure is under scrutiny at the School; after examining the "emeralds" that used to be in the last coronation crown (Karampelas *et al*., 2022), the museum associated again with the Laboratoire Français de Gemmologie (LFG) to conduct gemological investigations on the suite of amethysts, along with investigating their history. The goal of this study was to gather as much information as possible regarding the jewels that were once adorned by the amethysts, along with a complete gemological study of each of the 177 gems (Figure 1).

Gem characterization with classical gemmological tools (refractometer, specific gravity kit, a 3 Watt SW- and LW-UV lamps) was conducted at the Mineralogy Museum. The microscopic, chemical and spectroscopic analyses were done the LFG in Paris. The stones were brought in five different parcels for about a week each. Raman and PL spectra were carried out using a mobile Raman spectrometer with a 532 nm excitation wavelength and a Raman spectrometer with a microscope with a 514 nm excitation wavelength, Vis-NIR spectra were acquired from 365 to 1000 nm using a mobile instrument with an integrating sphere, FTIR spectra from 400 to 8000 cm^{-1} in transmission mode, using a beam condenser and EDXRF using a set of parameters (combining various filters and voltage) to optimize the analysis.

In his book, Morel (1988) presents a complete historical reconstruction of the French Crown Jewels, along with a listing of most jewels and gems they contained. The different attributions to the School of Mines can easily be identified. Concerning the "Siberian amethysts", Morel specified that they were part of the amethyst and diamond "parure" requested by Napoléon the First to jeweler Marie-Etienne Nitot, to be added to the Crown Jewels, and to be used by Marie-Louise (Morel, 1988, p. 276). The amethyst and diamond "parure" was constituted of a tiara, a belt, a necklace, a comb, a pair of earrings, and a pair of bracelets. In total, the set was constituted of 235 amethysts and 3630 diamonds. Morel mentioned that amethyst was at that time a gemstone that was highly in trend, reaching its time of

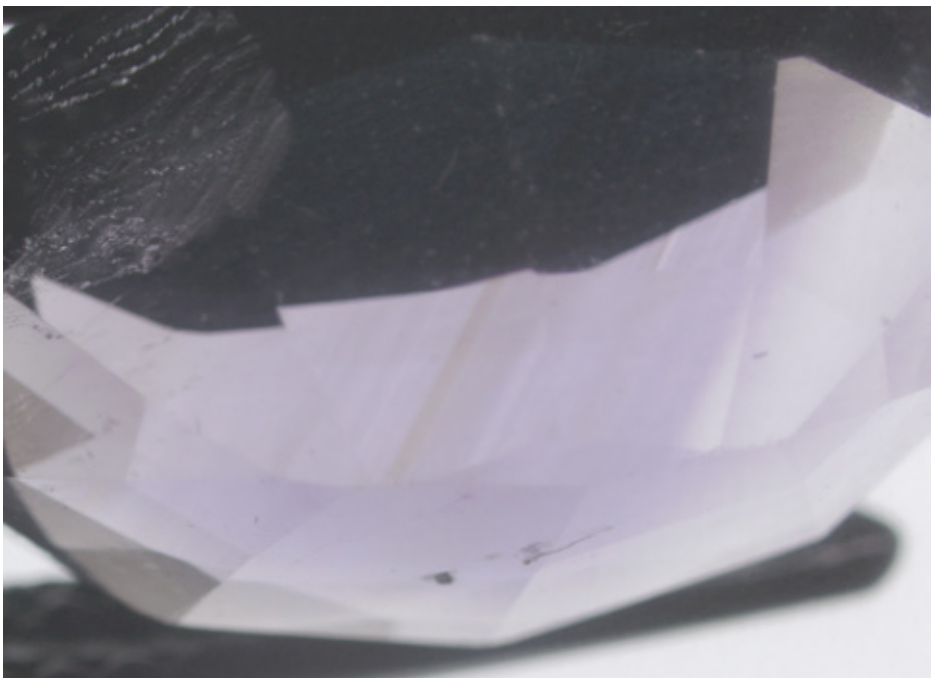

Figure 2. Colour zoning of the sample ENSMP 69828.14. Photomicrograph by U. Hennebois/LFG, © Mineralogy Museum, Mines Paris – PSL; image width 5 mm.

glory at the Romantic Era. The outcome of the amethyst and diamond set is also written in Morel's book (p. 385). During the Bourbon Restauration, King Louis the 18th, who reigned in 1814 to 1821, dismantled some jewels and alienated some 6000 gems from the French Crown Jewels. The amethyst and diamond parure was part of the jewels that were dismantled, but the amethysts were kept in the Crown Jewels. In 1887, the Crown Jewels were sold, while some lots were attributed to the Louvre Museum, the National Museum of Natural History and to the School of Mines, including the 177 samples "Siberian amethysts".

At the time of the preparation of a temporary exhibition, which ran from September 2023 to March 2024, the mineralogy museum curators contacted the descendant of Nitot Jeweler, the Maison Chaumet based place Vendôme in Paris to conduct some research into the past of these jewels. The Heritage Center of the Maison Chaumet found an important document: a drawing of the tiara, part of the amethyst and diamond ornament. Long searches in the heritage documents of the Maison did not reveal any other documents so far. The reproduction of this drawing was first shown during this exhibition.

The examined stones were all faceted with round to oval to cushion shapes, weighing from 0.10 to 77.42 ct. Most of the examined samples presented various natural inclusions, pronounced colourless zones (Figure 2). Thus, they were all natural without any indication of treatment observed. All these samples did not present reactions under UV lamps, having specific gravity of around 2.65 and refractive index from 1.54 to 1.55. Eight samples presented bubbles under microscope, showing artificial product, chalky blue luminescence under UV lamps with specific gravity around 2.50 and refractive index around 1.52. The 169 natural samples presented Raman spectra characteristic of quartz. Their FTIR spectra were varying, some with the characteristic three absorption bands of natural amethysts, situated at 3585, 3595 and 3614 cm^{-1}; in some spectra the band at 3595 cm^{-1} was missing. This was also observed before in natural amethysts with pronounced colourless zones (Karampelas *et al*., 2011). The eight samples presented Raman and FTIR spectra characteristic of artificial glass. The presence of Mn^{3+} as main colourant was identified by UV-Vis-NIR spectroscopy.

This article once again underscores the vital role of scientific research in the study of museum collections. We hope that ongoing research on this historic national collection-owned and curated by the Paris School of Mines since 1792- through the collaboration between the Laboratoire Français de Gemmologie and the Mineralogy Museum at Mines Paris – PSL, will inspire other institutions to actively document and share new insights about their specimens with both the scientific community and the wider public.

References:

- Karampelas S., Fritsch E., Zorba T. and Paraskevopoulos K.M., 2011. Infrared spectroscopy of natural vs. synthetic amethyst: An update. Gems & Gemology, 47(3), pp. 196-201.
- Karampelas, S., Gaillou, E., Herreweghe, A., Maouche, F., Hennebois, U., Leblan, S., Meslin Sainte Beuve, B., Lechartier, M., Nectoux, D., Delaunay, A., 2022. A Gemological and Spectroscopic Study with Mobile Instruments of Some "Emeralds" from the Coronation Crown of Napoleon III. Gems & Gemology, 58 (2), pp. 168-183.
- Morel, B., 1988. Les Joyaux de la Couronne. Fonds Mercartor, Anvers, Albin Michel Ed., 420 pp.

Cross-Cultural Provenance and Characterization of Turquoise Artefacts: A Multi-Analytical Non-Destructive Study of Reshui Tomb Cluster, China (744 AD) and Tepeh Zagheh, Iran (5200–4200 BCE)

Bahareh Shirdam[1,2*], Yang Mingxing[1,2], Andy Hsitien Shen[1,2], Hassan Fazeli Nashli[3]

[1] Gemmological Institute, China University of Geosciences, Wuhan, 430074, China

[2] Hubei Jewelry Engineering Technology Research Center

[3] Department of Archaeology, University of Tehran, Tehran, Iran

Turquoise has long held considerable cultural, economic, and symbolic significance across ancient civilizations, functioning both as a prestigious ornament and as a medium of exchange. Its distribution provides important insight into long-distance trade networks (figure 1), resource procurement strategies, and the sociopolitical structures that facilitated material mobility. This study presents a cross-cultural, comparative analysis of turquoise artefacts from two geographically distinct archaeological contexts: the Reshui Tomb Cluster (Xuewei Tomb No. 1, Qinghai Province, China, Tang Dynasty, 744 AD) (Ma *et al*., 2024) and Tepe Zagheh (Qazvin Plain, Iran, Transitional Chalcolithic period, 5200–4200 BCE) (*Vidale et al*., 2018).

A non-destructive, multi-analytical methodology was applied to characterize the mineralogical and geochemical composition of the turquoise samples. The analytical techniques included Raman spectroscopy, Fourier-transform infrared spectroscopy (FTIR), Energy-Dispersive X-ray Fluorescence (EDXRF), and Laser Ablation Inductively Coupled Plasma Mass Spectrometry (LA-ICP-MS). Provenance determination was supported by an extensive LA-ICP-MS dataset comprising over 2,000 measurements from turquoise deposits across China (Hubei, Henan, Shaanxi, Xinjiang, Gansu, Qinghai, and Anhui) and 586 measurements from main Iranian sources (Neyshabur, Baghu, and Meiduk). Together, these complementary methods enabled the identification of diagnostic mineral phases, trace-element patterns, and rare earth element (REE) distributions critical for accurate provenance attribution (*Shirdam et al*., 2024).

For the Reshui assemblage, preliminary hypotheses positioned Delingha (Wulan region, Qinghai) as the likely source, based on the presence of sedimentary-hosted min-

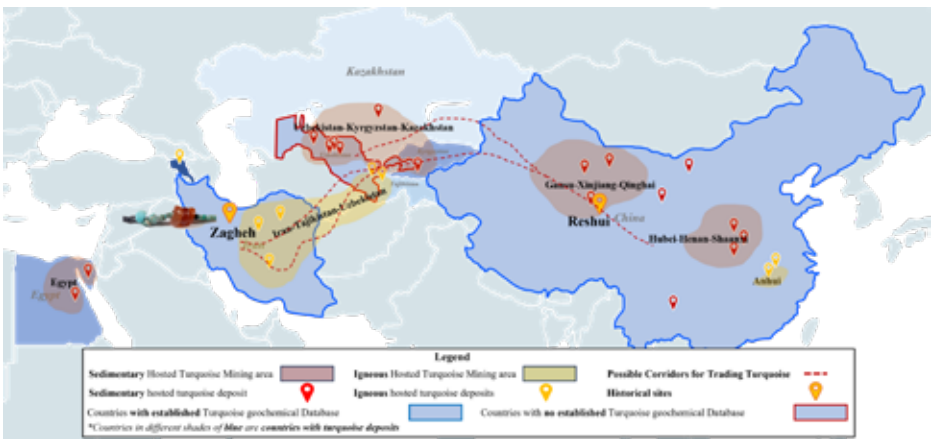

Figure 1. Major turquoise sources along the silk road and the location of studies artefacts to the trade routes

eral traits. However, detailed mineralogical and trace-element data, including rare earth element (REE) profiles and secondary mineral associations, didn't match with known Delingha specimens. Instead, geochemical consistency was found with turquoise from the Shuangying Mountain Formation in Beishan, Gansu Province. This reassignment redefines understandings of Tang Dynasty turquoise procurement, indicating that acquisition was likely integrated into formalized, state-regulated trade routes through the Hexi Corridor, a strategic segment of the Silk Road. The association of Gansu-sourced turquoise with elite tombs in Qinghai suggests centralized control over high-value resources and underlines the reach and sophistication of Tang economic networks.

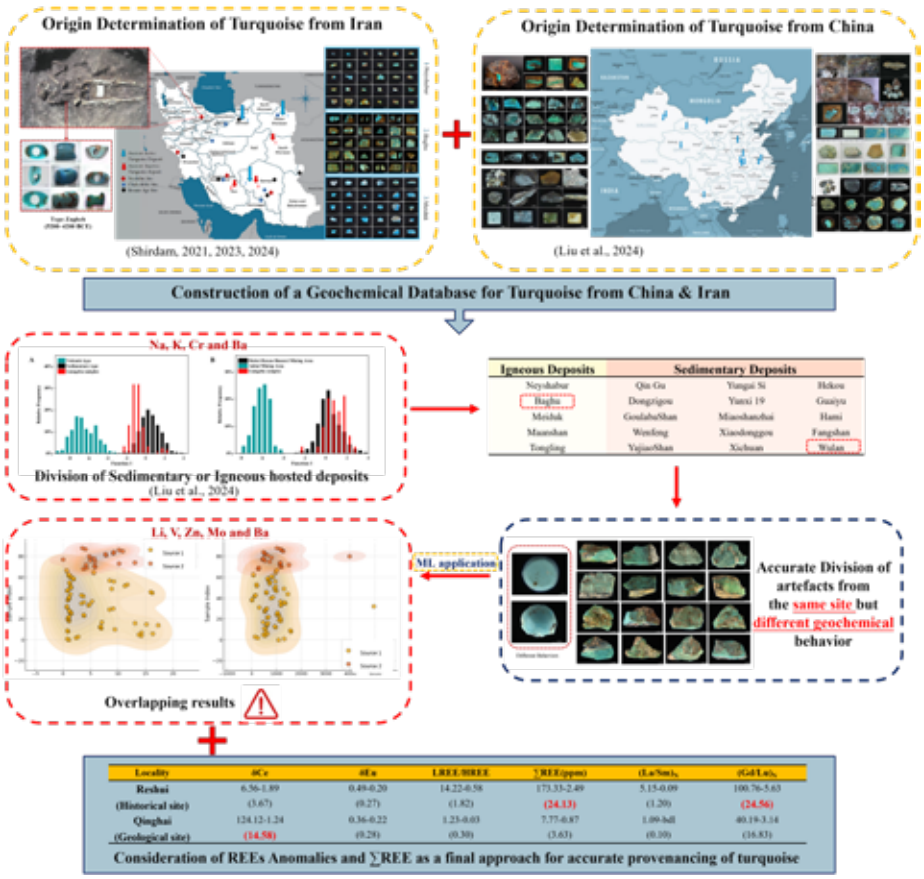

Figure 2. Technical workflow for turquoise provenancing, including an example of data processing and strategies for resolving overlapping geochemical signatures

References:

- Ma, B., Li, X., Qin, X., *et al*., 2024. A preliminary study on the origin of turquoise unearthed from the Xuewei No. 1 Tomb in the Reshui Tomb Group in Dulan, Qinghai Province in 2018. Archaeology and Cultural Relics, 2024(4), 121–128.
- Shirdam, B., Yang, M., Liu, J., Liu, L., Shen, A.H., 2024. Characterizing the provenance signatures and geochemical behaviors of turquoise in copper deposits: comparative case studies of Meiduk, Iran, and Tongling, China. Journal of Gems & Gemmology, 26(S1), 71–73.
- Vidale, M., Fazeli-Nashli, H., Desset, F., 2018. The late prehistory of the northern Iranian Central Plateau (c. 6000–3000 BC): growth and collapse of decentralised networks. In: Surplus without the state: political forms in prehistory. 10th Archaeological Conference of Central Germany, October 19–21, 2017, Halle (Saale).

Novel cultured pearls with ceramic nucleus and possible cause of their strong luster

Yan Li, Qing Su
Gemological Institute, China University of Geosciences, Wuhan 430074, China
*yanli@cug.edu.cn

Cultured pearls with a ceramic nucleus (bead) represent a new type of saltwater cultured pearls that has recently emerged. Its growth process is similar to that of ordinary cultured pearls and the detailed process of producing them is outlined in the supplementary material. While they resemble Akoya cultured pearls in appearance, they often show a stronger luster (Fig.1). In pearl valuation, luster is one of the most important criteria, which may enable cultured pearls with ceramic nucleus to be a new type of high-quality cultured pearls. Therefore, the underlying reason for their enhanced luster requires investigation, possibly linked to their unique ceramic nuclei and the structure and reduced thickness of their nacre layers. This report explores a new method for cultivating superior cultured pearls at a lower cost, demonstrating the feasibility and advantages of using ceramics as the nuclear material for pearl cultivation.

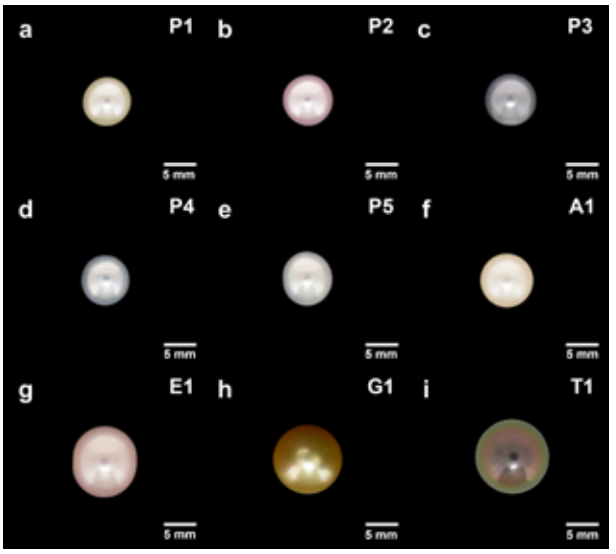

Fig. 1 Nine different pearl samples: (a-e) Novel cultured pearls with ceramic nucleus (P1-P5); Akoya cultured pearl (A1); Edison cultured pearl (E1); Golden cultured pearl from the South Sea (G1); Tahiti cultured pearl (T1), all with shell beads.

As technology continues to advance, a growing focus is placed on using non-destructive and rapid methods to detect and analyze pearls. Among these techniques, three-dimensional (3D) fluorescence and Energy Dispersive X-ray Fluorescence (EDXRF) are useful non-destructive testing methods to characterize pearls [L. Shi *et al*., 2018, Y.J. Li *et al*., 2023]. For this study, we analysed five cultured pearls with ceramic nucleus (samples P1-5) and four Akoya-type reference samples (A1, E1, T1, G1) using advanced characterization techniques such as EDXRF, 3D fluorescence spectroscopy, photoluminescence (PL) spectroscopy, UV-visible (UV-vis) spectroscopy, Fourier Transform Infrared (FTIR) Spectroscopy, and Scanning Electron Microscopy (SEM) (Fig.2). 3D fluorescence spectroscopy shows that the P1-5 (Fig.3a-e) and A1 (Fig.3f) are characterized by the presence of two fluorescence centers located at approximately 374/446 nm and 374/462 nm within the E_x / E_m range, which were distinctly different from those of the other pearl samples [Y.J. Li, C.Y.F. Chen and L.P. Li, 2023] (Fig.3g-i).The appearance of dual fluorescence peaks at 446 nm and 462 nm upon excitation at 374 nm is characteristic of humic acid luminescence [Y.J. Li and L.P. Li, 2023]. This indicates that the primary organic components of P1-5 and A1 include humic acid, distinguishing them from other samples. The presence of humic acid may lead to the fluorescence quenching of amino acids, such as tryptophan. The greater the concentration of humic acid, the more pronounced the fluorescence quenching phenomenon becomes [Z. Wang *et al*., 2015], which leading to the weaker tryptophan luminescence of P1-5 and A1. Therefore, it can be concluded that the pearl oysters producing cultured pearls with a ceramic bead are consistent with those that produce Akoya pearls. Therefore, it can be concluded that the pearl oysters producing cultured pearls with a

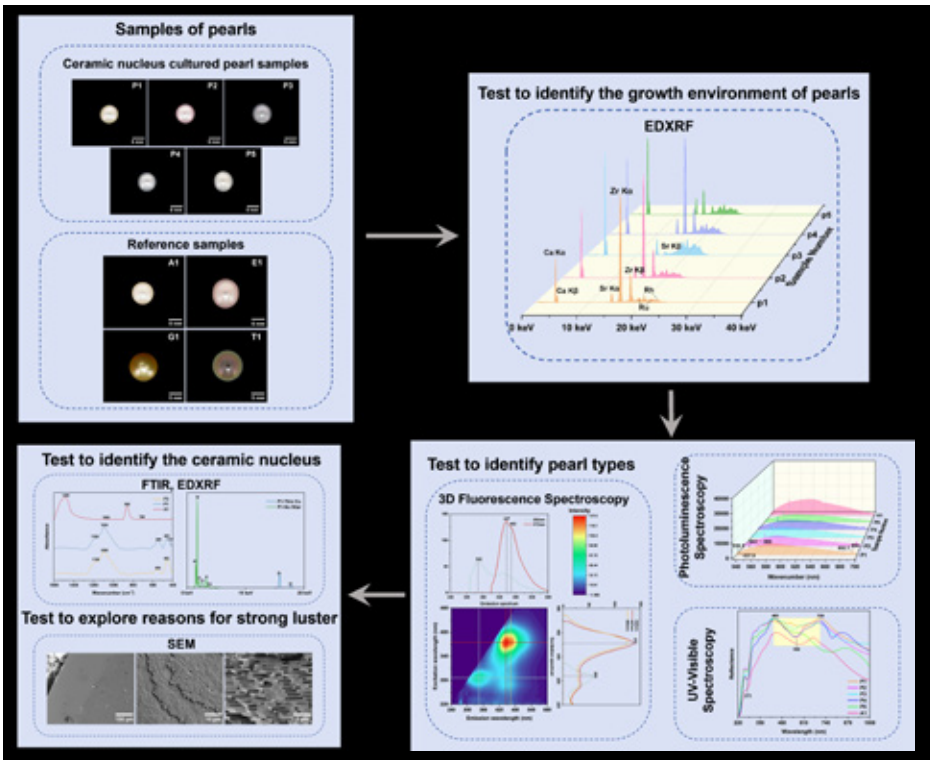

Fig.2 Flowchart of novel ceramic pearl analysis and testing.

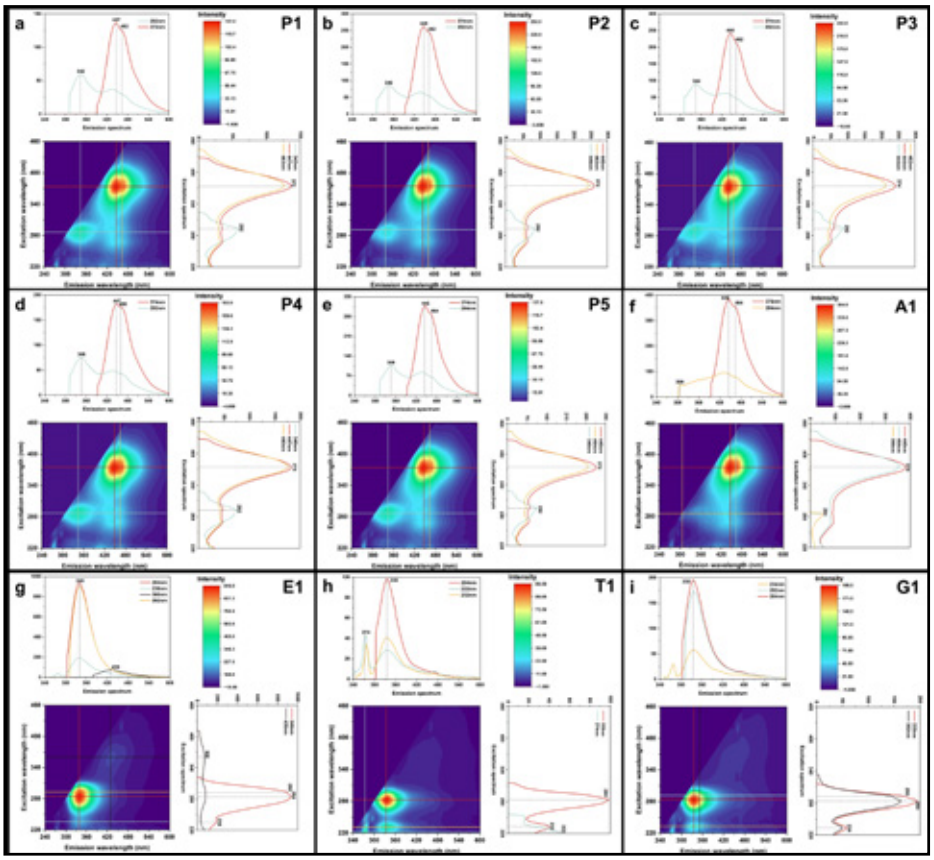

Fig.3 3D fluorescence spectra of (a-e) novel ceramic-nucleus cultured pearl samples P1-P5 and (f-i) reference samplesA1, E1, T1, G1.

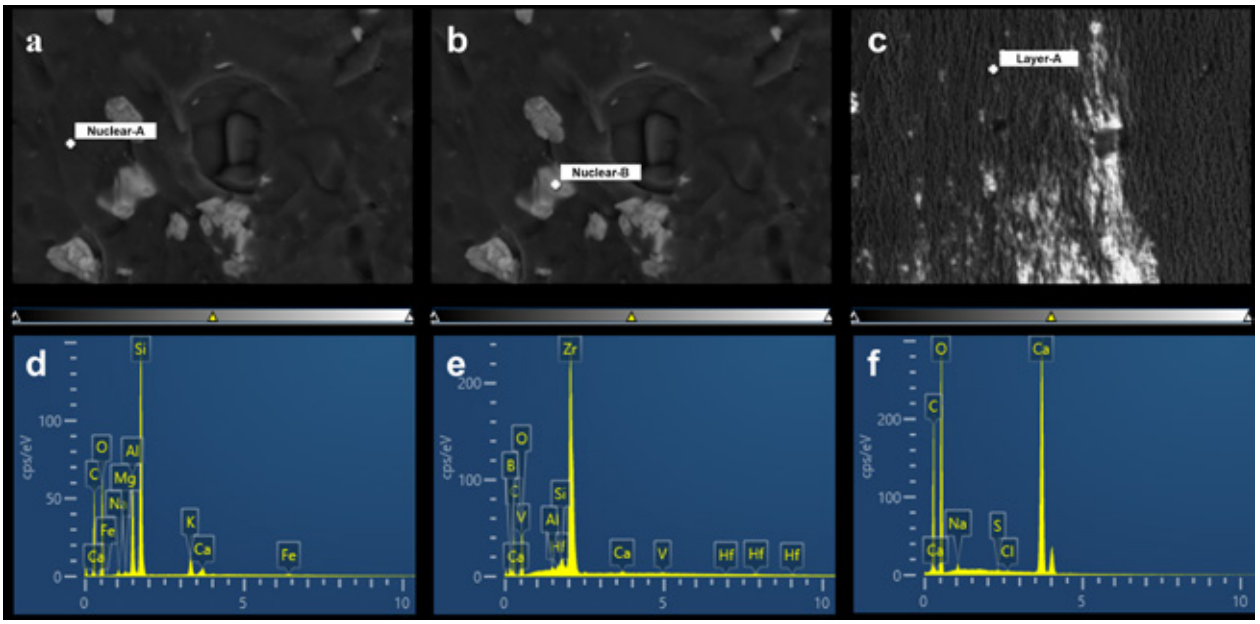

Fig. 4 (a-b) SEM images and (d-e) EDS spectrum of the bead of P1 at different positions; (c) SEM image and (f) EDS spectrum of the nacre layer of P1.

ceramic bead are consistent with those that produce Akoya pearls. Combing with the result of EDXRF which proves the cultivated environment of are sea water, we have confirmed that the mother oysters used for cultivating cultured pearls with ceramic beads are the same as those used for akoya cultured pearls (*Pinctada martensii* oyster). Based on our study, a key feature to differentiate cultured pearls with such a ceramic bead from traditional akoya cultured pearls using a bead from a shell (usually freshwater mollusc) can be found in the EDXRF testing. Our pearl samples with ceramic bead revealed strong and characteristic peaks of Zr due to the fact that their nacre layer was very thin and Zr (as a heavy element) from the bead material was easily detectable even through the nacre. This was confirmed by energy dispersive spectroscopy analyses of both, the nacre layer of the cultured pearl and the ceramic nucleus after cutting such a pearl into two halves (Fig.4). These analyses clearly confirmed that the abnormal Zr concentrations detected in EDXRF testing originated from the ceramic bead.

To further investigate the reasons for the stronger luster of cultured pearls with a ceramic bead, SEM analysis was conducted on the surface, and cross-section of the nacre layer [F. Fu *et al.*, 2014] (Fig.5). Obviously, the hexagonal aragonite platelets on the surface of our samples with ceramic beads (P1 and P3) exhibits a regular, relatively flat morphology, characterized by regular shapes and fewer cracks. But the interlayer of A1 possesses a lot of peeled aragonite debris, which increases surface diffuse reflection and easily reduces its luster (Fig.5d-i). From the perspectives of surface roughness, the strong bonding mechanism between the nacre layer and the ceramic nucleus was additionally analyzed: The uneven boundary between the layer and the nuclear indicates that the surface roughness of the ceramic bead is higher than that of the shell bead used in traditional Akoya-type pearl cultivation. (Fig.5a-c). Based on SEM analyses, we assume that the strong luster of the new cultured pearls originates from the use of ceramic nuclei, which facilitates the tight bonding of nacre layer and nuclei as well as the uniform growth and distribution of nacre layers. Additionally, the thinner nacre layer with an average thickness of 0.37 µm of these new cultured pearls with ceramic beads might be considered an advantage due to shorter cultivation time and lower production costs, although they might

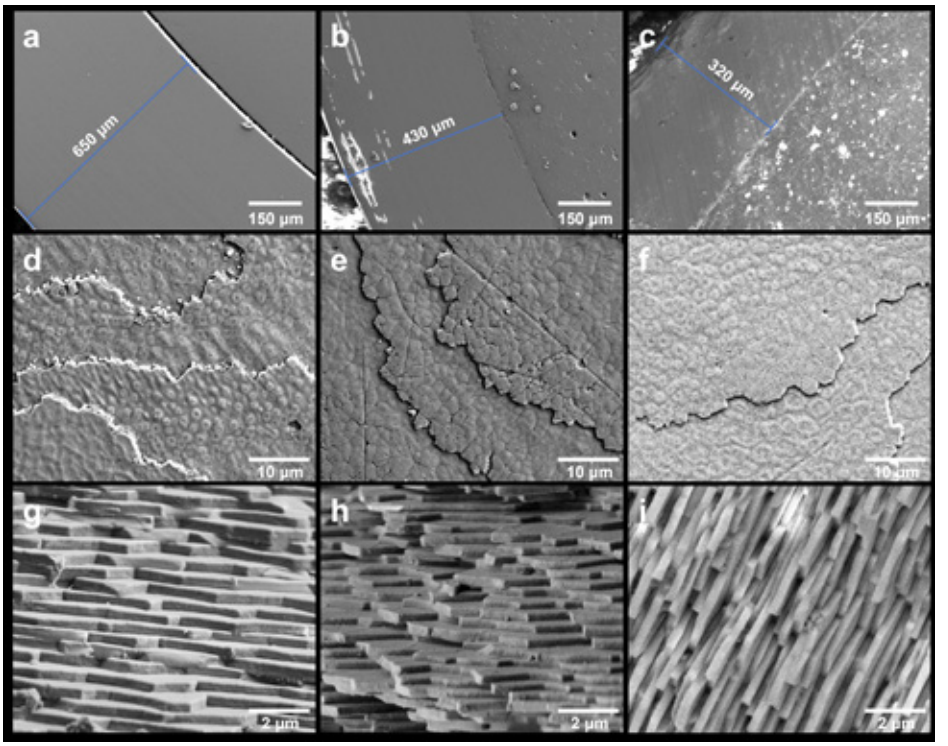

Fig.5 (a-c) SEM images of the nacre layer thickness of A1, P3 and P1, (d-f) SEM images of the surface structure of A1, P3 and P1 nacre layers, (g-i) SEM images of the cross-section of A1, P3 and P1's nacre layer.

be damaged easier than that of common cultured pearls. In summary, cultivating pearls with a ceramic nucleus may be an effective method for enhancing pearl luster, providing interesting ideas for pearl cultivation.

References:

- Shi, L., Wang, Y., Liu, X., & Mao, J. 2018. Component Analysis and Identification of Black Tahitian Cultured Pearls From the Oyster Pinctada margaritifera Using Spectroscopic Techniques. Journal of Applied Spectroscopy, 85(1), 98-102.
- Li, Y. J., Chen, C. Y. F., & Li, L. P. 2023. Spectroscopy Study of γ-Ray Irradiated Gray Akoya Pearls. Spectroscopy and Spectral Analysis, 43(4), 1056-1062.
- Li, Y. J., & Li, L. P. 2023. Application of Three-Dimensional Fluorescence Spectroscopy in Pearl Detection: A Case Study of Gray Akoya Pearl. Journal of Gems & Gemmology, 25(05), 46-53.
- Wang, Z., Cao, J., & Meng, F. 2015. Interactions between protein-like and humic-like components in dissolved organic matter revealed by fluorescence quenching. Water Research, 68, 404-413.
- Fu, F., G., T. L., G., X. X., S., X., & and Hu, X. B. 2014. Influence of microstructure on optical behaviour of freshwater cultured pearls. Materials Research Innovations, 18(4), 245-250.

Acknowledgement

This work was supported by "CUG scholar" Scientific Research Funds at China University of Geosciences, Wuhan (No. CUG2022185), China Arts and Crafts Society 2024 Arts and Crafts Research Project, Case Study on the Development and Brand Building of Tianjin Silk Craft Industry (No. CNACS2024-I-3).

Modern Cultivation of Freshwater Pearls in China: Advances in Materials, Technique

Niels Ruddy Hansen[1*]
Espedammen 9, 2605 Brøndby, Denmark
* nrh@ruddyhansen.dk

Keywords Cultured freshwater pearls; China; Hyriopsis cumingii

This presentation explores the modern advancements in freshwater pearl cultivation in China, focusing on the materials, techniques, and market orientation driving the industry. The process centers around the mussel Hyriopsis cumingii, which is utilised with two primary techniques: non-nucleated tissue-grafting for culturing smaller pearls, and bead implantation for culturing larger, spherical pearls. The development of fireball and baroque shapes, alongside the rise of Edison pearls—large, naturally colored pearls with exceptional luster—marks significant milestones in aquaculture technology. China, as the dominant global producer, has shifted towards higher-quality pearl production, with the help of integrating advanced sorting technologies and AI-assisted grading systems. The evolving market demand for superior quality pearls has led to innovations in breeding and environmental management, establishing China as a leader in the freshwater pearl industry.

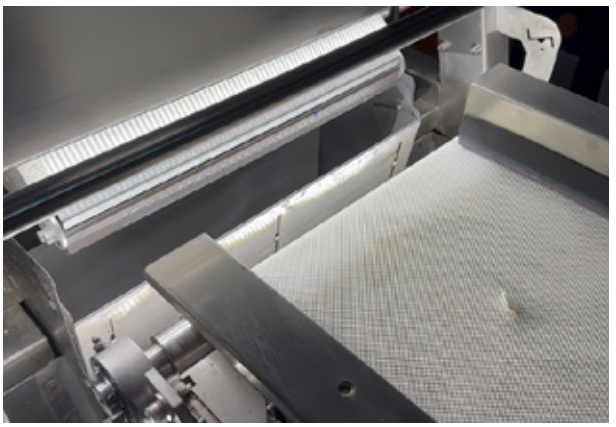

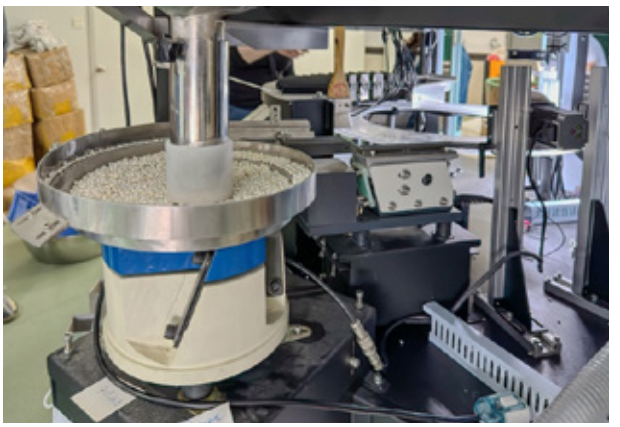

Amber and its treatments: A New Baltic Amber Classification Chart

Alessandra Costanzo[1], Agnieszka Klikowicz-Kosior[2], Michal Kosior[2]

[1] Earth and Ocean Sciences, School of Natural Sciences, University of Galway, Ireland; alessandra.costanzo@universityofgalway.ie

[2] Amber Experts Laboratory, Reduta Wyskok 4, Gdansk, Poland; mk@amberexperts.com; akk@amberexperts.com

Keywords: Baltic amber, treatments, enhancement

This paper aims to present the history of the modification of Baltic amber (succinite), and particularly the modern methods of its enhancement, along with a discussion of their objectives and characteristics. A new Baltic amber classification chart has been developed (Fig.1) and illustrates the variety of amber species found in nature as well as the vast array of enhanced varieties. In addition to aiding in the comprehension of amber modification, the classification aims to organize the body of knowledge on amber essential to gemmologists and to those working with amber as there has been in the past several incorrect attempts of describing and defining Baltic amber. This is the first time this type of classification is made for Baltic amber which is developed following the global standards of CIBJO and LMHC (CIBJO, 2022, LMHC, 2011) and also drawn by years of experience in identifying amber. This new classification does now include information on each treatment including treatment outcomes in terms of colours and durability as well as other information such as the type of inclusions produced, fluorescence, depth of treatment and indications on how to recognise it.

Amber is a fossilised resin from ancient trees (coniferous and deciduous), which underwent the process of fossilisation in various epochs and depositional environments. Baltic amber is derived from coniferous trees of Eocene age from several secondary deposits in Central and Eastern Europe (e.g. Baltic and North Sea coast, Poland, Russia - Kaliningrad region, Western Ukraine, Germany - Saxony). In addition to Baltic amber, we find fossilised resins on the jewellery market from other parent trees, other locations and other epochs such as Myanmar amber, Dominican amber, Mexican amber, Fushun amber (China). All of the above would have different characteristics from Baltic amber but most importantly mainly natural material from these areas is available in the market. Treatments to improve colour (e.g., dyeing), transparency (e.g., clarification), durability (e.g., durability enhancement) and done also to respond to market demand (e.g., ageing) are only recorded in Baltic amber. The treatments can be applied individually, combined, or sequentially to achieve the desired effect (e.g. clarification, decrepitation and heating in the presence of oxygen will result in an orange amber piece with sun spangles which is always in high demand in the Western countries and synonym of Amber in this part of the world. Depending on the selected treatment only the surface or the whole body of the stone might be affected. For example, hydrothermal treatment can fully change the stone throughout. Ageing instead is a natural process that can be reproduced in a laboratory environment and consists of superficial oxidation at low temperature of natural amber due to light and oxygen exposure. The various treatments aim to change the appearance and enhance the durability of natural Baltic amber while preserving its natural origin.

The composition and colour of amber (full body colour or superficial colouration only) and its transparency are determined by many factors, such as the origin of amber, the sediments in which the amber has been deposited, the local climate and the ground temperature. Baltic amber, also known as "Baltic gold", is available in colours from white, through various shades of yellow, orange, red up to darker shades of brown, and almost black. Yellow and orange amber (honey amber - Chinese trade name; cognac amber - Western trade name) is commonly seen and sold on the market and comes in a variety of hues. Sporadically, amber with a "cherry" colour can be also found, however its appearance is the effect of the oxidized top layer which can disappear after the amber is preformed and polished.

The practice of enhancing gemstones has its origins in ancient Egypt. The oldest record of improving colour and transparency of gemstones is dated back over 3,300 years (Nassau, 1984). Amber was also treated in ancient Rome not only to modify its colour to a darker tone and consequently to improve its clarity, but also to resemble the rare Simetite, a 25-million-year-old Miocene resin amber from Sicily. For this purpose, slow cooking in fat of young goats was used and sometimes dye was added to reproduce different colours and emulate different gemstones (e.g. purple amethyst) (Ball, 1950). The techniques developed at that time, mainly involving heating under controlled conditions combined with dyeing, have been improved to the present day even if not drastically changed. Currently, heating is still used to modify, not only amber but also precious gemstones including rubies and sapphires. It is believed that the majority of all the "cognac", "green" and "cherry" nuggets of Baltic amber found today on the market were heated to improve their appearance and to reach a more pleasing colour.

The modern market of gemstones is governed by international regulations and classifications and to safeguard the authenticity of the products, after thoroughly description and testing the amber cannot be called natural if it has been heated. The term used in these cases is treated amber which describe a stone that has been modified by one of more processes to change its appearance and/or durability (CIBJO, 2022). It is also essential to differentiate natural amber from artificial material: the latter consists only of imitations as no synthetic amber is available on the market. Pressed amber obtained from pressing together amber pieces can also be found. At the right temperature (120-180°C) they become soft and sticky and can be compacted together by mechanical pressing into larger chunks without any additional components (e.g. adhesives) and using several techniques. Pressed amber may also be additionally treated to improve appearance. However, the value of pressed amber put it, in most cases, a lower price category than treated. Many specialists even refer to pressed amber pieces as amber imitations (CIBJO, 2022).

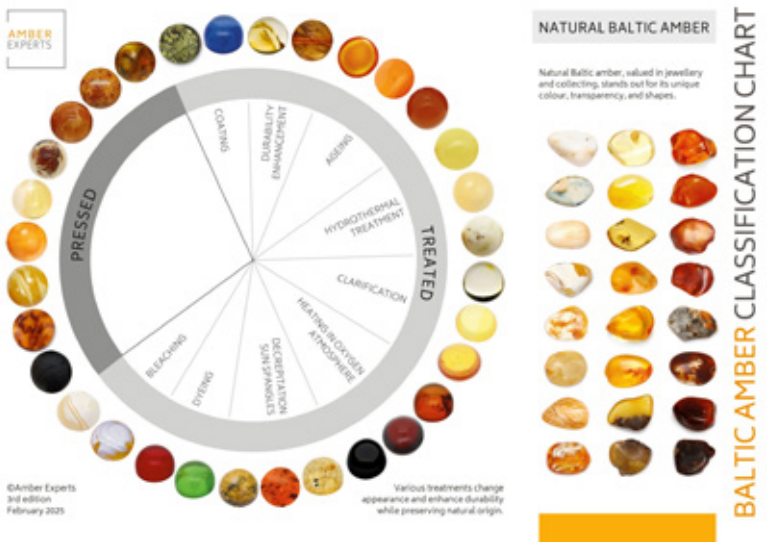

Figure 1: New Baltic amber classification chart showing the range of colours from natural (right chart) to the ones obtained with the various treatments (left wheel) and from the most common to the rarest colours available in the market.

References:

- Ball, S.H., 1950. A Roman Book on Precious Stones. Gemological Institute of America, Los Angeles.
- CIBJO Coloured Stone Commission, 2022. The Gemstone Book. The Blue Books. https://cibjo.org/rstoolkit/introduction-to-the-blue-books-2/.
- Laboratory Manual Harmonisation Committee. Standardised Gemmological Report Wording. LMHC Information Sheet # 10, Amber and Copal. Dec 2011.
- Nassau, K., 1984. The early history of gemstone treatments. Gems & Gemology, 20(1), 22-33.

Amber from the Thanbaya Gaing Coal Mine, Minbu Township, Magwe Region, Myanmar

Tin Nyunt Thet[1], Thye Sun Tay[2], Lwin Soe[3], Lock Cheyenne[4] et Hui Ying Loke[2]

[1] Director-General, Department of Geological Survey and Mineral Exploration, Ministry of Natural Resources and Environmental Conservation, Nay Pyi Daw, Myanmar. (thettinnyunt@gmail.com)

[2] Far East Gem Research Institute, Singapore. (tay@gem.com.sg)

[3] Freelance Geologist, Myanmar.

[4] Department of Chemistry, National University of Singapore, Singapore.

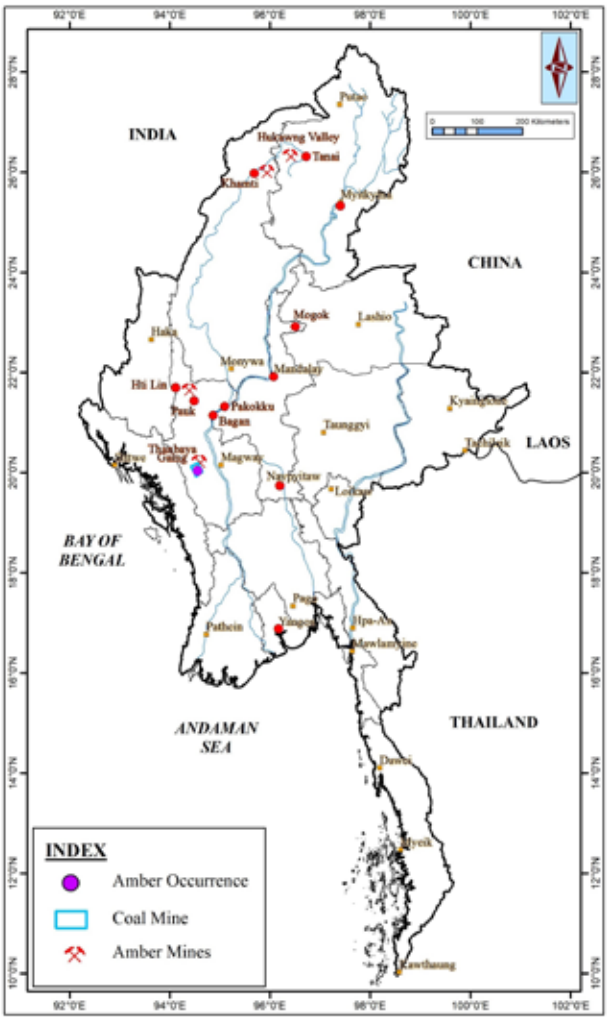

Figure 1: The location of the amber occurrences in Myanmar and the new occurrence of the amber at the coal field around the Thanbaya Gaing Coal mine, Magwe Region (Modified by Thet Tin Nyunt).

Amber was recently discovered by local coal miners at the Thanbaya Gaing Coal mine located 6.5 km northwest of Padaung village, and about 5 km west of Thanbaya Gaing village, Lat 20˚ 02' 54.8" Long 94˚ 33' 33.5" (Figure 1). The rock unit that is exposed in the study area is the Pondaung Formation (Late Eocene; Bender, 1983/Late Middle Eocene; Khin Zaw *et al*., 2014) which includes sandstone, sandy mudstone and shaly mudstone where the carbonaceous mudstone and the surrounding coal seams are exposed (Myint Myat Chan Aye, 2024). The amber occurs as a small band with 1 to 3 cm in thickness and 2 to 4 cm length and is also found as a lentoid and lenticular shape near the coal seams such as bituminous coal, brown coal and dull coal (Figure 2 a, b).

Materials and results

For the study of the samples, basic gemmological methods such as Gem-A refractometer, GIA binocular microscope, Mettler H800C for hydrostatic measurement, Mineralite Lamp Model UVSL-25 ultraviolet light, and JASCO FT/IR-4X were used.

The parcel of amber ranges in colour from yellow, yellowish-brown to very dark brown and almost all are black. Most of the samples are opaque and only a few are translucent useable for the observation of inclusions (Figure 3). The size of the samples ranges from 1 cm to 10 cm in length.

The gemmological properties of the amber are as follows: RI 1.54 to 1.55 and SG 1.01 to 1.04. Under magnification flow marks, gas bubbles, white minute specks of carbonate attached on the surface and some unidentified inclusions (probably organic debris) were found, but no insects were found (Figure 4 a to f).

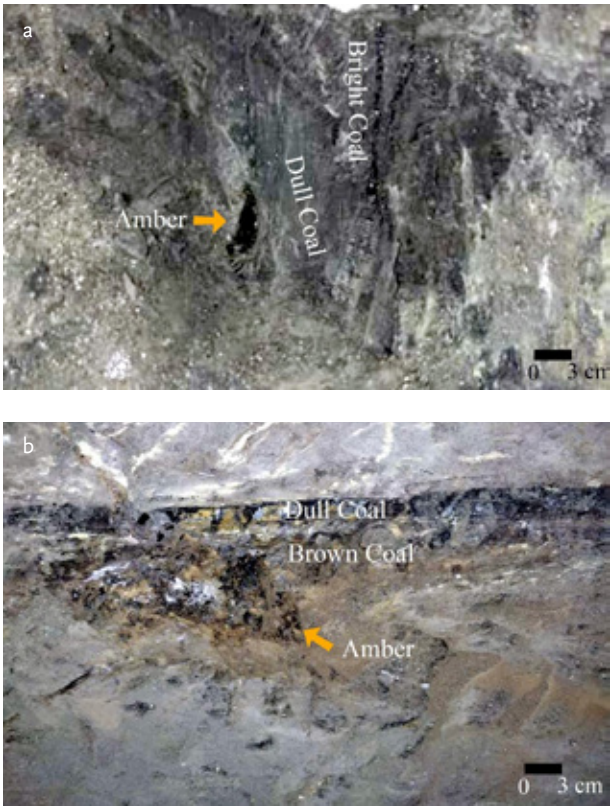

Figure 2 (a) Nature and occurrence of amber near the carbonaceous mudstone and the surrounding coal seams; (b) Lentoid and lenticular shaped amber near the coal seams (Photo by Soe Lwin).

Figure 3. Almost all the amber samples are black, other colours range from yellow to yellowish-brown and dark brown. The largest piece on the left weighs 28 grams (measure 6.5cm x 3.8cm) (Photo by Tay).

Under LWUV lighting, some of the sample fluoresce strong chalky blue in flow pattern with minute chalky blue droplets (Figure 5 a to d). Furthermore, when the long wave ultraviolet were switched off during the experiment, a dull greyish green appearance of the phosphorescence effect could be observed.

The FTIR analysis reveals spectral characteristics of amber, such as a broad O—H stretching peak at 3397 cm^{-1} and C—H stretching peaks at 2956 cm^{-1} and 2869 cm^{-1} (Garcia-Valles *et al*., 2023) (Figure 6). Other similar peaks with amber include C=O stretching at 1708 cm^{-1}, together with C—H bending at 1378 cm^{-1} and C—O stretching at 1042 cm^{-1} (Garcia-Valles *et al*., 2023), albeit minor shifts in wavenumber. Nearly all the samples have the presence of the C=C exocyclic methylene out of plane bending at 888 cm^{-1}, indicating unsaturated C=C structures. This shows that the Magwe amber had undergone the process of polymerization, i.e. maturation stages of amber from copal (Guiliano *et al*., 2007; Zheng *et al*., 2021). An interesting observation is that the presence of the peak at 2725 cm^{-1} is consistent in the Magwe amber samples, which is commonly identified as C—H stretch in aldehydes (Poinar & Mastalerz, 2000).

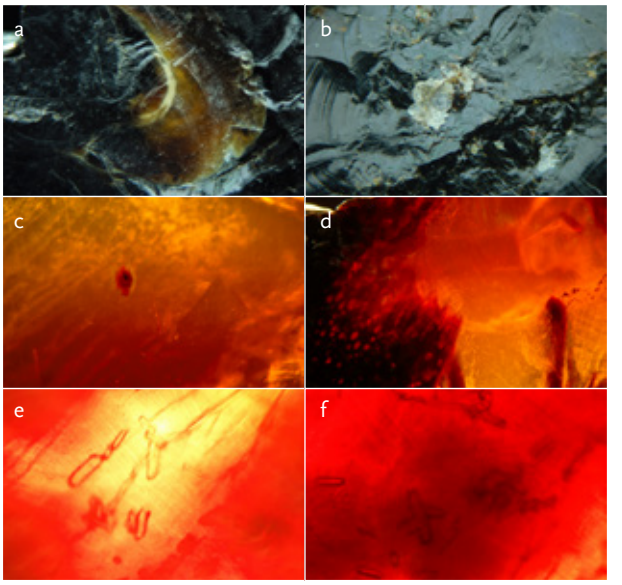

Figure 4. (a) Creamy white flow mark (10x); (b) white flaky carbonate mineral attached to the surface (10x); (c) minute organic debris (x40); (d) gas bubbles on the left side (20x) (Photomicrograph by Tay); (e-f) minute crystal inclusions in amber (x40) (Photomicrograph by Thet Tin Nyunt).

Conclusion

This study has highlighted that the dark brown ancient resin is amber, but the infrared spectroscopy showed the presence of C=C exocyclic methylene out of plane bending at 888 cm^{-1} indicates unsaturated C=C structure i.e. copal. The Magwe amber indicates a transitional process of polymerization into a purer form of amber. Unique observation of Magwe amber shows a strong bluish fluorescence in zoning and droplet, and on top of that, its phosphorescence in dull greyish-green when ultraviolet light was switched off. As this is the initial stage of study, more samples are needed to provide more data of Magwe amber.

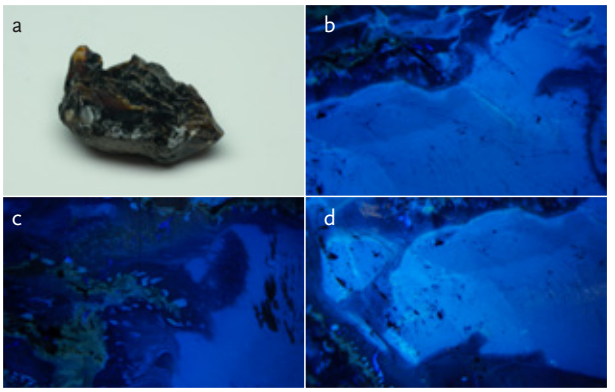

Figure 5. (a) Sample 14 showed opaque and dark yellowish-brown in colour amber (b) under LWUV, zoning fluorescence pattern; (c) bright chalky blue droplet and flow fluorescence; (d) patches of chalky blue fluorescence (10x) (Photo by Tay).

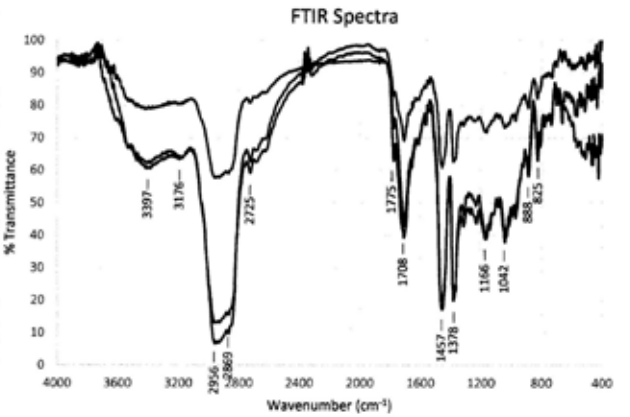

Figure 6. Representative infrared spectrum of amber from Thanbaya Gaing Coal mine, Magwe Region.

References:

- Bender, F. (1983). Geology of Burma, Borntraeger, Berlin, 293.
- Garcia-Valles, M., Di Mariano, A., Alfonso, P., Noguès, J., & Martinez, S. (2023). Differentiation between copal and amber by their structure and thermal behaviour. Journal of Thermal Analysis and Calorimetry, 148(23), 13027–13037. https://doi.org/10.1007/s10973-023-12333-8.
- Guiliano, M., Asia, L., Onoratini, G. & Mille, G. (2007). Applications of diamond crystal ATR FTIR spectroscopy to the characterization of ambers. Spectrochimica Acta Part A: Molecular and Biomolecular Spectroscopy, 67(5), 1407-1411, http:// de.doi. org/ 10. 1016/j.saa.2006.10.33.
- Khin Zaw, Meffre, S., Takai, M., Suzuki, H., Burrett, C., Thaung Hteik, Zin Maung Maung Thein, Tsubamoto, T., Egi, N., & Maung Maung, (2014). The oldest anthropoid primates in SE Asia: Evidence from LA-ICP-MS U-Pb zircon age in the Late Middle Eocene Pondaung Formation, Myanmar, Gondwana Research 26, 122-131.
- Myint Myat Chan Aye, (2024). Geological Exploration report of the Thanbaya Gaing Coal mine, Minbu Township, Magwe Region. Unpublished Exploration report, 59 p.
- Poinar, G. O., & Mastalerz, M. (2000). Taphonomy of fossilized resins: Determining the biostratinomy of amber. Acta Geologica Hispanica, 171–182.
- Tay, T. S., Kleismantas, A., Thet Tin Nyunt, Minrui, Z., Krishnaswamy, M & Loke, H. Y. (2015). Burmese amber from Hti Lin. The Journal of Gemmology, 34(7), 606-615.
- Thet Tin Nyunt, Tay, T.S., Loke, H. Y., Krishnaswamy, M., Cho Cho, Naing Bo Bo Kyaw, Wai Yang Lai Aung & Chutimun Chanmuang N. (2020). Amber from Khamti, Sagaing Region, Myanmar, The Journal of Gemmology, 37(3), 314-322.
- Zheng, T., Li, H., Lu, T., Chen, X., Li, B., & Liu, Y. (2021). Spectroscopic Identification of Amber Imitations: Different Pressure and Temperature Treatments of Copal Resins. Crystals, 11(10), Article 10. https://doi.org/10.3390/cryst11101223.

Acknowledgements

The co-author TTS like to thank Mr Murali Krishnaswamy, Dr Guanghai Shi, Dr Linda Sellou and Ms

A Photo Survey of Inclusions in Fossiliferous Amber

Nathan Renfro
GIA, Carlsbad California, USA, nrenfro@gia.edu

For many, fossiliferous tree resin, primarily amber, gained wide visibility to the public in 1993 where it was prominently featured in the movie, Jurassic Park. This was certainly where the author's awareness of such fossil bearing material was born. Amber provides a fossil record for a continuous 135 million years over 160 deposits (Penny, 2010). The most prominent localities for the amber examined by the author are the Dominican Republic, Burma and the Baltic region.

Many of the fossils examined for this study showcase a wide range of biodiversity including insect, arachnid, centipede and some plant and fungus examples. While these specimens may be scientifically relevant as a well-preserved record of the biodiversity that existed millions of years ago, it is the hope of the author that documenting the contents of fossil resins will continue to inspire the exploration of these materials in search of new secrets of the ancient world.

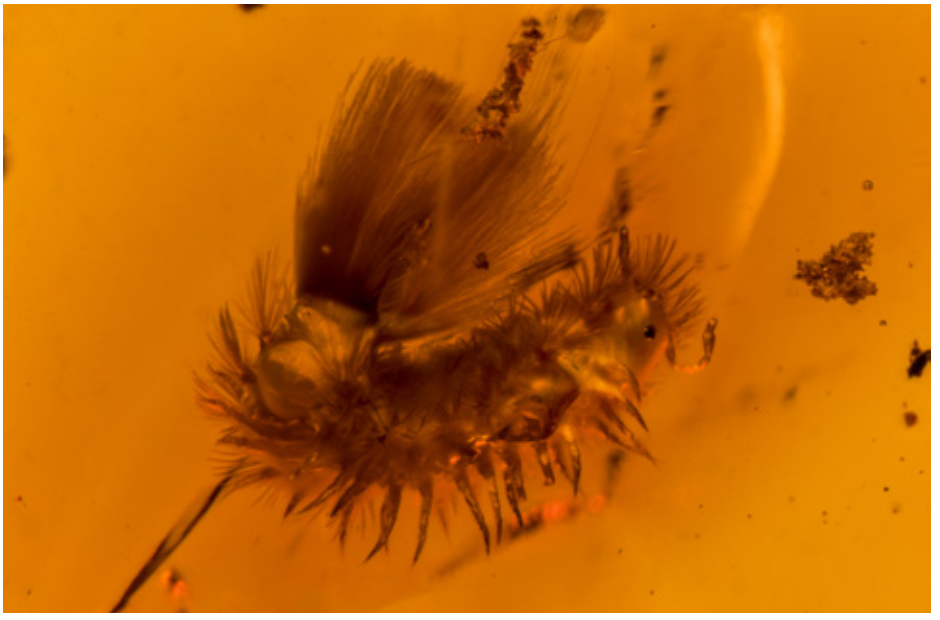

A polyxenoid millipede in fossil amber. Field of View 5.64mm

References:

• Penney, D, 2010. Biodiversity of Fossils in Amber from the Major World Deposits, Siri Scientific Press, Manchester, United Kingdom, 304pp

• The author would like to thank John Koivula for providing the majority of the fossiliferous resin samples examined in this study.

Fe-Ti charge transfers: A comprehensive review and its applications to minerals and gems

Maxence Vigier[1,2], Helen Evans[3], George R. Rossman[3], Stéphane Jobic[1], Emmanuel Fritsch*[1]

[1] Nantes Université, CNRS, Institut des Matériaux de Nantes Jean Rouxel, IMN, F-44000, Nantes, France.

[2] On leave from Nantes, Université, Institut des Matériaux de Nantes Jean Rouxel, currently at : Conditions Extrêmes et Matériaux: Haute Température et Irradiation (CEMHTI), UPR 3079 CNRS, 45100 Orléans, France.

[3] Division of Geological and Planetary Sciences, California Institute of Technology, Pasadena, California 91125-2500, U.S.A

emmanuel.fritsch@cnrs-imn.fr

The iron-titanium charge transfer (Fe-Ti CT) is mentioned in numerous articles as the source of the coloration of many natural minerals and some man-made materials, but no global review of this charge transfer phenomenon has been provided so far. Iron and titanium are ubiquitous in nature and are often found in the same material as Fe^{2+} and Fe^{3+}, and Ti^{4+} (Ti^{3+} is rare in nature, mostly the result of irradiation or extremely reducing conditions). When Fe and Ti ions are in close geometric proximity in an oxide or (alumino)silicate structure, charge transfer can occur between the two ions, even though their concentration might be below 100 ppm. The transfer occurs mostly between octahedral sites, sharing either an edge or a face, rarely a summit. This results in a variety of absorption features that contributes to the color of minerals.

Ascertaining a metal-metal charge transfer is often not straightforward. We compiled existing knowledge on Fe-Ti charge transfer in both crystalline and amorphous materials and identified several key characteristics in more than 40 different materials. A charge transfer is associated with broad, intense, optical absorption bands (Mattson & Rossman, 1987) with a decreasing intensity with high temperature (Evans & Rossman, 2024). It is also strongly pleochroic in non-isotropic materials (Mattson & Rossman, 1987). Until now, Fe-Ti charge transfers have been primarily described in the 2.25 to 3.1 eV range, corresponding to yellow to orange to brown colors, with notable exceptions such as blue sapphire or kyanite, and green andalusite.

This review suggests that Fe-Ti charge transfer can occur across the entire visible spectrum. More importantly, our major finding is that the position of the absorption band correlates with the estimated Fe-Ti interatomic distance (Figure 1). There is a fair dispersion of the data, as the Fe-Ti distance is exact only in Fe-Ti minerals. When both Fe and Ti are traces it may be the Al-Al distance before substitution, so relaxation after substitution is not taken into account. Yet, although this correlation is not a proof of the origin of color, it brings a robust argument to identify Fe-Ti charge transfer.

After discovering this correlation, we wondered if other minerals beyond sapphire could offer several Fe-Ti distances. Indeed, the existence of multiple crystallographic sites for both Fe and Ti in many oxides leads to multiple Fe-Ti CT bands within these materials, as illustrated in figure 2. In particular not two but four possible Fe-Ti CT bands have been identified in blue sapphire, and three in dumortierite, ilmenite and pseudobrookite. For dumortierite, this result implies that both pink and blue dumortierite may be colored by Fe-Ti CT. The rose fibers coloring rose quartz are not taken into account, as they represent a superstructure, with potentially different Fe-Ti distances.

The present compilation is a further step to confirm that Fe-Ti CT is the cause of color in some minerals. For example, for the brown color in beryl, the proposition of Fe-Ti CT seems reasonable. The Al-Si distance is 3.321 Å for a summit-sharing octahedral Ti^{4+} with a tetrahedral Fe^{2+}, which corresponds to an absorption at about 3 eV, just at the beginning of the visible range; This can generate - with an adequate width - the strongly pleochroic continuum observed.

On the other hand, the blue color of benitoite - $BaTiSi_3O_9$ - has long been attributed to Fe-Ti or Fe-Fe charge transfer based on the presence of titanium in its structure, with iron as impurity. Given the observed broad band position at about 1.77 eV, the estimated Fe-Ti distance (3.30 Å) is not close to the correlation line to support a Fe-Ti charge transfer mechanism. In addition, the pleochroism is not strongest when E is parallel to the Ba-Ti direction (the supposed Fe-Ti direction after substitution), but perpendicular to it. So the jury is still out on benitoite blue color.

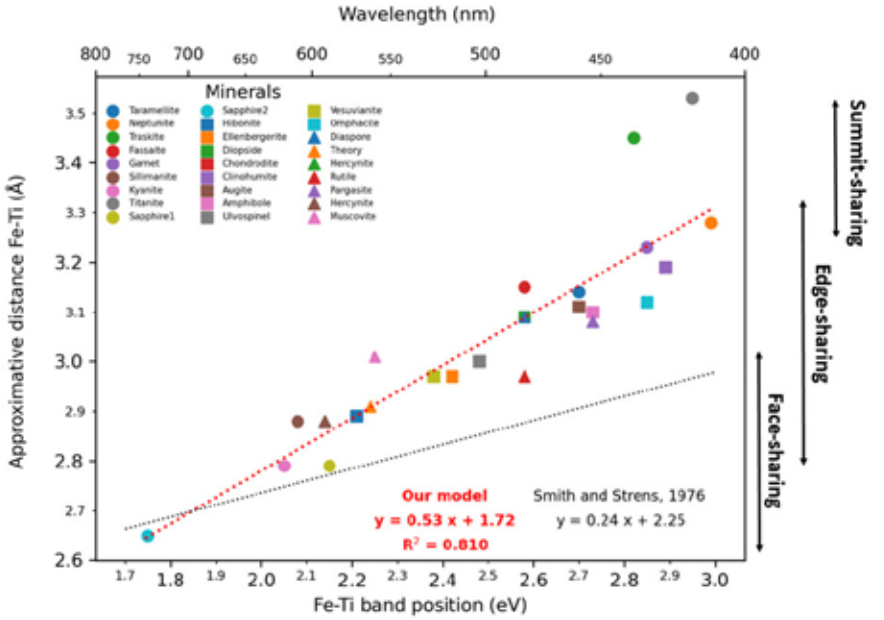

Figure 1: Correlation trend of Fe-Ti CT band positions (position of the center of the band in eV) with the estimated internuclear Fe-Ti distance in angstrom (red dotted line) for 26 different materials. Most of the distances are extrapolated from crystallographic data, and calculated between the two substituted atoms. Note the difference in slope with the proposition by Smith & Strens (1976; black dotted line)."Theory" refers to calculations on $(FeTiO_{10})^{-14}$ cluster. Sapphire 1 is related to edge-sharing, and sapphire 2, face-sharing octahedra in sapphire. Figure based on the data from 20 articles, not cited here for the sake of brevity.

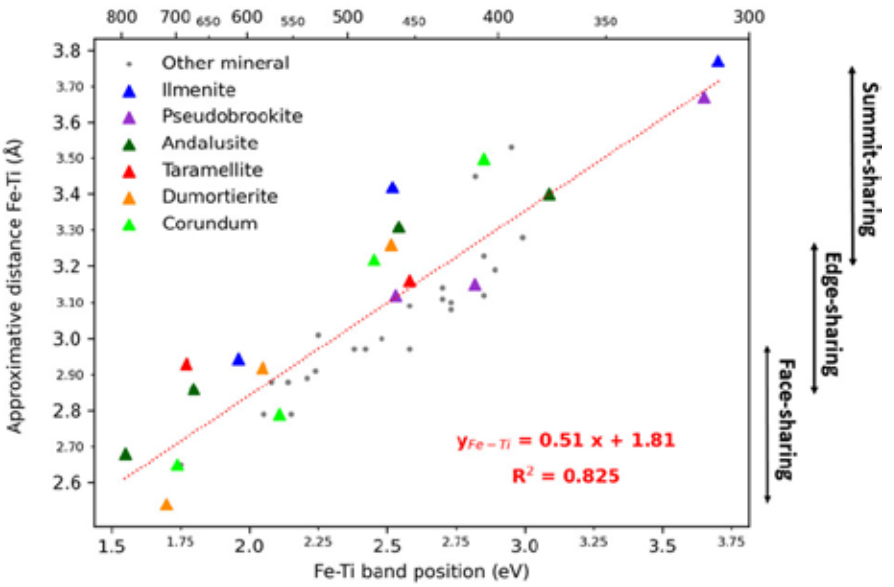

Figure 2: Correlation of Fe-Ti charge transfer band position in energy vs. the estimated internuclear distance in angstrom highlighted in six minerals presenting different Fe-Ti distances in their structure. 'Other minerals' refers to data presented in Figure 1. The linear plot has been calculated both on the data presented in figure 1 and with additional data from the six multi-bands minerals, leading to a slightly different equation.

References:

- Evans, H.V., and Rossman, G.R. (2024) Intervalence charge transfer in aluminum oxide and aluminosilicate minerals at elevated temperatures. American Mineralogist, 109, 2152–2161.
- Mattson, S. M. and Rossman, G. R. (1987) Identifying characteristics of charge transfer transitions in minerals. Physics and Chemistry of Minerals, 14, 94–99.
- Smith G, Strens R.G.J (1976) Intervalence transfer absorption in some silicate, oxide and phosphate minerals. In: Strens R.G.J (ed) The Physics and Chemistry of Minerals and Rocks, Wiley and Sons, London New York, pp 583–612.

Recent Progress on the Formation Mechanism of Copper Nanoparticle in Oregon Sunstone

Chengsi Wang, Andy H. Shen
Gemmology Institute, China University of Geosciences, Wuhan, Hubei, China
wangcs@cug.edu.cn; chance_w@foxmail.com

As a high-value gem mineral with unique optical properties, Oregon Sunstone has garnered attention in mineralogical and geochemical research. In our previous studies, we confirmed that its diverse coloration and optical properties arise from copper nanoparticles (NPs) of varying geometries, which induce by localized surface plasmon resonance. In the isotropic (red) zones, NPs manifest as randomly distributed nano-spheres, while in dichroic (green/red) zones, they appear as directionally aligned nano-rods (Wang *et al*. 2025). However, the formation mechanisms of these nanoparticles and the factors controlling their geometries remain unresolved. Resolving these questions will advance efforts to locate, synthesize and identify these gem crystals.

Comparative stability of nanoparticles with different geometries

Both previous studies and our experimental findings demonstrate significant differences in the thermal stability between spherical and rod-shaped nanoparticles. Hofmeister and Rossman (1985) observed that the green color zones in feldspar disappeared after heat treatment at 850°C, whereas the red zones required heating to 900°C for color re-absorption. Our results align with this trend, though the green reabsorption temperature was lowered to 800°C.

Similar instability is observed at the nanoscale: copper nanoparticles exhibit poor electron beam tolerance, rapidly decomposing and undergoing amorphization at visually observable rates during transmission electron microscopy (TEM) observations. Notably, spherical nanoparticles retain metallic Cu^0 even after their geometry and crystal structure are disrupted. In contrast, rod-shaped nanoparticles decompose faster under electron irradiation, and the valence state of Cu in rods increases due to progressive oxidation during decomposition (Figure 1). Both macroscopic and microscopic observations confirm that spherical nanoparticles exhibit superior stability compared to their rod-shaped counterparts.

Color transition by thermal treatment

During thermal treatment of sunstone samples, we serendipitously observed that anisotropic green samples transitioned to isotropic red at 750°C. Intriguingly, this transition could not be achieved when the temperature was lowered or raised. Below 750°C, no color change occurred; while above 750°C, the color completely disappeared (Figure 2). From a phase transition perspective, if rod-shaped and spherical nanoparticles represent distinct mineral phases, their phase transition temperature would be 750°C. However, attempts to reverse the process (converting red to green) proved unsuccessful despite extensive experiments involving multiple thermal pathways: varying temperatures and durations; direct heating at/around the transition temperature; and high-temperature "activation" followed by low-temperature annealing. These efforts either fully dissolved the nanoparticles or re-formed spherical nanoparticles.

This suggests that the interconversion between rod-shaped and spherical nanoparticles is not governed by a simple phase transition mechanism.

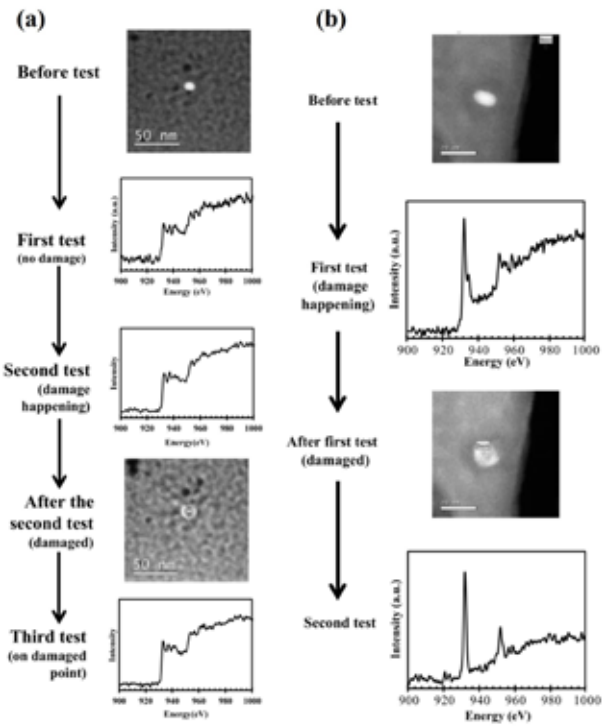

Figure 1. Electron beam damage of NPs during the collection of EELS spectra. (a) In the red zone, the NP was damaged after second test and the valence state of Cu reminded 0.
(b) In green zone, the NP resulted in a valence state about ~1.5 and was significantly damaged thereafter. After the second test, the valence state of the NP turned increased to ~2.

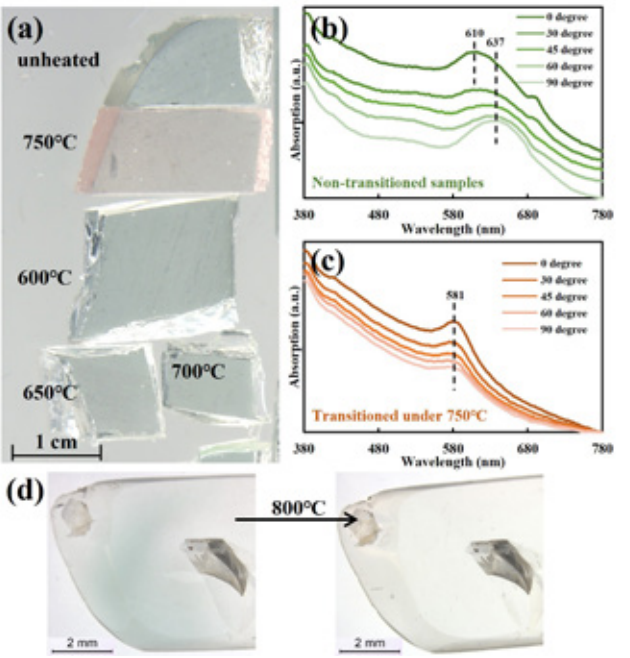

Figure 2. Color transition by thermal treatment.
(a) (d) Photographs for samples which has been heated under different temperatures. (b) Polarized UV-Vis spectra of sample before color transition. (c) Polarized UV-Vis spectra of sample after color transition.

Theoretical model for shape transformation of Cu nanoparticles

Inspired by the shape-control principles in nanomaterial synthesis (Xia *et al*. 2015), a model for shape transformation mechanism was proposed to explain the unidirectional rod-to-sphere transformation and its irreversibility. The most stable geometry corresponds to the global minimum free energy state, typically achieved under thermodynamic dominance. While, local minimum states form when kinetic factors control the pathway. In our system, spherical nanoparticles, represent the global minimum state, while rod-shaped nanoparticles correspond to a local minimum state (Figure 3). Heating rod-shaped NPs to 750°C enables them to overcome the energy barrier between these states, transitioning to the spherical global minimum via thermodynamic driving forces. Conversely, reversing this process (sphere → rod) fails may because rod formation requires the involvement of kinetic factor(s) (e.g., directional structural constraints), which cannot be replicated through thermal activation alone.

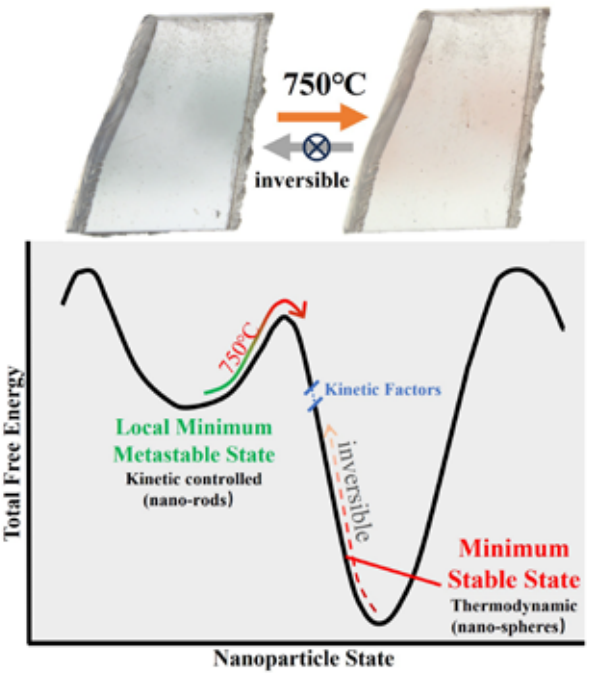

Figure 3. Theoretical model for shape transformation.

References:

- Hofmeister, A.M., and Rossman, G.R. (1985) Exsolution of metallic copper from Lake County labradorite. Geology, 13, 644–647.
- Wang, C., Heaney, P.J., Palke, A., Wang, K., Wang, H., Kiefert, L., and Shen, A.H. (2025) Nanoparticle geometry as the key to bicolor behavior in Oregon sunstones —— an application of LSPR theory in nanomineralogy. American Mineralogist, 110, 293–305.
- Xia, Y., Xia, X., and Peng, H.C. (2015) Shape-Controlled Synthesis of Colloidal Metal Nanocrystals: Thermodynamic versus Kinetic Products. Journal of the American Chemical Society, 137, 7947–7966.

Application of Fibre Optics Reflectance Spectroscopy (FORS) for the determination of mineral pigments in jasper

Ulrich Henn
German Gemmological Association, Idar-Oberstein, Germany
ulihenn@dgemg.com

The identification of pigments is carried out routinely mostly by X-ray diffraction, FTIR and Raman spectroscopy as well as visible absorption. An optical method which frequently is used in archaeology and art history has the advantages of quick, non-destructive and portable testing: Fibre Optics Reflectance Spectroscopy (FORS). Its wide application spectrum includes the determination of inorganic and organic pigments in e.g. antique ceramics, glass and paintings (Picollo *et al*., 2000; Cosentino, 2014). Gemmological application of FORS covers investigations of opaque gem materials i.e. the determination of colour causes, the proof of colour modifications and the detection of imitations.

Micro-crystalline quartz and especially the colourful group of jaspers offer a broad spectrum of applications in determination of colour causes by mineral pigments.

As an example, jaspers from the region of Idar-Oberstein, Germany were investigated by using an Ocean Optics FORS system (Figure 1), which consists of a halogen light source (1) and an Ocean Insight Flame Miniature Spectrometer (190-1100 nm) (2), both connected with a UV-visible bifurcated optical fibre (3) at the end of which the reflection probe (4) is coupled. This consists of six illumination fibres around one read fibre which is held over the smooth surface of the sample (5) in a distance of approx. 1 cm.

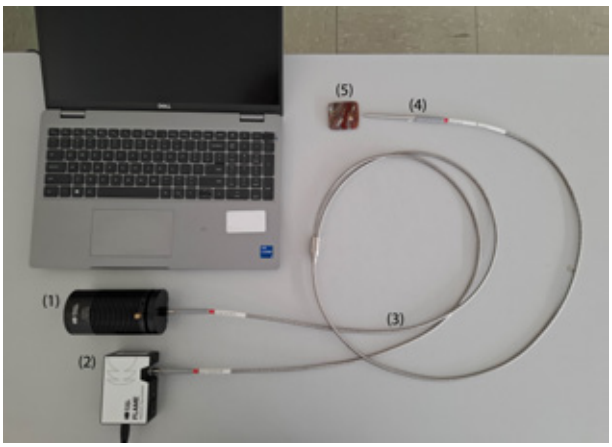

Figure 1. Fibre Optics Reflectance Spectroscopy (FORS). Ocean Optics system, described in the text.

The investigated samples originate from jasper veins in Permian intermediate volcanic rocks of the Saar-Nahe region and cover red, yellow, brown and green colours. Generally, colours of jaspers are caused by mineral impurities (Kostov, 2010). Red, yellow and brown colours are due to iron oxides or hydroxides, green to phyllosilicates.
Three representative types of Permian jasper from the Saar-Nahe region have been selected to demonstrate the results of FORS measurements. Indications of the respective pigments were additionally confirmed by Raman spectroscopy and chemical investigations.

Red and yellow jasper

Red and yellow jasper (Figure 2a) is frequently found in the Permian volcanic rocks of the Saar-Nahe region and a historically significant mining place is the Steinkaulenberg in Idar-Oberstein. There red and yellow jasper is found together with agate and moss agate in veins of an andesite. Generally, such material is known as jasp-agate (Campos-Venuti, 2012).

The reflection spectrum of the red jasper (Figure 2b) is characterized by a broad absorption in the range 550 nm to shorter wavelengths followed by a gradient between 550 and 600 nm with an inflection point at 580 nm. A second broad absorption band in the near infrared has a maximum at 850 nm. Between the two absorptions there is a broad reflection region with maximum at 740 nm which is responsible for the red colour.

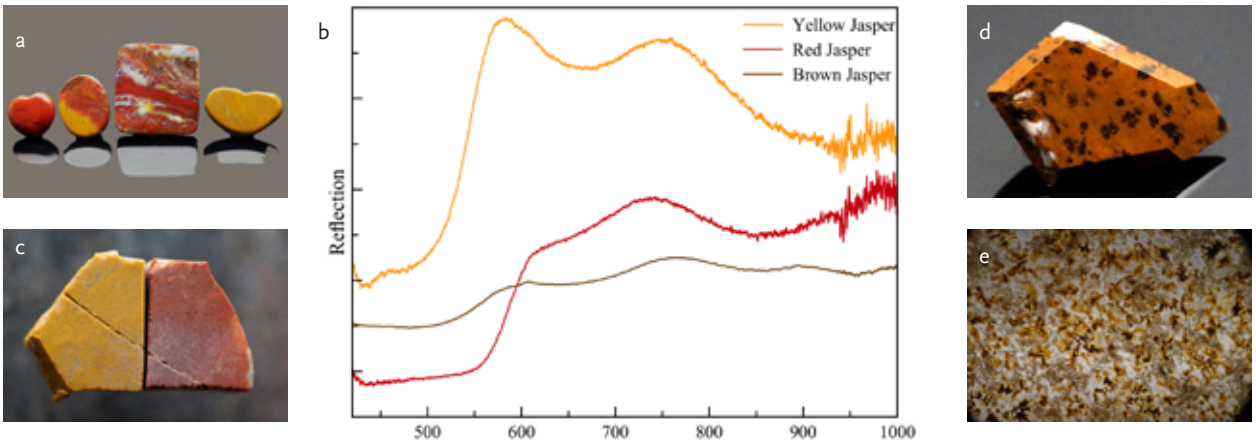

a. Red and yellow jasper from the Steinkaulenberg in Idar-Oberstein. Size of the large jasp-agate 47 x 42 mm.
b. Reflectance spectra of red, yellow and brown jasper.
c. Iron-rich jasper before (left) and after heating (right).
d. Dark spotted brown Panthera-jasper from Baumholder. Size 30 x 20 mm.
e. Thin section of Panthera-jasper. Size of the brownish-yellow, grey-brown and brownish-black pigments 0.1 – 0.5 mm.

In the reflection spectrum of the yellow jasper (Figure 2b) the main absorption lies in the range 500 nm to shorter wavelengths with a maximum at 430 nm. The inflection point of the following gradient is at 540 nm. Two more absorption bands have maxima at 660 and 950 nm. The reflection maximum is located at 575 nm in the yellow spectral range.

The spectral characteristics of the red and yellow jasper arise from crystal field transitions of Fe^{3+} and can be clearly attributed to hematite (red ochre) in the red material and goethite (yellow ochre) in the yellow one (Torrent & Barrón, 2002; Elias *et al*., 2006).

Heating the yellow jasper at 230°C causes a colour modification to red (Figure 2c), effected by a dehydration process which causes the transformation of the iron hydroxide goethite to the iron oxide hematite: $2\ FeO(OH) + Fe_2O_3 + H_2O$.

Brown jasper

A particular dark spotted brown jasper (Figure 2d) occurs near Baumholder, approximately 10 km south of Idar-Oberstein. The material is called Panthera jasper and is associated with baryte deposits. Even under magnification, various pigments could be observed, including brownish-yellow, grey-brown and brownish-black partly flake-like impurities (Figure 2e) in the fine-grained SiO_2 matrix.

The reflection spectrum (Figure 2b) is mostly characterized by the spectral features of goethite and differs mainly in the lower reflectance intensity. The curve is flatter in the 500 to 600 nm range and the subsequent edge shifts to longer wavelengths. An additional absorption band with a maximum at 850 nm can be assigned to hematite which suggests the presence of limonite as a goethite dominated mixture of iron hydroxides and oxides.

The brown colour impression is finally caused by these brownish-yellow pigments in combination with the grey-brown and brownish-black pigments composed of manganese oxides (probably hollandite and romanechite).

Similar to the yellow jasper from the Steinkaulenberg a colour modification from brown to red is produced by heat treatment which underlines the dominance of goethite as the main pigment.

Green jasper

A rarely found variety is the green jasper (Figure 3a) from a locality near Oberkirchen, aproxiamately 20 km south of Idar-Oberstein. These are also heterogeneously composed veins with jasper, moss agate and agate as well as zeolites and alteration products, e.g. phyllosilicates.

The reflection spectrum of the green jasper (Figure 3b) is characterized by a broad reflection band with maximum at 550 nm in the green spectral range and a second reflection peak at 830 nm. In between lies an absorption band with a maximum at 750 nm.

These features are typical for the green phyllosilicate celadonite (green earth) $K(Mg,Fe^{2+})(Fe^{3+},Al)Si_4O_{10}(OH)_2$ (Radpour *et al*., 2019). The 750 nm absorption band is caused by a Fe^{2+}-Fe^{3+} electron transition (Platonov *et al*., 2009) and the absorption band visible just before 1000 nm (approx. 980nm) is probably due to isolated Fe^{2+}.

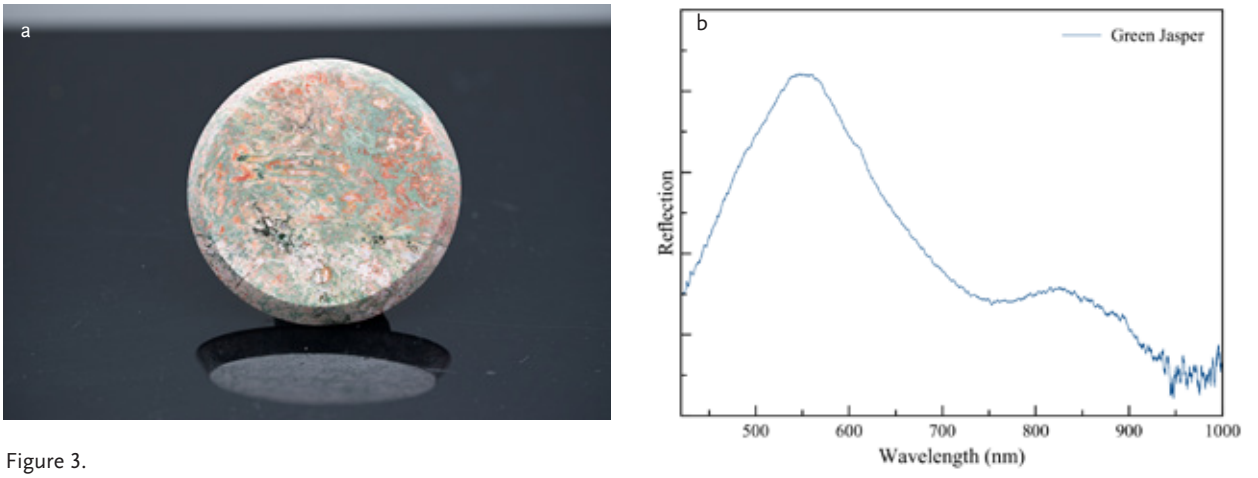

Figure 3.
a. Jasp-agate plate with green jasper from Pfeffelbach. Diameter 7 cm.
b. Reflectance spectrum of green jasper.

References:

- Campos-Venuti, M., 2012. Genesis and classification of agates and jaspers: a new theory.- Tipografia Luciani, Rome.
- Cosentino, A., 2014. FORS Spectral Database of Historical Pigments in Different Binders. Conservation Journal Issue 2, Autumn 2014.
- Elias, M., Chartier, C., Prévot, G., Garay, H., Vignaud, C. 2006. The colour of ochres explained by their composition. Materials Science and Engineering B 127, 70-80.
- Kostov, R.. I., 2010. Review of the mineralogical systematics of jasper and related rocks. Archeometriai Müheliy 3, 209-213.
- Picollo, M., Bacci, M., Casini, A., Lotti, F., Porcinai, S., Radicati, B., Stefani, L., 2000. In: Martellucci, *et al.* (Eds.), Fiber Optics Reflectance Spectroscopy, a Non-destructive Technique for the Analysis of Works of Art, Optical Sensors and Microsystems: New Concept, Materials, Technologies. Kluwer Academic/Plenum Publishers, New York, pp. 259-265.
- Platonov, A. N., Khomenko, V. M., Shuriga, T. N., (2009): Optical Absorption spectra and Fe distribution in the structures of Li-Fe-micas. Geochemistry International 47, 174-185.
- Radpour, R., Fischer, C., Kakoulli, I., 2019. New insight into Hellenistic and Roman Cypriot Wall Paintings: An exploration of artist´s materials, production technology, and technical style. Arts 8, 74.
- Torrent, J., Barrón, V., 2002. Diffuse Reflectance Spectroscopy of Iron Oxides. Encyclopedia of Surface and Colloid Science, 1438-1446.

Zoisite and its many colors

Clemens Schwarzinger[1], Steve Ulatowski[2], George R. Rossman[3]
[1] Johannes Kepler University, Linz, Austria, Clemens.schwarzinger@jku.at,
[2] New Era Gems, Grass Valley, CA, USA, [3] California Institute of Technology, Pasadena, CA, USA

The mineral zoisite is a calcium alumosilicate belonging to the class of silicates, more exactly sorosilicate minerals. Its chemical formula is $Ca_2Al_3(SiO_4)(Si_2O_7)O(OH)$ and it crystallizes in the orthorhombic crystal system. It was first found at the Saualpe in Carinthia, Austria at the end of the 18th century. After the initial finds in Austria, zoisite has been found in many other localities such as in Norway, USA, Pakistan, Afghanistan, Kenya and Tanzania. While the pink thulite from Norway and the ruby bearing green zoisite (also known as anyolite) from Longido, Tanzania are used for carving or decorative purposes, the only occurrences of gem quality material so far are Alchuri in Pakistan where small amounts of grey, brownish green and sometimes multi-colored crystals have been found, and Merelani in Tanzania. The latter one became famous mostly for the blue-to-violet V-bearing variety of zoisite which was first documented in the 1970ies by Manuel de Souza and made its way into the hands of Tiffany's who suggested to market this new gem material under the name tanzanite (reportedly as zoisite sounds too close to suicide) (Cairncross, 2020; Liddicoat, 1968; Wilson *et al*., 2009).

Of course, the most famous color of zoisite from Merelani is blue or violet. In the strict sense it is also only those colors that are allowed to be called tanzanite according to the CIBJO rules. All other colors must be called zoisite with the appropriate color descriptor, such as pink zoisite, however, the terms pink tanzanite or fancy tanzanite are frequently found, especially in the mineral trade where CIBJO does not apply. While in the early years much of the material found had a natural blue-to-violet color, most material mined later on was of yellow-brownish, purplish, or greyish color (Smith, 2011). Luckily, a simple heat treatment to temperatures of around 500-550 °C can turn such material into blue or violet (Schmetzer, 1978). The reason for the blue-to-violet coloration has soon been identified to be related to vanadium, however, there is still lots of discussion on its oxidation state – especially its fate during the heat treatment.

Figure 1. The various colors of zoisite in its rough and cut form.

We have collected samples mainly from the Merelani mines in Tanzania covering almost all known colors, including colorless, yellow, blue, green, pink and orange (Figure 1). Analysis of the material was carried out with UV-Vis-NIR spectroscopy as well as LA-ICP-MS to determine minor and trace elements (Table 1).

Colorless zoisite is much rarer than tanzanite and unsurprisingly the level of trace elements in such stones is very low. Despite the low abundancy of bands in the visible range, indicative bands in the NIR region can be found which allow identification of the crystallographic axes, as can be seen in Figure 2 (Smith, 2024). The α-ray has a band at 2470 nm, the β-ray one at 2300 nm and the γ-ray is indicated by a broad band at 1600 nm as well as strong absorption above 2400 nm.

Whereas the reason for the blue coloration of tanzanite is long known to be vanadium, the reason for the yellow to brown color, which often dominates in unheated tanzanite, is less well known. According to our findings, a correlation of titanium and a band at 445 nm in the γ-ray is given. Comparison of the band position and the bandwidth at half maximum of 5300 cm^{-1} leads us to the conclusion, that the reason for the yellow color is an Fe^{2+}-Ti^{4+} intervalence charge transfer (IVCT). This interpretation is in good agreement with data reported by Rondeau *et al*. (2018) and Taran and Koch-Müller (2011).

Green zoisites owe their color either a combination of the aforementioned chromophores vanadium and Fe-Ti-IVCT, where the contribution of yellow and blue have to be balanced, or there is a dominance of chromium, having absorption bands at 455, 488, 580, 650, 658 and 695 nm (Figure 3).

Pink zoisites, as well as thulite, owe their color trace amounts of manganese in its trivalent state. The oxidation state is very important, as only Mn^{3+} is a strong chromophore, whereas Mn^{2+} is almost colorless. Thus, conventional heating always results in destruction of the pink chromophore while heating under oxygen atmosphere can prevent discoloration along the α-ray (Schwarzinger, 2022).

A special unicorn amongst the zoisite colors is orange. While an easy explanation can again be given in the mixture of pink and yellow, some samples show an extremely high concentration of rare earth elements, of which Nd^{3+} can also be seen in the UV-Vis spectra. A summary of the coloring elements can be found in Table 1.

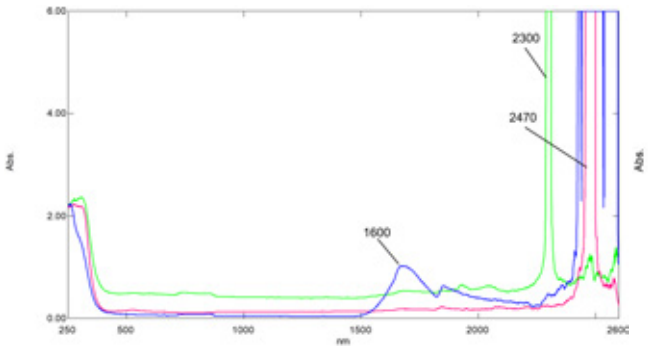

Figure 2. Polarized UV-Vis-NIR spectrum of a colorless zoisite (α-ray: red; β-ray: green; γ-ray: blue), optical pathlength 3.0 mm.

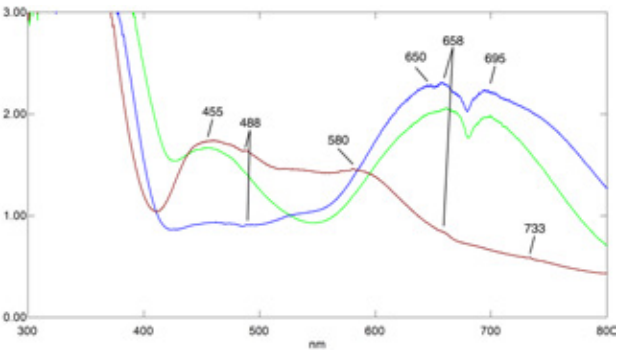

Figure 3. Polarized UV-Vis spectra of a 32.7 ct green zoisite dominated by chromium showing a green (γ-ray), bluish green (β-ray), and yellow-brown (α-ray) axis. Optical pathlengths are 16 and 17 mm.

Color	^{47}Ti	^{51}V	^{52}Cr	^{55}Mn	^{56}Fe	^{146}Nd
Colorless	190 (55-332)	172 (146-198)	9 (3-13)	40 (33-59)	0 (0-6)	0.6 (0.3-1.1)
Yellow	191 (26-927)	579 (78-1375)	34 (5-90)	46 (1-110)	30 (0-92)	54 (0.5-285)
Blue	225 (33-746)	1780 (392-3568)	150 (16-964)	69 (3-162)	121 (0-614)	54 (3-267)
Violet	144 (29-416)	922 (640-1476)	20 (8-48)	174 (64-428)	523 (38-1956)	70 (1-370)
Green	423 (45-1132)	1146 (675-2166)	144 (37-470)	20 (2-76)	9 (0-80)	15 (2-100)
Pink	156 (2-366)	318 (52-709)	14 (0-77)	298 (20-1067)	580 (16-2442)	387 (0.1-1666)
Orange	207 (118-422)	463 (456-1184)	50 (23-106)	132 (52-244)	171 (40-453)	998 (122-1882)
Greenish Brown	205 (132-345)	1234 (620-1899)	89 (31-147)	115 (64-212)	100 (26-238)	156 (30-599)

Table 1. Color contributing trace elements sorted by color.
Average values in ppmw with ranges in parentheses.

References:

- Cairncross, B. The Where of Mineral Names: Tanzanite, A Variety of Zoisite, Merelani Hills, Simanjiro District, Manyara Region, Tanzania. Rocks Miner. 2020, 95/5, 48-462. https://doi.org/10.1080/00357529.2020.1771156
- Liddicoat, R.T.; Crowningshield, G.R. More about zoisite. Lapidary Journal, 1968, 22, 736–40.
- Rondeau, B., Charmard-Bois, S., Fritsch, E., Notari, F., Chauvire, B. Reverse dichromatism in gem andalusite related to total pleochroism of the Fe^{2+}-Ti^{4+} IVCT. Spectrochim. Acta A 2018, 204, 611-619. https://doi.org/10.1016/j.saa.2018.06.053
- Schmetzer, K., Bank, H. Bluish-green zoisite from Merelani, Tanzania. Gems Gem. 1978, 16/4, 121-122.
- Schwarzinger, C. The Heat Treatment of Pink Zoisite. Minerals 2022, 12, 1472. https://doi.org/10.3390/min12111472
- Smith, C.P. Natural-color tanzanite. Gems Gem. 2011, 47/2, 119-120.
- Smith, C.P. Personal communication 2024.
- Taran. M.N., Koch-Müller, M. Optical absorption of electronic Fe–Ti charge-transfer transition in natural andalusite: the thermal stability of the charge-transfer band. Phys. Chem. Minerals 2011, 38, 215-222. https://doi.org/10.1007/s00269-010-0397-9
- Wilson, W.E.; Saul, J.M.; Pardieu, V.; Hughes, R.W. The Merelani Tanzanite Mines. Mineral. Rec. 2009, 40/5, 347-408.

Pink-orange gem quality euclase from Bahia, Brazil

Lætitia Gilles-Guéry
Sorbonne Université, Museum National d'Histoire Naturelle, CNRS, IRD, Institut de Mineralogie, de Physique des Matériaux et de Cosmochimie (IMPMC), Paris, France
Currently : Ecole des Arts Joailliers, Paris, France, laetitia.gilles-guery@vancleefarpels.com

Co-authors of publications related to the topic: Jurgen Schnellrath, Luiza Almeida Villar de Queiroz, Laurence Galoisy, Georges Calas, Brendan Laurs, Bear Williams, Cara Williams, Benoit Baptiste, Tiago Campolina Barbosa

Figure 1. This 2.99 ct shield-shaped euclase was studied for the article Gilles-Guéry *et al.* (2022-b). Courtesy of D. Clauwet; cutting and photo by B. Kosnar.

Euclase—$BeAl(SiO_4)(OH)$, monoclinic crystal system—is a seldomly occurring mineral and with a Mohs hardness of 7 and a perfect cleavage to (010) rarely faceted for use in jewellery, but crystal specimens are highly sought after by collectors. The mineral is most often colourless but can also be blue (mostly with colour zoning), bluish green, green and yellow (e.g. Chaves & Karfunkel, 1994). Few millimetre-sized pale pink euclases have been reported from the Borborema Pegmatitic Province in Brazil (Eeckhout *et al.*, 2002; Cassedanne & Philippo, 2015).

In 2016, finds of pink-orange euclase in Brazil have attracted considerable attention due to the material's unusual and beautiful colour, relatively high clarity and well-formed crystals. If the first samples were wrongly identified as Imperial topaz by a gemlab in Belo Horizonte, it was rapidly identified as euclase using Raman spectroscopy and standard gemmological testing at the Centro de Tecnologia Mineral (CETEM) laboratory and then analysed at Sorbonne University in Paris, France, to study the cause of their colour (Gilles-Guéry *et al*. 2022-a). The origin of the samples was reported as Livramento de Nossa Senhora in Bahia State. Pink euclases begun to spread in mineral fairs: in 2018 at Sainte Marie aux Mines and in 2020 at Tucson (Figure 1). Rapidly, it appears that the euclase samples look slightly different and were coming from two different places. In December 2020, part of the team (LAVQ and JS) visited the occurrence located approximately 18 km west-north-west of the town of Livramento de Nossa Senhora in the Paramirim mountain range of Bahia State. In October 2021, three members of the team (LG-G, LAVQ and JS) made a second trip to Livramento de Nossa Senhora to investigate the second source of the pink-orange euclase : Catoles mountain range, Bahia State, located approximately 30 km northnorth-east of the first occurrence (Gilles-Guéry *et al.*, 2022-b).

The pink-orange euclase samples were characterized by classic gemmological and Raman spectroscopy (plus a confirmation by X-ray diffraction). Both samples from the first and second occurrences had RIs of 1.652–1.673 (birefringence 0.021) and an SG value of 3.10. They were inert to long- and shortwave UV radiation.

Both samples displayed a strong pleochroism (Figure 2) (from orange to pink for the first occurrence and from pink to pale pinkish for the second occurrence) that was visible to the unaided eye by turning or by using a dichroscope. While the colour of the sample from the first occurrence was an almost homogenous pink-orange (Figure 3a), samples from the second one were strongly colour zoned (hourglass-shaped) (Figure 3b), varying from orange-pink at the pointed end of the faceted stone to almost colourless at its wider end.

Figure 2. Strong pleochroism from pink to pale pinkish is shown on the shield-shaped euclase from the second occurrence. Photo by C. Williams.

The samples from the first occurrence were typically less included than those from the second occurrence. Partially healed fissures with fluid inclusions were commonly observed, including those consisting of a liquid and a vapour phase. The samples from the second occurrence exhibited lower transparency. The most characteristic inclusions in our samples consist of various types of fibrous channels: straight fine-to-coarse ones (Fig. 4a) and curly/wooly fibers (Figure 4b). Other inclusions encountered in euclase from the second occurrence were dolomite, quartz, prismatic euclase and also partially healed fissures consisting of two-phase fluid inclusions. Moreover, some inclusions are still unidentified : flattened circular negative crystals, curly fibres and a hydrated La-Al phosphate/arsenate mineral (Gilles-Guéry *et al.*, 2022-b).

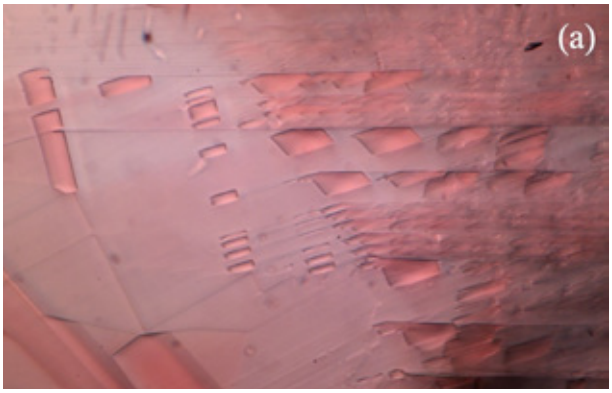

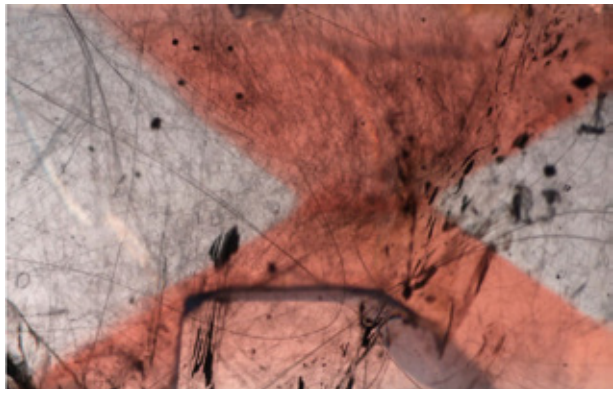

Figure 3. (a) the complex color zoning from pink to pinkish of the sample from the first occurrence and (b) the strong hourglass-shaped color-zoning from orange-pink to almost colourless of the sample from the second occurrence. Photomicrographs by J. Schnellrath and L. A. V. de Queiroz; image widths (a) 3.2 mm and (b) 6.0 mm.

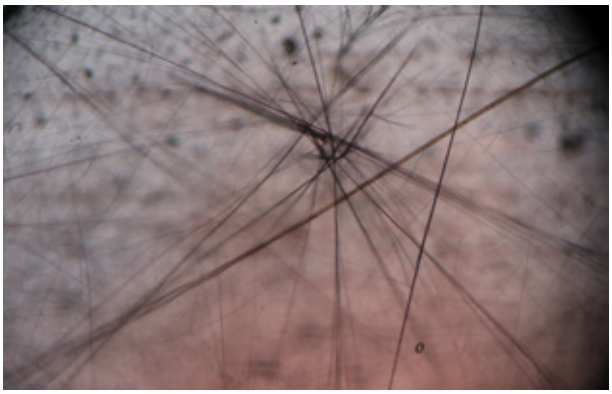

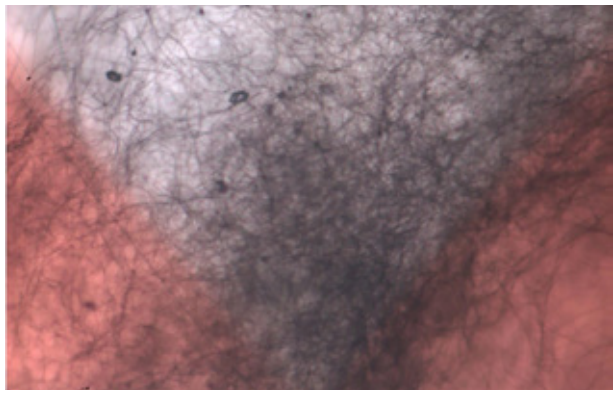

Figure 4. Various types of fibers observed in euclase from the second occurrence (a) straight fine-to-coarse inclusions and (b) curly/wooly fibers. Photomicrographs by J. Schnellrath and L. A. V. de Queiroz; image widths (a) 3.9 mm and (b) 2.5 mm.

Chemical analyses performed by EPMA reveal the presence of minor and traces elements: Fe (average content of 992 ppm), Mn (average content of 73 ppm), Ti (average content of 46 ppm), Ge (average content of 142 ppm).

The combination of spectroscopic techniques: unpolarized, polarized, low temperature, or in situ high temperature optical absorption spectroscopy, Electronic Paramagnetic Resonance (EPR) spectroscopy, and X-ray Absorption Near Edge Structure (XANES) spectroscopy (at SOLEIL synchrotron) allows Gilles-Guéry *et al*. (2022) to determine the causes of colour, pleochroism and heat-induced change of colour in pink-orange euclases. EPR and XANES spectroscopy prove that iron was only in ferric state (no redox change after heat treatment) and substitutes Al^{3+} in slightly distorted octahedral sites. EPR also shows the absence of paramagnetic radiation-induced defects. Thus, the colour and pleochroism from orange to pink have been related to the substitution of Mn^{3+} in the octahedral Al sites. An additional component, which might contribute to thermally unstable defects together with the rising slope towards the UV region, was assigned to an $O \rightarrow Fe^{3+}$ oxygen–metal charge transfer. Gilles-Guéry *et al.* (2022-a) found that heat treatment modifies the colour of this euclase from pink-orange to a stable pure pink by removing the thermally unstable defects that cause the yellow tint (Figure 5).

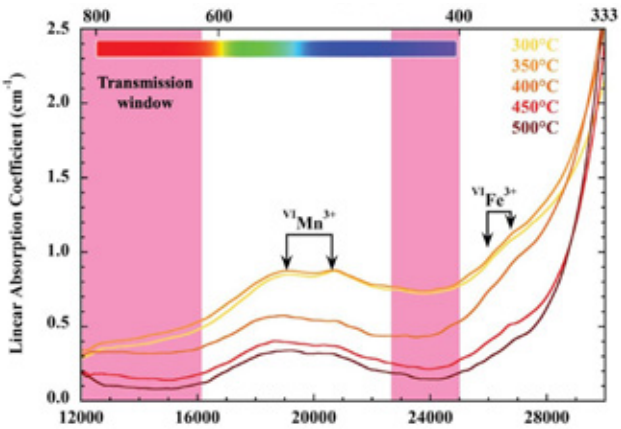

Figure 5 : Optical microspectroscopy study of the isochronal in situ measurements between 300°C and 500°C of pink euclase.

The formation of the pink-orange euclase from Bahia, Brazil appears to be in hydrothermal veins hosted by a schistose unit within metaarenite. The presence of many green Mn-bearing andalusite crystals in nearby schists indicates local oxidizing conditions. The presence of Ge in the samples is consistent with the contamination of the hydrothermal fluid by the surrounding rocks, as for Colombian euclase (Pignatelli *et al*., 2017). According to the overall gemmological properties and chemical composition, the euclase samples from both occurrences have the same geochemical signature but different internal features which allow their distinction (Gilles- Guéry *et al*., 2022-b).

The pink-orange euclase is still under research for unidentified inclusions and Mn content analyses of the color-zoning by LA-ICP-MS (LAVQ). Thus, euhedral pink-orange euclases have been given to the mineral collection of l'Ecole des Mines and of Sorbonne Université, in order to conserve samples for future research. Moreover, the School of Jewelery Arts has enriched its collections with a faceted pink euclase to introduce this rare gem to a wider audience.

References:

- Cassedanne, J., Philippo, S., 2015. Mineral and gem deposits of eastern pegmatites. Musée National.
- Chaves, M.L.S.C., Karfunkel, J., 1994. Novas ocorrencias de euclasio em Minas Gerais. Boletim IG-USP. Série Científica, 25, 53–60.
- Eeckhout, S.G., Castañeda, C., Ferreira, A.C.M., Sabioni, A., De Grave, E., Vasconcelos, D., 2002. Spectroscopic studies of spessartine from Brazilian pegmatites, American Mineralogist, 87(10), 1297-1306.
- Gilles-Guéry, L., Galoisy, L., Schnellrath, J., Baptiste, B., Calas, G., 2022-a. Mn^{3+} and the pink color of gem-quality euclase from northeast Brazil. American Mineralogist, 107 (3): 489–494.
- Gilles-Guéry, L., Queiroz L.A.V., Schnellrath, J., Williams, B., Williams, C., Laurs B.M., Galoisy, L., Calas, G., Barbosa, T.C., 2022-b. Pink-orange euclase from Bahia, Brazil, Journal of Gemmology, 38(1), 50-68.
- Pignatelli, I., Giuliani, G., Morlot, C., Rouer, O., Claiser, N., Chatagnier, P.Y., Goubert, D., 2017. Recent Advances In Understanding the Similarities and Differences of Colombian Euclases, The Canadian Mineralogist, 55(4), 799-820.

On the nature of blue rose quartz

Karen E. Fox[1*], Andrew M. McDonald[2], Chris Yakymchuk[1]
[1] Earth and Environmental Science, University of Waterloo, Waterloo, Canada; *kefox@uwaterloo.ca
[2] Harquail School of Earth Sciences, Laurentian University, Sudbury, Canada

Keywords: rose quartz, blue, dumortierite, fibre, scattering, inclusions, Tyndall

Introduction

Over the past several years, the market for pink-coloured rose quartz has been augmented by variants ranging from colourless through deep rose-pink, to lavender and blue. The blue material has been available since at least 2021, and internet sources refer to it as rose quartz because it occurs in the same deposits as common rose quartz and because it sometimes shows hints of pink colour (MysticCrystals, 2023). This study probes the definition of rose quartz in the context of how it is currently represented on the market.
Materials and methods

Five polished hand-specimens of blue rose quartz, three of which are depicted in Fig. 1, were compared with a variety of polished cobbles of pink-coloured semi-transparent "standard" rose quartz from Madagascar. Three of the blue specimens were labelled as "mined in Brazil", another was said to come from Madagascar, and the last was of unknown provenance. All were visually assessed and examined with a calcite dichroscope. Petrographic thin sections on glass slides without cover slips were prepared from blue rose quartz BRQ1 and from a standard rose quartz RQ1 and inspected using a Nikon Eclipse LV100Pol petrographic microscope.

Observations

All "blue" specimens appeared almost opaque, with an unsaturated, bluish grey, muddy colour when illuminated from the front or side on black background with minimal backlighting (Fig. 1). When photographed on white as shown in Fig. 2, the blue cast was minimized and hints of pink could be discerned in BRQ1 and BRQ2, while transmitted light produced a strong orangish yellow colour reminiscent of that seen in opalescent glass (Fig. 3). When fracture-free areas of blue quartz were probed with a He-Ne laser, a clearly visible light path was evident. Standard rose quartz specimens varied in transparency but were never as turbid and never showed the transmitted yellow to the same extent as the blue rose quartz, and did not scatter the laser beam as much. In the three most transparent blue cobbles, a silky reflected "cats-eye" line and hints of asterism were detected.

Figure 1. Blue rose quartz on black with illumination from the left front.

Figure 2. Blue rose quartz on white with top and side illumination.

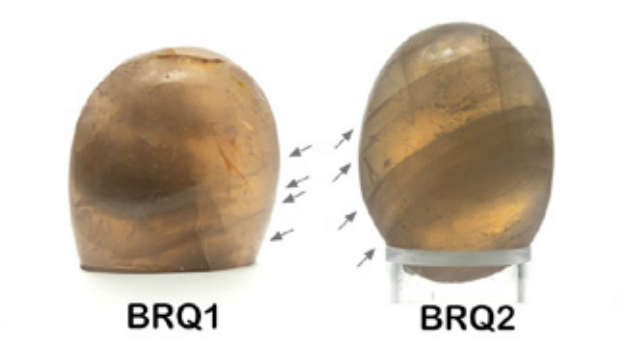

Figure 3. Light transmitted through blue rose quartz is a strong orange-yellow colour. Arrows indicate parallel planar fractures.

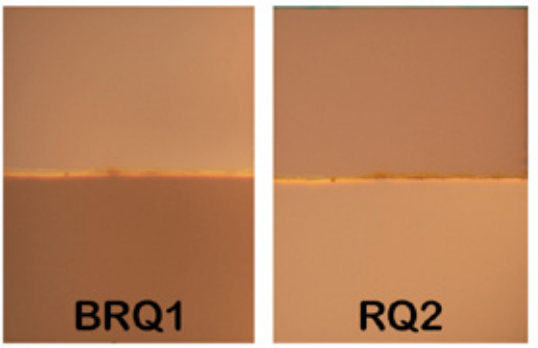

Figure 4. Dichroism in blue BRQ1 (left) and RQ2, a "standard" rose quartz (right).

Dichroscope examination of the transparent blue rose quartz specimens revealed two distinct colours that matched well with the dichroism of a distinctly coloured standard rose quartz, RQ2 (Fig. 4). In general, the blue rose quartz examined here was quite fractured, often displaying partially healed parallel planar fractures as indicated by arrows in Fig. 3.

Figures 5a and 5b show thin sections from blue and pink specimens, respectively, viewed between crossed polars. The blue rose quartz showed signs of dynamic recrystallization evidenced by a complex texture of small subgrains with diffuse boundaries aligned as indicated by the arrow in the figure, the largest averaging around 0.7 mm x 0.5 mm. The rose quartz showed fewer and much larger subgrains with only faint signs of directional structure. Both specimens contained abundant fibres oriented in three directions consistent with hexagonal axes, as revealed in Fig. 6a and Fig. 6b. The length of fibres was limited by cutting orientation and how parallel they were to the polished surface of the slide. Lengths up to 0.86 mm were measured on the rose slide, and up to 0.17 mm for the blue. Preliminary fibre counts suggested a density around 2500 fibres/mm2 for blue rose quartz and about 1800 fibres/mm2 for the rose quartz. A high density of pinpoint inclusions, barely visible at 500x magnification in Fig. 6a, accompanied by slightly larger more visible dark granules, was observed on the blue rose quartz slide and to a far lesser extent on the standard rose quartz slide.

Figure 5a. Blue rose quartz thin section between crossed polars. The arrow indicates a directionality to the texture.

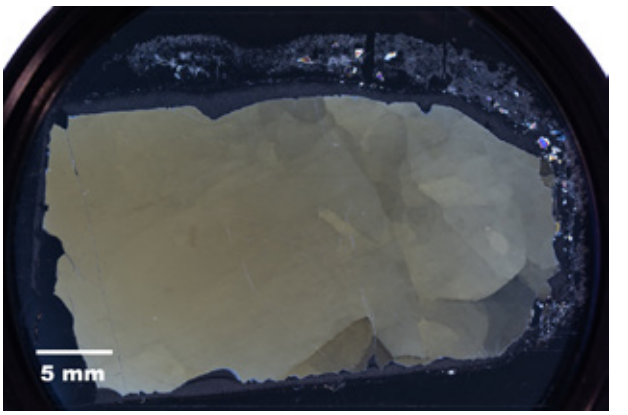

Figure 5b. "Standard" rose quartz thin section between crossed polars.

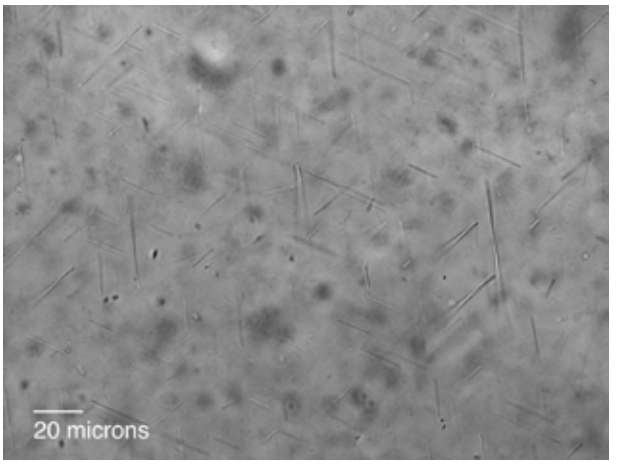

Figure 6a. Oriented fibres with granular and pinpoint inclusions in blue rose quartz.

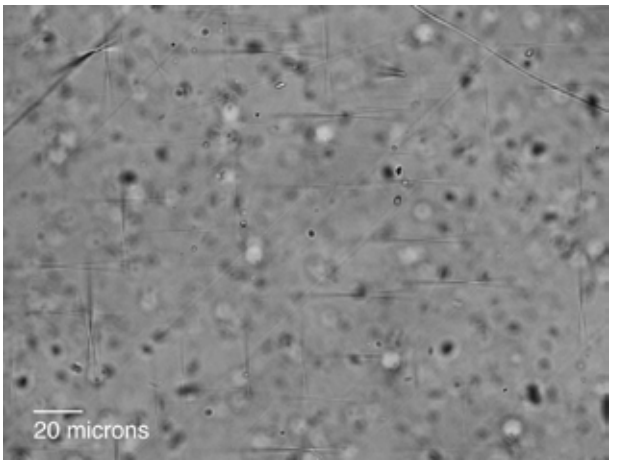

Figure 6b. Oriented fibres and granular inclusions in pink rose quartz.

Discussion and further investigation

The presence of oriented fibres in this blue rose quartz, along with hints of pink colour in some specimens, prompts comparison with the dumortierite-like fibres identified by Ma *et al*. (2002) as the cause of colour in pink rose quartz. The overall hazy blue colour with a transmitted yellow colour, plus the Tyndall scattering effect that makes the laser beam visible (Kerker, 1991), combined with the observed high density of almost invisible pinpoint inclusions, all suggest that the dominant blue is due to scattering phenomena as postulated by Seifert *et al*. (2011) for other examples of blue quartz. The similarity of the dichroism shown by the blue rose quartz to that in the standard rose quartz is consistent with reports that "even rather pale rose quartz may show medium to strong dichroism" (Liddicoat, 1989). However, since scattering phenomena polarize light (Strutt, 1919), the relative contribution of dichroic fibres versus scattering to the dichroism requires clarification. The muddy colour of this blue rose quartz may be linked to the yet-to-be-determined size distribution of pinpoint and granular particles present. Particles below and at the resolution of the microscope may contribute the blue, while larger ones may scatter white light or even act as absorbers. Beyond colour, the eye-visible fracturing and the nature of the quartz microstructures observed in the thin sections opens avenues for understanding temperatures and strain states associated with the deformational history of the deposits that sourced these quartz specimens.

References:

- Kerker, M., 1991. Founding fathers of light scattering and surface-enhanced Raman scattering. Applied Optics, 30(33), 4699–4705.
- Liddicoat, R.T., 1989. Handbook of gem identification. Gemological Institute of America, Santa Monica. 364 pp.
- Ma, C., Goreva, J.S., Rossman, G.R., 2002. Fibrous nanoinclusions in massive rose quartz: HRTEM and AEM investigations. American Mineralogist, 87, 269–276.
- MysticCrystals, 2023. Blog: What is blue rose quartz. Available from: <https://mysticcrystals.co.za/crystal-blog/what-is-blue-rose-quartz/>. Accessed 2025-04-20.
- Seifert, W., Rhede, D., Thomas, R., Förster, H.-J., Lucassen, F., Dulski, P., Wirth, R., 2011. Distinctive properties of rock-forming blue quartz: inferences from a multi-analytical study of submicron mineral inclusions. Mineralogical Magazine, 75(4), 2519–2534.
- Strutt, R.J., 1919. Scattering of light by solid substances. Proceedings of the Royal Society A: Mathematical, Physical and Engineering Sciences, 95, 476–479.

Gem-quality pink fluorite from Planggenstock, Switzerland: chemical and physical properties and a comparison with pink fluorites from other localities

Michael F. Hügi[1], Michael S. Krzemnicki[2], Markus Wälle[2]

[1] Swiss Gemmological Society, Hausmattweg 26, CH-3074 Muri b. Bern, Switzerland,

[2] Swiss Gemmological Institute SSEF, Aeschengraben 26. CH-4051 Basel, Switzerland

michael.huegi@gemmologie.ch

Introduction

In this study, first results of trace element analyses and various spectrometric investigations on pink fluorites from alpine deposits (Aar and Montblanc Massifs) as well as from the skarn de-posit near Huanggang, China, will be presented.

Pink fluorite is a typical mineral from Alpine extensional fissures, especially from the granitic central massifs of the Alps Aar Massif (Switzerland) and Mont Blanc Massif (France) (Stalder *et al*., 1998). It occurs exclusively in the form of octahedral crystals of usually less than 3 cm edge length, but very large crystals of over 15 cm are rarely found. The colour ranges from mostly pale pink to pinkish red and rarely intense raspberry red.

The formation of alpine pink fluorites occurs in connection with the formation of the minerals in alpine crystal clefts. The formation of these alpine fissures was caused by tectonic processes during the Alpine orogeny (Gnos *et al*., 2021). At a depth of about 13 to 18 km within crustal rocks and at temperatures of 450 to 550 °C, the tectonic stress about 20 My ago led to the for-mation of extensional fissures in the rocks, with cavities reaching up to several metres in size. These cavities were subsequently filled with supercritical hydrothermal aqueous fluids, which dissolved minerals from the rock of the fissure walls. The cooling associated with the uplift of the Alps led to supersaturation of the dissolved complexes and thus to the hydrothermal for-mation of minerals in these fissures. Quartz, the most common mineral species in these Alpine clefts, started crystal formation at temperatures between about 450 and 400°C, which represents the earliest stage of crystallisation. In contrast, the crystallisation of fluorite and chlorite began at lower temperatures in the final stage of growth of the rock crystals. This is why fluorites always are found grown on the surface of quartz crystals.

Probably the largest find of alpine pink fluorite to date was made in the fissure system of the Planggenstock mountain, canton of Uri, central Switzerland. This deposit is located in the so-called Central Aar Granite, which, with an extension of about 90 km from west to east, is the largest body of granitic rock in the Aar Massif and in Switzerland. The crystal deposit was dis-covered in 1993 and contained several very large fissure cavities which yielded mainly rock crystal in crystals up to one metre in size. In 2019, another cavity was discovered nearby containing numerous intensely coloured and large fluorite crystals (Fig. 1 and Fig. 2) together with large amounts of green chlorite sand.

Trace elements analysis of pink fluorite

At the time of submission of this abstract, trace elements of pink fluorites from Planggenstock and Huanggang, China have been analysed using Gem-TOF (LA-ICP-TOF-MS) at SSEF. Pink fluorite samples from the Montblanc Massif (France) are currently prepared and their data integrated later.

The most abundant trace element in pink fluorites from both Planggenstock and China is yttrium, which was measured in concentrations of 170 to 278 ppm in the alpine samples and between 205 and 273 ppm in the fluorites

Figure 1: Octahedral crystals of pink fluorite on gran-ite from the Planggenstock mountain, Switzerland. Total height approx. 30 cm. Photo: M. Hügi

Figure 2: Intensely coloured fluorite of 97.18 ct from the Planggenstock mountain, cut by Philipp Munsteiner. Photo: Atelier Munsteiner

from Huanggang. Based on our samples, a clear distinction between the alpine and Chinese pink fluorites is exhibited by the varying concentrations of Sr and Lu. For both elements, the alpine samples exhibited higher mean concentrations, with factors of 3 for Sr and 8 for Lu.

Despite the divergent geochemical formation conditions, the REE patterns of both deposits demonstrate remarkable similarity in terms of concentration ranges and the ratio of light REE (LREE) to heavy REE (HREE) (Fig. 3). The REE pattern exhibited by the Chinese samples deviates from that observed in the alpine samples, and is characterised by a negative Eu - anomaly. This discrepancy can be attributed to the divergent redox conditions that prevail in the respective geochemical growth environments, as generally described by Armbruster *et al*., (1996).

The LREE / HREE - ratio measured in the alpine fluorites also aligns with the observation by Armbruster *et al*., (1996). These authors reported that the REE patterns of alpine fluorites and the host rock (Central Aar Granite) are contrasting, which the granite showing a notably higher LREE/HREE ratio and a slight negative Eu anomaly (Schaltegger and Krähenbühl, 1990) compared to the fluorites. The enrichment of HREE in pink fluorites can be attributed to a post-magmatic fluid-rock interaction with F-bearing fluids, which have the capacity to form complex-es of HREE, in conjunction with Na, Nb, Y, Zr, Hf, Ta and U (Webb *et al*., 1985).

Cause of colour of pink fluorites

According to Bill and Calas, (1978), the attractive pink colour of fluorite is due to the presence of a YO^{2-}colour centre. This assertion is supported by UV-Vis spectrophotometry, which confirms the main absorption at 485 nm, and by the high Y concentrations that have been measured on samples both from Planggenstock and Huanggang. A weaker absorption band at 365 nm is attributed to Yb^{2+} (Armbruster *et al*., 1996).

Some fluorite crystals from the Planggenstock show a distinct inhomogeneous colour distribution gradually ranging from intense pink to colourless. Based on our GemTOF analyses, this colour distribution is not related to variations in Y concentration. So it can be assumed that the YO^{2-}colour centres may have been activated differently due to variable exposure to natural radi-oactive irradiation.

Inclusions in alpine pink fluorite.

So far, microscopic inclusion analysis was conducted on the polished pink fluorites from the Planggenstock deposit. The inclusion pattern demonstrates the presence of two-phase fluid inclusions, which are characteristic of hydrothermal mineral formations found in the alpine fissures of the Aar massif (Mullis, 1996). These inclusions are euhedral tetrahedral negative crystals in shape and are characterised by an aqueous filling with a water vapour bubble (Fig. 4). The most prevalent solid inclusions observed on or in close proximity to the crystal faces of the fluorite crystals were layers of fine-grained chlorite, which crystallised as the final phase of mineralisation within the alpine fissure.

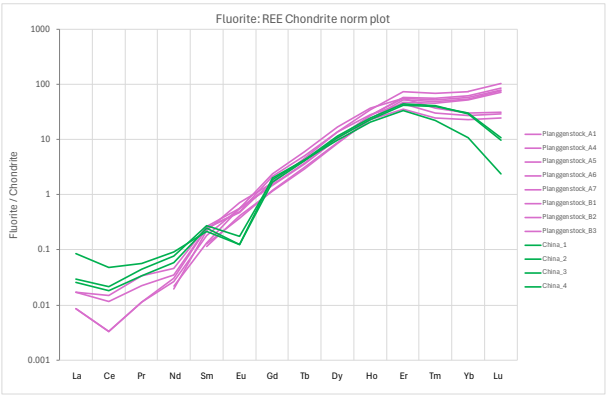

Figure 3: Chondrite-normed REE-pattern of pink fluorite of the Planggenstock mountain (red lines) resp. from the Huanggang Mine (green lines).

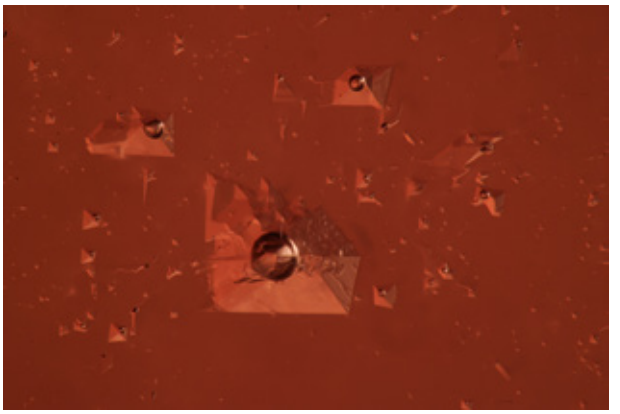

Figure 4: Two-phase inclusions in tetrahedral negative crystals in pink fluorite from Planggenstock mountain, Switzerland. Width of field 1.2 mm. Photo M. Hügi

Conclusions:

Although not a gemstone of great prevalence and value in the trade, fluorite, and especially attractive pink fluorite of gem-quality is considered an attractive collector stone and especially also sought after, even more so as rough crystals with or without matrix, due to their perfect octahe-dral shape.

With the discovery of the huge cavity with numerous pink fluorites at Planggenstock (Switzerland), and new pink fluorites emerging from Huanggang in China, it is the aim of this study to better characterise this new material from Planggenstock and to compare it with pink fluorites from Huanggang and the Montblanc Massif. Our preliminary results show that despite quite different geological setting and formation (Planggenstock: hydrothermal; Huanggang: skarn-related) their trace element concentrations and patterns only differ slightly.

References:

- Armbruster, T., Kohler, T., Meisel, T., Nägler, T. F., Götzinger, M. A., & Stalder, H. A., 1996: The zeolite, fluorite, quartz assemblage of the fissure at Gibelsbach, Fiesch (Valais, Switzerland): crystal chemistry, REE patterns, and genetic speculations. Schweizerische Mineralogische und Petrographische Mitteilungen, 76, 131–146.
- H. Bill, G. Calas, 1978: Color Centers, Associated Rare-Earth Ions and the Origin of Coloration in Natural Fluorites Phys. Chem. Miner. 1978, 3(2), 117.
- Gnos, E., Mullis, J., Ricchi, E. *et al.*, 2021: Episodes of fissure formation in the Alps: connecting quartz fluid inclusion, fissure monazite age, and fissure orientation data. Swiss Jour. Geosciences, 114, 14. https://doi.org/10.1186/s00015-021-00391-9
- Mullis, J., 1996: P-T-t path of quartz formation in extensional veins of the Central Alps. Schweiz. Min. Petrogr. Mitt., 76, 159–164
- Schaltegger, U. and Krähenbühl, U., 1990: Heavy rare-earth element enrichment in granites of the Aar Massif (Central Alps, Switzerland). Chem. Geol., 89: 49-63.
- Stalder, H. A., Wagner, A., Graeser, S., & Stuker, P., 1998: Mineralienlexikon der Schweiz Wepf: Basel, 579 pp.
- Webb, P.C., Tindle, A.G., Barrit, S.D., Brown, G.C. and Miller, J.F., 1985: Radiothermal granites of the United Kingdom: comparison of fractionation patterns and variation of heat production from selected granites. In: High Heat Production (HHP) Granites, Hydrothermal Circulation and Ore Genesis. Inst. Min. Metall., London, pp. 409-424.

Typomorphic features of tourmalines of the Malkhan pegmatite field from the Irkutyanka vein

Anna Y. Shelementyeva, Yuri B. Shelementyev, Olga V. Yarapova
Gemmological Center of Moscow State University, Moscow, Russia
shelementieva@gem-center.ru

This abstract presents the examination results of 5 tourmaline samples found in the Irkutyanka vein of the Malkhan pegmatite field in 2022 (Figure 1). The samples were studied using optical and scanning electron microscopy as well as LA-ICP-MS analyses. Conclusions are made on the chemical composition of the samples, noting the anomalous content of bismuth and lead in the studied samples.

The Malkhan pegmatite district is among the today active tourmaline deposits, which is the largest source of tourmaline in Russia. The deposit is located in the Krasny Chickoy area of the Zabaikalsky Krai, Transbaikalia, Russia. Geology, mineralogy, and geochemistry of the pegmatite field are described in detail by Zagorsky and Peretyazhko (1992). There are more than 15 tourmaline-bearing veins in the Malkhan pegmatite field including Danburitovaya, Geologicheskaya, Irkutianka, Karkadilovaya, Mokhovaya, Novaya, Oktyabrskaya, Oreshnaya, Skakunya, Solnechnaya, Sosedka, Svetlaya, Tabornaya, Zapadnaya-1 and Zimoveynaya (Zagorskiy *et al*., 2008).

The Irkutyanka vein has been known since 2018. It is a wedge-shaped body up to 390 m in length and from 5 to 12 m in diameter. The productive part with gem quality tourmaline is represented by an albite and quartz-albite pegmatite. The sizes of miaroles with tourmaline vary widely and have a variety of shapes. The distribution of miaroles and tourmaline in the productive zone is extremely uneven. Tourmaline crystals vary from several mm to 5 cm in size. In addition to the traditional colored varieties of elbaite from Malkhan, we found monochromatic translucent crystals of a light green (mint) color.

The chemical composition of the crystals was analyzed on a TESCAN VEGA 3 scanning electron microscope at an accelerating voltage of 15 kV. Average Li and B contents in each sample were determined using LA-ICP-MS measurements, carried out with an Elan DRC-e quadrupole inductively coupled plasma mass spectrometer. Laser ablation: NWR-213. Calibration was carried out using solid standard samples NIST SRM 610 and NIST SRM 620. The calculation of the elemental content was carried out with normalization to 100% of the sum for oxides.

Figure 1. Samples of the studied tourmalines from the Irkutyanka vein of the Malkhan pegmatite field. FOV 6.5 cm.

The tourmaline supergroup has the generalized chemical formula $^{[9]}X^{[6]}Y_3{}^{[6]}Z_6\ (^{[4]}T_6O_{18})\ (^{[3]}BO_3)_3V_3W$ (Henry *et al*., 2011) and can be classified into primary groups based on the dominant occupancy of the X-site. Twenty-one members of the tourmaline supergroup contain Na as the dominant cation on the X-site, seven Ca, six □ (vacancy) and only one K.

Occupation of structural positions in chemical formulas was carried out step by step in accordance with the procedure specified in the current nomenclature of tourmalines (Henry *et al*., 2011). First, Na and Ca were placed in the

X-position. The fraction of a vacancy (□) in this position was calculated from the stoichiometric ratio based on the equation Na + Ca + □ = 1 apfu. The assignment of a particular composition to a specific mineral species was carried out in accordance with the rules on the dominant valence approved by the KNMNK MMA (Bosi *et al*., 2019). First, based on the predominant component in the X-position, the mineral was determined to belong to the group of alkaline tourmalines (Na> Ca and Na > □) or tourmalines with a dominant vacancy (□ > Na and □ > Ca) (Figure 2).After that, the dominant anion in the W– F–, OH– or O2– position was taken into account. At the last stage, the dominant end-member determining the formula of the end-member of the corresponding mineral species in the tourmaline supergroup was calculated based on the results of the Y-position occupancy.

All the examined tourmalines Contain Li (0.76-0.94 apfu) and Al (7.76-8.11 apfu) in octahedral positions. Other octahedral cations (Mn, Fe, Ti) contain less than 1 apfu. Tourmalines do not show a deficiency of Si (5.90-6.00 apfu) and are represented by species with a predominance of F (0.78-0.83 apfu).

As a result, we have calculated the compositions of tourmalines that fall into the fields of the following two mineral species:
Fluor-elbaite $Na(Li_{1.5}Al_{1.5})Al_6(Si6O_{18})(BO_3)_3(OH)3F$
Fluor-rossmanite $□(LiAl_2)Al_6(Si_6O_{18})(BO_3)_3(OH)3F$

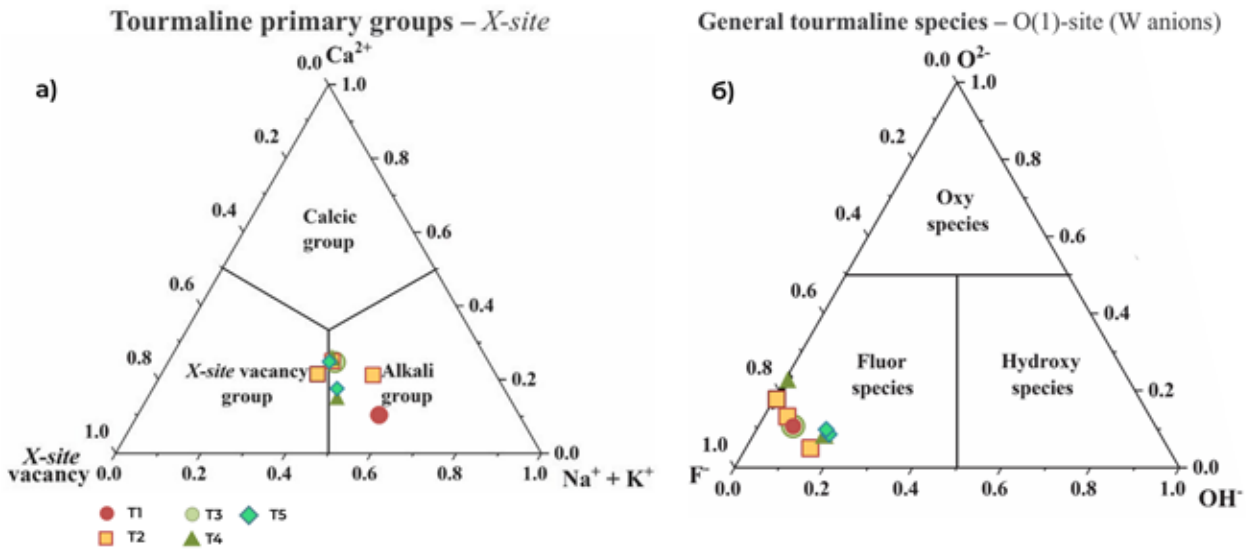

Figure 2.
a) The ratio of cations and vacancies (□) in the X position in tourmaline supergroup minerals from the Irkutyanka vein,
b) The ratio of anions occupying the W position in tourmaline supergroup minerals from the Irkutyanka vein.

It is worth noting that elbaite and fluor-elbaite are common mineral species not only in the Malkhan pegmatite field, but also in other tourmaline deposits. Fluor-rossmanite is endemic to Malkhan and was approved as a new mineral species in 2022. The studied tourmaline samples were found to contain higher lead (up to 0.5 wt.%) and bismuth (up to 0.7 wt.%) contents (figure 3). The largest amount of lead was found in sample T1, and the largest amount of bismuth was found in samples T4 and T5. Bismuth and bismuth-containing minerals have already been described in separate veins on the Malkhan Ridge. The bismuth-columbite mineral was discovered in the Danburitovaya albite-pegmatite vein, and Bi- and Pb-rich tourmalines were found in the Zapadnaya-1 pegmatite vein (Peretyazhko *et al*., 1989). The lead and bismuth content in our samples may be a typomorphic property. Vereshchagin *et al*. (2022) suggested in their article that trivalent cations can also occupy the X-position of tourmaline. It can be predicted that the general classification scheme for tourmalines based on the occupancy of the X-position will include not only vacancies, monovalent (e.g. Na, K) and divalent (e.g. Ca, Pb) cations, but also trivalent (e.g. Bi) cations. (Vereshchagin et. al. , 2022)

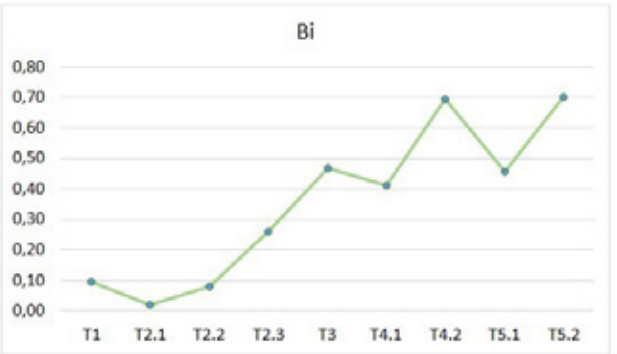

Figure 3. Bismuth content in the studied tourmaline samples in mass percent.

References:

- Bosi, F., Hatert, F., Hålenius, U., Pasero, M., Miyawaki, R., Mills, S.J., 2019. On the application of the IMA-CNMNC dominant-valency rule to complex mineral compositions. Mineralogical Magazine, 83, 627–632.
- Henry, D.J., Novák, M., Hawthorne, F.C., Ertl, A., Dutrow, B.L., Uher, P., Pezzotta, F, 2011. Nomenclature of the tourmaline supergroup minerals. American Mineralogist, 96, 895–913.
- Peretyazhko, I.S., Zagorskiy, V.E., Bobrov, Y.D, 1989. First find of Bi- and Pb-rich tourmalines. Doklady AN SSSR (Doklady Academy of Sciences), 307(6), 1461–1465. (in Russian).
- ereshchagin, O.S., Kasatkin, A.V., Škoda R., 2022. New data on Bi-, Pb-bearing and Mn-rich gem tourmaline from the Malkhan pegmatite district (Transbaikalia). Zapiski Rossiyskogo Mineralogicheskogo Obshchestva (Proceedings of the Russian Mineralogical Society), 6, 46–57.
- Zagorskiy, V.E., 2010. Malkhan deposit of tourmalines: types and origin of miaroles. Doklady RAN (Doklady Earth Sciences), 431(1), 81–84. (in Russian).
- Zagorskiy, V.E., Peretyazhko, I.S., 2008. The Malkhan gem tourmaline deposit in Transbaikalia, Russia. Mineralogical Almanac, 13b, 4–41.

Colored gemstones of metamorphic origin: Progress report in understanding how they crystallize at depth in East Africa, the Hindu Kush, Pamir Mountains, and the Middle-Urals Ring Structure

John M. Saul
Paris, France, john.saul@wanadoo.fr

Two problems

It is difficult to reconcile the existence of deposits of transparent gems of metamorphic origin with the observation attributed to Robert Boyle (1627–1691) that the best crystals grow in cavities. A problem arises for the gem-rich areas in East Africa, the Urals, the Hindu Kush, Pamirs and elsewhere because cavities do not exist at the depths where regional metamorphism occurs.

In the absence of actual cavities, we might seek regions at depth where the constraining pressure is somehow regionally reduced. But such circumstances are also absent from metamorphic terrains.

To be clear, isolated 3–D spots or groups of spots with low pressure do exist and may indeed contribute to gem-formation. Low pressure spots at Merelani where tanzanite crystallized in association with boudins are a clear example (Olivier, 2008). But localized spots such as furnished by boudins or at the apexes of tight folds are only contributing factors. As a matter of scale — cm vs. km — they throw no light on the existence of extended metamorphic terrains (in East Africa, the Urals...) that host multiple gem deposits formed at depth.

There is another problem too: all the colored gemstones in a given region crystallized within one particular short-lived window of time. In East Africa, for example, all the gems crystallized approximately 550 million years ago.

Elements of a solution

The pressure at any depth in the Earth is essentially fixed, but this is not necessarily true for temperature.

An increase in temperature at depth would allow certain minerals to crystallize higher in the Earth, hence under lower constraining pressure, hence, in some cases, as gems.

A rise in temperature leading to the formation of gems under metamorphic conditions cannot, however, be achieved by familiar sources of heat such as volcanism or igneous intrusions. For whereas volcanism and igneous intrusions are common, gem-producing regions are rare.

Thus, for the gem-rich areas in East Africa, for example, it is necessary to identify a source of heat that was active. c.550 million years ago *but not before that time and not after*.

A candidate-source of heat available for the formation of metamorphic gems is furnished by thrust faults whereby thick sheets of rock, thrust one over another, produce temperature inversions that place hot rocks from deep in the Earth on top of cooler rocks from closer to the surface; Figure 1.

Such temperature inversions are locally augmented by transient frictional heat whose magnitude is determined by the types of rocks and the thickness and temperature of the thrust sheets (Fritz, *et al*., 2009).

Heat was dispersed *upward* into overlying rocks *though only temporarily*, producing elevated temperatures at unusually shallow depths. Certain minerals were then "tricked" into crystallizing higher in the Earth than usual, hence with better quality crystallization. And in East Africa, the Urals, Himalayas, Hindu Kush, Pamirs, and presumably elsewhere, the time of thrusting and the time of gem formation are correlated.

Such scenarios, along with secondary contributing factors such as faults, the formation of boudins, or the production of temperature-lowering fluxes, provide circumstances that might allow high-quality crystallization at depth throughout a sizable region.

But we are confronted with the fact that large thrusts, which characterize continent-to-continent collisions, are not uncommon. And, to repeat, gem-rich regions are rare. So there must be differences between large-scale thrusting in general and those particular large-scale thrusts (in East Africa, the Urals...) that actually lead to the formation of gems.

One difference may be the thickness of individual thrust sheets, and another difference would be their initial temperature (see Fritz, *et al*., 2009).

Another difference, potentially affecting heat production, is the distance inland from the collision zone. For, as has been shown for the India–Eurasia (Hindu Kush, Pamirs) convergence (Figure 2), the initial subduction of coastal sediments causes a "temporary acceleration in subduction rates" by a factor of >2, a phenomenon responsible for additional frictional heat, and thought to be "a common feature at the final stage of continental assembly" (Zhou *et al*. 2024). The incoming plate sprints at the end of its marathon!

Yet this is not the last word for, as can be observed (Figure 2), gems are preferentially formed at the passive edges of the "target" continent in places where the incoming plate encounters a circular plug of resistant rock, which is the case, as I have long argued in East Africa, the Hindu Kush, Pamirs and the Middle Urals Ring Structure (Saul, 2014, 2016, 2017, 2022, 2023; Burba, 1991, 2003a, 2003b). In such places thrusting over the resistant plug is much like that of sandpapering over a knot.

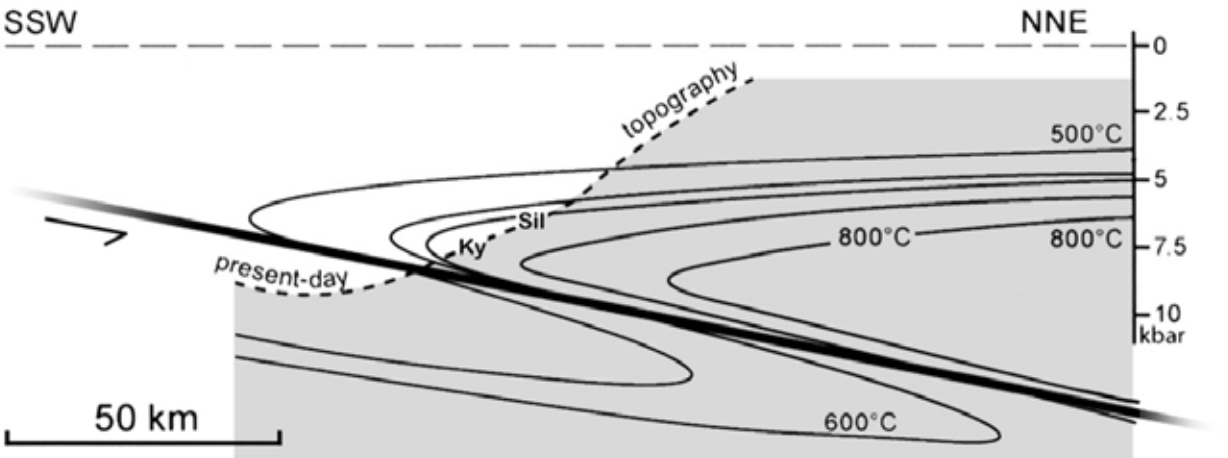

Figure 1: Thermal profile along the Himalayas in central Nepal. A thrust fault (thick line) caused overlying rocks to be metamorphosed at higher temperatures than those below. This allowed minerals to crystallize higher in the Earth than is usual, hence with less constraining pressure. "Sil" indicates sillimanite and "Ky", below it, indicates kyanite, which normally crystallizes above sillimanite. Adapted from Le Fort (1975). Similar profiles for East Africa or the Urals were not available for this study.

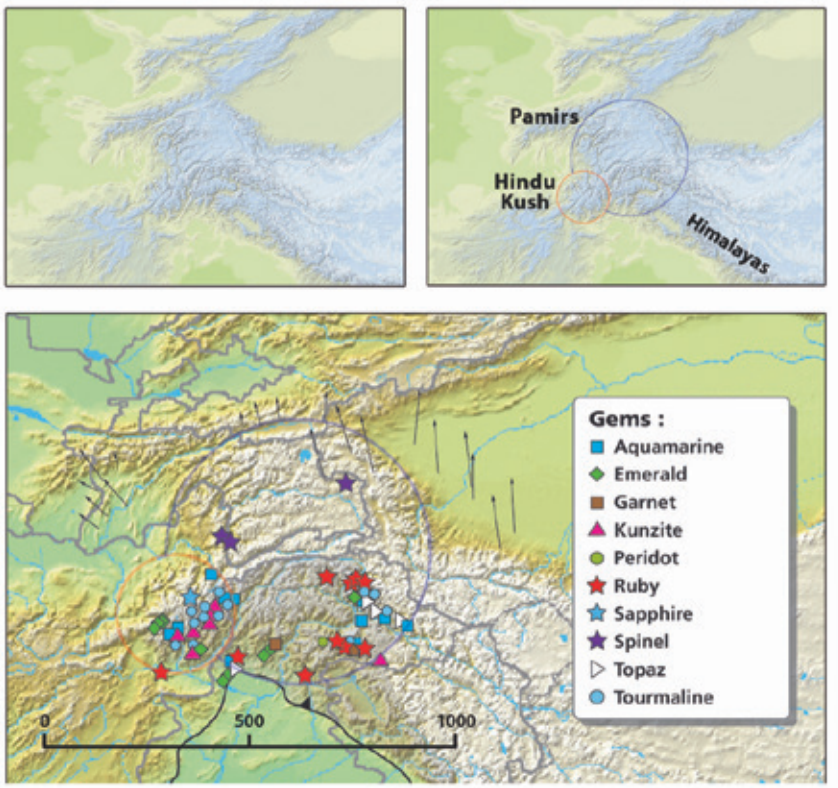

Figure 2: Gemstone locality map of the Hindu Kush and the Pamirs, both of which have faint circular outlines.

References:

- Boyle, Robert. An Essay About the Origine and Virtues of Gems (1672). In The Works of Robert Boyle. Edited by Michael Hunter and Edward B. Davis, vol. 7, 4–72. Brookfield: Pickering & Chatto, 1999–2000.
- Burba, G.A., 1991. Middle-Urals Ring Structure, USSR: Definition, description, possible planetary analogues. Lunar and Planetary Science Conference XXII, 153–154.
- Burba, G.A., 2003a. Effect of the supposed giant impact crater on the geologic evolution of the Ural Mountain range. Large Meteorite Impacts, LPI, Houston, Abstract 4117.
- Burba, G.A., 2003b. The geological evolution of the Ural Mountains: A supposed exposure to a giant Impact. Vernadsky/Brown Microsymposium, 38, Abstract MS011.
- Fritz, H., V. Tenczer, C. Hauzenberger, E. Wallbrecher, and S. Muhongo, 2009. Hot granulite nappes – Tectonic styles and thermal evolution of the Proterozoic granulite belts in East Africa. Tectonophysics, 477(3-4), 160–173.
- Le Fort, P., 1975. Himalayas, the collided range: Present knowledge of the continental arc. American Journal of Science, 275(A), 1–44.
- Olivier, B., 2008. The geology and petrology of the Merelani tanzanite deposit, NE Tanzania. Ph.D. Thesis, University of Stellenbosch, 453 pp.
- Saul, J.M. 2014. A Geologist Speculates. Les 3 Colonnes, Paris, 159pp.
- Saul, J.M., 2016. Deep 'plugs' caught in continent-to-continent collisions, gemstones, deposits of metals, oil & gas. 35th International Geological Congress, Cape Town, Paper 149.
- Saul, J.M., 2017. Transparent gemstones and the most recent supercontinent cycle. International Geology Review, 60(7), 889–919.
- Saul, J.M., 2022. Gemstone Deposits of Eastern Kenya and Tanzania Controlled by Ancient Meteorite Impacts and Continental Collision – an Exploration Model. Australian Gemmologist, 28(1), 15–24.
- Saul, J.M., 2023. Gemstone Occurrences and Circular Meteorite-Impact Scars: the gemmology tail wags the geology dog. Australian Gemmologist, 28(3), 130–135.
- Zhou, H., J. Hu, L. Dal Zilio, M. Tang, K. Li and X. Hu, 2024. India–Eurasia convergence speed-up by passive-margin sediment subduction. Nature, 635, 114–120.

Hessonite garnet from Angul district of Odisha, India

Jayshree Panjikar[1, 2] and Aatish Panjikar [1, 2]
[1] Pangem Testing Laboratory, Pune, India
[2] PANGEMTECH – Panjikar Gem Research & Tech Institute, Pune, India
jayshreepanjikar@gmail.com

Keywords: Hessonite garnet, inclusions, Angul, Odisha

Introduction

This study describes hessonite (Fe-bearing variety of grossular garnet), found in the Birlamunda village, located in Palalahada tehsil of Angul district (N 20° 50' 56.508", E 85° 3' 38.844") of Odisha state. Rocks in this region are a part of the Precambrian khondalite-charnockite-granite gneiss. Hessonite occurs along the contact zone of garnetiferous-gneiss and the amphibolite. Gemmological properties have been determined. Semi-quantitative analyses carried out using EDXRF show presence of iron, titanium and chromium. Material shows distinct turbidity or roiled structure like treacle commonly known as heat-wave effect. Crystalline inclusions identified with Raman were apatite, calcite, diopside, ilmenite, quartz, rutile and zircon.

Materials and methods:

Hessonite garnet from Birlamunda village with prominent inclusions were selected. Using gemmological methods their optical properties, refractive index, specific gravity, UV fluorescence etc. were determined. Inclusions crystallizing near the surface were identified by Raman spectroscopy. Semi-quantitative analyses were carried out using EDXRF and electron microprobe.

Results

Visual Appearance: Hessonite garnet from Birlamunda village of Angul District of Odisha were found to be having turbidity, treacly appearance with a brownish yellow to bright orangish yellow body color and a large number of crystalline inclusions. The coloration in these hessonite garnets is due to Cr and Fe content.

Gemmological Properties: Specific gravity was found to be in the range of 3.69 to 3.72, refractive indices fell in the range of 1.743 to 1.746. All samples showed no fluorescence under LWUV as well as under SWUV.

Microscopic Observations: Birlamunda hessonite garnet display a characteristic turbidity or roiled appearance which looks more like heat wave effect (Fig 1&2). Most samples were included with very tiny transparent crystals of apatite and some other crystals (Fig 3). Calcite rhombs were also seen in some specimen (Fig 4). In many of these hessonite garnets there were euhedral apatite crystal inclusion (Fig 5). These apatite crystals were of prismatic shape. some were grouped together with quartz crystals, which manifest as stumpy crystals (Fig 6). Some samples contained rutile in the form of fine needles arranged in three directions (Fig 7). In four specimen there were ilmenite crystals as inclusions (Fig 8). Diopside crystals were prominently observed in many of the specimen (Fig 9). Some diopside crystals were grouped together in a straight line (Fig 10). The yellowish-brown specimen had more of zircon halo type inclusions (Fig 11). In one unique case there were 'fused' crystals of apatite looking like a 'giant' crystal inclusion (Fig 12).

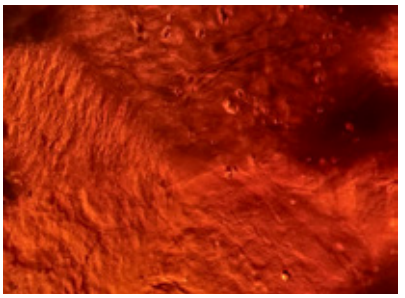

Fig 1: Heat wave like appearance

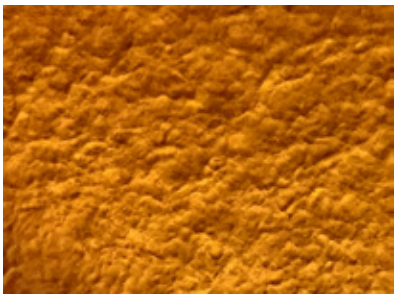

Fig 2: Roiled treacle-like appearance

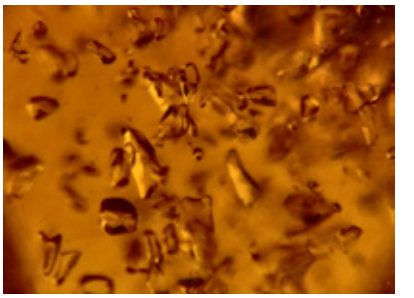

Fig 3: Variety of crystals observed

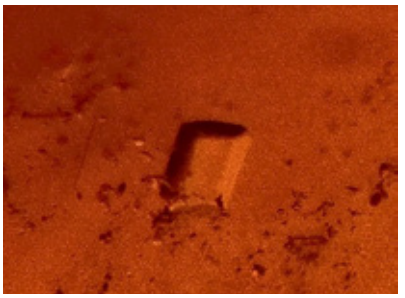

Fig 4: Calcite crystal inclusion

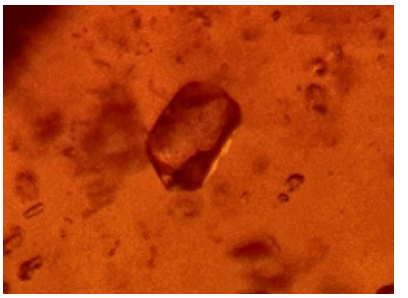

Fig 5: Apatite crystal inclusion

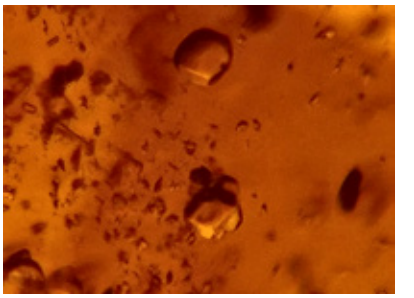

Fig 6: Stumpy quartz crystals

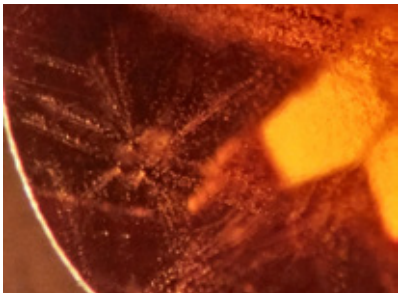

Fig 7: Fine rutile needles

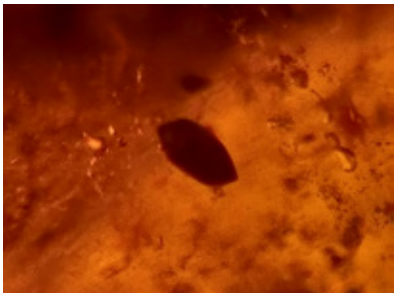

Fig 8: Ilmenite crystal inclusion

Fig 9: Diopside crystal inclusion

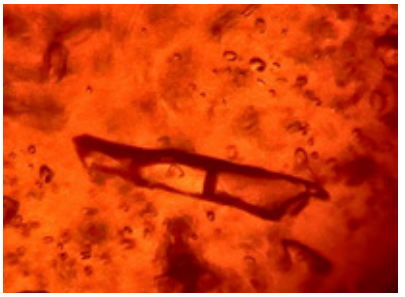

Fig 10: Diopside crystals

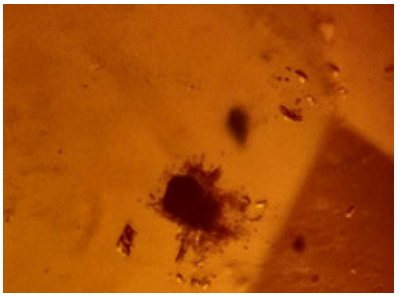

Fig 11: Zircon inclusion with halo

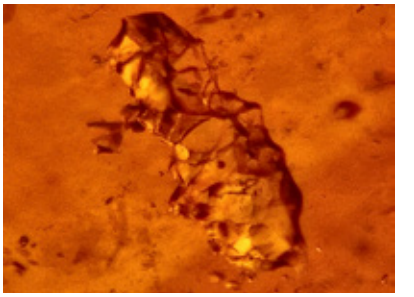

Fig 12: Fused crystals of apatite

Fig 13: Position of Odisha state

Chemical Analyses: Semi-quantitative chemical analyses by EDXRF for hessonite garnet gave the oxide weight % for SiO_2=37.98 to 38.82, Al_2O_3 =20.47–20.05, for CaO=38.98–39.01 and for FeO = 1.12-1.15, whereas the oxide weight % for $Cr_2O_3$and TiO_2 was determined as 1.08 and 0.37 respectively. No manganese was detected in our samples by EDXRF.

Discussion: The inclusions in hessonite described by Kanis & Redmann (1994) from four different localities, viz. Ghatpara, Burubura, Budhido and Dahikbala (Fig13 & 14) in Orissa (now Odisha) are somewhat similar to the ones observed in the present study. All hessonites described by them from these four occurrences contain traces of MnO based on their chemical analyses, in contrast to this we did not analyze any manganese in our hessonite samples from Birlamunda. Besides, the Ghatpara and Burubura hessonite display two and three phase inclusions. Whereas the hessonite from Dahikbala contain needlelike inclusions. Budhido hessonite garnets have orthoclase mineral inclusions. None of the specimen investigated in this study displayed neither orthoclase inclusions nor two or three-phase inclusions. They contain, however, other inclusions such as zircon, apatite, diopside and calcite crystals.

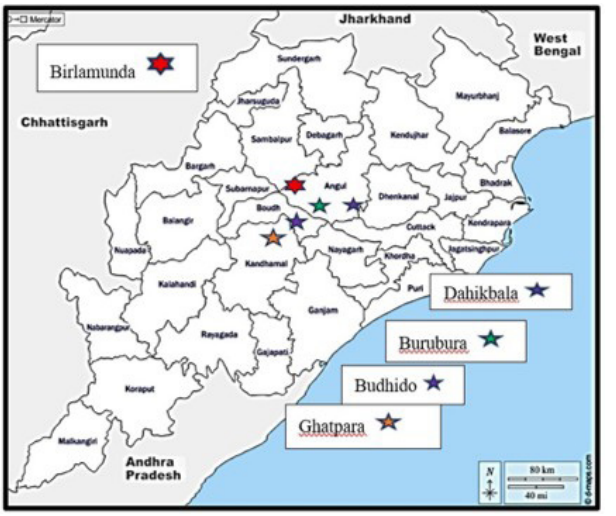

Fig 14: Localities described in *Kanis & Redmann* and Birlamunda

The Birlamunda hessonite garnet occurs in a variety of color shades of orangish- brown to yellowish brown tending towards honey color. The coloration is mainly due to Fe with possibly minor contributions by Cr. The Birlamunda hessonite garnet contain a large number of solid inclusions in a distinct roiled or treacle like 'background' in which the crystalline inclusions are present. According Gübelin and Koivula (1986) the treacle effect is due to the colloidal separation of calcite. The authors are of the opinion that this roiled treacle-like appearance is mainly due to the drastic changes in temperature and pressure during the crystallization of the hessonite garnet. These variations in pressure and temperature had created disturbances in the solid solutions and given rise to polycrystalline aggregate of small hessonite garnet. The small RI differences between the single grains of the polycrystalline structure are responsible for the roiled type effect. The large number of crystalline inclusions of apatite, diopside, zircon, calcite, rutile, quartz and ilmenite indicate the mother-liquor was having a characteristic metamorphic assemblage. Some of the inclusions of apatite and diopside appear to be fused together to form large giant crystals.

Conclusion

The Birlamunda hessonite garnets have some inclusions similar to those studied by Kanis & Redmann, (1994), indicating that the emplacements of these garnets may have been in a similar type of metamorphic rock mentioned in that study. The geology of the Indian subcontinent is extremely complicated with numerous metamorphic events, so it is indeed difficult to indicate whether the geological period was also similar to that in the study done by Kanis &Redmann (1994), it could be similar. There are crystals of rutile and ilmenite in some of the specimens which were not described in the hessonites studied by Kanis & Redmann or by Gübelin and Koivula (1986). Rutile needles seem to be perfectly oriented. Oriented acicular inclusions of the Birlamunda hessonite garnet could be the result of crystallization at ultrahigh temperature of above 1000°C and pressure above 3 GPa as stated in Axler & Ague (2015).

References:

- Amthauer G., 1975: Zur Kristallchemie und Farbe grüner und brauner Grossulare aus Tansania. Z. Dt. Gemmol. Ges. Vol24, pp 61-72
- Anderson B.W. 1959: Properties and classification of individual garnets. Journal of Gemmology, Vol. 7, No. 1, pp. 1-7.
- Arbunies-Andreu M., Bosch-Figueroa J.M., Font-Altabi M., Traveria-Cros A., 1975: Physical and optical properties of garnets of gem quality. Fortschritte Mineralogie, Vol. 52, pp. 531-538.
- Axler J.A. and Ague J.J., 2015: Oriented multiphase needles in garnet from ultrahigh-temperature granulites, Connecticut, U.S.A. American Mineralogist, Volume 100, pages 2254–2271.
- Gübelin, E.J., Koivula, J.I., 1986: Photo atlas of inclusions in gemstones. ABC Verlag, Zurich pp.829
- Kanis J., Redmann M., 1994: Four hessonite garnet occurrences in Orissa, India. Journal of Gemmology, Vol 24, No.2, pp75-83
- Li W., Zheng J., Pei J., Xu X., Chen T., 2022: Correlations between Garnet Species and Vibration Spectroscopy: Isomorphous Substitution Implications. Crystals, Vol. 12, pp 103-119
- Slack G.A., Chrenko R.M., 1971: Optical absorption of natural garnets from 1000 to 30,000 wavenumbers. Journal of the Optical Society of America, Vol. 61, No. 10, pp. 1325- 1329.
- Stockton C.M., Manson D.V., 1982: Gem Quality Grossular Garnets, Vol. 2, No. 4, pp. 204-213
- Stockton C.M., Manson D.V., 1985: A proposed new classification for gem-quality garnets. Vol. 21, No. 4, pp. 205-218

Acknowledgements

Authors thank Mr. N. Sharma for his help to procure the samples. Authors express gratitude to the technical staff of National Chemical Laboratory, of Dept. of Geology, University of Pune and of Pangemtech for carrying out the analyses.

Hurlbutite from Myanmar

Denis Gravier[1], Aurélien Delaunay[2], Julien Boemo[3], Jean-Marie Arlabosse[4], Emmanuel Fritsch[5], Stefanos Karampelas[2,6]

[1] Gravier & Gemmes, Poncin, France
[2] Laboratoire Français de Gemmologie, LFG, 30 rue de la Victoire, 75009 Paris, France, a.delaunay@lfg.paris
[3] GemForest, Lot, France
[4] Nuvisan, Sophia Antipolis, France
[5] Institut des Matériaux Jean Rouxel (IMN), Université de Nantes & CNRS, Nantes, France
[6] School of Geology, Aristotle University of Thessaloniki, 54124, Thessaloniki, Greece

A crystal of the very rare mineral hurlbutite $CaBe_2(PO_4)_2$ originating from Myanmar (without further locality details) was studied and faceted afterwards in two gems, which we also studied. This specimen is of particular interest because the species rarely produces well-formed crystals, but rather masses or globules (spherulites; Mindat, 2025). The crystal is a near-colorless, short lozengic prism, measuring approximately 17 x 10 x 7 mm and weighing about 2 grams. It is naturally etched, with few inclusions visible through the frosted surface, and a dissolved dislocation near the broken base. The ultraviolet (UV) luminescence is weak, greenish white in longwave, and weak orange in shortwave UV. The rough was faceted into two stones, a 0.64 ct round brilliant cut and a 2.56 ct rectangular scissor cut (RSC; Figure 1).

Figure 1: The rough hurlbutite crystal (height about 17 mm), and the two fashioned gems, a 2.56 ct rectangular scissor cut and a 0.64 ct round brilliant cut. Photos LFG

The refractive indices measured on the faceted stones are $n\alpha = 1{,}593$, $n\beta = 1{,}600$ and $n\gamma = 1{,}606$, close to values provided in the original description $n\alpha = 1.595(3)$ $n\beta = 1.601(3)$ $n\gamma = 1.604(3)$ (Mrose, 1952). It is optically biaxial negative. The specific gravity measured by the hydrostatic method is 2,88 compared to 2.877(5) (measured: Mrose, 1952) and 2.90 (calculated) (Mindat).

To verify the exact nature of this rare gem, on which very limited literature is available, we combined Raman scattering with X-ray diffraction and chemical analysis using Energy Dispersive X-ray Fluorescence (EDXRF).

The Raman scattering was obtained on a Renishaw InVia Raman microscope with a 514 nm laser and a 4 cm^{-1} resolution. The main peak is that of phosphates, at about 1017 cm^{-1} (Figure 2). The patterns obtained on the rough and the two faceted gems match both RRUFF references R070612 (from Finland) and R090048 (from the type locality in the USA).

Powder X-ray diffraction was performed on a D6 Phaser de Bruker, with a copper anode, a 30 kV voltage and a 18 mA current, on ground fragments remaining from the cutting process. The diffractogram obtained in the 5 to 90° 2θ angle range matches hurlbutite references in RRUFF and the Crystallography Open Database (COD).

The semi quantitative chemistry on the rough and afterwards on the faceted stones using EDXRF was measured on a ThermoScientific QUANTX. As expected from the chemical formula, calcium and phosphorus are responsible for the strongest signals, confirming identification indirectly. The main impurity is strontium (Sr) known to substitute for Ca. Additionally minor Mn, Pb, Al, Si and S were detected. The beryllophosphate hurlbutite is typical of the pegma-

titic environment; Two of its components, beryllium and phosphorus, are generally found concentrated in pegmatitic fluids. In its original occurrence, Chandlers Mill Quarry, Newport, New Hampshire, USA, hurlbutite appears in a complex granitic pegmatite (Mrose, 1952).

Photoluminescence (PL) excited at 514 nm (RSC 2.56 ct) shows a broad band centered about 580 nm (greenish yellow) extending from about 500 to 650 nm, and a more intense one with apparent maximum about 737 nm in the red and near infrared (Figure 3). The 580 nm band may correspond to the greenish white emission observed in LWUV. There are in addition a few sharp lines at 543 nm, as well as a group at 854, 859, 869, 874, 886 nm, possibly caused by trivalent rare earth elements ions (REE^{3+}).

To our knowledge, there was no existing description of hurlbutite as a gem material in the literature before our contribution. We were able to confirm properties from the mineralogical references and gather some gemological properties, which are awaiting confirmation if another gem-quality hurlbutite is found.

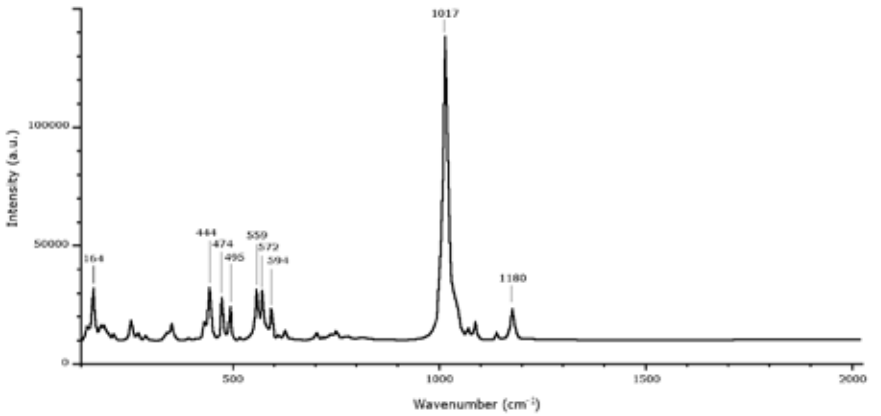

Figure 2: Raman spectra of the hurlbutite crystal. Vertical scale arbitrary.

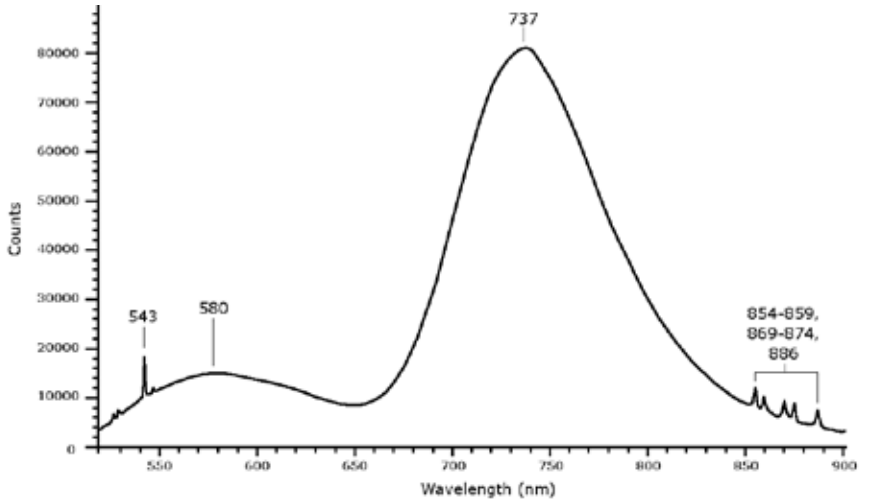

Figure 3: Photoluminescence spectrum of the 2.56 ct hurlbutite excited with a 514 nm laser at room temperature, from 500 to 900 nm. Vertical scale arbitrary.

References:

- Mrose, M., 1952. Hurlbutite, $CaBe_2(PO_4)_2$, a new mineral. American Mineralogist, 37, 931–940.
- Mindat https://www.mindat.org/min-1953.html (consulted 04-2025)

A convincing glass imitation of larimar (pectolite)

Gagan Choudhary
IIGJ-Research & Laboratories Centre, Jaipur, India; gagan.choudhary@iigjrlc.org

Larimar, a massive blue variety of the mineral pectolite ($NaCa_2Si_3O_8(OH)$), belonging to the wollastonite group of minerals is known in the trade for few decades now. However, in recent times it has gained popularity amongst jewellery designers and consumers, as suggested by high frequency of submissions at the laboratory for certification. Originating only from the Dominican Republic, its striking blue colour with light blue to white waves or web like patterns caused by the spherulitic growth has made larimar a sought-after gemstone.

With increasing popularity, larimar has been subject to imitation by various materials, including ceramics (Kiefert and Groenenboom 2013) and naturally dyed stones such as chalcedony (Miura, 2020). Similar man-made ornamental materials were produced as early as the 1950s, including the well-known 'Victoria Stone' (Renfro, 2017).

The present author has examined numerous specimens of translucent to opaque partly devitrified glass submitted to the laboratory, many of which closely resemble larimar in both appearance and colour—making them convincing imitations. These materials are reportedly being presented as larimar at both online and offline platforms. This study documents the gemmological characteristics of this glass imitation of larimar encountered at the laboratory over the past one and a half years, sourced from a local gem dealer.

Results and Discussion

Visual appearance

Rough samples, slices, and polished cabochons of both larimar and the larimar imitation were selected for this study. Majority of larimar as well as imitation samples were opaque, however, using strong fibre optic light few sections appeared translucent. Larimar specimens exhibited colours ranging from blue to greenish blue, with characteristic white web-like patterns (Figure 1, left). In comparison, the larimar imitation (partly devitrified glass) samples ranged from greenish blue to bluish green and displayed similar white webbing, particularly evident in sliced sections (Figure 1, right). In cabochon form, the imitation samples often featured a darker central core surrounded by a radiating fibrous and whitish zone. This fibrous zone also exhibited a noticeable sheen or chatoyant effect.

Cross-section of rough imitation samples displayed radiating fibrous structure typically associated with spherulitic growth, while the outer surface (crust) had a transparent glassy layer with botryoidal pattern (Figure 2, left and right).

Properties

Gemmological properties of the studied samples of larimar and larimar imitation are summarized in Table 1.

Raman spectroscopy was performed on larimar and larimar imitation samples using a 532 nm excitation laser, covering the spectral range of 100–2000 cm^{-1} (Figure 3). The larimar samples exhibited a rising background absorption from 200 to 2000 cm^{-1}, attributed to fluorescence, with major peaks observed at approximately 651and 1025 cm^{-1}, along with smaller features at ~317, 375, 413 and 970 cm^{-1}.

The opaque or crystalline areas of the imitation samples displayed a consistent spectral pattern across multiple spots, characterized by major peaks at approximately 635 and 970 cm^{-1}, and additional smaller or broader features at ~331, 413 and 1042 cm^{-1}. Interestingly, few features such as ~413 and 970 cm^{-1} were present in spectra of both, larimar and crystalline areas of imitation samples suggesting a similarity in composition and structure. Raman spectra of crystalline areas of the imitation were consistent with that of wollastonite given in the RRUFF database and elsewhere (e.g., Hänni *et al*., 2001). Peak at ~970 cm^{-1} is present as

the major feature in glass, while present only as a weak feature in pectolite. Further, the peak at ~635cm^{-1} present in glass shifts to peak at 651cm^{-1} in larimar, while the peak at 1025cm^{-1} present in larimar shifts to 1042cm^{-1} in the devitrified glass. In contrast, the transparent glass crust of the larimar imitation exhibited broad bands in the ranges of approximately 370–620 cm^{-1} and 800–1100 cm^{-1}, consistent with the spectral signature typical of amorphous glass.

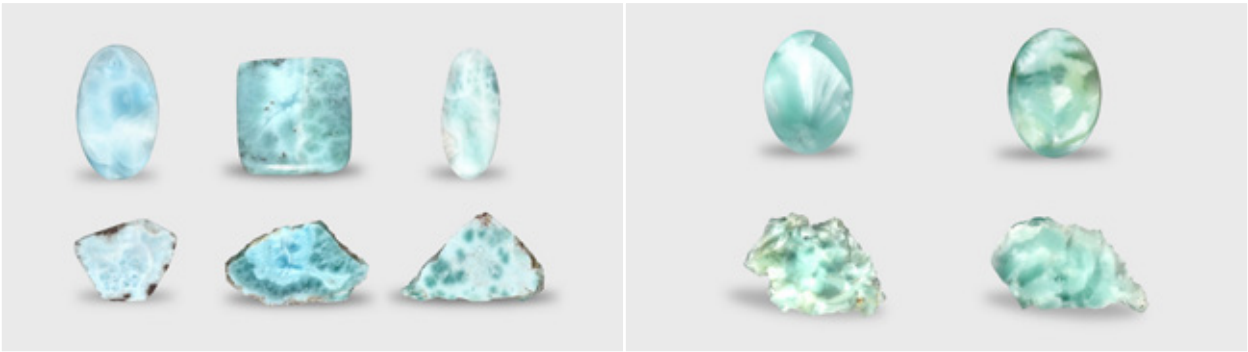

Figure 1: Representative cabochon and sliced rough samples of larimar (left) and glass imitation (right), displaying a close resemblance in colour—ranging from greenish blue to bluish green—and white web-like patterns. The left cabochon in glass (right image) also exhibits a notable sheen effect due to fibrous inclusions. Photos by G. Choudhary.

Figure 2: Rough sample of devitrified glass showing an opaque radiating pattern originating from a central core and terminating in circular edges, indicative of spherulitic growth (left).
In contrast, the surface or crust of the same sample exhibits a transparent, glassy layer with a botryoidal pattern (right).
Photos by G. Choudhary.

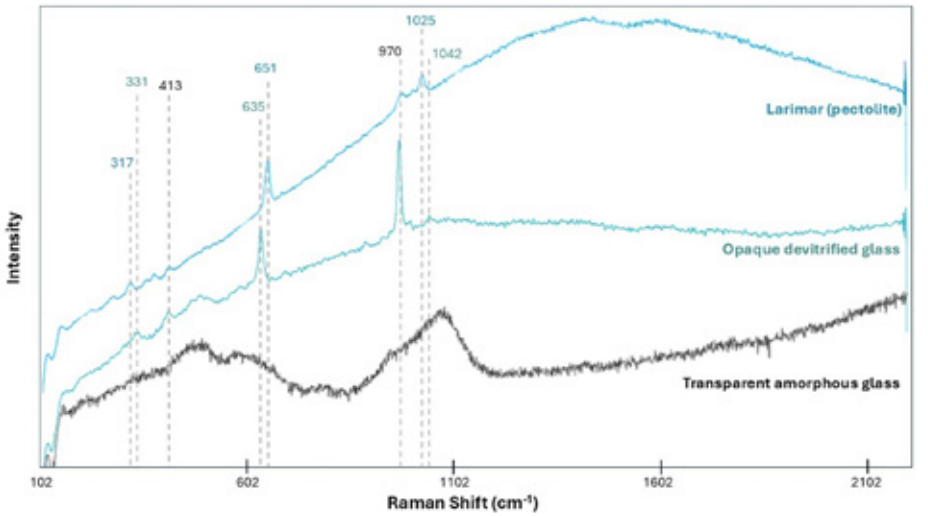

Figure 3: Raman spectra of larimar (blue), opaque devitrified glass (blue-green), and amorphous glass matrix (black).

Property	Larimar	Larimar imitation
Colour	Blue to greenish blue; white webbing	Greenish blue to bluish green; white webbing
Diaphaneity	Opaque under standard lighting; few sections translucent under fibre optic light	Opaque under standard lighting; few sections translucent under fibre optic light. Top surface transparent.
RI	~1.60 (spot); distinct birefringence blink ranging from ~1.58 – 1.62	~ 1.49 (spot); no birefringence blink
SG (hydrostatic)	2.83 – 2.87	2.54 – 2.58
UV Fluorescence	Moderate to distinct yellowish green in shortwave; inert under longwave	Weak yellowish green in shortwave; inert under longwave
EDXRF analyses	Major: Ca, Si, Al, Na, Mg Minor: Cu, Fe, Mn, K Traces: V, Sr, Zn, Ti, Ni	Major: Si, Ca, Al, Na, K, Fe, Mg Minor: Ti, Zr, Traces: Sr, Rb, W, Mn, Sn, Zn, Pb
Raman analyses	Major peaks: ~651 and 1025 cm^{-1} Weaker features: ~317, 375, 413 and 970 cm^{-1}	Crystalline areas Major peaks: ~635 and 970 cm^{-1} Weaker features: ~331, 413 and 1042 cm^{-1} Amorphous areas (glass crust) Broad bands in the range ~370-620 and 800-1100 cm^{-1}

Microscopic examination

The larimar imitation samples exhibited fine fibrous inclusions (Figure 4) arranged in a radiating pattern originating from distinct cores. In several specimens, multiple such cores were present, resulting in a botryoidal or spherulitic appearance. These fibrous inclusions often produced a sheen effect, contributing to the visual similarity with natural fibrous minerals. The inclusions themselves were colourless, showed well-defined growth striations along their lengths, and displayed fine cracks reminiscent of cleavage features commonly observed in minerals with prominent cleavage perpendicular to the crystallographic c-axis.

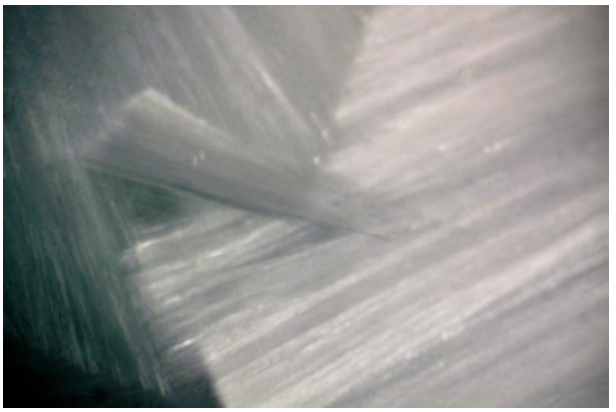

Figure 4: Fine, tightly packed, intergrown fibrous crystals arranged in a radial to subparallel pattern in opaque areas of glass-imitation of larimar. Photomicrograph by G. Choudhary; image width 5.08mm

Similar lath-like crystals in a glass matrix have previously been reported to be wollastonite (Hänni *et al*., 2001) or apatite (Renfro, 2017), tanohataite and cristobalite (Fayed *et al*., 2025). However, Raman spectroscopic analysis of the inclusions in the present study was consistent with that of wollastonite.

Conclusions

The described partly devitrified glass serves as a convincing imitation of larimar (pectolite) due to its similar webbing pattern and visual appearance, which may potentially mislead gemmologists and gem dealers. However, standard gemmological properties, including RI and SG, allow for easy distinction between partly devitrified glass and larimar, supplemented by Raman spectroscopy and chemical analysis. These imitations typically show higher concentrations of Si and Al, and lower Ca content compared to larimar. Additionally, the presence of coarse, needle-like microscopic structures resulting from devitrification provides further diagnostic evidence for separation. Although the identification and separation of this partly devitrified glass are not particularly challenging, raising awareness about its existence is crucial to prevent misidentification in the gem trade.

References:

- Fayed M.G., Abdel Ghany A.E., El-Tawi R.S., Hashem A.H., Hamzawy E., El-Bassyouni G.T., Mohamed S.G., 2025. Devitrified silica minerals glass of tanohataite ($LiMn_2Si_3O_8F$) mineral as anode material for lithium-ion batteries. Ceramics International, 51(1), 401-410
- Hänni H.A., Tien S., Xingqiang Y., Wen-Po T., 2001. A glass imitation of blue chalcedony. Journal of Gemmology, 27(5), 275-285
- Kiefert L., Groenenboom P., 2013. Imitation larimar. Gems & Gemology, 49(2), 124
- Miura M., 2020. Quench-Crackled Dyed Blue Chalcedony Resembling Larimar. Gems & Gemology, 56(2), 281-283
- Renfro N., 2017. Colorful Chatoyant Glass. Gems & Gemology, 53(2), 256-257

Bertrandite in Emeralds

Shane F. McClure
Global director of colored stone services
Gemological Institute of America, Carlsbad, CA, USA, smcclure@gia.edu

Over the past few years we have been seeing more and more lower quality stones in the lab. The reasons for this may be related to lack of supply of finer goods, rising prices, the global pandemic or others. Among these lower quality stones have been large numbers of heavily included emeralds (Figure 1).

We began to notice that a number of these emeralds were highly fractured with the fractures being very low relief. They appeared to be filled with a clarity enhancing substance and for a while were treated as such. However, we noticed that there were differences between these fractures and ones we knew to be filled with polymers to enhance the clarity of emeralds.

When testing for clarity enhancement, we look for certain clues. These include flash effect, high relief unfilled areas, gas bubbles, UV fluorescence, sweating of filler out of the fractures, polymers in the FTIR spectra and more. We use these indications to support the conclusion that there is a filler present and it is affecting the appearance of the stone. However, it is possible that many of these things may not be present in a given stone. So the lack of these indications in suspicious looking fractures can make it challenging to decide if a stone is clarity enhanced or not.

For the emeralds in question what looked like a filler in many of them did not show bubbles or unfilled areas, did not have a flash effect or UV fluorescence of any indication of polymer int the FTIR. The fractures sometimes appeared brownish when viewed down the length of the fracture (Figure 2) and also sometimes showed interference colors when viewed under crossed polaroids. Sometimes there was an irregular structure within the fractures that resembled a roiled effect.

Many of these fractures are very narrow but some get wide enough that the material in them can be seen at the surface. The luster of this material is somewhat different than the host emerald and often slightly undercut, indicating that it is softer than the emerald (Figure 3). Raman analysis came up with a match for two minerals – some phlogopite but mostly a beryllium mineral called bertrandite.

Figure 1: An example of a heavily included emerald that contains bertrandite filled fractures. 1.82 carats.

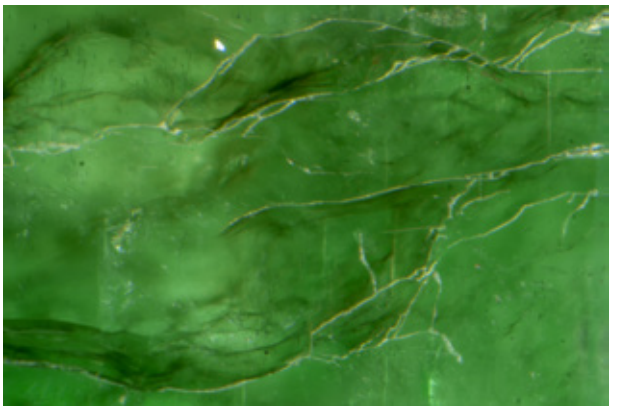

Figure 2: Fractures filled with bertrandite sometimes look brownish when viewed down the length of the fractures. Photomicrograph by Chandler Powers, field of view 1.83 mm

Phlogopite is fairly common in emeralds from a number of localities but typically as an inclusion, not as a filler in fractures. Bertrandite, while commonly associated with beryl in some environments, has been mentioned a few times as an inclusion in emerald, but we could only find one reference of it filling fractures.

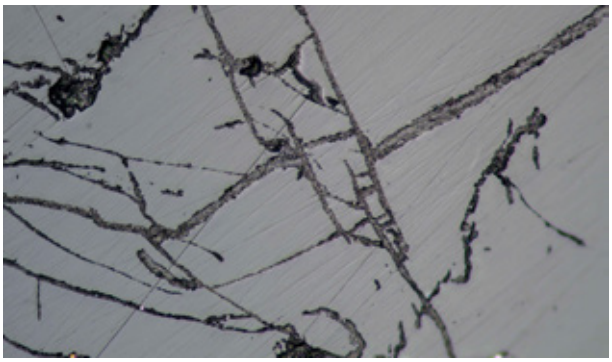

Figure 3: Extensive fracture system with bertrandite showing different surface luster and slight undercutting. Photomicrograph by Nathan Renfro, field of view 0.72mm

A search of the literature revealed a note by Zellagui (2022). In this article he documented an instance where they identified a wide fracture system in an emerald with bertrandite and phlogopite filling it. He showed the bertrandite along the edges of the fractures with the phlogopite filling the middle.

In our experience we have not yet seen an example where there was a clear difference in surface luster in a single fracture which might indicate both minerals being present. This could possibly be attributed to the width of the fractures we have observed being narrower than the example mentioned in the note.

In an attempt to see if we could identify the presence of bertrandite in these fractures in the FTIR spectra we found that in some cases the two strongest peaks in the FTIR spectrum of bertrandite showed up as tiny broad peaks at approximately 6981 and 6930 cm^{-1} within the emerald spectrum (Figure 4). Unfortunately these peaks are often too weak to be visible even though spectra were run in multiple directions.

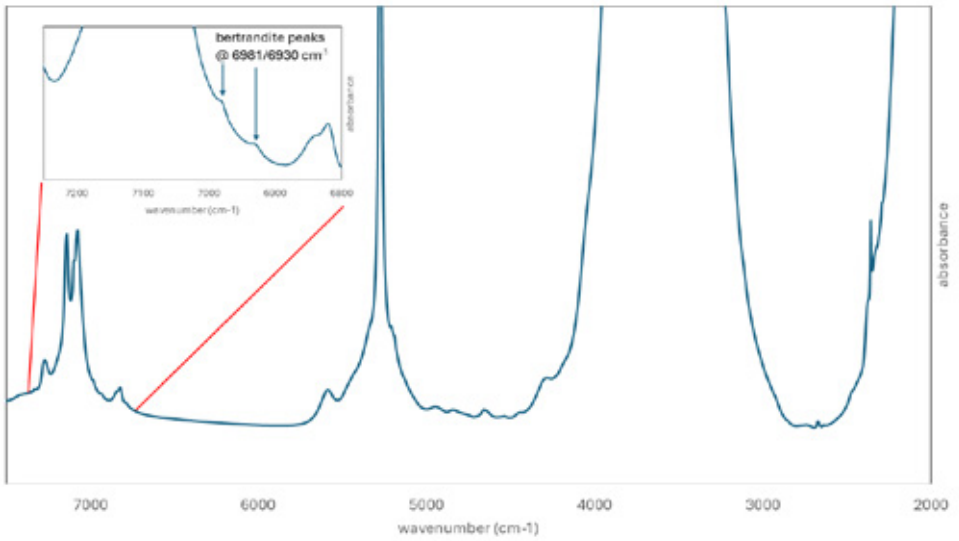

Figure 4: FTIR spectrum of an emerald showing two small bands at 6981 and 6930 cm^{-1} indicating the presence of bertrandite in this stone.

Bertrandite is a beryllium silicate - $Be_4(Si_2O_7)(OH)_2$ - that Mindat.org describes as "a common hydrothermal alteration product of beryl". It has an R.I. of approximately 1.59 – 1.61, which explains why fractures filled with it in high iron emeralds have such low relief. It is said to commonly replace beryl, often with a sheet silicate such as mica taking up the aluminum content of the beryl (Barton 1986). This could explain the detection of phlogopite in association with the bertrandite in fractures.

Most references discuss the formation of bertrandite in pegmatites, although there is some mention of it forming in non-pegmatitic environments (Barton,and Young, 2002). It is one of the last minerals to form in such pegmatites and requires water vapor to be present to form (Jacobson, 1988). Theoretically this could explain how bertrandite could form in the open fractures of a beryl crystal.

So, if all the fractures present in an emerald are filled with another mineral, then the stone has not been clarity enhanced and we have seen quite a few stones where this was the case. However, we also have seen quite a few where some fractures were not filled with a mineral and these fractures were usually filled with a polymer. We have seen both oil and artificial resin that exhibited the properties we would expect from such fillers, such as flash effect with the artificial resin. These fractures fluoresce weakly while all the other fractures filled with bertrandite do not fluoresce at all. The polymers show up in the FTIR. The challenge then becomes trying to separate which fractures are filled with what and how much that is affecting the appearance of a stone.

At this point in time, the origin of these stones is still unclear. The people submitting the stones to the lab say they do not know the origin. In comparing the chemical plots against known samples from the GIA reference collection, some of these stones are similar to samples originating in Russia, while others are similar to Zambia. However, all of the stones containing bertrandite look very similar to one another, so we are convinced that they are coming from the same locality.

References:

- Barton, M.D. 1986, Phase equilibria and thermodynamic properties of minerals in the BeO-Al_2O_3-SiO_2-(BASH) system, with petrologic applications, American Mineralogist, 71, 277-300
- Barton, M.D. and Young, S. 2002, Non-pegmatitic deposits of beryllium: Mineralogy, geology, phase equilibria and origin. In Grew, E.S. (ed) Mineralogical Society of America, Washington DC, USA 591-692
- Jacobson, M.I. 1988, Mount Antero sings the blues: Some beryl discoveries of note which exhibit offkey mineral association, Conference paper, Friends of Mineralogy 9th symposium on beryl – paragenesus and descriptive mineralogy, Tucson Gem and Mineral show, 14 February, 1988
- Zellagui, R. 2022, Emerald with bertrandite – phlogopite veins resembling fracture fillings, The Journal of Gemmology, 38(3) 216-217

Found, Lost, and Found Again: The Geological and Gemological Significance of the Salininha Emerald Deposit, Brazil

Rainer Alois Schultz-Güttler[1], Andressa Roberta Borotti[2], Ivan Pereira Marques[3], André Luiz Silva Pestilho[4]

[1] University of São Paulo, Rua do Lago 562, São Paulo, Brazil, rainersgut@gmail.com

[2] A Gemmologist, Travessa Dona Paula 13, São Paulo a.gemmologist@gmail.com

[3] Geological Survey of Brazil, Rua Costa 55, São Paulo, Brazil, ivan.marques@sgb.gov.br

[4] University of São Paulo, Rua do Lago 562, São Paulo, Brazil, andrepestilho@usp.br

Abstract

The Salininha emerald deposit (Figure 1), located in the municipality of Pilão Arcado, Bahia State, represents the first economically significant discovery of gem-quality emeralds in Brazil (Sauer 1982; 1992). Upon its recognition, controversy arose among specialists who questioned the classification of the Salininha crystals as true emeralds due to the predominance of vanadium, rather than chromium, as the chromophore element. The deposit was mined out after approximately one year of extraction (Sauer 1992) and subsequently abandoned. Currently, there are efforts underway to resume exploration activities in the region, with new material being extracted. Geologically, the occurrence is situated within the domain of deformed granitic rocks, which locally preserve remnants of metatexites, diatexites, and metabasalts that were not fully digested by granitization (Souza *et al.* 1979). These remnants can be interpreted as Archean granite-greenstone complex, later intruded by Paleoproterozoic granitoids, and deformed at ~2 Ga. in the events of the Transamazonian orogeny (Hurley *et al.* 1967). The emeralds are hosted within a talc-schist lens approximately 100 meters long and 50 meters thick, which is intruded by pegmatoid veins (Souza *et al.* 1979). In the samples analyzed, the emerald crystals grew over the meta-ultramafic host rock, showing no structural alignment with the main foliation of the talc-schist (Figure 2A). Micro-Raman spectroscopy was conducted on rough crystals and their inclusions, revealing the presence of talc and calcite. The inclusions in emeralds are also preferentially aligned with this foliation and are interpreted as relicts of the meta-ultramafic protolith, which likely served as the source of vanadium. The emerald crystals exhibit a flattened hexagonal prismatic habit and vary in color from very light to light yellowish green (Figure 2B and Figure 2C), with pleochroism ranging from yellowish green to bluish green. Additionally, the analyzed crystals exhibit no fluorescence under UV light and display a stable green color when observed through the Chelsea filter, consistent with vanadium-based coloration. They exhibit specific gravity values ranging from 2.67 to 2.75 g/cm³ (measured in rough material) and refractive indices from Ne = 1.588 to No = 1.595 (measured in faceted samples from the same locality - Figure 2D). Given the absence of deformation in the emerald crystals, the mineralization is attributed to a metasomatic process similar to that observed in the Campo Formoso emerald district, located ~300 km to the southeast. In Campo Formoso emeralds are hosted in metavolcano-sedimentary sequences of Greenstone affinity, tectonically inserted into the granitic rocks of the Archean basement, sometimes intruded by younger granitic rocks. The emeralds crystallized within discordant pegmatitic veins and adjacent metasomatic zones under moderate temperature and pressure conditions, without direct genetic association with the nearby granitic intrusions (Capovilla 1995). The Salininha deposit not only marked the inception of Brazil's prominence in the global emerald market but also contributed significantly to the understanding of vanadium-induced coloration mechanisms in beryl. Its geological setting, characterized by the metasomatic transformation of meta-ultramafic rocks and the crystallization of emeralds within discordant pegmatitic veins, provides valuable insights into emerald genesis in greenstone-related environments. Renewed geological and mineralogical investigations can highlight the potential to identify new emerald occurrences in the Salininha area and its surroundings.

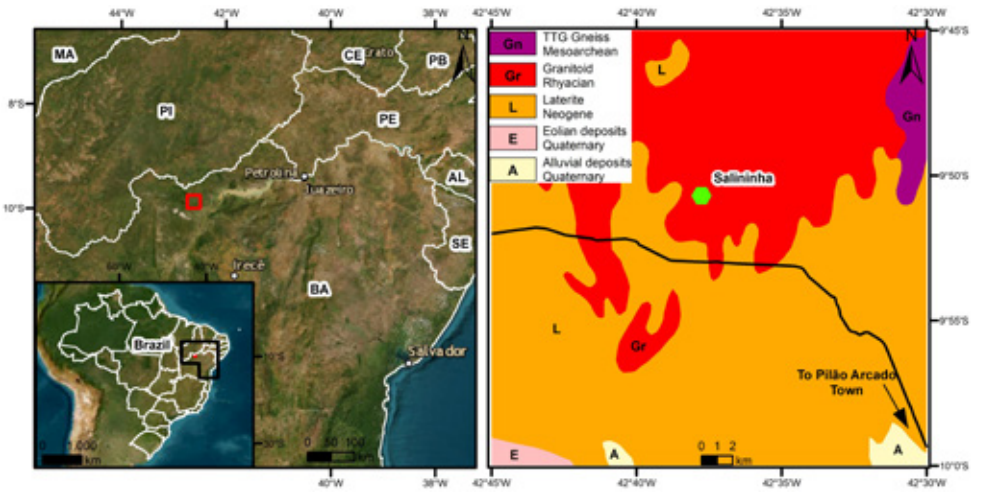

Figure 1: Location and geological map of the Salininha mine area. The geological mapping was modified from Souza *et al.* (2003)

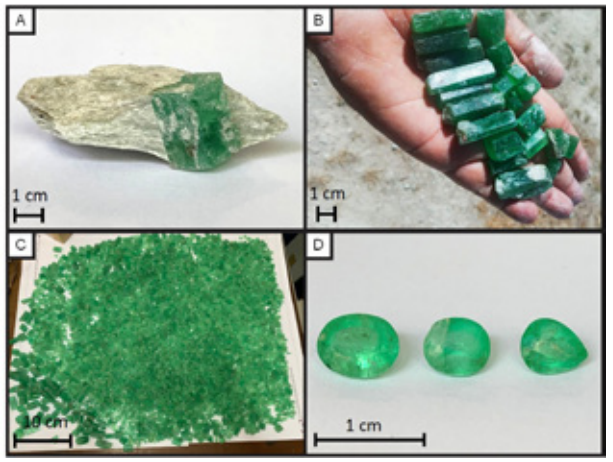

Figure 2A: Emerald crystal from Salininha overgrowing the foliated talc-schist, with the main foliation of the sample lying horizontally in the image. Figure 2B: Artisanal miner (garimpeiro) holding rough emerald crystals. Figure 2C: Lot of rough emeralds including both small and large crystals. Figure 2D: Faceted emerald crystals displaying a light green color.

References:

- Capovilla, Maria Manuela Galvão Monteiro. 1995. "Aspectos petrogenéticos e metalogenéticos das jazidas de esmeraldas de Carnaíba e Socotó, BA." Text, Universidade de São Paulo. https://doi.org/10.11606/D.44.1995.tde-28102015-102127.
- Hurley, P. M., F. F. M. de Almeida, G. C. Melcher, U. G. Cordani, J. R. Rand, K. Kawashita, P. Vandoros, W. H. Pinson, e H. W. Fairbairn. 1967. "Test of Continental Drift by Comparison of Radiometric Ages". *Science* 157 (3788): 495–500.
- Sauer, Jules Roger. 1982. *Brasil: Paraíso de Pedras Preciosas*. Rio de janeiro, RJ, Brazil: Gráfica JB S.A.
- ———. 1992. *Die Welt der Smaragde*. Rio de Janeiro, RJ, Brazil: Jules Roger Sauer.
- Souza, João Dalton de, Roberto Campelo de Melo, e Marília Kosin. 2003. "Mapa geológico do estado da Bahia". Map. CPRM. http://rigeo.sgb.gov.br/jspui/handle/doc/8665.
- Souza, João Dalton de, Leo Rodrigues Teixeira, Ivo Figueroa, Roberio Ribeiro de Azevedo, Newton Macedo Barral, Ivanaldo Vieira Gomes da Costa, Edgard Lázaro de Andrade Filho, Rui Boni D'Araujo e Oliveira, e Jane Nobre Lopes. 1979. "Projeto Colomi. Geologia e prospecção geoquímica da região de Remanso - Sento Sé: relatório final". Technical Report. CPRM. http://rigeo.sgb.gov.br/jspui/handle/doc/9193.

Acknowledgements

We would like to thank the Laboratory of Fluid Characterization in Geological Systems (GeoFluid), of the Institute of Geosciences of the University of São Paulo for the micro-Raman analyses.

Automated Data Processing of Raman Spectra for Supporting Spinel Origin Determination

Tasnara Sripoonjan[1,2], Montira Seneewong Na Ayutthaya[3], Sirinapa Saengdech[3], Sutas Singbamroong[4], Alongkot Fanka[2]

[1] G-ID Laboratories, Yan Nawa, Bangkok 10120 Thailand; *tasnara@hotmail.com

[2] Department of Geology, Faculty of Science, Chulalongkorn University, Bangkok 10330 Thailand

[3] The Gem and Jewelry Institute of Thailand (Public Organization), Bangkok 10500 Thailand

[4] Dubai Central Laboratory Department, Dubai Municipality, Dubai, UAE

Keywords: Spinel, Raman spectroscopy, provenance, automated data processing, origin determination, machine learning

Introduction

Spinel is a highly valued gemstone, with its color and quality influenced by trace-element chemistry and crystal structure. Accurate determination of its geographic origin is crucial for gemmological authentication, scientific research, and maintaining supply-chain integrity. Raman spectroscopy provides a non-destructive analytical approach, offering vibrational fingerprints that reflect both the crystal lattice and impurity-related features. However, manual interpretation is time-consuming and susceptible to operator bias, particularly when dealing with large datasets or subtle spectral variations. To address these challenges, we present an end-to-end automated pipeline that integrates spectral preprocessing, feature extraction, and chemometric analysis. Machine learning (ML) models are then applied to classify spinel samples according to their geographic origin. The performance of this approach is demonstrated using both red and blue spinels from three major deposits.

Materials and Methods

A total of 315 spinel samples (Figure 1) were sourced from local, trusted dealers and verified by gemmological means. Red spinel ($MgAl_2O_4$; n = 154) originated from Mogok (Myanmar), Luc Yen (Vietnam) and Lukande (Tanzania), while blue samples (n = 161) comprised spinel ($MgAl_2O_4$) from Luc Yen and Lukande and gahnite (ideally $ZnAl_2O_4$; n = 52) from Jemaa (Nigeria). Each sample was polished to present at least one flat surface for Raman analysis. Raman spectra were collected on a confocal Renishaw inVia Raman microscope equipped with a 50× objective (NA 0.50) using a 785 nm excitation laser. Three accumulations of 10s each were acquired over 200–1000 cm^{-1} with 1 cm^{-1} spectral resolution, conditions verified to avoid local heating (no peak drift between successive scans). Raw spectra were exported as CSV files and processed via the automated data processing pipeline.

Figure 1. Representative spinel samples used in this study, with weights ranging from 0.37 to 2.70 carats. (Photo by M. Seneewong Na Ayutthaya)

Automated Data Processing Pipeline

Our data-processing pipeline was implemented in Python 3.12 and proceeds as follows. First, Raman spectra are smoothed using a Savitzky–Golay filter (window length 7, polynomial order 3) to suppress high-frequency noise while preserving peak shapes. The smoothed spectra are then baseline-corrected via Asymmetric Least Squares (ALS) algorithm with $\lambda = 10^7$ and $p = 0.01$, followed by max-normalization (I/Imax) to remove intensity scale effects. Next, we isolate the four vibrational bands at 310, 405, 665, and 765 cm^{-1} and fit each with a Lorentzian profile (accepting fits only if $R^2 \geq 0.95$) to extract the full width at half maximum (FWHM). The resulting FWHM values, together with two dimensionless ratios (e.g., 405/665 and 405/765), are assembled into feature vectors and visualized in bi-scatter plots to assess natural clustering by geographic origin. Finally, we train both an artificial neural network (ANN) and a random forest (RF) models using 10-fold cross-validation and a 20% held-out test set (red spinel n = 28; blue spinel n = 30), optimize hyperparameters by grid search, and report overall accuracy, macro F1-score, and mean cross-validation accuracy (mean CV).

Results and Discussion

The full dataset of 315 spectra was processed on a MacBook Pro (M1 Pro, 16 GB RAM) in 149 seconds, averaging 0.47 seconds per spectrum. FWHM-based plots reveal well-defined clusters corresponding to geographic provenance. For red spinel, plotting the FWHM of the 405 cm^{-1} band against that of the 665 cm^{-1} band distinguishes samples from Myanmar (MM), Vietnam (VN), and Tanzania (TZ), though some overlap occurs between MM and VN. In blue spinel ($MgAl_2O_4$), the 405 cm^{-1} and 665 cm^{-1} modes are decisive. Nigerian gahnite ($ZnAl_2O_4$) occupies a distinct field due to homologous peak shifts to approximately 415 cm^{-1} and 657 cm^{-1}. Applying adaptive fitting windows of ±10 cm^{-1} further isolates gahnite without disturbing the true-spinel clusters (Fig. 2). While gahnite is also distinguishable from blue Mg–Al spinels by RI, SG, and Zn-rich chemistry, Raman provides a complementary method, especially for small or mounted stones. These FWHM shifts likely reflect variations in A–B site inversion and mass-related frequency shifts from Mg^{2+} substitution with heavier Zn^{2+} (Malavasi *et al*., 2002; Wang *et al*., 2020). Additionally, the separation—and remaining overlap—between TZ and VN blue spinels may be influenced by Fe/Co variations affecting site distortion (Furuya, 2023). Classification models trained on FWHM features performed strongly, as summarized in Table I. Confusion matrix analysis indicates most misclassifications occurred between MM and VN red spinels, and between TZ and VN blue ones, reflecting partially overlapping geological and chemical characteristics (Chauviré *et al*., 2015; Chankhantha *et al*., 2020; Krzemnicki *et al*. 2023, Wu *et al*., 2023). Overall, these findings demonstrate that deposit-specific FWHM features provide an effective foundation for automated, machine learning–based provenance determination of spinel.

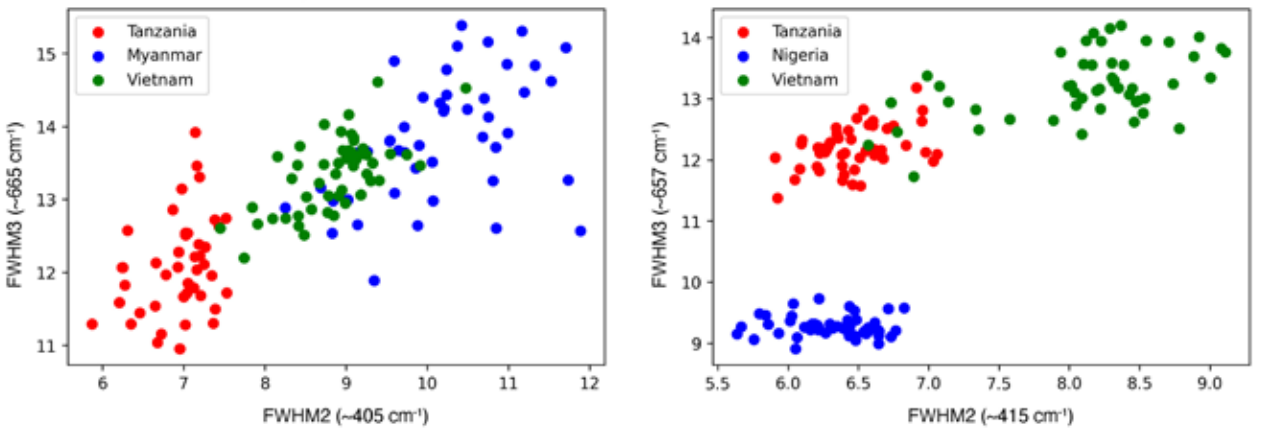

Figure 2. Scatter plots illustrating FWHM-based feature distributions for classification: (left) red spinel samples from Myanmar, Vietnam, and Tanzania; (right) blue spinel (Vietnam, Tanzania) and gahnite (Nigeria).

Dataset	Model	Accuracy	Macro F1	Mean CV	Misclassified samples
Red spinel	ANN	93	93	89% ± 6.6%	2/28: (1MM→VZ, 1VN→TZ)
	RF	93	93	88% ± 7.1%	2/28: (1MM→VZ, 1VN→TZ)
Blue spinel & gahnite	ANN	97	97	95% ± 4.0%	1/30: (1VN→TZ)
	RF	93	94	96% ± 4.1%	2/30: (2VN→TZ)

Table I Performance summary of ML models applied to red and blue spinel classification

Conclusion

We present an automated, high-throughput workflow for Raman spectral processing and provenance classification of blue and red spinel. By using FWHM of key vibrational bands as features, the pipeline captures subtle lattice variations associated with geographic origin. This approach achieves over 90 % classification accuracy on the current dataset and significantly reduces analysis time, enabling scalable and reproducible gemmological assessments. The strong performance of FWHM-based features highlight their sensitivity to crystallographic disorder and trace-element chemistry—factors that are critical for provenance differentiation. Building on these results, future work will expand the geographic diversity of the spinel dataset and extend the pipeline to a broader range of gemstone species.

Limitations and Outlook

The current model is calibrated using a limited set of deposits; incorporating additional localities will likely introduce greater spectral variability, necessitating model retraining or, at minimum, site-specific recalibration. Broader datasets may also increase class overlap, which could complicate cluster separation and reduce classification accuracy. Furthermore, heating above ~800 °C has been shown to broaden the same Raman bands (Saeseaw *et al*., 2009) used for provenance discrimination, potentially obscuring geographic signals. As a result, Raman-based FWHM classification should be integrated with complementary techniques—such as trace-element analysis—to disentangle provenance from heat treatment effects and establish a more robust, multimodal framework for origin determination.

References:

- Chankhantha, C., Amphon, R., Rehman, H.U., and Shen, A.H. 2020. Characterisation of Pink-to-Red Spinel from Four Important Localities. Journal of Gemmology, 37(4).
- Chauviré, B., Rondeau, B., Fritsch, E., Ressigeac, P., and Devidal, J.L. 2015. Blue spinel from the Luc Yen District of Vietnam. Gems & Gemology, 51(1).
- Furuya, M. 2023. Cobalt spinel from Bai Buoi mine, Yen Bai, Vietnam. 37th IGC2023, Tokyo, Japan
- Krzemnicki, M.S., Leuenberger, A. and Walter, A.B. 2023. Cobalt-bearing Blue Spinel from Lukande, near Mahenge, Tanzania. Journal of Gemmology, 38(5).
- Malavasi, L., Galinetto, P., Mozzati, M.C., Azzoni, C.B., & Flor, G. 2002. Raman spectroscopy of AMn2O4 (A= Mn, Mg and Zn) spinels. Physical Chemistry Chemical Physics, 4(15).
- Saeseaw, S., Wang, W., Scarratt, K., Emmett, J.L., and Douthit, T.R. 2009. Distinguishing heated spinels from unheated natural spinels and from synthetic spinels. GIA Res. News, 13.
- Wang, C., Shen, A.H., and Liu, Y. 2020. Characterization of order-disorder transition in $MgAl_2O_4$: Cr^{3+} spinel using photoluminescence. Journal of Luminescence, 227, 117552.
- Wu, J., Sun, X., Ma, H., Ning, P., Tang, N., Ding, T., Huihuang, L., Zhang, T., and Ma, Y. 2023. Purple-Violet Gem Spinel from Tanzania and Myanmar: Inclusion, Spectroscopy, Chemistry, and Color. Minerals, 13(2), 226.

Acknowledgments

The authors sincerely acknowledge the support provided by the Gem and Jewelry Institute of Thailand (GIT) and its staff throughout the course of this research. Hub of Talents in Gem and Jewelry funded from National Research Council of Thailand is gratefully acknowledged.

Spinel from Sri Lanka - An update

Gamini Zoysa, Dietmar Schwarz, Arunas Kleismantas

Most of the spinels are found in shades of red to purple. Colourless, green and cobalt bearing varieties also been recorded in few locations. Same as other gemstones from Sri Lanka. Spinels also occur in alluvial deposits in south-western and north central parts of the island.

The following subjects will be discussed in the presentation.

1. Mineralogy and Crystallography
2. Geology and Genetic Aspects
3. Gemological and Mineralogical Properties
4. Internal Features
5. Comparison of Properties of Spinel from Different Locations from Sri Lanka (Ratnapura, Horana, Eheliyagoda, Elahera)
6. Chemical Fingerprinting
7. Spectral Fingerprinting

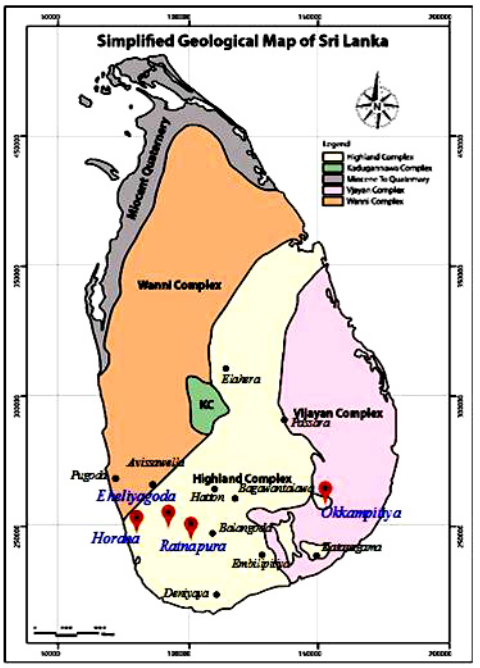

Fig. 1 - Geological map of Sri Lanka with litho-tectonic subdivisions. The locations of the spinel sampling areas used in this study are indicated.

The global distribution of spinel deposits is closely linked to collision, rift and subduction geodynamics. Spinel deposits located in marbles or in neighboring pelitic gneisses are widely known as sources of gem quality spinels. For example deposits in Myanmar, Vietnam, Afghanistan, Tajikistan, Tanzania. The formation of these deposits is explained by metamorphism of Limestones primarily contaminated by aluminous products of weathering , metasomatic transformations of terregenous layers of marble by metamorphic solution and influx of Al into marbles by endogenic solutions related to alkalic magmatism.

Fig. 2 - Orangey-brown, transparent, irregular-rounded crystal of unknown natural hosted by a Horana spinel

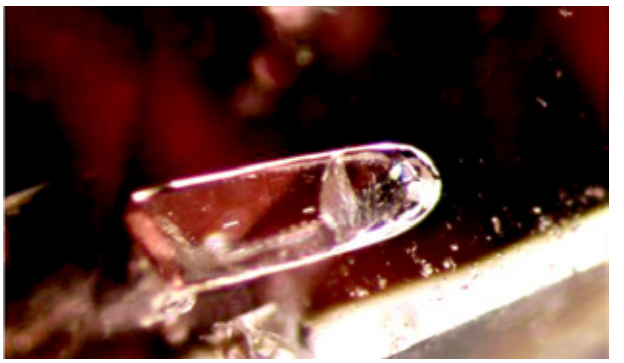

Fig. 3 - Colorless-transparent, elongated-prismatic, rounded apatite crystal.

The Importance and Methodology of Undertaking a Literature Search for Gemmological Research and Article Publishing

Brendan M. Laurs
Gem-A, Encinitas, California, USA, brendanlaurs@gmail.com

If I have seen further... it is by standing on the shoulders of giants. Sir Isaac Newton

Introduction

Performing a literature search is a very important—but often neglected—part of doing gemmological research. As indicated by Davis *et al*. (2012), "Any scientist needs to be familiar with the work that has been done in his or her area of research and with what others are doing concurrently. No scientist, however, can read all the books, articles and other printed matter related to a given area...Therefore, we need to be selective and to find the most pertinent literature on a subject as efficiently as possible and to use it effectively." A literature review should be conducted *before* starting a research project, in order to avoid "reinventing the wheel" and to keep up with the most current methods for pursuing an experiment, as well as to gather data and information critical to a proper understanding of the subject matter. A literature search involves collecting, cataloguing and evaluating information in the literature in order to determine salient works and refine the subject of one's research (Machi & McEvoy, 2022). Research findings and other scientific information can be published in books, monographs, proceedings, journals, dissertations, patents, standards, governmental bulletins or reports, and a variety of other sources.

In general, it is best to avoid using unpublished references (although in some cases a personal communication or report from a mining company etc. may be necessary to cite). As a general rule, it is also best to avoid referencing online chat groups/blogs or Wikipedia, due to variations on the quality of the information and lack of expert peer review.

Gemmological Literature Search

Gemmology poses special challenges for undertaking a literature search. Unlike other areas of earth sciences and related fields, there are no comprehensive reference tools for gemmological literature. Therefore, gem researchers will benefit from independently making their own literature collections and databases (typically composed of articles and other works in PDF and hardcopy formats). These can be organised and catalogued using reference management tools such as Endnote, Zotero, Mendeley and Papers, which also allow reference lists to be easily formatted according to numerous bibliographic style templates.

Scholarly journals (e.g. Figure 1) constitute a main source of primary literature (i.e. publications authored by the scientist(s) who personally carried out the research). An exhaustive list of 20 gemmological journals and 10 gem laboratory publications—including information on their time span, accessibility, website, etc.—is available by contacting the author. Only some of them offer indexes or table-of-contents listings that can be searched for keywords, authors, etc. These include *The Journal of Gemmology, Australian Gemmologist, Revue de Gemmologie A.F.G. and Gemmologie: Zeitschrift der Deutschen Gemmologischen Gesellschaft*. (Note that researchers should not omit foreign-language journals from their search, due to the availability of online translators such as Google Translate, DeepL, etc.)

It is highly recommended to download the entire available journal back-issue collections, so that the PDFs are readily accessible even without internet access, while travelling, etc. The PDFs for each journal should be saved into a separate folder. For those journals without indexes or contents

Figure 1: Examples of some scholarly gemmological journals in various languages.

listings, keyword searches can then be done for all files in a particular folder by using the "Advanced Search" function of Adobe Acrobat Pro. (Most PDFs are searchable, but those consisting of scanned images will first need to be processed using Adobe Acrobat Pro's "Recognize Text" function.) Although more time-consuming than using indexes or contents listings, with this technique it is possible to search for specific content in any collection of PDFs within a single folder, whether from a particular journal or from miscellaneous sources that are grouped together according to gem material, locality, etc.

Other sources of gemmological information include the following:

- Gemmological reference books (e.g. Gübelin & Koivula, 1986, 2005, 2008; O'Donoghue, 2006; Dominy, 2024)
- GIA Library search (https://g30010.eos-intl.net/G30010/OPAC/Index.aspx)
- GIA's historical reading lists (https://www.gia.edu/historical-gemology-reading-lists) and bibliographies (https://www.gia.edu/search?q=bibliography)
- CIBJO Blue Books and guidelines (https://cibjo.org/industry-standards-resources)
- Laboratory Manual Harmonisation Committee (LMHC) Gemstone Information Sheets (https://www.lmhc-gemmology.org/gemstones)
- Sheahan Diamond Literature Reference Compilation (https://secure.kaiserresearch.com/a13/Education.asp?ReportID=364130)
- For gem localities: John Sinkankas' textbooks (*Gemstones of North America, Emerald and Other Beryls*, etc.); mineral locality compilations (Bernard & Hyršl, 2015; Moore, 2016); and Mindat (https://www.mindat.org)
- For spectroscopic data: Mineral Spectroscopy Server (http://minerals.caltech.edu), RRUFF database (https://rruff.info) and Spec4Gem (www.spec4gem.info); the first two can be searched to provide reference listings for particular minerals.

Useful general search engines include Google Scholar (https://scholar.google.com) and Google Books (https://books.google.com); see search tips by Trauth and Sillmann (2018). A relatively new tool is R Discovery, which is an artificial intelligence tool for literature searches (https://discovery.researcher.life). In addition, keyword searches can be done using CrossRef (https://search.crossref.org), and this website can also be used to look up DOIs (digital object identifiers) for specific articles. DOIs should always be included in reference lists when available.

A tremendous amount of literature (mostly older works that are not under copyright) is freely accessible online via the Internet Archive (https://archive.org) and the HathiTrust Digital Library (https://www.hathitrust.org/the-collection). The Internet Archive contains resources of particular interest to gemmologists, such as a collection of documents from the GIA Library (https://archive.org/details/gialibrary) and gem-and-mineral bibliographies by John Sinkankas, Curtis P. Schuh and Joseph O. Gill. Valuable historical information on gem materials can also be found within archives contained in museums, monasteries, research institutions and government offices.

Local public university libraries are valuable assets for performing literature searches, encompassing numerous resources beyond the scope of this review (see, e.g., Mann, 2005). In addition to obtaining assistance from a reference librarian, it may be possible to use an interlibrary loan service to obtain materials held at other academic libraries. In addition, university libraries commonly have public computers that allow access to online academic databases including "online public access catalogues" (OPACs), WorldCat, GeoRef, Geobase, Web of Science, Scopus, ProQuest, EBSCO, Gale, etc. Importantly, these computers may also have full access to an extensive collection online journals, allowing members of the public to freely download selected articles and books in PDF format to a flash drive. Local community libraries also have digital collections (although usually not academically oriented) and interlibrary loan services. Another way to obtain access to online journal collections is through membership with the Geological Society (London), which allows members to remotely access content from more than 100 earth science journals.

In conclusion, gemmologists have various options for performing literature searches and electronically accessing journals, books, etc., either using their own computer or by visiting local libraries, even without being a student or member of a university.

References:

- Bernard, J.H. & Hyršl, J. 2015. Minerals and Their Localities, 3rd edn. Granit, Prague, Czech Republic, 920 pp.
- Davis, M., Davis, K.J. & Dunagan, M.M. 2012. Chapter 4: Searching and Reviewing Scientific Literature. In: Scientific Papers and Presentations, 3rd edn. Elsevier and Academic Press, London, UK, 33–46, https://doi.org/10.1016/B978-0-12-384727-0.00004-5.
- Dominy, G.M. 2024. The Handbook of Gemmology, 5th edn. Amazonas Gem Publications, Mallorca, Spain, 1,236 pp.
- Gübelin, E.J. & Koivula, J.I. 1986. Photoatlas of Inclusions in Gemstones. ABC Edition, Zurich, Switzerland, 532 pp.
- Gübelin, E.J. & Koivula, J.I. 2005. Photoatlas of Inclusions in Gemstones, Vol. 2. Opinio Publishers, Basel, Switzerland, 829 pp.
- Gübelin, E.J. & Koivula, J.I. 2008. Photoatlas of Inclusions in Gemstones, Vol. 3. Opinio Publishers, Basel, Switzerland, 672 pp.
- Machi, L. & McEvoy, B.T. 2022. Step 3: Search the literature. In: The Literature Review: Six Steps to Success, 4th edn. Corwin Press, Thousand Oaks, California, USA, 237 pp.
- Mann, T. 2005. The Oxford Guide to Library Research, 4th edn. Oxford University Press, Oxford, UK, 359 pp., https://doi.org/10.1093/oso/9780195189971.001.0001.
- Moore, T.P. 2016. Moore's Compendium of Mineral Discoveries 1960–2015. Mineralogical Record Inc., Tucson, Arizona, USA, 2 vols., vii + 809 pp. and ii + 813 pp.
- O'Donoghue, M. (ed) 2006. Gems, 6th edn. Butterworth-Heinemann, Oxford, UK, 873 pp.
- Trauth, M.H., & Sillmann, E. 2018. Searching and reviewing scientific literature. In: Collecting, Processing and Presenting Geoscientific Information: MATLAB® and Design Recipes for Earth Sciences, 2nd edn. Springer Nature, Berlin, Germany, 15–40, https://doi.org/10.1007/978-3-662-56203-1_2.

An approach to understanding the factors in the emerald enhancement clarity grading system used at CDTECGemlab

Javier Garcia-Toloza[1], Juan David Rincón[1], Cristian Ochoa[1], Julio Cedeño Carlos[1]

[1] Technological Development center for the Colombian Emerald CDTEC, Bogota, Colombia. ceo@gemlabcdtec.com

[2] National University of Colombia, Bogota, Colombia jagarciato@unal.edu.co

Emerald is the green variety of beryl, with its distinctive color resulting from trace amounts of chromium, vanadium, and iron. These elements replace aluminum in the octahedral positions of its crystal structure. The clarity of an emerald depends on the presence of internal characteristics such as inclusions (solid and/or fluid) and fissures. Since ancient times, the clarity of emeralds has been improved through various treatments (Nassau K. 1984). Among these, fissure filling is the most common procedure, where substances with optical properties like the host material are used to enhance clarity by improving light transmission within the gemstone. Emeralds may undergo treatments and/or enhancements before, during, and after the cutting process (Fig.1). Sometimes, the application of specific substances helps increase the material's stability, making it more resistant to damage during cutting, especially when large fissures or voids are present (Scarratt K. 2015). In most cases, fissures are filled after the cutting process to improve the gem's appearance.

Figure 1. Possible stages during which the enhancement of the stone can occur throughout its transformation.

Sometimes, an untreated gemstone with visible fissures can undergo treatments or enhancements that lead to a significant improvement in appearance changes that may not be apparent to the final consumer (Fig.2). For this reason, certification is essential, as it provides detailed information about any enhancement treatments, including the extent of the improvement and, in some cases, the type of substances used. Such certification serves as a reliable disclosure to the consumer, offering transparency regarding the gemstone's condition and the nature of any treatments at the time the report was issued.

Figure. 2 Emerald before enhancement (left) and after enhancement (right).

Gemlabs face the challenge of identifying both the type and quantity of substances used in clarity enhancement. This task involves considering various factors, such as identifying the diversity of substances—including vegetable oils, hydrocarbon-derived oils, resins, balsams, and waxes—which can be of natural or artificial origin (Johnson M. *et al,*

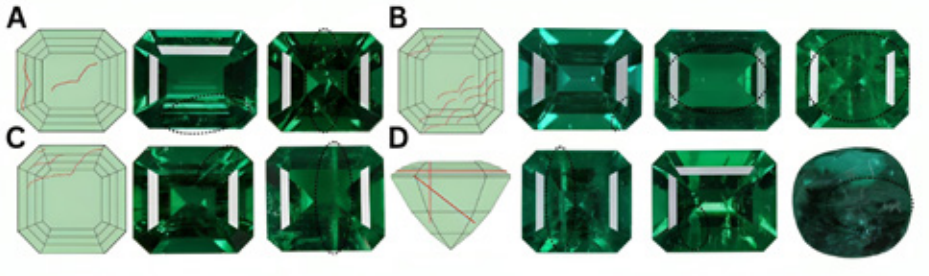

Figure 3. Primary factors used in grading emerald enhancement include, Location (A), quantity of fissures (B), length (C), and tilt (D)

1990; Kammerling R. et al, 1991; Hanni H. 1992; Kiefert L. et al, 1999; Hainschwang & Notari. 2022), as well as the mixtures employed. Although cedar oil was historically a commonly used product, it is now less prevalent. Currently, substances such as natural hydrocarbon-derived oils—commonly known as mineral oil (e.g., baby oil)—and liquid or hardened artificial resins are predominantly used.

Additionally, it requires developing an assessment as objective as possible of the extent of clarity modification by fissure filling through qualitative analysis. The assessment of the extent or intensity of clarity improvement has been addressed by Shane McClure *et al*., 1999, who classified the enhancement into three main categories: minor, moderate, and significant. This classification is based on factors such as the size, extent, or length of the treated areas; the number of fissures; the amount of treatment within fissures; and the location of filled fissures. The description of emerald enhancement is provided in Sheet # 5 (LMHC, 2014), which outlines a guide for determining the amount of filled fissures. This serves as the basis for quantifying the enhancement and assigning a corresponding quality grade.

However, one of the most important aspects of classification is the ability to identify fissures or voids containing substances. To achieve this, various methodologies have been developed that utilize different instruments and illumination techniques, along with careful inspection of various parts of the stone. These include transmitted light (bright field - dark field), reflected light, and UV light. Regarding UV illumination, caution should be exercised with certain UV ranges, as they may cause harmful effects on substances, such as polymerization. Additionally, it is important to remember that not all substances fluoresce, for example, some oils (Notari F. *et al*., 2022). This comprehensive approach ensures the collection of complete information necessary for an accurate and reliable classification process.

The purpose of grading is to assess the extent of improvement in the clarity of the stone. While the number of fissures present may be important, it does not necessarily determine the degree of improvement. For example, a single fissure that is oriented parallel to the table and covers a large portion of the stone can result in a moderate grade because it significantly affects the stone's clarity. Conversely, several small fissures that are perpendicular to the table, located on the crown facets (not the table), and aligned with the edges of the crown facets, especially if they are small relative to the stone's dimensions—may warrant a minor grade.

Fissures typically behave as three-dimensional features, either resembling a plane or acting as pores or hollows within the stone, such as in emeralds. This means they possess volume. Factors such as their location, length, quantity, and inclination are highly important for determinate improve clarity. In certain areas of the stone, the presence and arrangement of fissures may have a greater impact on clarity than in other regions. Additionally, if a wide fissure is in a region that could affect the stone's integrity—such as on the pavilion, girdle, or crown—its significance increases. For example, a fissure that crosses the stone completely or is blunt can lead to chipping or even a fracture that splits the stone into two nearly equal parts (integrity factor). Another important consideration is size. It is rare to find stones over 5 carats—or even over 10 or 15 carats—that are free of fissures. However, a stone with several fissures that appear dense relative to its small volume does not necessarily indicate a similar density in a much larger stone (size factor). The clarity factor provides a general measure of the impact of fissures on the stone's overall appearance. If a stone has high clarity, filled fissures will be more visible. In such cases, the presence of fissures may be more significant in an untreated stone with high clarity than in one with lower clarity, where the abundance of inclusions makes fissures less noticeable (clarity factor). Other factors may also influence

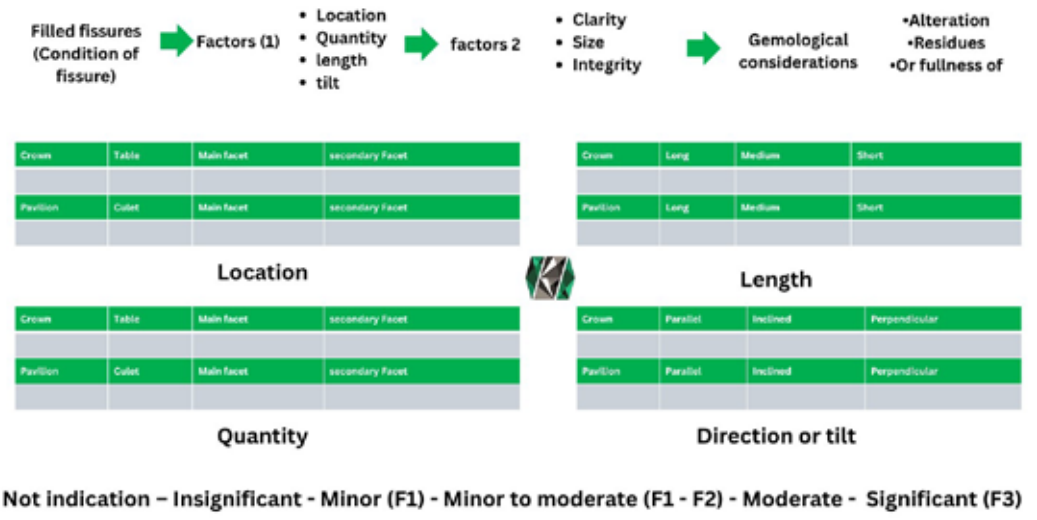

Figure 4. Grading emerald enhancement system by CDTEC

the grading based on gemological considerations. These include residues, alterations of substances, or any other features within the stone that could impact its clarity. Such features should be identified, described, and evaluated to determine their effect on the stone's overall clarity.

To define the factors that enable the improvement of quality grade assignments related to enhancement and/or treatment is an ongoing task for gemological laboratories, which helps foster consumer confidence. However, one of the objectives of this work is to contribute to the enhancement of methods that promote consistency in laboratory procedures. This includes supporting aspects such as record-keeping, traceability, and repeatability, all within the framework of international standards—not only for the gemstone industry but also for testing and analysis laboratories.

References:

- Hainschwang T. & Notari F. 2022. L´analyse gemmologique de l´emeraude. Émeraudes, tout un monde! 273-282.
- Hanni H.A. 1992 Identification of fissure -treated gemstones. Journal of gemmology, 23 (4). 201-205
- Kiefert L., Hanni H.A., Chalain J.P., Weber W. 1999. Journal of gemmology. 26 (8). 501–520.
- Nassau K. 1984. The early history of gemstones treatments. Gems & gemmology, 20 (1), 22-33
- LMHC (2023) Emerald. Information sheet No. 5; https://www.lmhc-gemmology.org/wp-content/uploads/2023/06/LMHC-Information-Sheet_5_V5_2023.pdf
- Mary L. Johnson, Shane Elen, and Sam Muhlmeister. 1990. On the Identification of Various Emerald Filling Substances. Gems & Gemology, Summer 1999, Volume 35, No. 2. 83-107
- Notari F., Caplan C., Hainschwang T., and Natch C., 2022. Les substances de remplissage des émeraudes. Émeraudes, tout un monde! 295-302.
- Robert C, Kammerling, John I. Koivula, Robert E. Kane, Patricia Maddison, James E. Shigley, and Emmanuel Fritsch. 1991. Fracture filling on emeralds. Gems & Gemotow, W. 27, Mo. 2, pa 70-85
- Scarrat Kenneth. 2015. Beautifying emeralds. Incolor special issue, December 2015. 50-55
- Shane F. McClure, Thomas M. Moses, and Maha Tannous, John I. Koivula. 1999. Classifying Emerald Clarity Enhancement at the GIA Gem Trade Laboratory. Gems & gemmology. Volume 35, No. 4. 176-185

Acknowledgements

The authors would like to thank all the organizations and institutions that made this work possible. This study was supported by the National Emerald Federation (FEDESMERALDAS), the association of Colombian Emerald Producers (APRECOL), the Colombian association of trade in emeralds (ASOCOESMERAL), Colombian Association of Emerald Exporters (ACODES) and the Ministry of Mines and Energy of Colombia.

Noble gas in corundum: interests in gemology

Boris Chauviré[1], Marianna Corre[2], Martial Curti[3], Cécile Gautheron[4], Sarah Figowy[5], Lauriane Pinsault[6]

[1] GeoGems, Nantes, France, boris.chauvire@geogems.fr [2] GeoGems, Nantes, France
[3] Bellerophon Gemlab, Paris, France [4] ISterre, Université Grenoble-Alpes
[5] Université Paris-Saclay, Paris, France [6] GeoGems, Nantes, France

Noble gas in geology

Noble gases —elements of the last column of the periodic table—are chemically defined by their full outer electron shells, making them highly inert and very volatile under ambient conditions. In geology, they are used to trace a wide range of processes, including mantle circulation and degassing, hydrocarbon reservoir formation, climate change, and ocean circulation (Burnard, 2013). Among the noble gasesthe lightest (helium, neon and argon) are the most commonly used and possibility present in gems. Their lack of chemical interaction makes them useful in gemology for two main purposes: detecting heat treatment and determining geographic origin.

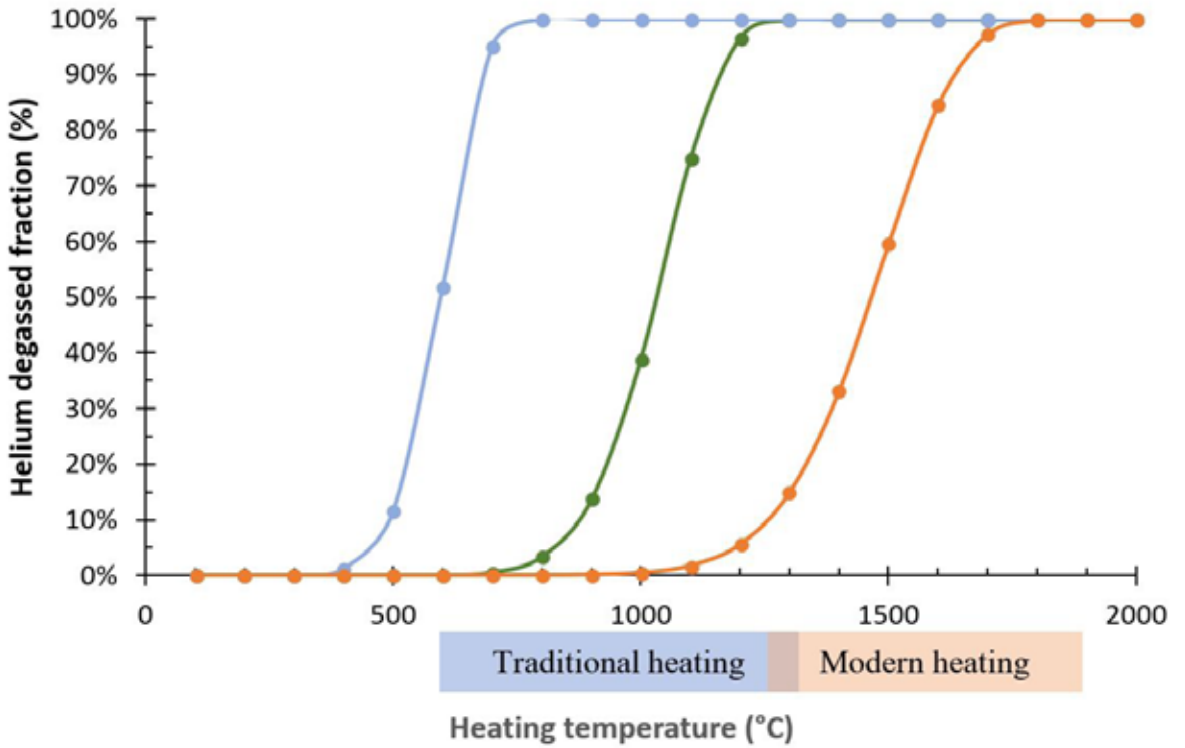

Figure 1 : Fraction of helium degassed during heating according to theoretical data from Zhang *et al.* 2016, with activation energy of 100 (blue), 150 (green) and 200 (orange) kJ/mol, calculated from the equation from Fechtig and Kalbitzer (1966).

Heat-treatment

Traditional heat treatment (~600°C–1200°C) is one of the oldest known gemstone enhancements, used over 4,000 years ago for improving corundum color (Notari *et al*., 2019). Modern treatments reaching up to ~1850°C leave detectable traces, while low-heat methods remain to date an important challenge to identify and spur further research (Saeseaw *et al*., 2021; Hughes & Vertriest, 2023; Karampelas *et al*., 2023).

Due to their volatility, noble gases—especially helium—could serve as scientific indicators of heat treatment. Quantifying diffusion of noble gases in crystals is then necessary to use these volatiles as tracers. Theoretical models and experiments on synthetic materials suggest that helium diffuses out of the crystal between 500 °C and 1700 °C, depending on the nature of the defects in which it is trapped and the duration for which the temperature is maintained (*e.g.*: Campbell, 1960; Fechtig & Kalbitzer, 1966; Zhang *et al*., 2016). The diffusion of noble gases is highly dependent on the local environment of diffusion, as demonstrated in high-density SiO_2 polymorphs (Figowy *et al*., 2024). As noble gases easily may easily diffuse as low as 500°C, the absence of helium in natural corundum may indicate human-induced heating, potentially calling for a reassessment of current heat treatment detection methods. Ongoing experiments on six samples treated at various temperatures aim at better constraining the conditions required for helium degassing. In parallel, new *ab initio* molecular dynamics calculations are performed and compared with experimental results to provide a quantification of diffusion processes and investigate the role of defects.

Origin

Noble gases are commonly used as tracers of geological processes, and their analysis may represent a novel approach for determining the origin of corundum. To date, no data on noble gases in natural corundum have been reported in the literature. To explore this potential, we measured the helium concentration from 116 crystals from 14 different sources. Our results show that sapphires from Kenya, Greenland, and Madagascar have significantly higher concentrations (>100 pmol/g) compared to those from other localities (<30 pmol/g), including Colombia, Vietnam, Mozambique, Kashmir, France, Sri Lanka, Cambodia, Australia, Myanmar, Tanzania, and Thailand. While most conventional provenance methods discriminate between deposit types (magmatic and metamorphic type), it seems that helium content does not directly correlate with the deposit type. While not immediately applicable to the gem trade yet, noble gas analysis could serve as a complementary scientific tool in the study of gem geology and origin determination.

References:

- Heidelberg, Berlin, Heidelberg. DOI: 10.1007/978-3-642-28836-4.
- Campbell, W.B. (1960, October 30) Diffusion rate and activation energy of helium through single crystal and polycrystalline alumina. Georgia Institute of Technology.
- Fechtig, H., & Kalbitzer, S. (1966) The Diffusion of Argon in Potassium-Bearing Solids. In *Potassium Argon Dating* pp. 68–107. Springer Berlin Heidelberg, Berlin, Heidelberg. DOI: 10.1007/978-3-642-87895-4_4.
- Hughes, E.B., & Vertriest, W. (2023) A Canary in the Ruby Mine: Low-Temperature Heat Treatment Experiments on Burmese Ruby. *Gems & Gemology*, 58, 400–423. DOI: 10.5741/GEMS.58.4.400.
- Karampelas, S., Hennebois, U., Mevellec, J.Y., Pardieu, V., Delaunay, A., & Fritsch, E. (2023) Pink to Purple Sapphires from Ilakaka, Madagascar: Insights to Separate Unheated from Heated Samples. *Minerals*, 13. DOI: 10.3390/min13050704.
- Saeseaw, S., Khowpong, C., & Vertriest, W. (2021) Low-Temperature Heat Treatment of Pink Sapphires from Ilakaka, Madagascar. *Gems & Gemology*, 56, 448–457. DOI: 10.5741/GEMS.56.4.448.
- Zhang, G., Xiang, X., Yang, F., Peng, X., Tang, T., Shi, Y., & Wang, X. (2016) Helium stability and its interaction with H in α-Al_2O_3: A first-principles study. *Physical Chemistry Chemical Physics*, 18, 1649–1656. DOI: 10.1039/c5cp06496a.

Gem zircon and sapphire age dating and application of origin determination: A study from New England sapphire fields, New South Wales, Australia

Ahmadjan Abduryim[1,2], Frederick Lin Sutherland[3], Terry Coldham[4], Elena Belousova[5]

[1] Tokyo Gem Science LLC; tgs@gemscience.tokyo

[2] GSTV Gemological Laboratory

[3] Australian Museum

[4] Gemmological Association of Australia

[5] Department of Earth and Planetary Sciences, Macquarie University

Abstract

Chemical composition and U-Pb age determined by laser ablation (LA) ICP-MS are presented for zircon megacrysts found in alluvial gem corundum deposits associated with alkali basalts in the Inverell district in New England, New South Wales, eastern Australia. The three mine localities, Kings Plains, Swan Brook, and Mary Anne Gully, produce gem-quality brown to yellow zircon megacrysts characterized by relative enrichment in Hf and REE. We observed no differences in relative concentrations of transition metals in relation to color. Chemical homogeneity within the single zircon crystals indicates stable crystallization conditions. The 206Pb/238U age of zircon megacrysts from these three localities fall into two groups, an older group of about 174-216 Ma and a younger group of about 37.7-45 Ma, respectively. Based on our data, the zircons in the New England alluvial gem deposits may be related to two formation episodes, one in the Upper Triassic-Lower Jurassic and one in the Eocene (late Oligocene). Most originated from the lithospheric mantle, and later hosted basaltic magmas brought up. Gem quality blue sapphires are also directly collected from these mines, and zircon inclusions in Kings Plains and Mary Anne Gully sapphires gave U-Pb ages of about 35 to 37 Ma which fall within the range of basalt K-Ar ages of 19 to 38 Ma and close to the younger group of zircon megacrysts (37.7-45 Ma) thus indicating the timing of volcanism of the Inverell district-New England field.

Introduction

Zircon megacrysts are common within eluvial, paleo-alluvial, and alluvial sapphire/ruby deposits derived from basaltic sequences, with gem properties suitable for cutting as an accessory gemstone. Such zircons and sapphires/rubies are widely distributed along eastern Australia (Figure 1). The largest gem field in New England, New South Wales, has a limited systematic spread of U-Pb ages (Coenraads *et al*., 1990; Sutherland & Fanning 2001; Sutherland *et al*., 2002; Zaw *et al*., 2006; Abduriyim *et al*., 2012). In 2010, the authors visited sapphire mines in Kings Plains, Mary Ann Gully, and Swan Brook and investigated the geological distribution and mining at each deposit. This study presents U-Pb age dating of zircon megacryst and zircon inclusion in host sapphire from the Inverell district in the New England gem field. These data are used to characterize and discuss the crystallization ages and source affinities (or genesis) of gem-quality zircon and sapphire megacrysts from a world-class basaltic gem field.

Figure 1. Distribution of sapphire/ruby and zircon in eastern Australia, showing mining locations of the New England, New South Wales, Anakie and the Lava Plains gem fields in Central and Northern Queensland, other sapphire/Ruby gem fields in Victoria and Tasmania.

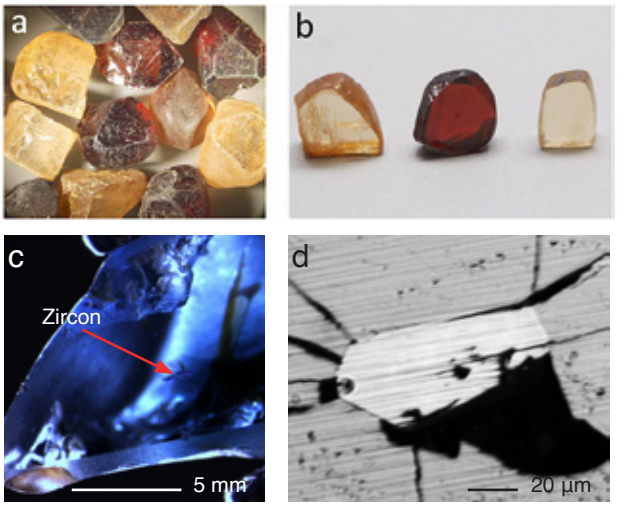

Figure 2. Zircon megacryst concentrate (a: left top) from Kings Plains mine. Zircon megacryst color range with polished surface for analysis (b: right top, sample weight, 2.46~4.11cts). (c) Blue sapphire from Mary Anne Gully (sample S-MA-0001) with a small zircon inclusion surrounded by tension cracks. (d) Zircon inclusion in sapphire (sample S-MA-0001) which was carefully polished to expose the zircon to the surface for LA-ICP-MS analysis.

Materials and Methods

Zircons from the Inverell district-New England gem deposits selected for analysis included 7 brown and yellow zircon megacrysts collected from the alluvial corundum mine in Kings Plains, 3 from the Mary Anne Gully mine and a color range of 5 faceted megacrysts from Swan Brook (Figure 2a and b).

125 samples of blue and greenish blue sapphire megacrysts were collected from the exact three mine locations. They show a glossy natural surface which is typical as a result of magmatic dissolution and etching. Two blue sapphire samples contained several large transparent euhedral zircon inclusions, and these sapphires were carefully orientated and polished to expose the zircon inclusion to the surface of the sapphire (Figure 2c and d). Their size (100 and 80 µm in length), was suitable for dating with conventional LA-ICP-MS (Agilent 7700 ICP-MS with 213nm YAG laser).

Results and Discussions

Chemical Composition: Zircon megacrysts from the Inverell district are significantly HREE-enriched over LREE (Figure 3). The chondrite-normalized REE patterns are moderately fractionated and show a positive Ce anomaly. Only a few samples show negligible Eu anomalies. The total content of LREE in the Inverell zircons is 0.01 to 0.3 (La) up to 20 to 300 (Dy) chondrite units. HREE content ranges from 30 to 500 (Ho) to 100 to 1250 (Lu) chondrite units. The REE patterns of the zircons from three localities in the Inverell district sapphire mine field have similar profiles, indicating related origins.

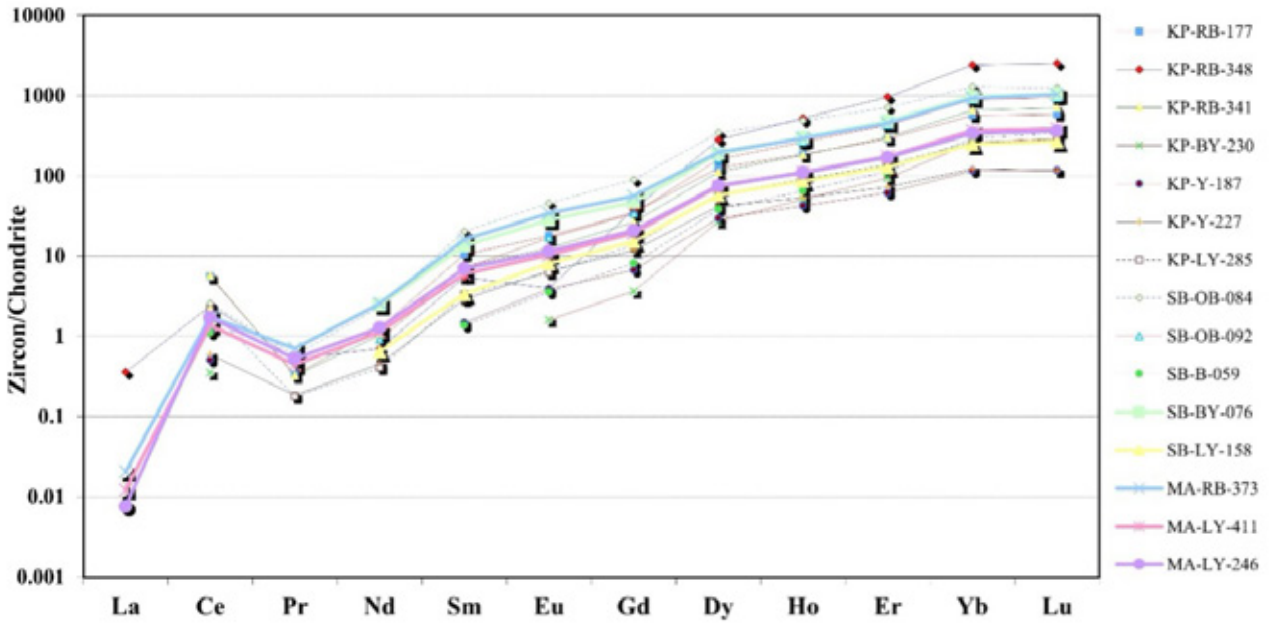

Figure 3. Chondrite-normalized REE patterns of zircon megacrysts from Kings Plains, Swan Brook, and Mary Anne Gully in the Inverell district, New England gem field, Australia.

The blue, yellow-blue (parti-color type) and greenish blue sapphires from three mine locations in Inverell district show relatively high Ga (> 120 ppm), low Mg (< 18 ppm) and low Cr (< 10 ppm), features that typify magmatic sapphires. The blue sapphire group, however, shows lower Fe, V, and Mg and higher Ti than the greenish blue group. Other minor trace elements such as Ni, Sn, and Ta values are mostly <1 ppm in blue and yellow-blue sapphires and below detection in greenish blue sapphires.

Geochronology: Six samples among the 7 zircon samples from Kings Plains reveal older ages, from the U-Pb concordance of 206Pb/238U age around 188.9 ± 4.5 Ma, 185.9 ± 3.3 Ma, 208 ± 4 Ma, 176 ± 6.1 Ma, 174 ± 7 Ma, and 207 ± 17 Ma at the 95% confidence level. One zircon gave a younger 45 ± 0.52 Ma age (Figure 4). Based on these results we assume that the deposits may represent two different volcanic activity periods, one in the upper Triassic and later in the late Oligocene.

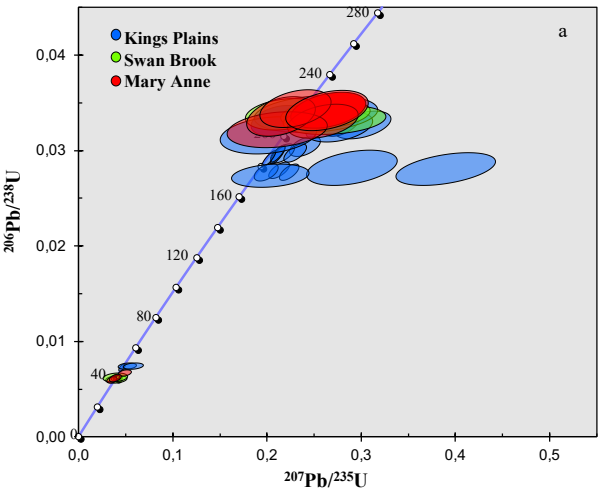

Figure 4. Concordia diagram showing U-Pb age data of zircons from Kings Plains, Swan Brook and Mary Anne Gully from the Inverell district, NSW, Australia.

Four samples among the 5 Swan Brook zircons show a younger concordant age around 37.94 ± 0.34 Ma, 37.22 ± 0.28 Ma, 36.2 ± 6.4 Ma, 37.66 ± 0.35 Ma at the 95% confidence level, except one zircon grain with an older U-Pb age of 215 ± 2 Ma.

This trend of two age groups is also found in zircons from the Mary Anne Gully alluvial deposit. Two samples resulted in a concordant age of 206 ± 11 Ma and 216±5.7 Ma, while one zircon shows a concordant age of 37.7 ± 0.9 Ma.

Most of the zircons from the Kings Plains alluvial deposits belong to the older age group (the weighted mean 206Pb/238U age of 174 Ma to 216 Ma) and suggest its main volcanic eruption episode was in Triassic to Jurassic, but Swan Brook zircons are dominantly the younger age group (37.7 Ma to 45 Ma), relating them to the Eocene Maybole volcano eruptions.

In the blue sapphire sample from Kings Plains, two spot analyses were obtained on the zircon inclusion carefully polished to be exposed at the surface. The U-Pb concordant ages of this zircon inclusion were 37.2 ± 1.9 and 36.9 ± 1.6 Ma (Figure 5). Another zircon inclusion in the Mary Anne Gully sapphire gave similar concordant ages of 35.7 ± 2.1 and 34.9 ± 1.4 Ma, revealing that there is no significant difference between these two mine locations in terms of formation ages. These results show that the sapphires originated during the Eocene volcanism in the Inverell district. In addition, the age of the zircon inclusions in sapphires fully overlaps with the young age of the zircon megacrysts from the same locations, indicating that the zircon inclusions probably formed together with the sapphires or shortly before. Based on literature and our data, it is assumed that the sapphires formed from strongly evolved magmas in the deep crust or upper mantle and that they were carried up in large quantities within alkali basaltic magmas during volatile-rich and explosive volcanic eruptions.

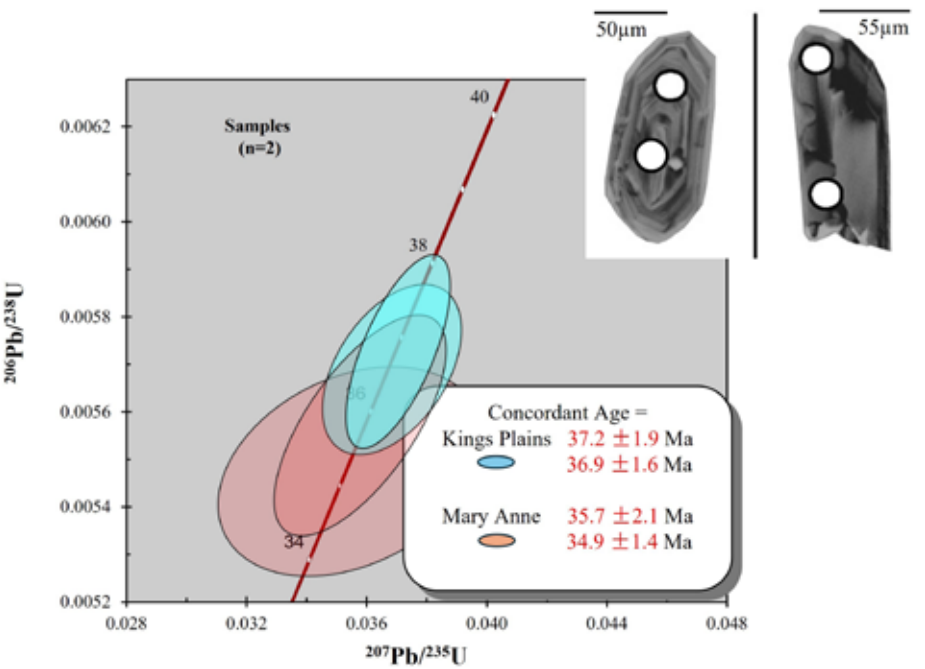

Figure 5. Concordia diagram for the zircon inclusion in sapphires from Kings Plains and Mary Anne Gully.

Geographic Origin Determination of Natural Yellow Sapphires: The Preliminary Study

Montira Seneewong-Na-Ayutthaya[1*], Bhuwadol Wanthanachaisaeng[1], Thanong Leelawatanasuk[1], Wilawan Atichat[1], Sirinapa Saengdech[1], Pimlapat Kamkaew[1] and Tasnara Sripoonjan[2]

[1] The Gem and Jewelry Institute of Thailand (Public Organization), ITF-Tower Building, Silom Road, Suriyawong, Bangrak, Bangkok, 10500 Thailand

[2] G-ID Laboratories, Yan Nawa, Bangkok, 10120 Thailand

[*] smontira@git.or.th

Keywords: Yellow sapphire, Geographic origin, Geochemical fingerprinting

Introduction

Determining the geographic origin of yellow sapphires plays a critical role in the gem trade, as origin often dictates both perceived quality and market pricing. Yellow sapphires, a popular variety of corundum, form in diverse geological environments, each imparting unique internal features and chemical profiles. In today's market, where ethical sourcing and traceability are increasingly prioritized, reliable methods for origin determination are essential. Traditional gemmological approaches, such as analyzing inclusions, can offer helpful insights but are often insufficient—particularly when stones have undergone heat treatment or when inclusions appear similar across different mining regions. This research seeks to overcome these challenges by analyzing yellow sapphires from importantly global sources, including Sri Lanka, Madagascar, Tanzania, and Thailand. Through detailed geochemical profiling, the study aims to uncover distinguishing chemical traits that can serve as dependable indicators of geographic origin. The goal is to improve precision in origin determination, thereby reinforcing consumer trust, enhancing valuation, and promoting transparency across the gemstone supply chain.

Materials and Methods

In this investigation, a total of 151 yellow sapphire samples were analyzed. These originated from Sri Lanka (36 samples), Ilakaka, Madagascar (22), Tanga, Tanzania (45), and Bang Kacha, Chanthaburi, Thailand (50), with weights ranging from 0.23 to 4.30 ct and displaying various yellow colour tones (Figure 1). All samples had undergone traditional heat treatment, except for the Thai samples, which were treated using beryllium heat treatment. The gemmological properties of these samples were examined using both standard gemological tools and advanced analytical instruments, including Raman (Renishaw inVia Qontor Raman microscope), UV-Vis-NIR (PerkinElmer Lambda 1050), and LA-ICP-MS (LA: ESI Industrial NWR-213, ICP-MS: ThermoScientific iCAP™ RQ).

Figure 1: Representative samples of yellow sapphire from Sri Lanka, Madagascar, Tanzania, and Thailand ranging in weight from 0.23 to 4.30 ct (Photograph by M. Seneewong-Na-Ayutthaya)

Results and Discussions

Internal features.

Sri Lankan yellow sapphires are frequently characterized by rectilinear, zigzag-shaped fingerprint inclusions (Figure 2a) and CO_2-filled negative crystals (Figure 2b) (Palke *et al*., 2019). Additional commonly observed internal features include silk, various fingerprint patterns, needle-like inclusions, minute particles, milky clouds, twinning, as well as crystalline inclusions such as apatite and graphite. In contrast, yellow sapphires from Ilakaka, Madagascar typically contain abundant rounded zircon inclusions (Figure 2c) (Saeseaw *et al*., 2020). Other diagnostic features in these samples include rutile needles (Figure 2d), silk, complex fingerprint patterns, iron staining, and mica inclusions. Tanzanian yellow sapphires are often distinguished by the presence of hematite silk (Figure 2e) and rose channels (Figure 2f). Additional inclusions observed in these stones include iron staining, hematite, zircon, amphibole, apatite, rutile, black inclusions, various crystalline phases, fingerprint patterns, silk, needles, clouds, and lamellar twinning. Notably, the zircon inclusions in Tanzanian sapphires may closely resemble those from Madagascar, complicating origin determination based solely on inclusion characteristics and necessitating further analytical investigation. Thai yellow sapphires frequently exhibit dissociated inclusions, particularly following high-temperature heat treatment (Figure 2g), along with angular bands of brownish particles (Figure 2h) (Saeseaw *et al*., 2017). Other internal features include feldspar, crystals, negative crystals, minute particles, clouds, blue colour zones, fingerprint patterns, silk, needles, and iron staining.

a) Rectilinear zigzag fingerprint in Sri Lankan stone

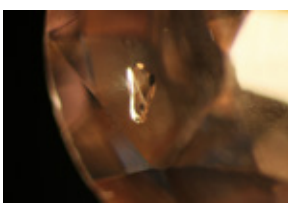

b) CO_2-filled negative crystals in Sri Lankan stone

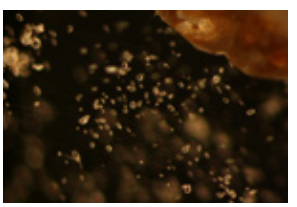

c) Cluster of rounded zircon inclusions in Madagascan stone

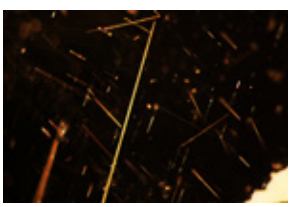

d) Rutile needle-like inclusions in Madagascar stone

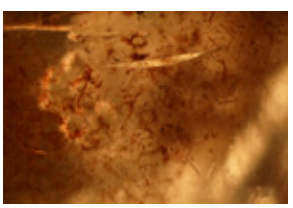

e) Hematite silk in Tanzanian stone

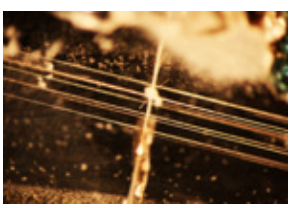

f) Rose channels in Tanzanian stone

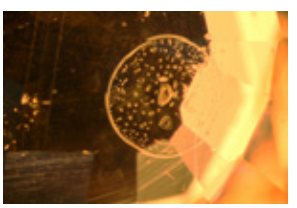

g) Dissociated crystal (heat treatment) in Thai stone

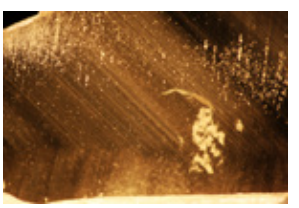

h) Angular bands of brownish particles in Thai stone

Figure 2: Inclusions observed in yellow sapphire samples from various deposits examined in this study; field of view 3.8 mm (a, d, e, g), 2.8 mm (b), 1.8 mm (c), 4.5 mm (f) and 9 mm (h). (Photomicrographs by M. Seneewong-Na-Ayutthaya)

UV-Vis spectra.

Yellow sapphires exhibit characteristic UV/Vis/NIR spectra, with their colouration primarily attributed to two distinct mechanisms: colour centres (h•-Fe^{3+}) and the presence of the iron (Fe^{3+}) trace element (Dubinsky *et al*., 2020). Figure 3 illustrates the absorption spectrum of a yellow sapphire from Sri Lanka, which is representative of the colour produced predominantly by the colour centre chromophore. In contrast, for yellow sapphires with higher iron concentrations, such as those from Madagascar, Tanzania, and Thailand, their spectra are characterized by absorption features at approximately 378 nm and 450 nm attributed to Fe^{3+}/Fe^{3+} pairs, and an absorption band at approximately 387 nm indicative of isolated Fe^{3+} (Emmett *et al*., 2023; Dubinsky *et al*., 2020). These spectral features confirm the dominant role of iron (Fe^{3+}) as the primary chromophore for yellow colouration in these latter groups.

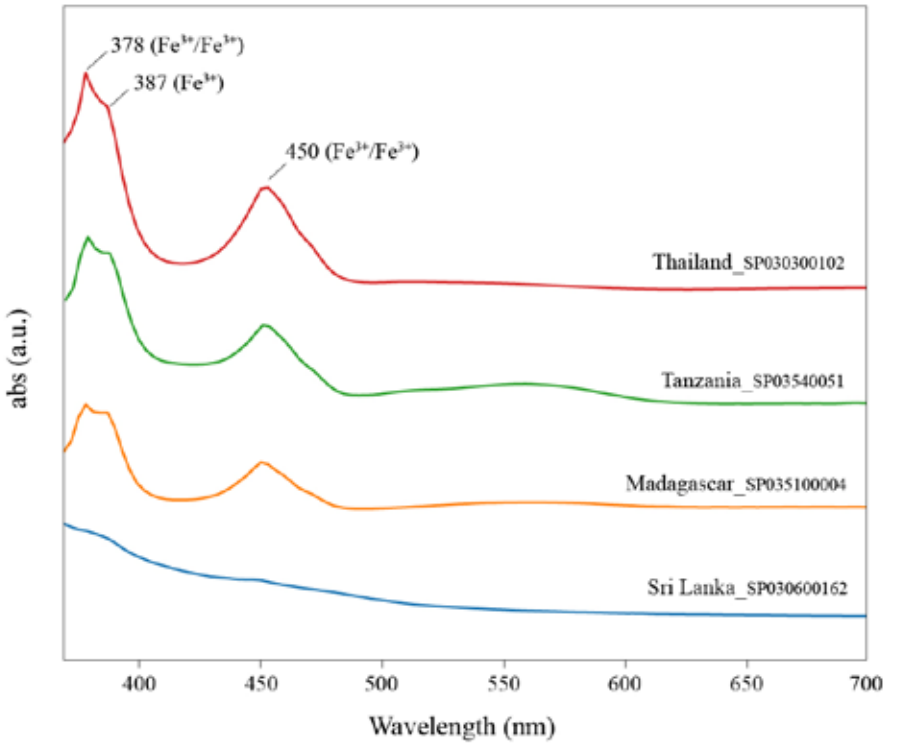

Figure 3: UV-Vis-NIR spectrum of yellow sapphire samples from various deposits examined in this study

Chemical analysis.

Chemical composition analysis of yellow sapphire samples using LA-ICP-MS revealed the presence of important trace elements, including Fe, Mg, Ga, Ti, Cr, and V. Yellow sapphires from Thailand exhibited the highest average Fe content (~15,000 ppm), followed by samples from Tanzania (~7,800 ppm), Madagascar (~4,500 ppm), and Sri Lanka (~440 ppm). The relatively high Fe content in Thai is attributed to their basalt-related geological origins, in contrast to Sri Lankan sapphires, which are typically associated with metamorphic rocks. As shown in Figure 4, 2D (Fe–Cr) and 3D (Fe–Mg–Cr) scatter plots clearly illustrate the differentiation of Sri Lankan yellow sapphires from those of other origins. Distinct clustering patterns were observed for each locality, enabling effective discrimination among samples from Sri Lanka, Madagascar, Tanzania, and Thailand. Among the trace elements, Fe, Mg, and Cr are identified as a key indicator for determining the geographical origin of yellow sapphires.

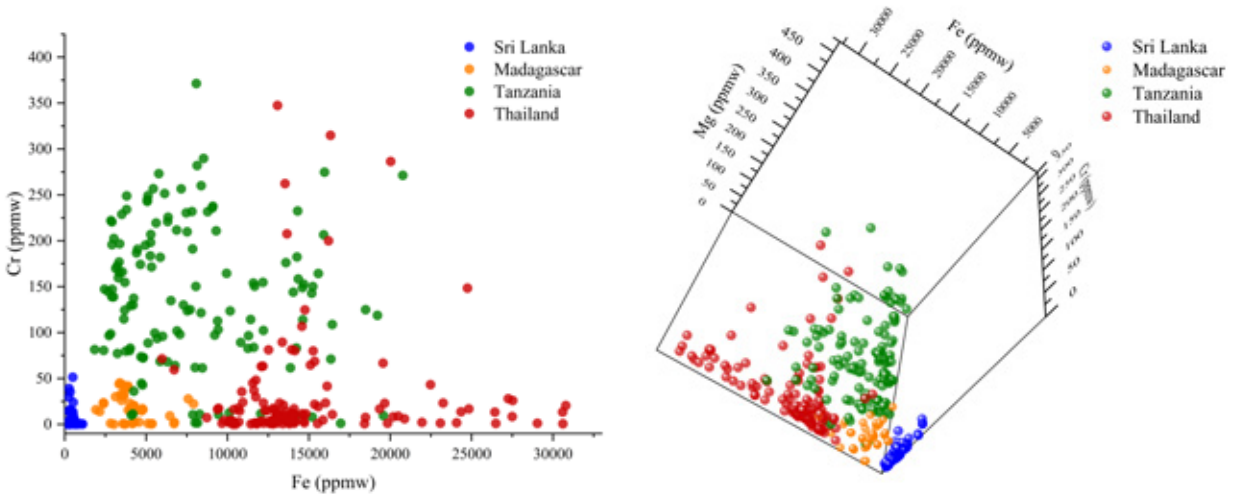

Figure 4: 2D and 3D scatter plots of trace element contents in yellow sapphires in this study.

Conclusion

This preliminary study demonstrates the potential for determining the geographic origin of yellow sapphires using a combination of various analytical techniques. The results highlight the ability to distinguish samples from Sri Lanka, Madagascar, Tanzania, and Thailand. Scatter plots of Fe-Cr and Fe-Mg-Cr concentrations show good clustering patterns, with Fe, Mg and Cr emerging as a key geochemical marker that reflects differences in geological formation. The integration of multiple methods, including inclusion observation, chemical analysis, and spectroscopic techniques, further enhances the accuracy of origin identification. For future research, increasing the sample size and incorporating a broader range of sample types and origins, colour variations, and treated stones from each locality will help strengthen and validate these findings.

References:

- Dubinsky, E.V., Stone-Sundberg, J., Emmett, J.L., 2020. A Quantitative Description of the Causes of Color in Corundum. Gems & Gemology, 56(1), 2–28.
- Emmett, J.L., Scarratt, K., McClure, S.F., Moses, T., Douthit, T.R., Hughes, R., Novak, S., Shigley, J.E., Wang,W., Bordelon, O., Kane, R.E. 2003. Beryllium Diffusion of Ruby and Sapphire. Gems & Gemology, 39(2), 84–135.
- Palke, A.C., Saeseaw, S., Renfro, N.D., Sun, Z., McClure, S.F., 2019. Geographic Origin Determination of Blue Sapphire. Gems & Gemology, 55(4), 536–579.
- Saeseaw, S., Sangsawong, S., Vertriest, W., Atikarnsakul, U., Raynaud-Flattot, L.V., Khowpong, C., Weeramonkhonlert, V., 2017. A Study of Sapphire from Chanthaburi, Thailand and Its Gemological Characteristics. Gems & Gemology, 53, 1-42.
- Saeseaw, S. Khowpong, C., Vertriest, W., 2020. Low-Temperature Heat Pink Sapphires for Ilakaka, Madagascar. Gems & Gemology, 56(4), 448–457.

Rubies from Greenland

Vincent Pardieu
VP Consulting WLL, Manama, Kingdom of Bahrain, vince@fieldgemology.org

"Rubies from Greenland – A Field Gemology Travelogue" a book by Vincent Pardieu

Gemology is traditionally practiced in laboratories, focused on identifying and analyzing gemstones. Vincent Pardieu's journey, however, took a different path. In 2005, he coined the term *field gemology* to describe the practice of studying gems at their source—in mines, markets, and remote locations. Since 2004, he traveled the world collecting research samples, carefully documenting each using what he calls the "Four Ws": When, Where, From Whom, and How it was collected. As Sir David Attenborough aptly noted, without context, a specimen loses much of its scientific value (Pardieu, 2020).

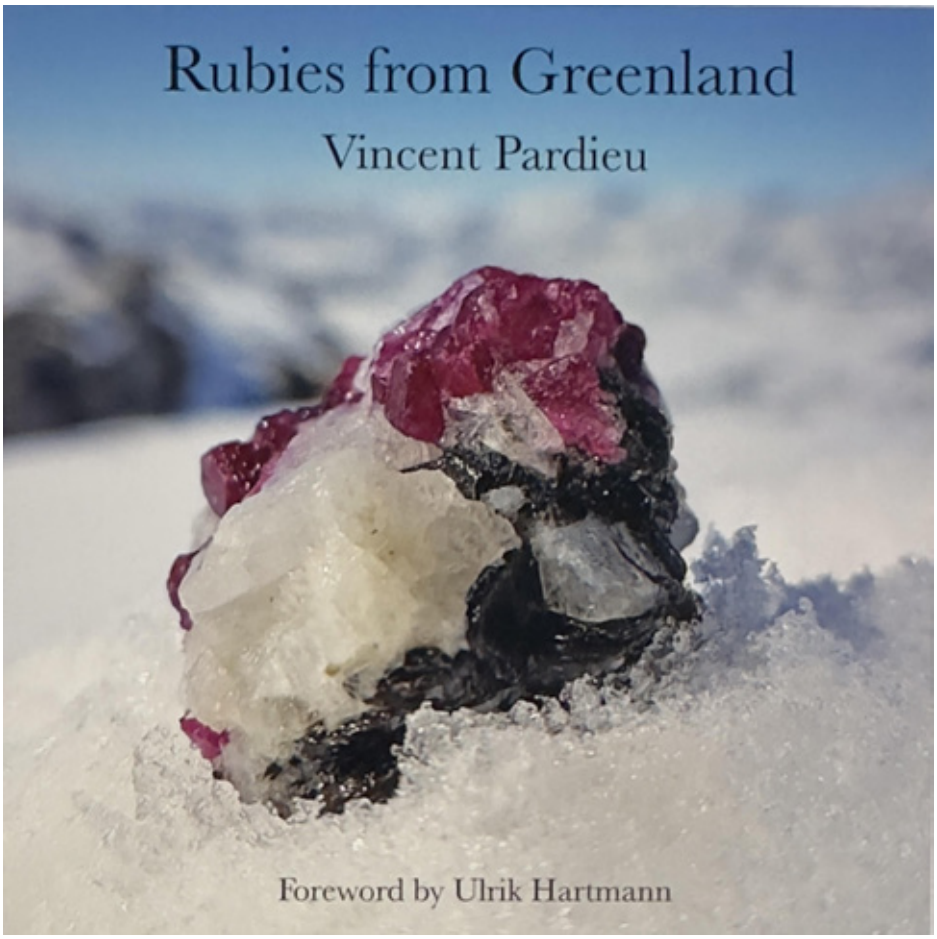

Beyond collecting reliable reference samples for gemological research, the author aims to capture the full story—through photographs of landscapes, miners, and the often-overlooked realities of extraction. While most in the gem trade focus on the polished final product, the origin of a gem profoundly influences its scientific, commercial, and cultural significance. This book, *Rubies from Greenland – A field gemology travelogue*, offers a visual and narrative account of the eleven visits Vincent Pardieu had to the Aappaluttoq ruby mine in Greenland. It follows the journey of these rubies from the mine to Bangkok—where they are heat-treated, cut, and polished—and finally to Denmark, where Hartmann's sets them into fine jewelry, some of which is now worn by Queen Margrethe II.

Rubies were first discovered in Greenland in 1965 (Herd & al, 1969). In the early 2000s, commercial interest grew, eventually leading to the development of a mining project. VP was invited in 2017 as a consultant when the mine officially began production. Remarkably, the rubies from Greenland belong to the same geological type as those from East Africa (Madagascar, Tanzania, Mozambique, and Malawi), associated with amphiboles—deposits that have now overtaken marble- and basalt-related sources as the primary origin of rubies in the global market (Giuliani *et al*, 2020). Yet, aside from Greenland, these amphibole-related ruby deposits remain under-researched. Beyond the scientific value, VP was struck by the paradox of a modern, high-tech mining operation in such a remote, untouched landscape. He proposed conducting heat-treatment experiments in Thailand to enhance the rubies' suitability for the jewelry market. The successful results led to the establishment of a Bangkok office and the development of traceability software that tracked each gem from mine to market. From 2017 to 2022, VP worked closely with the Aappaluttoq team—offering training, technical advice, and documenting the process through photography and video. Despite significant achievements, the mine struggled with challenges, especially during the COVID-19 pandemic (Pardieu, 2021). It ceased operations in 2022, and in 2024, Greenland Ruby declared bankruptcy.

This book is a tribute to those five unforgettable years. With hundreds of photos over 280 pages, it is visual reference on an extraordinary project. It offers a unique window into the complex and often secretive world of gemstone sourcing; sheds light on Greenland's mining potential and logistical challenges and honors the people who brought to life what are now recognized as the oldest known rubies on Earth.

References:

- Giuliani, G., Groat, L.A., Fallick, A.E., Pignatelli, I. & Pardieu, V. (2020). Ruby deposits: A review and geological classification. Minerals, 10(7), article 597 (83 pp.), https://doi.org/10.3390/min10070597
- Herd, R.K, Windley, B.F. & Ghisler, M. (1969): The mode of occurrence and petrogenesis of the sapphirine-bearing and associated rocks of West Greenland. Rapp. Grønlands geol. Unders. 24, 44 pp.
- Pardieu, V. (2020) Field gemology: The evolution of data collection. InColor, No. 45, pp. 37–42.
- Pardieu V., (2021) Back in the Field: An Expedition to Greenland's Ruby Mines, Gems & Jewellery Autumn 2021, pp.12-17

Blue sapphire from Malacacheta of Minas Gerais, Brazil

Masaki Furuya
Japan Germany Gemmological Laboratory, Kofu, Japan E-mail: jggl@sapphire.co.jp

Malacacheta, located in Minas Gerais, Brazil, is renowned for its alexandrite deposits and com-plex geological setting. Mining of alexandrite began in 1975, peaked around 1987, and contin-ued into the 2000s. Brazilian cat's eye alexandrite from this locality remains available in the mar-ket today. In addition to alexandrite, sapphires of various colors have also been reported from Malacacheta (Liccardo *et al*., 2006). However, sapphire has not been the primary focus of min-ing activity. These sapphires are recovered from the same alluvial deposits as alexandrite and are estimated to have formed in a metasomatic environment.

In this study, 13 faceted blue sapphire samples (Figure 1) from Malacacheta, commercially available on the market, were analyzed. According to the supplier, the sapphires were recovered together with alexandrite as a byproduct. The samples ranged in size from 0.35 to 0.69 ct and displayed colors ranging from light blue to vivid violetish blue, with some exhibiting visible color zoning. All samples were transparent, although some contained visible inclusions.

The sapphires exhibited gemological characteristics consistent with typical blue sapphire. Re-fractive indices ranged from 1.76 to 1.77, and specific gravity ranged from 3.98 to 4.00. Pleoch-roism ranged from pale to vivid blue. The samples were inert to both long-wave and short-wave UV radiation.

About microscopic features, most samples showed strong strain and color zoning (Figure 2). Comet tail-like inclusions were observed in some samples (Figure 3). Numerous samples con-tained crystal inclusions identified as plagioclase (Figure 4). Other mineral inclusions were rare; only one sample exhibited carbon and calcite inclusions within a surface-reaching cavity. Raman spectroscopy of a negative crystal inclusion (Figure 5) revealed CO_2 peaks at 1279.8 and 1384.6 cm^{-1} (Frezzotti *et al*., 2012). Additionally, no two phase inclusions were found in the samples.

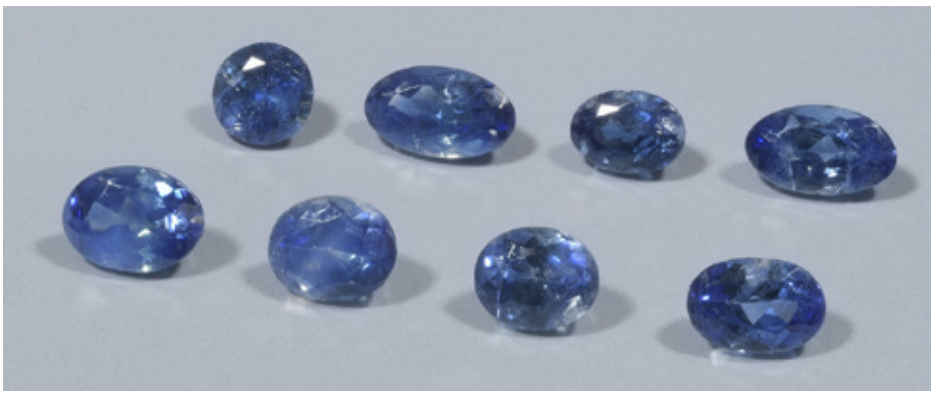

Figure 1. Tested samples of blue sapphire from Malacacheta

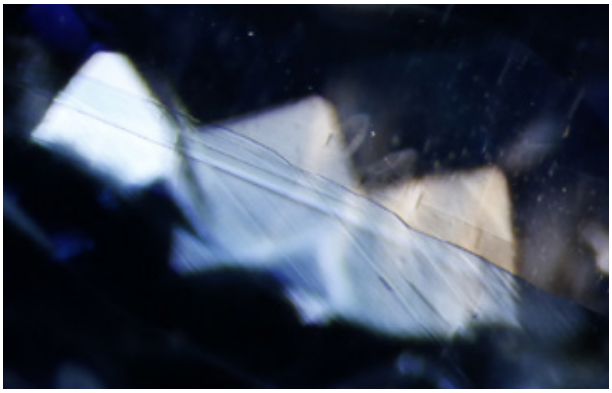

Figure 2. Strong strain with colour zoning

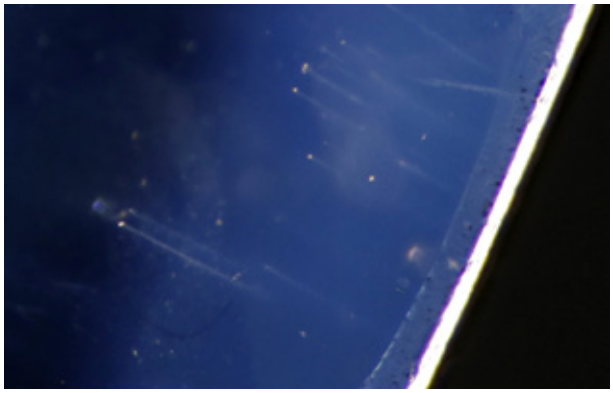

Figure.3 Comet like inclusions

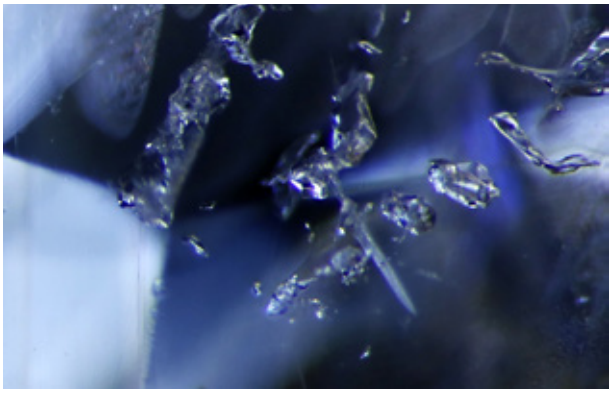

Figure 4. Plagioclase inclusion

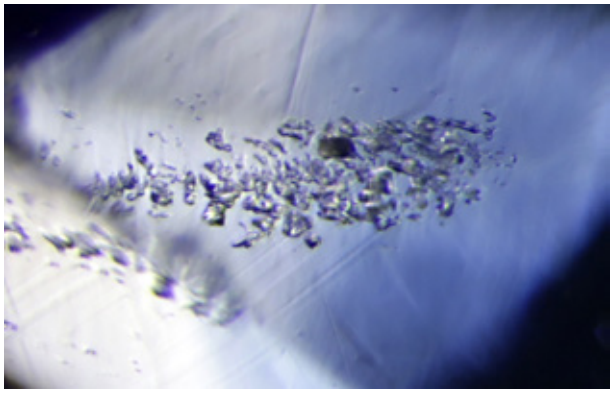

Figure.5 Negative inclusions tested with Ra-man

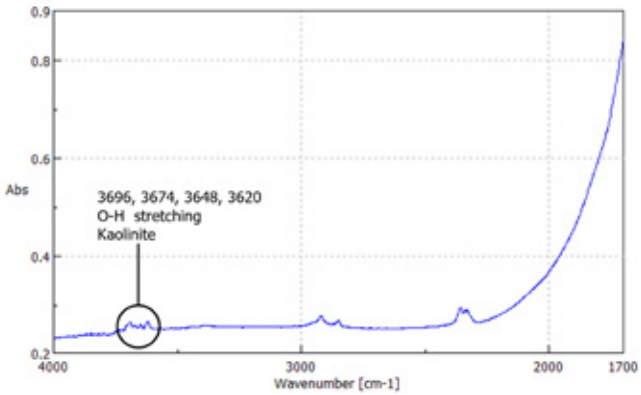

Figure 6. FT-IR spectrum with kaolinite absorption

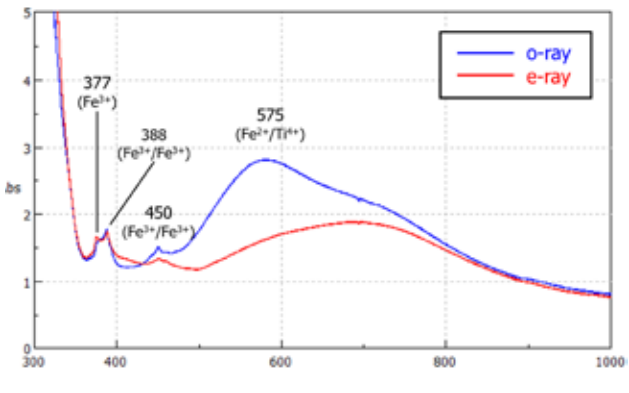

Figure.7 Polarized UV-Vis spectra

Origin	Malacacheta		Myanmar	Madagascar	Sri Lanka	Montana (Blue)
Elements	range	mean				
Be	0.2-3.1*	1.2*	-	-	-	-
Mg	41.9-138.4	81.5	25	63	63	37
Ti	127.2-608.5	320.2	59	164	138	50
V	8.7-30.5	20.3	1.5	23	9.4	5.2
Fe	1,845-6,393	3,722	2,040	924	997	4,598
Ga	53.7-124.0	83.0	89	63	97	54
Source	This study		Kreb, 2020			Zwaan, 2016

(* except high points)

Table 1. Trace elements of sapphire from Malacacheta and other origins (in ppmw)

FT-IR spectroscopy revealed almost no significant absorptions, except for weak kaolinite peaks in one sample. No OH-related absorptions around 3309 cm^{-1} were detected, not even as an al-most insignificant feature (Figure 6). UV-Visible spectroscopy indicated characteristics typical of non-magmatic sapphires, with no broad-band absorption near 880 nm and a UV cut-off be-tween 320 and 330 nm (Figure 7). These features suggest a metamorphic origin and the absence of heat treatment under reducing conditions.

LA-ICP-MS analysis detected Be in all samples, with concentrations ranging from 0.2 to 3.1 ppmw across most areas, and up to 6.8 ppm in specific regions containing cloud-like inclusions. High field strength elements such as Sn, Nb, and Ta were also detected in proportion to Be. Compared to the average trace element concentrations reported by Kreb *et al*. (2020) and Zwaan *et al*. (2016), the Malacacheta sapphires exhibited higher levels of Fe, Ti, and Mg than meta-morphic sapphires from Myanmar, Madagascar, and Sri Lanka. In particular, the Fe concentra-tions were similar to those found in Montana sapphires.

The Malacacheta sapphires are mined from alluvial deposit together with alexandrite. As the host rock for alexandrite formation in Malacacheta remains unidentified (Basílio *et al*., 2013), the exact origin of the sapphire is also uncertain. However, Basílio (2013) proposed that the alexandrite in this region formed via a Cambrian-aged metasomatic system, in which beryllium-rich fluids from nearby granite intrusions interacted with meta-ultramafic rocks and peralumi-nous schists. The features observed in this study—including strong strain patterns, CO_2 rich fluid inclusions and plagioclase inclusions, the absence of OH absorption in FT-IR spectra, and elevated Be, Fe, Mg, Ti concentrations—support the hypothesis that these sapphires might have crystallized in peraluminous schists and undergone metasomatic alteration by Be-rich fluids de-rived from granite intrusions.

References:

- Basílio M.S., Pedrosa-Soares A.C., Jordt-Evangelista H. 2013. Depósitos de alexandrita de Mala-cacheta, Minas Gerais. Revista Geonomos, 8(1), 47-54.
- Frezzotti M.L., Tecce F., Casgali A. 2012, Raman spectroscopy for fluid inclusion analysis. Journal of Geochemical Exploration, 112, 1–20.
- Krebs M.Y., Hardman M.F., Pearson D.G., Luo Y., Fagan A.J., Sarkar C. (2020). An evaluation of the potential for determination of the geographic origin of ruby and sapphire using an expand-ed trace element suite plus Sr–Pb isotope compositions. Minerals, 10(5), 447.
- Liccardo A., Jordt-Evangelista H., Oliveira E.F. 2006. Coríndon no Brazil: Química, inclusões, espectroscopia e aspectos genéticos. Revista Brasileira de Geociências, 36, 157-166.
- Zwaan J.C., Buter E., Regina M.K., Kane R.E. 2016. Alluvial Sapphires from Montana: Inclu-sions, Geochemistry, and Indications of a Metasomatic Origin. Gems & Gemology, 51(4), 370-391.

Gemological Characteristics of New Transparent Brown Sapphire

Sutas Singbamroong[1], Tasnara Sripoonjan[2], Montira Seneewong Na Ayutthaya[3], Pukkapon Piantumdee[4], Tanyawit Sutipanya[5], Khaled Hussein[1] and Nazar Ahmed[1]

[1] Dubai Central Laboratory, Dubai, United Arab Emirates, sutas.singbamroong@gmail.com

[2] G-ID Laboratories, Yan Nawa, Bangkok 10120, Thailand

[3] The Gem and Jewelry Institute of Thailand (Public Organization), Bangkok 10500, Thailand

[4] Sunset Gems Co., Ltd., Sam Khok, Pathum Thani, 12160, Thailand

[5] Department of Earth Sciences, Faculty of Science, Kasetsart University, Bangkok 10900, Thailand

A newly observed variety of faceted transparent brown sapphire has recently entered the gem market, prompting gemological attention due to its highly unusual appearance (Figure 1). Unlike traditional brown sapphires—commonly referred to as geuda in Sri Lanka or brown sapphires from basaltic-related origins—which are generally opaque or only weakly translucent due to dense microscopic inclusions and iron-related chromophores (Li and Shaokui, 2022; Wongkokua *et al*., 2023; Zheng *et al*., 2013; Zwaan, 1998). These new samples exhibit high transparency and attractive brown coloration. Such features suggest a treated origin rather than a naturally occurring chromophore system. This study investigates the gemological, spectroscopic, and chemical properties of these stones, with a focus on identifying the origin of color, the presence of any treatments, and the probable geological source.

Gemological testing confirmed that the stones are corundum, with refractive indices between 1.760 and 1.770 and specific gravities close to 3.98–4.00. Spectroscopic analysis revealed a gradual absorption rise beginning near 550 nm and extending into the UV region (Figure 2), attributed to charge transfer between trapped holes (h') and Fe^{3+}, as well as a small distinct absorption at 388 nm caused by isolated Fe^{3+} ions (Dubinsky *et al*., 2020). Notably, absorptions typically associated with Fe^{3+}– Fe^{3+} pairs, particularly at 377 and 450 nm, were absent, indicating that iron does not serve as the dominant chromophore in these samples. Microscopic observation revealed minute particulate inclusions and hazy zones causing Tyndall scattering. In some specimens, discoid fissures, glassy internal features, and dotted whitish minute particles consistent with rutile breakdown were observed—

Figure 1 Rough and faceted transparent brown sapphires. The pear-shaped stone in the middle weighed 2.29 ct. Photo: T. Sripoonjan

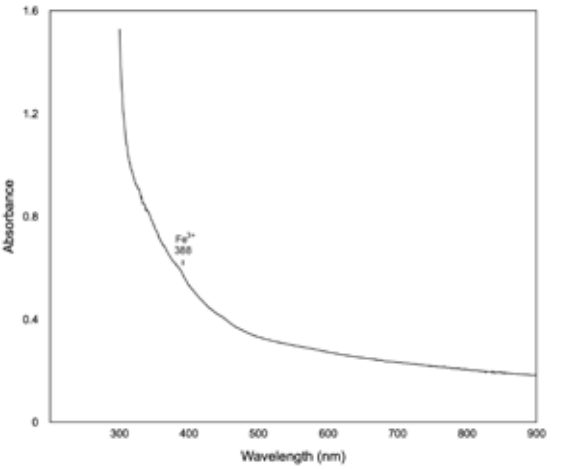

Figure 2 Representative UV-Vis-NIR spectrum of brown sapphire from this study

features indicative of exposure to extreme temperatures and supporting evidence of high-temperature heat treatment.

Laser ablation ICP-MS analysis detected beryllium concentrations ranging from 5 to 62 ppma, strongly suggesting that these sapphires have undergone heat treatment involving the diffusion of beryllium. Iron concentrations were low and closely aligned with those typical of metamorphic sapphires such as those from Sri Lanka, as opposed to those derived from basaltic sources. FTIR spectroscopy showed no hydrous or hydroxyl-related absorption bands, consistent with oxidative heating at elevated temperatures. DiamondView imaging revealed chalky blue fluorescence localized in the brown zones, attributed to titanate group-related structural features (Vigier *et al*., 2023). This fluorescence behavior, combined with the low iron content, reinforces the hypothesis that the brown coloration is primarily due to submicroscopic titanate-related particles and associated defect centers, rather than conventional Fe-based chromophores.

These findings reveal a previously undocumented treatment-induced appearance in sapphires and highlight the importance of advanced analytical methods in establishing origin and treatment history. This study underscores the need for continued research; particularly experimental work aimed at reproducing this brown color through controlled heating processes—a technically complex challenge that may yield deeper insights into color development mechanisms in corundum.

References:

- Dubinsky, E.V., Stone, J., Emmett, J.L., 2020. A quantitative description of the causes of color in corundum. Gems and Gemology, 56(1), 2-28.
- Li, Y., Shaokui, P., 2022. Gemological characteristics of brown sapphire from Guinea, Africa. Journal of Gems and Gemmology, 24(3), 10-19.
- Vigier, M., Fritsch, E., Cavignac, T., Latouche, C., Jobic, S., 2023. Blue shortwave luminescence of gems: the role of titanate groups. 37th International Gemmological Conference, Tokyo, Japan 23-27 October, 55-56.
- Wongkokua, W., Lhuaamporn, T., Monarumit, N., Kajornboonsook, P., Wathanakul, P., 2023. Explanation on yellow, green and brown coloration series of basal related Bangkaja sapphires. 37th International Gemmological Conference, Tokyo, Japan 23-27 October, 147-149.
- Zheng, Y., Zhao, K., Tang, X., Xie, Z., Zu, E., 2013. Study on color change of brown sapphire in Changle, Shandong. Advanced Mineral Research, 842(2014), 160-164.
- Zwaan, J.C., 1998. Geuda sapphire from Sri Lanka, Australian Gemologist, 20(11), 429-436.

Acknowledgements

The authors gratefully acknowledge the Gem and Jewelry Institute of Thailand (GIT) for their valuable assistance in providing advanced analytical facilities for this study. Special thanks are extended to Mr. Pukkapon Piantumdee of Sunset Gems Co., Ltd. for generously supplying the sapphire samples that were critical to the completion of this research.

HFSE-enriched sapphires of gem quality: A combined FTIR and trace element study and implications for heat treatment detection

Michael S. Krzemnicki[1,2], Wei Zhou[1], Pierre Lefèvre[1], Markus Wälle[1], Hao Wang[1]

[1] Swiss Gemmological Institute SSEF, Basel, Switzerland

[2] Department of Environmental Sciences, University of Basel, Switzerland

Corresponding author: michael.krzemnicki@ssef.ch

Gem-quality sapphires containing 'exotic' elements such as Sn, Nb, Zr, Ta, W, are of special interest in gemmological research, as the concentration of these so-called high-field-strength-elements (HFSE) often correlate with detectable traces of naturally incorporated beryllium (Whatanakul *et al*. 2004, Pardieu 2007, Shen 2007, Zhou *et al*. 2022 & 2024). It is this correlation, which enables gemmologists in most cases to safely separate them from Be-diffusion treated sapphires which show no such correlation when analysed with LAICPMS. In addition, some of these sapphires may also contain thorium and lead traces, which enable us to carry out direct radiometric dating on such sapphires (Wälle & Wang 2023).

Interestingly, such 'exotic' trace elements are found in both, basaltic sapphires (e.g. Nigeria, Tasmania, N-Madagascar) and metamorphic sapphires (e.g. Madagascar, Sri Lanka, Afghanistan) and are commonly related to metasomatic processes during crystal growth. How these incompatible elements and beryllium were incorporated into sapphires has been investigated in several studies, with models explaining the presence of these elements either by primary integration of nano-inclusions during growth of the sapphire or by direct incorporation of these elements into the corundum structure with a possible epigenetic segregation into nanoclusters or precipitates as nanoparticles of separate phases (Shen & Wirth 2012, Emori et al 2019; Oto *et al*. 2023, Jin *et al*. 2024 and references therein).

This study focuses mainly on FTIR spectroscopy of HFSE-enriched sapphires of metamorphic origin from Madagascar and Sri Lanka. We analysed 18 untreated but gem-quality sapphires ranging in weight from 0.45 ct to 50 ct, partly from the SSEF research collection and from reliable trade members (Figure 1). All samples contained either goethite (e.g. in deep hollow tubes) or diaspore in fluid inclusions,

Figure 1: Selection of investigated sapphires (5.7 ct to 50 ct) from Madagascar and Sri Lanka.

thus confirming them to be unheated samples (Sripoonjan *et al.* 2016; Krzemnicki *et al.* 2023). Interestingly, most of the investigated samples were of very fine quality with a velvety blue colour generally related to a certain amount of turbidity and occasionally dense growth structures and thin laces of very dark ink-blue colour.

Most of these HFSE-sapphires showed a broad absorption band at about 3300 cm^{-1}, partly accompanied by peaks at 3182, 3232, and 3308 cm^{-1} related to OH- groups associated with Al vacancies (Moon & Phillips 1991; Beran & Rossman 2006; Jollands *et al.* 2023 and references therein). By comparing their trace element content, we found best correlation with the tantalum concentration in these samples, although contribution by other HFSE-elements including Sn cannot be fully excluded. In general, HFSE-bearing sapphires with a low Ta concentration exhibited none to a small band, whereas stones with higher Ta were characterised by an increasingly strong band at 3300 cm^{-1}. As a special case, we found in sample 032 a similar but slightly shifted broad band centred at about 3385 cm^{-1} with two small side peaks at 3254 and 3310 cm^{-1}. Although high in tantalum (Ta_{mean} 67 ppm), the reason for this 'shift' and the side peak at 3254 cm^{-1} is not yet fully understood and needs further research.

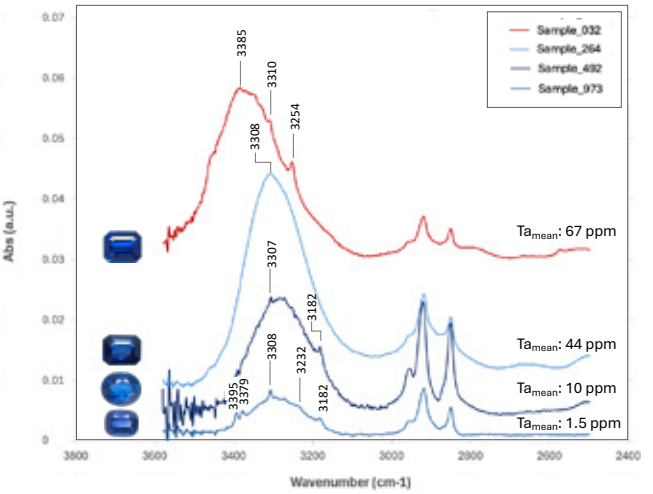

Figure 2: FTIR spectra of selected HFSE-sapphires characterised by a broad band centred at 3300 or 3385 cm^{-1}. Sample 973 generally has a mean Ta concentration of 1.5 ppm, but contains a micro-zonation enriched up to 345 ppm Ta, which may have a certain (small) influence on the observed FTIR spectrum.

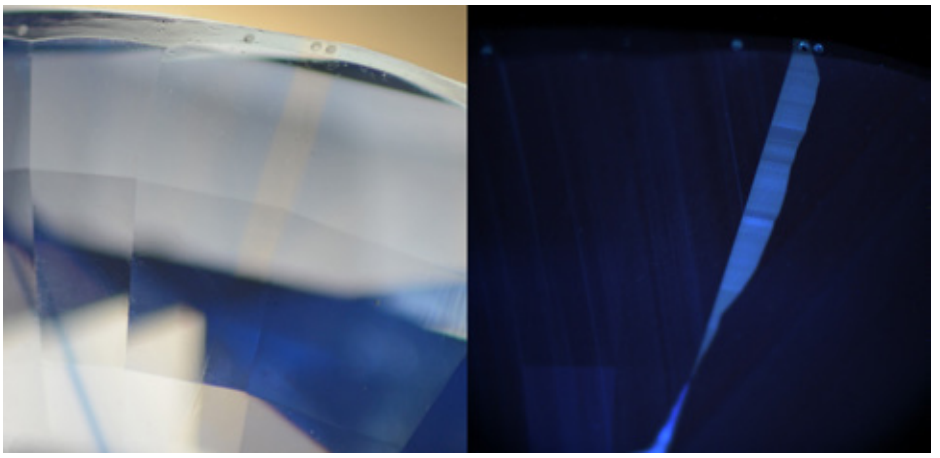

Figure 3: Thin Ta-rich (and HFSE-rich) zone in HFSE-sapphire sample 973 seen under microscope as colourless band and as chalky white zone in deep UV (DiamondView™).

Conclusions:

This study on unheated sapphires enriched in HFSE-elements reveals the presence of a broad absorption band at about 3300 cm^{-1}, seemingly best correlated with the Ta-concentration in these sapphires. The 'shift' of this band to 3385 cm^{-1} observed in one sample (Sample 032) is yet not fully understood, although assumed to be also related to some extent to tantalum.

Notably, some of these unheated sapphires show small OH- related peaks (3182, 3232, and 3308 cm^{-1}). In addition, these unheated sapphires also exhibit varying intensities of chalky white reactions. Although both features (OH- peaks in FTIR and chalky reaction in SWUV) are well known and described in heat treated metamorphic sapphires, this study reveals that such features may also be encountered in unheated stones. As such this study further underlines, that a simplistic approach for no-heat/heated distinction can be erroneous specifically for metamorphic sapphires with velvety appearance and turbidity. Only a full characterisation of these sapphires including Raman spectroscopy on inclusions (diaspore, goethite, zircon) and detailed trace element analyses (LAICPMS) may provide the answer whether such a sapphire had been heated or not.

References:

- Beran, A., Rossman, G.R. 2006. OH in naturally occurring corundum. Eur. J. Mineral., 18, 441–447.
- Emori K., Kitawaki H., Miyake A., 2019. Be-containing nano-inclusion in untreated blue sapphire from Diego, Madagascar. International Gemmological Conference Nantes-France Proceedings, 124-126.
- Jin, S., Saxey, D.W., Quadir, Z. *et al*., 2024. Nanoparticles in natural beryllium-bearing sapphire: incorporation and exsolution of high field strength elements in corundum. Contrib Mineral Petrol 179, 110 (2024).
- Jollands M. C., Jin S., Curti M., Guillaumet M., Béneut K., Giura P., and Balan E., 2023. Vibrational properties of OH groups associated with divalent cations in corundum (α-Al_2O_3), Eur. J. Mineral., 35, 873–890.
- Moon A.R., Phillips M.R., 1991. Titania precipitation in sapphire containing iron and titanium. Phys Chem Min, 18, 251–258.
- Oto S., Miyake A, Igami Y.. Emori K Kitawaki H., 2023. Crystal structure of Nano inclusions in blue sapphire from Diego, Madagascar. International Gemmological Conference Tokyo Proceedings, 135-137.
- Pardieu, V., 2007. Discovering beryllium in Madagascar blue sapphires. InColor 2007.
- Shen A., McClure S., Breeding C. M., Scarratt K., Wang W., Smith C., Shigley J., 2007. Beryllium in Corundum: The Consequences for Blue Sapphire. GIA Insider, Vol. 9, Issue 2 (January 26, 2007)
- Shen, A., Wirth, R., 2012. Beryllium-bearing nano-inclusions identified in untreated Madagascar sapphire." *Gems & Gemology*, Vol. 48, No. 2, 150-151.
- Sripoonjan T., Wanthanachaisaeng B., Leelawatanasuk T., 2016. Phase transformation of epigenetic iron staining: Indication of low-temperature heat treatment in Mozambique ruby. J. Gemmol., 35, 156–161.
- Wälle M., Wang H.A.O., 2023. 'Direct' Thorium-Lead dating of gem quality corundum by laser ablation ICP-TOF-MS. EuroAnalysis 2023 Geneva, Abstract Book, 64-65.
- Wathanakul, P., Atichat, W., Pisutha-Arnond, V., Win, T.T., Singbamrung, S., 2004. Evidence of the unusually high Be, Sn, Nb, Ta content in some trapiche like sapphires from basaltic origin, Proceedings of the 29th International Gemmological Conference, Wuhan, China.
- Zhou Wei, Krzemnicki M.S. and Wang H.A.O, 2022. Cases studies of chemical variation vs. zonation within single blue sapphire. The 23rd International Mineralogical Association General Meeting 2022, July, 2022, Lyon, France. Abstract-Proceedings.
- Zhou Wei, Krzemnicki M.S. and Wang H.A.O, 2024. Trace element in blue sapphire: Challenge or potential of element analyses by LA-ICP-TOF-MS for origin determination? The 37th International Geological Congress 2024, August, 2024, Busan, Korea. Abstract-Proceedings.

Low Temperature Heat Treatment of Madagascar Sapphire

E. Billie Hughes[1] and Rosey Perkins[2]
[1] Lotus Gemology, Bangkok, Thailand [2] London, UK
billie@lotusgemology.com

One of the challenges facing gemologists today is the detection of low temperature (below 1200°C) heat treatment in corundum (Hughes *et al*., 2017). At these temperatures, the color of ruby and sapphire can be altered, but some common features such as rutile silk mav remain intact.

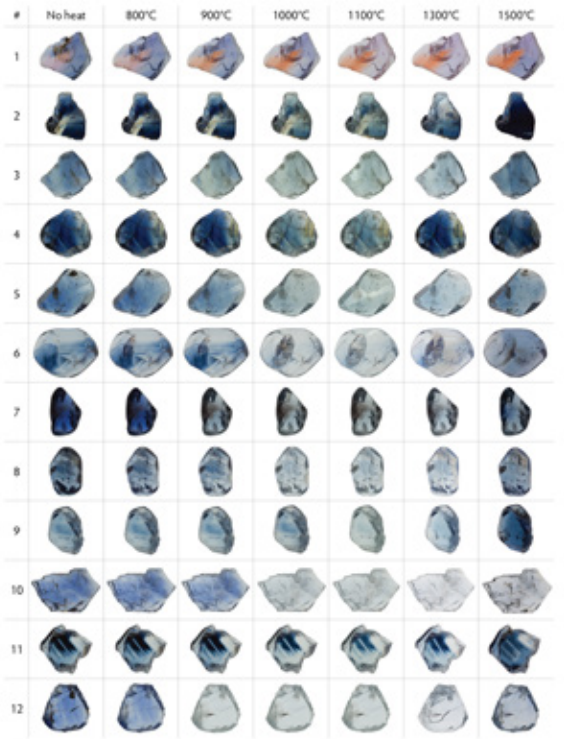

Figure 1. Madagascar sapphire before and after heating the 12 samples, shown before and after heating to each temperature. Most of the samples began to lighten significantly after heating to about 900–1000°C and started to deepen in color again around 1300°C. After heating to 1500°C, many pieces became significantly deeper in color. Photos not to scale. Photos by Rosey Perkins and Sora-at Manorotkul.

To aid in detection, the authors heated Madagascar sapphires at a range of temperatures from 800°C to 1500°C. The samples were documented using macrophotography in the untreated state and after heat treatment at elevated temperatures (figure 1), photomicrography of inclusions (figure 2), ultraviolet fluorescence imaging (figure 3), and spectroscopic analysis (ultraviolet/visible/near infrared and infrared) to record any changes, with a focus on features that could help detect heat treatment.

Results showed that a combination of inclusion studies, infrared spectroscopy, and observation of fluorescence could help detect treatment. We also noticed a fascinating change in UV-Vis-NIR spectra that can have implications for origin determination of blue sapphire (figure 4) (Schmetzer and Bank, 1980 and Emmett and Douthit, 1993). Many of the samples developed a peak at 880 nm after heat treatment. This can make it challenging to separate heated metamorphic sapphires from Madagascar from the basalt related material.

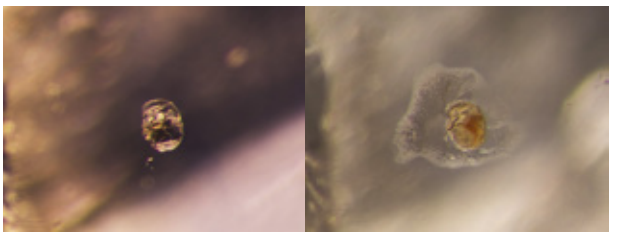

Figure 2.
Left: A small, flat crystal is pictured in sample 10 before heat treatment.
Right: After the first heating to 800°C, a reflective fissure begins to appear around the crystal. By 1100°C (pictured), the fissure has begun to heal at the edges.

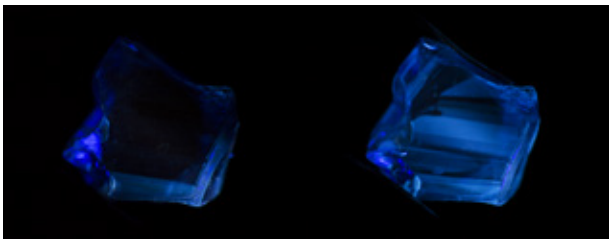

Figure 3. Short-wave UV fluorescence reaction of a Madagascar sapphire during heating
Left: Sample 11 began to show a short-wave fluorescence reaction after heating to 1000°C. This was mainly limited to one side of the stone, where a chalky blue band can be seen.
Right: After heating to 1100°C, the chalky blue reaction became stronger and more widespread, with chalky blue bands across the stone.

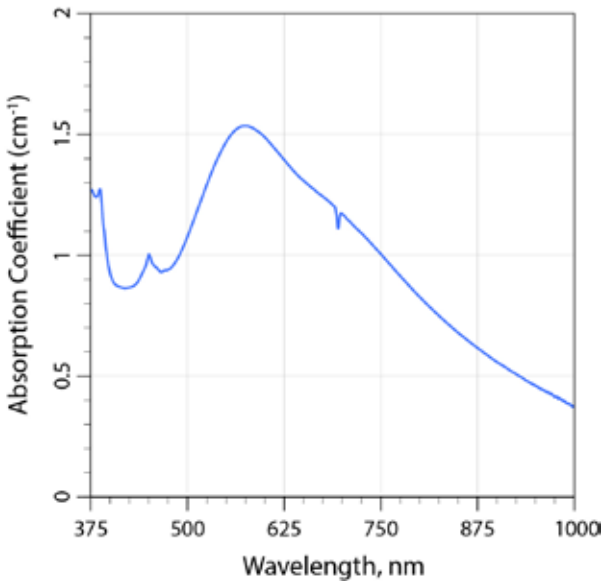

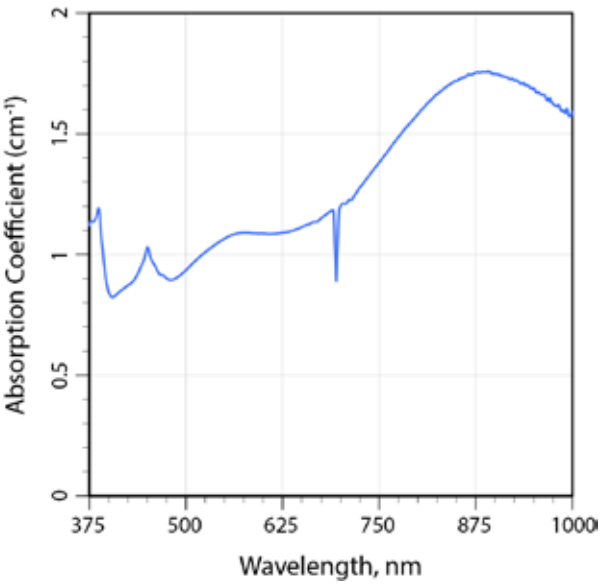

Figure 4. UV-Vis-NIR spectrum of a Madagascar sapphire before and after heating
Left: The UV-Vis-NIR spectrum of sample 7 before heat treatment. Note that the most prominent feature is the absorbance between 500 and 600 nm, as well as a small Fe-related peak around 450 nm.
Right: The UV-Vis-NIR spectrum of sample 7 after heating to 900°C. Note the development of a large peak at ~880 nm.

References:

- Emmett J., Douthit T. (1993) Heat treating the sapphires of Rock Creek, Montana. Gems & Gemology, Vol. 29, No. 4, pp. 250–272.
- Hughes R.W., Manorotkul W., Hughes E.B. (2017) Ruby & Sapphire: A Gemologist's Guide. RWH Publishing/Lotus Publishing, Bangkok, 816 pp.
- Schmetzer, K. and Bank, H., 1980, Explanation of the absorption spectra of natural and synthetic Fe- and Ti containing corundums, Neues Jahrbuch für Mineralogie, Abhandlungen, Vol. 139, No. 2, pp. 216–225.

Effects of Gamma Irradiation on Corundum: Towards a Potential Detection Method

Hao A.O. Wang[1], Markus Wälle[1], Vladimir Hutanu[2], Xiaosong Li[2], Michael S. Krzemnicki[1,3]

[1] The Swiss Gemmological Institute SSEF, Basel, Switzerland; hao.wang@ssef.ch

[2] Research Neutron Source Heinz Maier-Leibnitz (FRM II), Garching, Germany;

[3] Department of Environmental Sciences, University of Basel, Basel, Switzerland.

Introduction

Corundum, encompassing the highly prized ruby and sapphire varieties, stands as a cornerstone of the global gemstone market. The allure and value of these gems have historically driven the development of various treatment techniques aimed at enhancing their colour and clarity. While many treatments are stable and widely accepted when properly disclosed, the emergence of new or less understood methods presents an ongoing challenge for the gemological community. Accurate detection and disclosure of all treatments are paramount for maintaining market confidence and ensuring fair trade. Gamma irradiation has been explored as a potential method to alter the colour of various gemstones, including corundum (Ashbuugh, 1988; Pardieu *et al*., 2022). However, the effects of such irradiation on corundum, the stability of any induced colour changes, and robust methods for their detection remain areas requiring comprehensive investigation. This contribution builds upon our preliminary work, presented at the IGC Tokyo 2023 (Wang et al., 2023), to provide a more in-depth understanding of gamma irradiation effects on a diverse suite of corundum samples and to outline a potential detection method.

Materials and methods

• **Sample selection:** For this study, we carefully selected 29 natural and synthetic corundum samples. This selection was designed to represent a variety of colours, including colourless, pink to purple fancy sapphires, rubies and sapphires. The rationale was to assess how differing trace element compositions, which are fundamental to corundum's colour, influence the response to gamma irradiation. Four selected samples representing different initial colours and elemental concentrations (Mg, Ti, V, Cr, Fe) are presented in Table 1. Elemental concentrations were determined by LA-ICP-TOF-MS.

		Init. Colour	Mg	Ti	V	Cr	Fe
Sample 1	Nat. Crd.	blue	100	175	11	10	2800
Sample 2	Nat. Crd.	purple	25	50	10	400	540
Sample 3	Syn. Crd.	purple	-	60	0.6	360	95
Sample 4	Syn. Crd.	purplish red	-	5	1	1700	-

Table 1. Information and initial colours of the selected four corundums as well as their trace element composition. All numbers are in unit of ppm. "-" indicates that the concentrations are below detection limit ~1ppm.

• **Gamma irradiation:** The samples were subjected to gamma irradiation at FRM II Facility for a continuous period of 70 hours, achieving a total dose of approximately 33 kGy (Li, *et al*. 2022). This represents a substantially higher dose than in our preliminary investigations, intended to maximize any potential colour alterations.

• **Post-irradiation handling:** Immediately following irradiation, samples were carefully transferred into an aluminum container. This precaution was taken to shield them from ambient light exposure, thereby preserving any unstable colour centers that might have been restored until systematic laboratory analysis could start. Upon return to the laboratory, the initial post-irradiation colour of each sample was documented.

• **Colour stability testing:** To test the colour stability we followed an altered procedure based on the standard testing procedure as used also for client stones in the SSEF laboratory (Krzemnicki, 2022). The colour shift of 4 selected samples after each step are shown in Figure 1.

o Fading test: To assess the light stability of any induced colour, samples were exposed to a 20 W high-power LED light source, for a duration of 3 hours. Importantly, this LED source was characterized by the absence of long-wave UV (LWUV) component at 365 nm and only a negligible contribution of short-wave UV (SWUV) at 254 nm (Palke *et al.*, 2023).

o Activation test: Following the fading test, samples were exposed to standard gemological UV lamps to probe for the presence of colour centers that could be reactivated. This primarily involved exposure to LWUV (365 nm) for 10 minutes. For specific samples that showed no discernible colour shift after LWUV activation (e.g., Sample 3), more energetic activation methods were employed, including LWUV exposure for 2 hours, SWUV exposure for 1 hour and deep UV exposure using a DiamondView instrument for 10 minutes, to explore the potential activation of other types of colour centers.

o UV-VIS-NIR spectroscopic analysis: UV-VIS-NIR absorption spectroscopy was the primary analytical technique used to characterize colour and to identify specific chromophores or colour centers. Spectra were recorded over a range of 290 nm to 1600 nm. While the majority of analyses focused on polarized light through C-axis (O-ray), E-ray measurements were also conducted on select samples to further investigate anisotropic absorption features.

o Mild heat treatment: After the colour stability test, a mild heat treatment at 350 °C for 20 minutes was applied to all samples, in order to see the colour stability under heat condition.

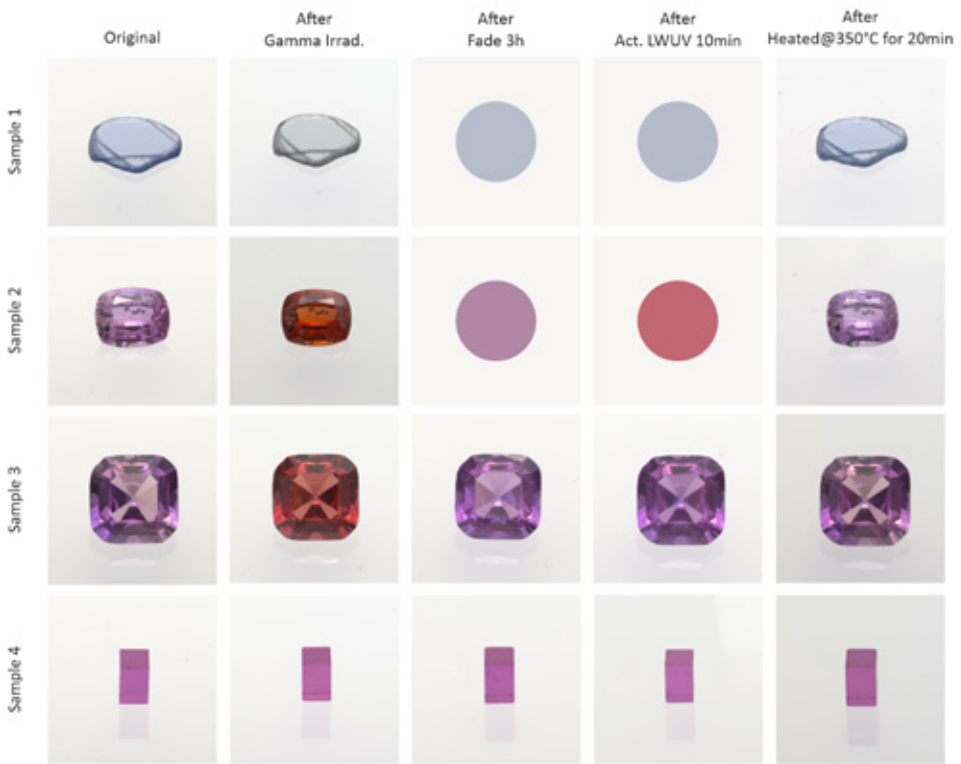

Figure 1. Photos of selected four corundums undergoing colour shift (except for sample 4 no obvious colour shift) after Gamma irradiation, colour stability test in the lab and a mild heat treatment. After fade and after activation photos of Sample 1 & 2 were unfortunately not properly taken, hence the colours are represented by the colour disks.

Results and conclusion

Gamma irradiation induces diverse, chemistry-dependent colour shifts in corundum, which we have categorized into four distinct groups based on their behaviours (Figure 1). These responses include irreversible (during fading or UV activation) blue colour reduction in Fe-Ti rich sapphires (Group 1), which might be one of the reasons that blue/purple hue can be reduced in some rubies. We also observed the development of unstable, light-sensitive, colour reversible orange hues in some natural pink/purple corundum (Group 2) and the appearance of semi-stable orange hues in certain varieties (Group 3) that are bleachable by intense light but not readily reactivated by standard UV sources, nor higher energy UV lights. Notably, high concentration Cr-only synthetic corundum (Group 4) showed an inert response to the irradiation. Those samples with colour shift after irradiation can be restored to their original colours after a mild heat treatment.

The variability and potential transience of these induced colour shifts require a detection approach beyond simple observation. We will propose a strategy based on differential UV-VIS-NIR spectroscopy, meticulously tracking spectral changes during colour stability tests (controlled fading and UV activation). This method involves comparing spectra taken before, during, and after these tests to identify characteristic patterns of colour centres which are unstable, or which can be activated again. We will also discuss spectral features serving as illustrative examples of ongoing investigations into diagnostic markers. This emphasis on the dynamic response of the stone offers greater diagnostic potential than static measurements.

In conclusion, while gamma irradiation effects in corundum are complex and present detection challenges, our methodology may hold promising potential. Future research will focus on expanding the sample database, refining stability testing protocols to enhance diagnostic spectral features, correlating these features with specific colour centres and defects, and validating the method through broader studies. This work aims to provide the gemmological community with more robust tools for identifying gamma-irradiated corundum, thereby supporting market transparency and consumer confidence.

References:

- Ashbuugh, C. E., 1988. Gemstone Irradiation and Radioactivity. Gems & Gemology 24, no. 4, 196-213.
- Krzemnicki, M. S., 2022. New Additional Test at SSEF for The Colour Stability of Rubies SSEF Newsletter. https://www.ssef.ch/new-additional-test-at-ssef-for-the-colour-stability-of-rubies/
- Li, X., Hutanu, V., Bulla, S., Molch J., Jeschke, F., "Gamma irradiations using spent fuel elements at FRM II", RRFM 2022 proceedings, p310-318.
- Palke, A., McClure, S., Renfro N., 2023. Additional Observations on Unstable Color in Padparadscha Sapphires, International Gemmological Conference, Tokyo Japan Proceedings, p132-134.
- Suwanmanee, W., Kittikunlayaworakun, C., Lhuaamporn, T., Jakkawanvibul, C., Leelawatanasuk, T., Atichat, W., Pisutha-Arnond, V., Jangsawang, N., Pangza, K., 2023, Influence of Irradiation on Colour Modification and Colour Stability of Rubies: A Preliminary Study, International Gemmological Conference, Tokyo Japan Proceedings, p138-141.
- Wang, H.A.O., Weltz, D., Krzemnicki, M.S., Mack, A., Wälle M., 2023, Effects of Gamma Irradiation on Ruby and Pink Sapphire and Potential Detection Methods in Gem Labs, International Gemmological Conference, Tokyo Japan Proceedings, p132-134.

Challenges in the Detection of Ruby and Sapphire Treatment in the Thai Market

Supparat Promwongnan, Wilawan Atichat, Cheewaporn Suphan, Wassana Chongraktrakul, and Visut Pisutha-Arnond

The Gem and Jewelry Institute of Thailand (Public Organization), Bangkok, 10500, Thailand, psupparat@git.or.th

Keywords: ruby, sapphire, corundum, treatment detection, heat treatment, FTIR, Raman spectroscopy, diffusion, glass filling, gemology

Abstract

The detection of treatments in ruby and sapphire remains a critical aspect and has become an increasingly complex issue in the gem trade and laboratories alike. Treatments such as traditional heating, flux-assisted heating, various types of glass filling, lattice diffusion heating using elements from an external source, irradiation, and pressure-assisted heating have been widely applied to enhance colour, clarity, and durability of corundum, directly affecting the stone market values and ethical disclosure. The advancement of these techniques, particularly those designed to evade detection, have outpaced many traditional gem detection methods, necessitating the integration of advanced analytical technologies.

Introduction

The commercial value of ruby and sapphire is closely linked to their natural, untreated or treated state. The treatments, usually common, must be accurately detected and disclosed to ensure transparency and maintain consumer trust. However, as treatment technologies evolve, so do the challenges in their detection. This presentation is aimed at reviewing and updating both traditional and advanced methods for identifying treatments in the ruby and sapphire and discusses the identification challenges, ongoing research and future directions in this field.

Overview of Treatment Methods

Corundum treatments are commonly employed to enhance a gem's appearance, and they can be broadly categorized into heat-involved and non-heat-involved methods (Pisutha-Arnond, 2017). Heat-involved treatments include conventional heating (typically around 1200 – 1700 °C), flux-assisted heating using substances like borax and/or silica to (partially) assist healing of fissures. In addition, heat treatment combined with diffusion is used, such as shallow surface-diffusion with added colouring agents such as Ti alone or Ti with Be (as well as Ti and Fe in case of synthetic colourless sapphire) to create blue colouration (e.g., Kane *et al*., 1990, Leelawatanasuk *et al*., 2014, Pisutha-Arnond *et al*., 2019), Cr to produce red hue (McClure *et al*., 1993), and high-temperature beryllium diffusion (above 1700°C) often resulting in yellow colour (e.g., Emmett *et al*.,2003, Pisutha-Arnond *et al*., 2004). Other heat treatments of corundum include fracture filling with high-refractive-index glasses (e.g., lead or bismuth-based, colourless or coloured) at rather moderate temperatures and heating under pressure (e.g., Krzemnicki *et al*., 2019), as well as other low temperature heat treatments. In contrast, non-heat-involved treatments of corundum consist of oil or resin filling to improve clarity, dyeing to enhance or alter colour, and irradiation to induce a change of stone colour (e.g., introducing an unstable yellow hue). Each treatment may produce specific diagnostic features. However, certain corundum treatments - particularly low-temperature heating and recent glass filling – often are challenging for gemologists to accurately identify and properly disclose the treatment of a stone.

Basic and Advanced Techniques for the Detection of Ruby & Sapphire Treatments

- Microscopy: Identification of specific diagnostic features, e.g., altered inclusions, newly healed fissures, presence of flux residue, colour concentration along stone surface and fractures.
- FTIR Spectroscopy: May assist heat treatment detection of corundum, e.g. based on characteristic absorption bands

(e.g., 3232, 3309, 3185 cm^{-1}), though not always conclusive for all samples (Soares *et al*., 2025, Phlayrahan and Homkhajorn, 2021)
- Raman Spectroscopy: Detects phase transformation of some inclusions (e.g., goethite to hematite). The presence of goethite (or diaspore) in corundum is a strong indication that a corundum sample has not been heated (Krzemnicki *et al*., 2023)
- EDXRF and LA-ICP-MS: Identify trace elements and diffusion of foreign elements (e.g., Be, Pb, Ba, Bi) associated with specific treatments (Krzemnicki *et al*., 2004)
- LIBS: Elemental analysis for diffusion treatments, especially Be-diffusion (Krzemnicki *et al*., 2004)
- Luminescence Analysis: Observes changes in silk inclusions and UV-induced luminescence as indicators of heating, especially in Geuda sapphires (Pluthametwisute *et al*., 2025)

Key Challenges in Identification

- Low-temperature heat treatment of corundum is often difficult to detect, as it may not altered inclusions significantly or produce clear spectroscopic markers (e.g., Atichat *et al*., 2011, Hughes *et al*., 2022)
- Heat treatment detection in corundum from basaltic origins is particularly difficult, as natural heating during ascent in alkali basalt and high iron content— which suppresses diagnostic spectral features—complicate differentiation from heated stones. Accurate trace element analysis and close inclusion observation are essential. (e.g., Soonthorntantikul *et al*., 2019).
- Some glass-filled stones may appear highly transparent, masking fractures quite effectively; detection may be supported by chemical analysis (e.g., lead content) and X-ray imaging (see figure 1).
- Surface diffusion treatments create color only on the outer rim, requiring immersion techniques and careful chemical profiling for identification (see figure 2).
- Irradiation treatments can create an unstable (in some cases also stable) yellow colouration, but it could also induce a subtle change of colour that is difficult to distinguish from natural colouration. Currently, only the colour stability of such stones can be checked by a fading test, whereas the irradiation treatment itself cannot be detected up to this day. Recently, advanced spectroscopic and fluorescence techniques are under investigation allowing possibly a reliable detection in the near future (e.g., Wang *et al*., 2023).
- Detection the presence of oil in ruby and sapphire: especially colourless or low-viscosity oil could be a challenge without the backing of other techniques, such as Raman microprobe, FTIR spectroscopy, and hot point tester.
- Overlapping spectroscopic features in treated and untreated stones complicate detection, but the most reliable results come from combining multiple analytical techniques (Soares *et al*., 2025, Phlayrahan and Homkhajorn, 2021).

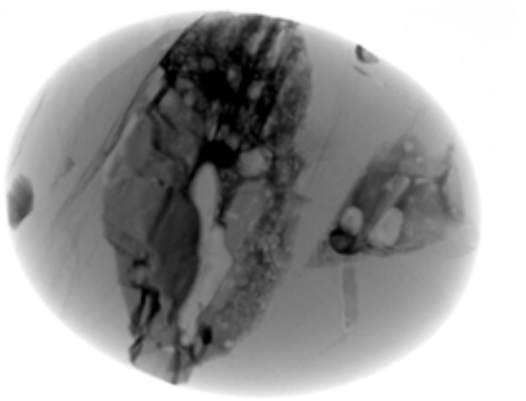

Figure 1. X-ray image of a glass-filled (and heated) ruby showing high density glass along the fractures within the stone. Photo by W. Chongraktrakul; image widths 7.0 mm.

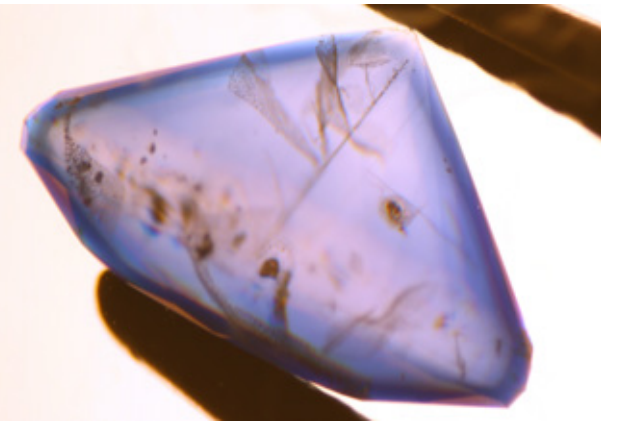

Figure 2. A diffusion-treated sapphire exhibits blue colour concentration along the stone surface, while the interior is noticeably lighter or even colorless. Photomicrograph by S. Promwongnan; image widths 7.0 mm.

Conclusion

The detection of treatments in ruby and sapphire is an ongoing challenge due to the sophistication of modern enhancement techniques. Accurate identification requires a combination of traditional gemological skills and advanced analytical technologies. Continued research, method development, and collaboration among laboratories are essential to keep pace with evolving treatment methods. Above all, transparency and full disclosure of treatments are essential to uphold ethical standards and maintain consumer confidence in the gemstone industry.

References:

- Atichat, W., Leelawatanasuk, T., Sriprasert, B., Pisutha-Arnond, V., Wathanakul, P., Suthirat, C., 2011. Low temperature heat treatment of Mozambique ruby. Proceedings of the 32nd International Gemmological Conference (IGC 2011), Interlaken, Switzerland, 157-259
- Emmett, J.L., Scarratt, K., McClure, S.F., Moses, T., Douthit, T.R., Hughes R, Novak, S., Shigley, J.E., Wang, W., Bordelon, O., Kane, R.E., 2003. Beryllium diffusion of ruby and sapphire. Gems & gemology, 39(2), 84-135
- Hughes, E.B., Vertriest, W., 2022. A Canary in the Ruby Mine: Low-Temperature Heat Treatment Experiments on Burmese Ruby. Gems & gemology, 58(4), 400-423
- Kane, R.E., Kammerling, R.C., Koivula, J.I., Shigley, J.E., Fritsch, E., 1990. The identification of blue diffusion-treated sapphires. Gems & gemology, 26(2), 115-133
- Krzemnicki, M.S., Hänni, H.A.,Walters, R.A., 2004. A new method for detecting Be diffusion-treated sapphires: Laser-induced breakdown spectroscopy (LIBS). Gems & gemology, 40(4), 314-322
- Krzemnicki, M.S., Cartier, L., Hughes, R.W., Leelawatanasuk, T., Kiefert, L., Choudhary, G., McClure, S., Milisenda, C., Gambini, E., Kim, S., Schwarz, D., Dunaigre, C., and Horikawa, Y., 2019. Sapphires Heated with Pressure – A Research Update. InColor, 42, 87–90
- Krzemnicki, M.S., Lefèvre, P., Zhou, W., Braun, J., Spiekermann, G., 2023. Dehydration of Diaspore and Goethite during Low-Temperature Heating as Criterion to Separate Unheated from Heated Rubies and Sapphires. Minerals, 13(12), 1557
- Leelawatanasuk T., Susawee N., Saengbuangamlam S., Promwongnan S., Atsawatanapirom N., Atichat W., Pisutha-Arnond V., Sriprasert B., 2014. Treated black sapphire. Proceedings of the 4th International Gem and Jewelry Conference (GIT 2014), 126-130
- Phlayrahan, A., Homkhajorn, H., 2021. The new evidence from the fingerprint region in FT-IR spectra indicates the heat treatment of blue sapphire sample. In Journal of Physics: Conference Series 2145(1), 012023
- McClure, S.F., Kammerling, R.C., Fritsch, E., 1993. Update on diffusion treated corundum: Red and other colors. Gems & gemology, 29(1), 16-28
- Pisutha-Arnond, V., Häger, T., Wathanakul, P., Atichat, W., 2004. Yellow and brown coloration in beryllium-treated sapphires. Journal of gemmology, 29(2), 77-103
- Pisutha-Arnond,V., 2017. Ruby & sapphire treatment and identification: Decade of advancement. Technical article, The 20th Anniversary of GIT Achievement, Bangkok, Thailand, 96pp.
- Pisutha-Arnond V., Promwongnan S., Narudeesombat N., Ounorn P., Leelawatanasuk T., Sripoonjan T., Nilhud N., Atichat W., 2019. Blue diffusion-treated natural & synthetic sapphires recently available in the market. Journal of the gemmological association of Hong Kong, 40, 87-95
- Soonthorntantikul W, Khowpong C, Atikarnsakul U, Saeseaw S, Sangsawong S, Vertriest W, Palke A., 2019. Observations on the heat treatment of basalt-related blue sapphires. Gemological Institute of America Report.
- Soares de Sousa, A., Gomes, E.M.C., Bayés-García, L., Di Mariano, A., Garcia-Valles, M., 2025. Fingerprinting of ruby and sapphire gemstones through Fourier-transform infrared (FTIR) methodologies. European journal of mineralogy, 37(1), 53-62
- Wang, H.A., Weltz, D., Krzemnicki, M.S., Mack, A., Wälle, M., 2023. Effects of Gamma Irradiation on Ruby and Pink Sapphire and Potential Detection Methods in Gem Labs. Proceedings of the 37th International Gemmological Conference (IGC 2023), Tokyo Japan, 119-122

Acknowledgements

The authors would like to thank Mr. Thanong Leelawatanasuk for the collaborative work and shared expertise in conducting advanced spectroscopy analysis and treatment detection

Padparadscha Sapphire & heat treatment

Stephen Kennedy
The Gem & Pearl Laboratory Ltd, Unit 23, Arundel House, 43 Kirby Street,
London EC1N 8TE; info@thegemlab.co.uk

Keywords: Padparadscha sapphire, heat treatment, Laboratory Manual Harmonisation Committee

In 2018 the Padparadscha engagement ring of Princess Eugenie (Figure 1), the niece of the king, gave a boost to the popularity of the gemstone in the UK. Its subtle colour makes it ideal for the independently minded looking for something different (Figure 2).

Figure 1 –Princess Eugenie's engagement ring. Photo: Hello Magazine.

Figure 2 – Padparadscha Sapphire. Photo: SSEF.

In gemmological circles the Padparadscha sapphire moved centre-stage with the discovery of beryllium diffusion in 2002 - treatment may have been occurring the year before (Emmett, J.L., et al 2003). There is much on the accepted colour of padparadscha and treatments (Notari, Franck, 1996). The present Laboratory Harmonisation Committee Information Sheet 4 (Version 10, February 2023) standardises the nomenclature they use to describe a 'padparadscha sapphire' (www.lmhc-gemmology.org) I wish to thank the individuals involved, who have provided these Information Sheets on many gemstones over the years. They are an excellent tool to explain the issues of report wording to both trade and public alike. In general I inform customers that I follow the World Jewellery Confederation (CIBJO) and LMHC guidelines. However I do not issue reports on heated 'padparadscha' sapphires', which is still acceptable according to LMHC wording. It is this I would like us to consider.

Many gem dealers in the UK have informed me that they do not trade in heated padparadscha sapphires. It may be due to the lack of availability of heated (not diffused) material, or maybe those seeking Padparadschas for commissioned jewellery are only interested in unheated gemstones. It may be a pragmatic decision in that the gem dealer or trader, in the UK or from abroad, may be asked to provide a laboratory gem report to prove it is only heated and not diffusion treated. The LA-ICP-MS spectroscopy to check for diffusion is not widely available and testing them might be expensive. So it is likely they will be traded as untested heated padparadschas. This temptation is removed if any heated pink/orange sapphire, along with diffused pink/orange sapphire, is not allowed to have the padparadscha label.

I understand the quandary of the LMHC. If padparadscha is a variety name then it has to follow the allowances for all variety names in that they can be heated or unheated. I would prefer the variety name to be pink/orange sapphire and the commercial name of padparadscha only applied to unheated gemstones. However the variety name of padparadscha is so well established in the trade it probably cannot be changed. Even if we keep the variety name as padparadscha a precedent has already been set that padparadscha cannot be applied to diffusion-treated pink/orange sapphire and it is therefore only a small step further to say it cannot be applied to heated pink/orange sapphires. I know padparadscha is arguably only a colour decription in Sinhalese but the term has taken on a meaning in its own right of a premium gemstone with a premium price. We have 'outlawed' padparadscha being applied to diffused orange/pink sapphires so let's take it a small step further and remove the premium padparadscha label being applied to heated orange/pink sapphires.

References:

- Emmett, J.L., et al (2003), Beryllium Diffusion of Ruby and Sapphire, Gems & Gemology, Vol.39, No.2, p.84-135
- Notari, Franck (1996) The Padparadscha Sapphire, Diploma presentation at the Geology Department of the University of Nantes https://gemmologie-francophonie.com/wp-content/uploads/2021/10/Notari_1996-DUG_Padparadscha.pdf

Acknowledgements:

Laboratory Manual Harmonisation Committee (LMHC) Dr. Michael S. Krzemnicki/Dr Laurent Cartier of SSEF and Dr Stefanos Karampelas of LFG for their help in a late change of topic

Advancing Fei Cui Origin Authentication: A comparison of green Fei Cui from Myanmar, Guatemala, Italy and Russia

Shang-I (Edward) Liu[1], Ka-Yi (Angela) Man[1,2], Montira Seneewong-Na-Ayutthaya[3], Bhuwadol Wanthanachaisaeng[3]

[1] The Gemmological Association of Hong Kong, Hong Kong, China; gemedward@hotmail.com

[2] Department of Food Science and Nutrition, The Hong Kong Polytechnic University, Hong Kong, China; mankayi_plus2@yahoo.com.hk

[3] The Gem and Jewelry Institute of Thailand (GIT), Bangkok, Thailand; smontira@git.or.th, wbhuwadol@git.or.th

Keywords Origin determination, Fei Cui, Jadeite jade, Omphacite jade

In recent years, an increasing number of sources of fei cui, such as Guatemala, Italy and Russia, have entered the Chinese market, leading to a growing demand for precise origin determination of fei cui. Building upon our previous study (Liu *et al*., 2024), this study progresses towards a more comprehensive understanding. In November 2024, author Liu conducted a geological field trip to the fei cui mines in Guatemala (Figure 1), collecting a new set of Guatemalan samples directly from the source. To expand the study's scope, green samples from Russia were also included (Figure 2).

Following the standard tests outlined in the fei cui standards (GAHK, 2016; GIT, 2022), which encompass RI, SG, and FTIR analyses, all samples (BU, n =21, GU, n = 29; RU, n = 13; IT, n = 7) have been confirmed as fei cui, devoid of any resin or dye. Moreover, the FTIR results, consistent with the literature (Abduriyim *et al*., 2017; Miura *et al*., 2019), support the classification of the Russian samples as jadeite jade. In alignment with our previous study, the recent batch of Guatemalan samples collected between 2023 and 2025 also exhibits jadeite dominance, while the Italian samples are characterised by chrome-omphacite dominance (Liu *et al*., 2024). Compared with other localities, Russian fei cui relatively coarse granular and loose texture, and contains phlogopite and molybdenite (Figure 3).

Figure 1. Outcrop of jadeitite and omphacitite (white area on the left) with intrusive dykes of albitite and amphibolite in serpentinite mélange in a new mining site on the north - eastern side of the Motagua fault zone in Guatemala. Photo © S.I Liu

Figure 2. The samples of green fei cui from Russia (left, RU-01 1.03 ct), Guatemala (centre, GU-G31 0.83 ct), and Myanmar (right, BU-41 0.78 ct) analysed in this study

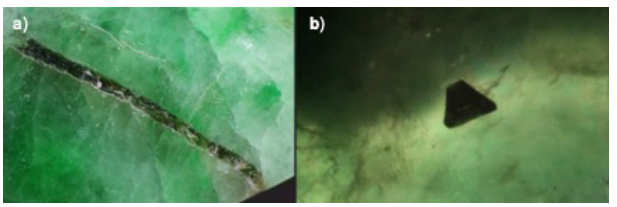

Figure 3. (a) Phlogopite and (b) molybdenite inclusions found in Russian fei cui

LA-ICP-MS were used to analyse the characteristic trace element profile of fei cui from different origins. The 3D-PCA score plot of LA-ICP-MS (Figure 4a) indicates a distinct separation of Italy from other regions, with slight overlap observed among Myanmar, Guatemala, and Russia. Among the four localities, Russian fei cui has the highest Ga, Zn, Li, and Fe content, while Italy has the highest Cr content (Figure 4b) due to its chrome-omphacite-dominated nature.

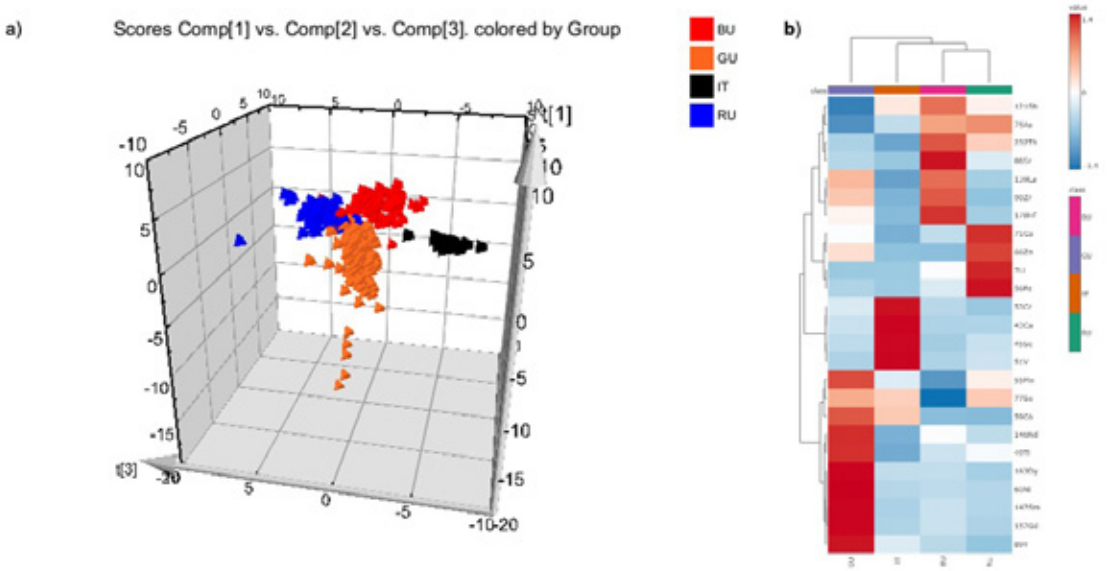

Figure 4. (a) 3D-PCA score plots of LA-ICP-MS data of green fei cui from Myanmar (BU), Guatemala (GU), Italy (IT) and Russia (RU); (b) Heatmap of LA-ICP-MS data.

References:

- Liu, S.I, Man, K.Y., Seneewong-Na-Ayutthaya, M., Jakkawanvibul, C., Lee. A. T.-Y. (2024). Geographic Origin Determination of High-quality Green Jadeite-Omphacite Jade (Fei Cui) from Myanmar, Guatemala and Italy Using Statistical Processing Coupled with Spectroscopic and Chemical Analysis. The Journal of Gemmology, 39(2), 124-145
- The Gemmological Association of Hong Kong (GAHK). (2016). Standard Methods for Testing Fei Cui for Hong Kong (HKSM/FCT-2016), GAHK. http://www.gahk.org/attachment/fc_std_eng.pdf
- The Gem and Jewelry Institute of Thailand (GIT). (2022). The Gem and Jewelry Institute of Thailand Standard-Testing of jade and Fei Cui (GIT 1013.1-2564), GIT.
- Abduriyim, A., Saruwatari, K. & Katsurada, Y. (2017). Japanese jadeite: History, characteristics, and comparison with other sources. Gems & Gemology, 53(1), 48–67
- Miura, M., Arai, S., Ishimaru, S., & Shmelev V. (2019). Ornamental Jadeites from the Levoketchpel Deposit in the Polar Urals of Russia. Gems & Gemology, 55(2), 278-281
- Franz, L., Sun, T. T., Hänni, H. A., De Capitani, C., Thanasuthipitak, T., Atichat, W. (2014). A comparative study of jadeite, omphacite and kosmochlor jades from Myanmar, and suggestions for a practical nomenclature. Journal of Gemmology, 34(3), 210-229.
- Wang, L., Zhang, H., Liu, J., Wang, L., Ouyang, Q., Liu, D. & Liu, W. (2022). Mineral component and genesis of high-grade green jadeite jade from Guatemala. Journal of Gems & Gemmology, 25(5), 11–30.
- Zhang, Y. & Shi, G. (2022). Origin of blue-water jadeite jades from Myanmar and Guatemala: Differentiation by non-destructive spectroscopic techniques. Crystals, 12(10), 1448,

Color Genesis Analysis and Characteristics for Origin Identification of Purple Jadeite

Elizabeth Su
Gemsu Rona Jewellery (Shanghai) Co., Ltd, Shanghai, China,
esu_gems@yahoo.com

Introduction

Purple jadeite, renowned for its distinctive purple hues and rich cultural connotations, is highly admired and sought after. This study investigates purple jadeite samples from Burma and Guatemala, each exhibiting different color variations, as shown in Figure 1. The research commences with a conventional gemological analysis, followed by a comprehensive examination of the color genesis through various spectroscopic techniques, including X-ray fluorescence (XRF) spectra analysis, ultraviolet-visible (UV-Vis) absorption spectra analysis, infrared spectroscopy (IR), Raman spectra analysis and Photoluminescence Spectroscopy (PL) analysis.

Figure 1: Purple Jadeite Samples from Burma and Guatemala.

Results

The results reveal that the coloration of purple jadeite is primarily attributed to the presence of manganese ions (Mn), iron ions (Fe), and titanium ions (Ti). The intensity of the purple coloration is directly correlated with the concentration of manganese ions, while iron ions and titanium ions producing a more violet color. Notably, there are significant differences in trace element concentrations between the two sources: Burmese purple jadeite exhibits higher manganese and lower titanium content (MnO: 0.038-0.065%, TiO_2: 0.015-0.200%), whereas Guatemalan purple jadeite shows lower manganese and higher titanium content (MnO: 0.011-0.032%, TiO_2: 0.506-0.697%). Furthermore, the jadeite samples examined in this research all exhibit purple hues, primarily attributed to the chromophoric contributions of manganese (Mn), iron (Fe), and titanium (Ti) ions, with no significant relationship to chromium (Cr) ions. The chromium content is relatively low, as seen in Table 1.

Sample	Fe_2O_3%	MnO%	Cr_2O_3%	TiO_2%	NiO%
B-001	0.098	0.044	0.012	0.024	0.052
B-002	0.073	0.040	0.004	0.015	0.043
B-003	0.115	0.038	0.001	0.029	0.045
B-004	0.246	0.041	0.027	0.079	0.043
B-005	0.087	0.034	0.017	0.054	0.044
B-006	1.291	0.055	0.013	0.200	0.056
B-007	0.093	0.044	0.005	0.025	0.040
G-001	0.210	0.013	0.001	0.643	0.032
G-002	0.193	0.011	0.009	0.557	0.027
G-003	1.063	0.030	0.014	0.506	0.021
G-004	0.133	0.032	0.011	0.697	0.025
G-005	0.188	0.027	0.009	0.559	0.037

Table 1: Trace element content in Burmese and Guatemalan Purple Jadeite.

The ultraviolet-visible absorption spectra of purple jadeite from the two regions exhibit distinct differences. Burmese purple jadeite is primarily characterized by absorptions at 314, 437, and 581 nm, as illustrated in Figure 2, whereas Guatemalan purple jadeite displays characteristic absorptions at 309, 380, 437, 551, 626, 768, and 947 nm, as shown in Figure 3. The absorptions at 381 and 437 nm are attributed to d-d electronic transitions of Fe^{3+}, while the absorption at 581 nm is associated with d-d electronic transitions of Mn^{3+}. The absorption at 626 nm is due to electronic transitions of Ti^{3+}, the absorption at 768 nm results from charge transfer between Fe^{2+} and Fe^{3+}, and the absorption at 947 nm is attributed to d-d electron transitions of Fe^{2+}[which reference?].

Therefore, 581 nm represents a characteristic peak for Burmese purple jadeite (Minghui *et al.*, 2023), while 551 nm is a characteristic peak for Guatemalan purple jadeite. The 581 nm feature appears as a peak in the UV-Vis spectra of Burmese purple jadeite, whereas it manifests as a trough between 551nm to 626nm in the spectra of Guatemalan purple jadeite. The UV-Vis spectra of Burmese purple jadeite in the 580–950 nm range exhibit a single peak, whereas the spectra of Guatemalan purple jadeite within the same range display multiple peaks.

In terms of infrared spectroscopy, Guatemalan purple jadeite lacks the absorption lines at 1167 cm^{-1} and 745 cm^{-1}. However, no significant differences were observed in the Raman spectroscopy and photoluminescence spectra. The Raman spectral results indicate that purple jadeite from both sources is relatively pure jadeite.

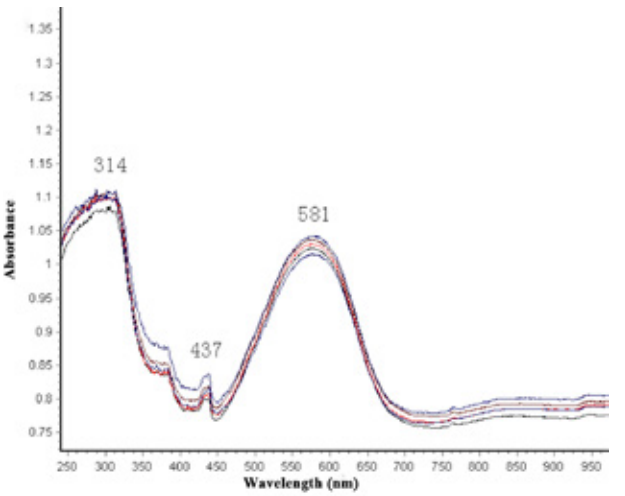

Figure 2: UV-Vis absorption spectra of the purple jadeite from Burma.

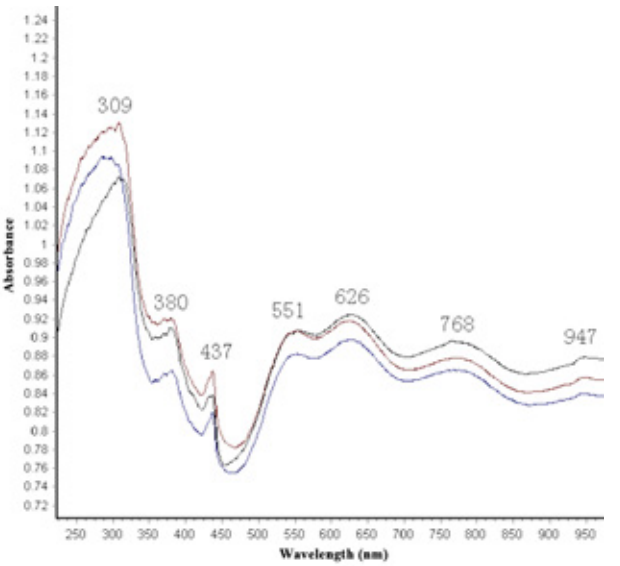

Figure 3: UV-Vis absorption spectra of the purple jadeite from Guatemala.

Conclusion

The findings of this study indicate that both Burmese and Guatemalan purple jadeite are primarily composed of relatively pure jadeite. However, significant differences in trace elements are observed, with Burmese purple jadeite exhibiting elevated manganese and lower titanium concentrations, whereas Guatemalan purple jadeite displays reduced manganese and higher titanium levels. These compositional variations contribute to the distinct differences in their absorption spectra. Through detailed compositional analysis and ultraviolet-visible absorption spectroscopy, a reliable distinction between Burmese and Guatemalan purple jadeite can be made.

The samples examined in this abstract predominantly consist of purplish-red jadeites from Burma and bluish-purple jadeites from Guatemala. However, it should be noted that bluish-purple jadeites are also present in Burmese jadeite on the market, and premium-quality Guatemalan jadeite may exhibit purple hues similar to that of the Burma origin. For instance, B-004 (purple jadeite sample from Burma) and G-002 (purple jadeite sample Guatemala) display remarkably similar purple coloration in both hue and saturation, rendering them difficult to differentiate by visual observation alone. Therefore, I conducted a comprehensive analysis using several types of advanced instrumentation. Among these, the ultraviolet-visible (UV-Vis) absorption spectroscopy proved to be diagnostically significant, offering an effective means of distinguishing the origin of the jadeite samples.

References:

- Minghui Tang & Chuyan Hu, 2023. Gemological and Mineralogical Characteristics of Purple Jadeite. Master thesis. Guilin University of Technology
- Xiao Wu, Zhenyu Bao, Yan Kang, Xiaozhen Han, Xueliang Liu & Mingyi Qu, 2019. Color Origin of Burmese Lavender Jadeite, Laser & Optoelectronics Progress, 56 (7). Doi: 10.3788/LOP56.073001
- Xueliang Liu, Jianliang Fan & Shouguo Guo, 2011. Spectroscopical Characteristics and Color-Causing Mechanism of Light Pink-Red Jadetite, Laser &Optoelectronics Progress, Doi: 10.3788/ LOP48.093002
- Yanran Shang, Weizhao Wang, Tianli Jin, Linming Huang, Zhongyun Wu & Ying Guo, 2024. Colouration in purple jadeite-jade from Myanmar: A spectroscopy and chromaticity investigation, ACTA PETROLOGICA ET MINERALOGICA, 43 (3), 643-651. Doi: 10.20086/j. cnki. yskw.2024.0312

Acknowledgements

I would like to express my sincere gratitude to Professor Lijian Qi and Zhengyu Zhou of Tongji University for providing access to advanced gemological analytical instrumentation. I also gratefully acknowledge Professor Lijian Qi and Doctor Xueliang Liu of East China University of Science and Technology for their valuable academic guidance throughout the course of this research.

Dyed purple Jade (Lavender jade or purple “Fei Cui”) from Mandalay's jade market, Myanmar

Montira Seneewong-Na-Ayutthaya, Bhuwadol Wanthanachaisaeng*, Thanapong Lhuaamporn, Waratchanok Suwanmanee, Wilawan Atichat, and Thanong Leelawatanasuk

The Gem and Jewelry Institute of Thailand (Public Organization), ITF-Tower Building, Silom Road, Suriyawong, Bangrak, Bangkok, 10500 Thailand

* wbhuwadol@git.or.th

Keywords: Fei Cui, Jadeite, Lavender jade, Dyed jade

Introduction

Jade or "Fei Cui" are trade names for a stone that typically contains only one or more main mineral components, including jadeite, omphacite, and kosmochlor. These mineral components exist in the form of small crystallites tightly packed together (aggregate), with many grain boundaries between them. As a result, jade also known as “fei cui” commonly exhibits varying degrees of translucency. Not only green jade, but also purple jade is increasingly popular in the gem market. This is due to its beautiful, rare and unique colouration. Moreover, there is a belief that purple jade (also known as lavender jade or purple “fei cui”) is an auspicious gem, bringing good luck to the person who owns or wears it. Due to the rarity of such shades in nature, high-quality purple jade holds significant value and is in demand in the current market. Since 2023, The Gem and Jewelry Institute of Thailand (Public Organization) or GIT, has received reports from entrepreneurs indicating an increase in the quantity of various shades of purple jade entering the market compared to previous years. Furthermore, there is a significant possibility that some of the purple jade available in the market may have been artificially enhanced colour through dyeing processes. This situation has raised significant concerns within the trade, impacting both entrepreneurs' and consumers' confidence in the authenticity of purple jade available in the trade and market.

Materials and Methods

GIT received a collection of purple jade samples, acquired from a dealer at the Mandalay Jade and Gemstone Market in Myanmar. The collection comprises 15 samples with a weight range of 3.30 to 9.16 ct. Among these, three samples were identified as natural purple jade while the remaining twelve were suspected to have been dyed, as illustrated

Figure 1. 12 Dyed purple jade samples from the Mandalay jade market in Myanmar, ranging from 0.11 to 1.04 ct. Photo by M. Seneewong-Na-Ayutthaya.

in Figure 1. To determine evidence of dye treatment, the samples were analyzed using both microscopic examination and advanced instruments, including a Raman microscope spectrometer (Renishaw inVia), FTIR spectrometer (Thermo Scientific, Nicolet iN10) and UV-Vis-NIR spectrophotometer (PerkinElmer, Lambda 1050).

Results and Discussions

All samples have been confirmed to be natural jadeite-jade through basic instrument testing. Fluorescence testing revealed that all samples were inert when exposed to short-wave and long-wave UV radiation. Visual observation of the samples with the naked eye and a 10x loupe revealed that they can be grouped into two categories: dark purple and light purple. Most of the samples exhibited irregular colour and texture characteristics, typical for jade which is dyed. Poor-quality jade, characterized by pale colour and larger crystal grain size, are often treated by a dyeing process. This textural property allows the dye to penetrate and spread more effectively along the crystal grain boundaries. Additionally, it's worth noting that jade with purple colour is rare in the famed jade deposits in Myanmar. High-magnification observation under a gem microscope, as illustrated in Figure 2 , revealed distinct internal characteristics. The natural purple jade sample exhibited a light purple colour that is smoothly distributed among the fine, small crystal grains. The more intense purple jade samples revealed evident features indicating that they were dyed, such as distinct colour patches and concentrations along grain boundaries as a result of the dyeing treatment.

Subsequently, the purple jade beads were cross-sectioned to study the extent of dye penetration, as represented in Figure 3. The results revealed significant colour modifications in all the purple jade samples through the dyeing treatment. Strong evidence of dye infiltration was observed within the central area of the samples, with the intensity of the dye gradually decreasing to a very light colour toward the edge of the samples (in the thinnest area of the cross-section). Based on the observed characteristics of the dye penetration we assume that a vacuum-assisted dyeing technique was used. For this, the jade bead is first placed in a vacuum chamber to remove air, water, or small particles from the grain boundaries. This pre-treatment enables the jade to absorb the dye more effectively, as the dye can quickly

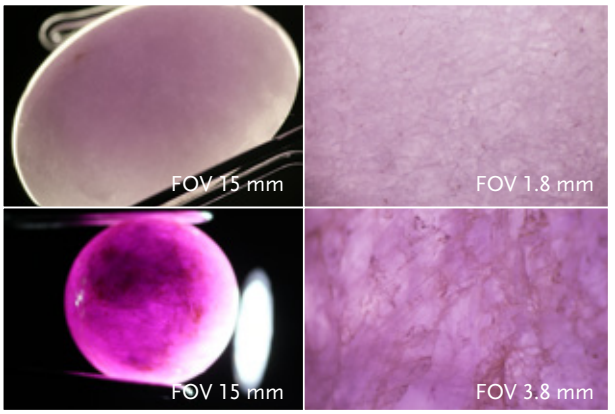

Figure 2. (top) Natural purple jade exhibiting a light purple colour with smooth distribution in fine crystal grains, and (bottom) dyed purple jade displaying areas of colour patches caused by dyeing, with dye concentration observed along the crystal grain boundaries. Photomicrographs by M. Seneewong-Na-Ayutthaya.

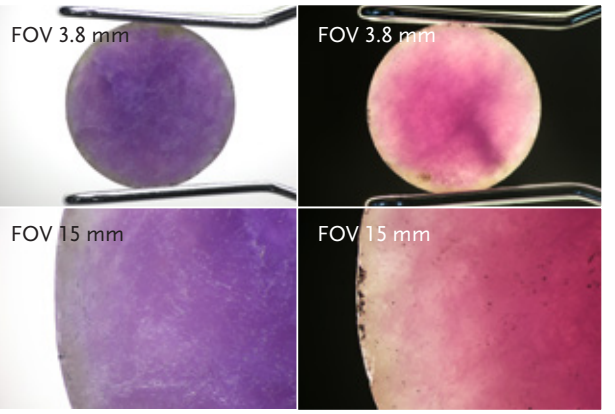

Figure 3: A cross-section of dyed purple jade sample was studied in bright-field and dark-filed illumination to observe the extent of dye penetration. Dye concentration was observed in the centre of the bead, while a pale colour was evident near the surface of the bead. Photomicrographs by M. Seneewong-Na-Ayutthaya

penetrate between the crystal grain boundaries (Ou Yang & Humphrey, 2015) and thus allows the dye to penetrate deeply into the crystalline texture of the jade bead. Furthermore, the lighter colouration observed at the edge of the cross-section sample may result from cleaning procedures commonly employed during the process of making jade jewelry. Specifically, washing the bead with a mild acidic solution, such as plum juice, is a traditional practice. used to clean off various chemical residues from the grinding and polishing process (Yan, 2019).

An additional experiment involved soaking purple dyed samples in ethyl alcohol for 48 hours. After this test it was observed that the jade samples displayed their original colour (pale yellowish green) near the edge of the samples (see Figure 4) as they had assumingly before the dyeing treatment.

Figure 5 displays the absorption spectra of a purple jade of natural colour (spectrum at the bottom), a reference sample of dyed purple jade, and two spectra of dyed jade

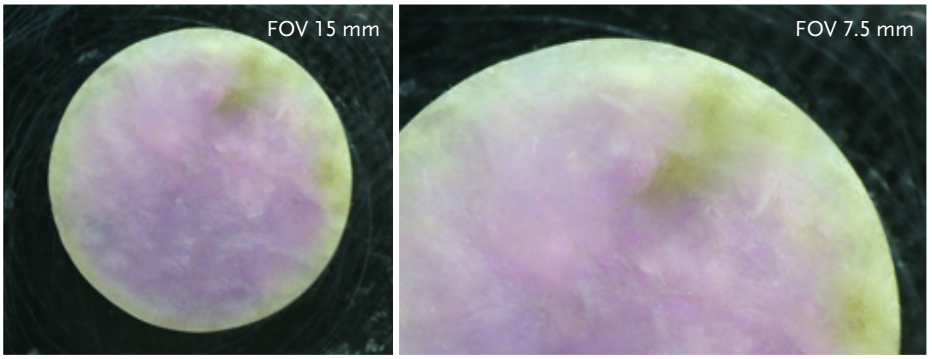

Figure 4: A purple dyed jade cross-section after soaking in ethyl alcohol for 48 hours. It clearly displays its original colour before the dyeing treatment along the edge of the sample. Photomicrographs by M. Seneewong-Na-Ayutthaya

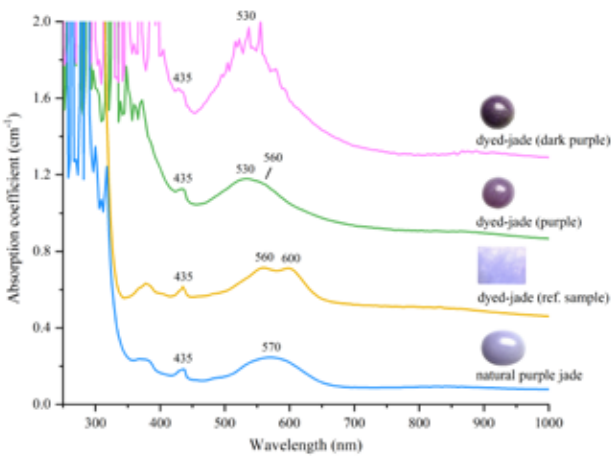

Figure 5: UV-visible spectra of natural purple jade and dyed purple jade samples.

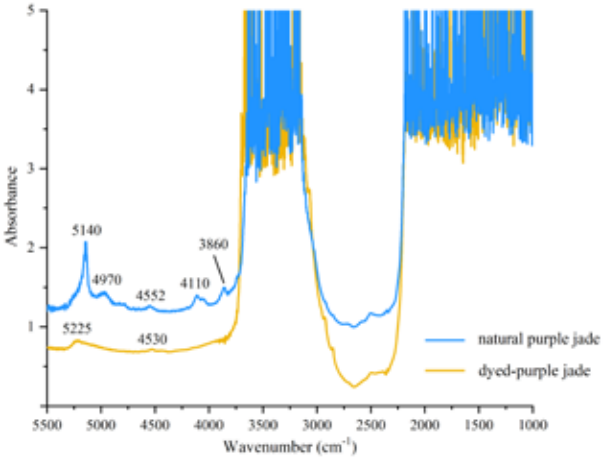

Figure 6: FTIR spectra of natural purple jade and dyed purple jade samples.

of purple and dark purple colour. In dyed samples investigated for this study, a main absorption band was observed at 530 (with a small shoulder at 560 nm) related to the purple dye. The dyed reference sample of light purple colour exhibits two broad absorption bands at 560 and 600 nm, respectively. In contrast to this, the purple jade of natural colour exhibits an absorption peak at 573 nm due to the presence of manganese (Mn^{3+}), causing the purple colour in natural jade, and in addition a peak at 453 nm, which represents iron (Fe^{3+}) (Lu, 2012; Abduriyim *et al*., 2017). The comparison of the absorption spectra clearly indicates that the purple jade beads investigated had been dyed. Figure 6 shows the FTIR spectra of a dyed purple sample compared to the untreated natural purple jade. A small wax-related appears around 2900 cm^{-1}, with no absorption peaks indicating polymer treatment (Zhang *et al*., 2013; Seneewong-Na-Ayutthaya, 2022; Promwongnan *et al*., 2023). This suggests that the dyed purple jade sample can be classified as C-Jade, a type of jade that has only been enhanced in quality through dyeing.

Concluding remarks

From the analysis of purple jade (also known as lavender jade or purple "fei cui") samples from the Mandalay Jade Market in Myanmar, it was suspected that the colour had been modified by dyeing. From a total of 15 purple jade beads investigated for this study, 12 samples were found to be impregnated with purple dye. The experimental results showed that the dye penetrated deeply into the jade, likely facilitated by using a vacuum technique to help spread the dye along crystal grain boundaries. Consequently, this type of treatment can be identified through careful microscopic examination and confirmed using standard spectroscopic techniques by experienced gemmologists.

References:

- GIT 1013.3-2564, Jade and Fei Cui identification by Fourier Transform Infrared Spectrometer, Date of enactment: 30 September 2021.
- Abduriyim, A., Saruwatari, K. and Katsuruda, Y., 2017. Japanese Jadeite: History, Characteristics, and Comparison with Other Sources. Gems & Gemology, 53(1), 48-67
- Lu, T., 2012. Colour Origin of Lavender Jadeite: An Alternative Approach. Gems & Gemology, 48(4), 273-283
- Ou Yang, C.M., Humphrey, Y., 2015. Fei Cui Jade A stone & A culture. Shanghai Translation Publishing House, Shanghai, China, 248 pp.
- Seneewong-Na-Ayutthaya, M., 2022. The Study of Five Jade Imitations from Bangkok's Yaowarat Road: Gem-A Student Project. *Gems & Jewellery*, summer, 32-35.
- Shurvell, H.F., Rintoul, L., and Fredericks, P.M., 2001. Infrared and Raman spectra of jade and jade minerals. The Internet Journal of Vibrational Spectroscopy, 5(5).
- Promwongnan, S., Atichat, W., Fueangaksorn, K., Pisutha-Arnond, V., Leelawatanasuk, L. 2023. Treated jadeite-jade: Unusually bright fancy colours. *Proceedings of the 37th International Gemmological Conference (IGC)*, Tokyo, Japan, 165–168.
- Yan, W., 2019. Dyed Jade Bangles in Myanmar. Jade Jewellery-education. Source: https://mays.com.au/blogs/jade-education/dyed-jade-bangle-myanmar-2019
- Zhange, J., Lu, T., Chen, H., 2013. Gemological Characteristics of Coated Jadeite Jade. *Gems & Gemology*, 49(4), 246-254.

Acknowledgements

Special thanks also go to Mr. Chanon Pongcharoenkul (Executive of JADE FOR YOU), who kindly provided natural purple jade and dyed purple jade from the Mandalay Jade Market in Myanmar.

Pink to Red and Violet Diamonds from the Argyle Mine, Australia: Properties, Color Origin and Latest Research Results.

Thomas Hainschwang
GGTL Laboratories Liechtenstein/GGTL Laboratories Belgium
thomas.hainschwang@ggtl-lab.org

Fig. 1. A range of pink to red to violetish gray to violet diamonds from the Argyle mine in Australia.

The Argyle Mine was by very far the largest producer of pink to red diamonds worldwide and the only producer of violet diamonds (Fig. 1). The mine that started its operation in 1983 was finally closed in November 2020, after 37 years of successful operation. While the mine was famous for these rare colored diamonds, these represented only a very small percentage of its production, far more what was produced by the Argyle deposit were brown diamonds.

Significant research has been conducted by our laboratory concerning the still puzzling color origins of these diamonds and their defect characterization. While being produced in the same Lamproite body which is characterized by its high percentage of diamonds that have undergone plastic deformation – namely brown, pink and red diamonds – the extremely rare and unusual violet diamonds have no link to plastic deformation whatsoever. These stones are much higher in nitrogen and hydrogen than the pinks and reds and we found that their color is linked to a combination of absence of N3 center absorption and distinct content of nickel nitrogen defects, possibly in conjunction with hydrogen. Whether the hydrogen plays an actual role in the coloring defects is not clear, as contrary to the classical attribution of the violet color to hydrogen, we could not find any major link between the color and (IR active) hydrogen content. During this research we have defined the spectral structures of the major defects that are responsible for the violet color, and curiously one of the main defects involved has its ZPL quite far in the NIR, namely at 1330 nm (Hainschwang et al, 2021). We were able to define the spectral structure of the 1330 nm center at 77K and define its link to part of the absorptions seen in the visible spectral range (Fig. 2).

Work performed by our lab on "olive", brown to pink and red diamonds with the aim to understand why plastic deformation can produce these colors has pointed towards the temperature during plastic deformation events being responsible for the different hues. The different temperature conditions result in somewhat different vacancy-cluster-type defects and in consequence the different colors. Annealing experiments of type I diamonds exhibiting two colors of "graining" revealed that the "olive" hue is least stable, the brown hue is more stable and the pink hue is most stable to annealing. A link between the amber center (AC) absorption in the infrared spectrum at 4063 cm^{-1} with "olive" color and the AC at 4167 cm^{-1} with brown color could be clearly established: diamonds of "olive" color with distinct 4063 cm^{-1} AC absorption turned brown upon annealing at 1500°C and the AC at 4063 cm^{-1}

annealed out while the AC at 4167 cm^{-1} increased distinctly (Fig. 3). The brown colors start to anneal out at temperatures from 1900°C while pink seems to remains unaffected to over 2000°C. Since at that temperature other defects emerge in type Ia diamonds, it is difficult to define a temperature when the pink color is effectively annealed out. From experiments with type IIa diamonds of mixed brown-pink color, we know that pink color in type IIa diamonds is more stable than brown color, as such stones can be HPHT treated into a purely pink color, hence the brown color anneals out earlier than the pink color. All indications show that the same is true for the pink color of type Ia diamonds.

It is suggested that the three different colors of plastically deformed diamonds are the result of plastic deformation at different temperatures: olive is the result when plastic deformation occurs at the lowest temperature, brown is the resulting color when plastic deformation occurs at an intermediate temperature and pink results from plastic deformation at the highest temperature. This model is the only way one can logically explain pink and brown graining in one and the same diamond: two separate events of plastic deformation, the first one at higher temperature resulting in pink graining, and the second one at lower temperature resulting in brown color (Hainschwang *et al*., 2020b).

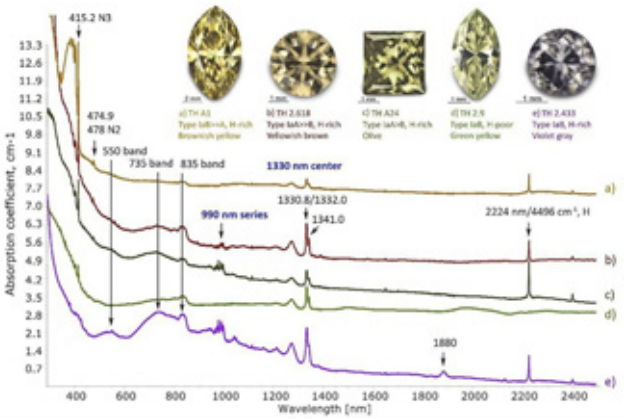

Fig. 2. The normalized and extended low temperature UV–Vis-NIR spectra of some differently colored "1330 nm diamonds" included in this study. It is obvious that sample TH 2.9 is different to all others, since while it exhibits a strong 1330 nm center, it is very low in hydrogen and lacks the broad bands at 735 and 550 nm. The spectra have been shifted vertically for clarity.

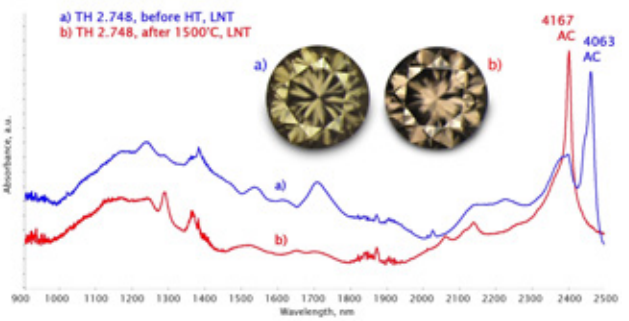

Fig. 3. The normalized and low temperature NIR spectra of a type Ia "olive" diamond before and after annealing at 1500°C. The sample changed color from "olive" to brown by the annealing while the amber center at 4063 cm^{-1} anneals out and the amber center at 4167 cm^{-1} increases distinctly.

References:

- Hainschwang T., Notari F., Pamies G. (2020), The origin of color of 1330 nm center diamonds. Diamond and Related Materials, Vol. 110, pp. 108151.
- Hainschwang T., Notari F., Pamies G. (2020b). A defect study and classification of brown diamonds with deformation-related color. Minerals, Vol. 10, pp. 903.

Shining light on "480 nm band" diamonds: Gemmological characteristics of an unusual group of diamonds with yellow and red luminescence

Marleen Bouman and Jelena Zarupski
HRD Antwerp-Research, Antwerp, Belgium
marleen.bouman@hrdantwerp.com

Fancy colour diamonds that derive their colour from nitrogen-related defects (such as N3/N2 centers or C-centers) are relatively common and well-studied. An underexplored group derives its colour from a broad absorption band centered around 480 nm, which is hypothesized to be related to oxygen impurities (Hainschwang *et al*. 2008). These diamonds are referred to as "480 nm band diamonds" and their properties have been described in a number of studies (e.g. Breeding *et al*. 2020, Lai *et al*. 2024). A rare subgroup of "480 nm band" diamonds are "chameleon diamonds", which temporarily change colour upon heating or prolonged storage in the dark. Common features of these diamonds are (De Weerdt & Van Royen, 2001, Fritsch & Delaunay, 2018):

1) A band at 426 nm in UV-Vis-NIR absorption spectroscopy, related to the 480 nm absorption band.
2) A peak at 1241 cm^{-1} in FTIR, which is thought to be linked to the 480 nm band.
3) Yellowish-green fluorescence in DiamondView, often accompanied by irregular zones of blue and bright green fluorescence.
4) Nickel-related defects in Photoluminescence Laser spectroscopy (PL), such as the 883/885 nm doublet, S2 and S3 centers.
5) Hexagonal or rounded plate-like inclusions, identified as graphite platelets by Shiryaev *et al*. (2023)
6) Hydrogen-related absorptions in FTIR spectroscopy.

An often-overlooked feature of "480 nm band" diamonds, however, is their luminescence reaction. When illuminated with long-wave ultraviolet (LWUV) light (365 nm) these diamonds typically show a yellow luminescence, whereas under blue light (450 nm) they display red luminescence (Collins & Mohammed, 1982). The red luminescence is produced by the 480 nm absorption band (2.6 eV), while yellow luminescence is linked to a vibronic system with a zero-phonon line (ZPL) at 456 nm (2.721 eV).

The aim of this study is to provide a detailed gemmological characterization of the relatively unknown "480 nm band" diamonds. Diamonds were screened with a custom-made luminescence tester, containing a LWUV and blue light source (Figure 1). In this way, we could quickly identify whether diamonds have yellow and red luminescence, which implicates that they contain the "480 nm band".

More than 50 diamonds were selected for detailed spectroscopic and gemmological analysis. All diamonds show yellow and red luminescence under the luminescence tester. The diamonds were studied by FTIR and UV-Vis-NIR spectroscopy, DiamondView imaging, microscopy, long-wave and short-wave UV excitation, and some of them by other techniques such as PL and ED-XRF spectroscopy. Special attention was paid to the presence of Y centers and CO_2 content in FTIR, since a genetic relation with "480 nm band" diamonds has been suggested before (Kupriyanov *et al*., 2020, Hainschwang *et al*. 2008).

Figure 1: Two"480 nm band" diamond under normal light (left), LWUV light (middle) and blue light (right). Both display yellow and red luminescence under LWUV and blue light, respectively.

For the selected diamonds, brown is the dominant colour grade (usually 'reddish brown'), followed by yellow, orange and rarely olive and pink. Weights are in the range of 0.14 ct to 2.27 ct. FTIR results show that two diamonds contain distinct CO_2 bands around 655 and 2370 cm^{-1}, known as the υ2 and υ3 bands (Schrauder & Navon, 1993). The main Y center band at 1145-1150 cm^{-1} is found in 7 diamonds. This is lower than expected, as Kupriyanov *et al.* (2020) concluded that the typical "480 nm" red luminescence is genetically related to Y centers. Therefore, we would expect to find Y centers in all studied diamonds. It is, however, possible that the Y centers are overshadowed by other defects (A, B, C centers), and further analysis using spectral deconvolution is necessary.

Although the "480 nm band" is responsible for red luminescence, only 15 diamonds show a distinguishable 480 nm band in their UV-Vis spectrum (Figure 2, red spectrum). Most of the studied diamonds owe their colour to a broad absorption continuum (Figure 2, black spectrum). For these stones, other properties such as inclusions, DiamondView and PL spectroscopy correspond to those of typical "480 nm band" diamonds. We can conclude that red luminescence is a more sensitive indicator than UV-Vis spectroscopy for the presence of the "480 nm band" defect.

In conclusion, our study shows that screening for luminescence reaction is a useful gemmological tool to quickly identify diamonds with "480 nm band" properties, since the combination of yellow and red luminescence is unique to these diamonds. We identified "480 nm band" diamonds over a range of colours, extending beyond the yellow and orange diamonds that have been typically studied. This allows us to investigate possible genetic links between the "480 nm band", CO_2 diamonds and Y centers.

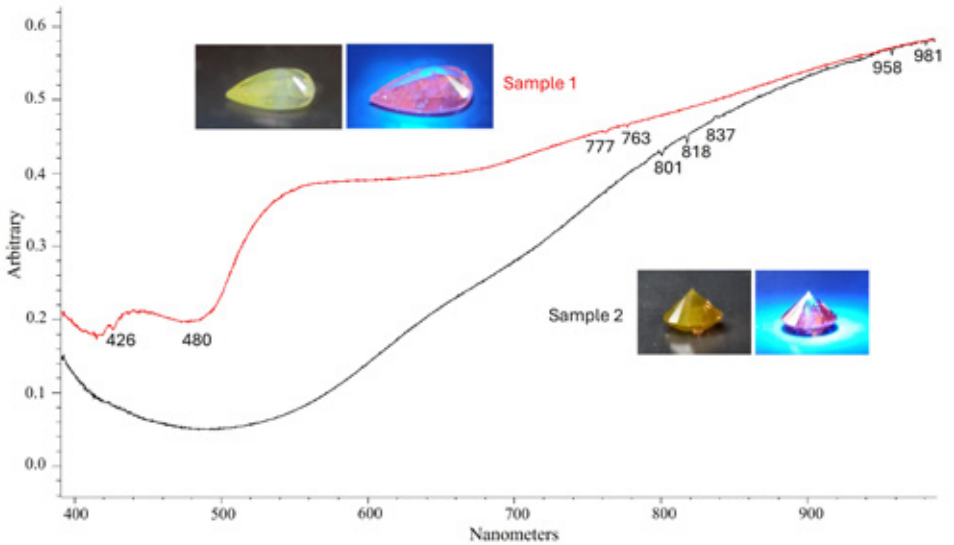

Figure 2: UV-Vis-NIR transmission spectra of two "480 nm band" diamonds. Red spectrum: Diamond with a typical 480 nm absorption band (Sample 1). Black spectrum: Diamond with yellow and red luminescence but no 480 nm band in UV-Vis-NIR (Sample 2). The samples are the same as those shown in Figure 1.

References:

- VBreeding, C. M., Eaton-Magaña, S., & Shigley, J. E., 2020. Naturally Colored Yellow and Orange Gem Diamonds: The Nitrogen Factor. Gems & Gemology, 56(2).
- Collins, A. T., & Mohammed, K., 1982. Optical studies of vibronic bands in yellow luminescing natural diamonds. Journal of Physics C: Solid State Physics, 15(1), 147.
- De Weerdt, F., & Van Royen, J., 2001. Defects in coloured natural diamonds. Diamond and related materials, 10(3-7), 474-479.
- Fritsch, E., & Delaunay, A., 2018. What Truly Characterises a Chameleon Diamond? An Example of an Atypical 25.85 ct Stone. Journal of Gemmology, 36(2).
- Hainschwang, T., Notari, F., Fritsch, E., Massi, L., Rondeau, B., Breeding, C. M., & Vollstaedt, H., 2008. HPHT treatment of CO_2 containing and CO_2-related brown diamonds. Diamond and related materials, 17(3), 340-351.
- Kupriyanov, I. N., Palyanov, Y. N., Kalinin, A. A., & Shatsky, V. S., 2020. Effect of HPHT treatment on spectroscopic features of natural type Ib-IaA diamonds containing Y centers. Crystals, 10(5), 378.
- Lai, M. Y., Hardman, M. F., Eaton-Magaña, S., Breeding, C. M., Schwartz, V. A., & Collins, A. T., 2024. Spectroscopic characterization of diamonds colored by the 480 nm absorption band. Diamond and Related Materials, 142, 110825.
- Schrauder, M., & Navon, O., 1993. Solid carbon dioxide in a natural diamond. Nature, 365(6441), 42-44.
- Shiryaev, A. A., Chesnokov, Y., Vasiliev, A. L., & Hainschwang, T., 2023. Exsolution of oxygen impurity from diamond lattice and formation of pressurized CO_2-I precipitates. Carbon Trends, 11, 100270.

Identification of melee size synthetic coloured diamond for jewellery

Kentaro Emori, Hiroshi Kitawaki, Mio Hisanaga, Masahiro Yamamoto
(Central Gem Laboratory, Tokyo, Japan, emori@cgl.co.jp)

Introduction

Synthesis methods to produce large and high-quality diamond for jewellery have been improved over the years, and large, colourless faceted stones weighing more than 50 ct have been realized (Eaton-Magaña *et al*., 2024). In addition, melee size fancy-coloured diamonds are also useful as components of jewellery, and the melee size synthetic coloured diamonds have been seen at jewellery shows in Japan and at the Tucson Show in USA. Jewellery assembled with the melee size diamonds is also sold in shops. Two methods are used to produce synthetic diamonds for jewellery: the HPHT method and the CVD method. It is important for gemmological identification to know clearly the different characteristics of the synthetic diamonds made with the two methods.

Material and Methods

Samples we bought at the 2024 IJT (International Jewelry Tokyo) for the present study are 35 pieces of melee size synthetic fancy-coloured diamonds with size of 0.10 ct or less which were labeled as CVD synthetic diamonds. After testing with standard gemmological instruments, the 35 samples were classified into seven categories according to colour, with five pieces for each category: (1) Green, (2) Greenish Blue, (3) Yellow, (4) Pink, (5) Orangy Pink, (6) Reddish Orange and (7) Orange (Figure 1).

These stones were observed under a gemmological microscope, and were measured with infrared and UV-VIS absorption spectroscopy. Deep UV luminescence images were obtained using DiamondView™. Photoluminescence spectra were taken for all samples being immersed in liquid nitrogen, using a Raman spectrometer with microscope with five different lasers for excitation at 457, 488, 514, 633 and 830 nm.

Figure 1: Fancy colour melee size diamond studied in this study (Upper row, from left: Orange, Reddish Orange. Middle row, from left: Yellow, Pink, Orangy Pink. Lower row, from left: Green, Greenish Blue)

Results and Discussion

(1) Green and (2) Greenish Blue: In all samples in these categories, the concentrations of nitrogen were below the detection limit according to the IR absorption spectroscopy, and deep UV fluorescence images showed characteristic patterns of HPHT synthetic diamond. From both green and greenish blue samples, a distinct 741 nm (GR1) peak was observed in the UV-VIS absorption spectra (Figure 2) and PL spectra. For green samples, peaks at 575 nm (NV^0), 741 nm (GR1), 488.9 nm and 470.2 nm (TR12) were detected in the PL spectrum. The 575 nm peak was stronger than the 741 nm peak. These results suggest that the green and greenish blue samples have been produced by irradiation of type IIa HPHT-synthetic diamonds. The greenish blue samples have been annealed at a lower temperature (around 500 °C) after the irradiation.

(3)Yellow: All samples are type Ia with high concentrations of A-centre nitrogen according to the IR absorption measurements. Weak C-centre and 3107 cm^{-1} (N_3VH) peaks were also detected. In addition, deep UV fluorescence images confirmed that all of them are HPHT synthetic diamond. 544.5 nm and 523.8 nm peaks associated with cobalt were detected in PL spectra (Figure 3). These suggest that they are so called "HIH" diamond which means a HPHT diamond were irradiated and treated in a HPHT condition (Hainschwang and Notari, 2011.)

(4)Pink, (5)Orangy Pink, (6)Reddish Orange and (7)Orange: In all samples, faint nitrogen-related absorption was observed in the IR absorption spectra. A very strong 575 nm (NV^0) peak and a weak 637 nm (NV^-) peak were observed in

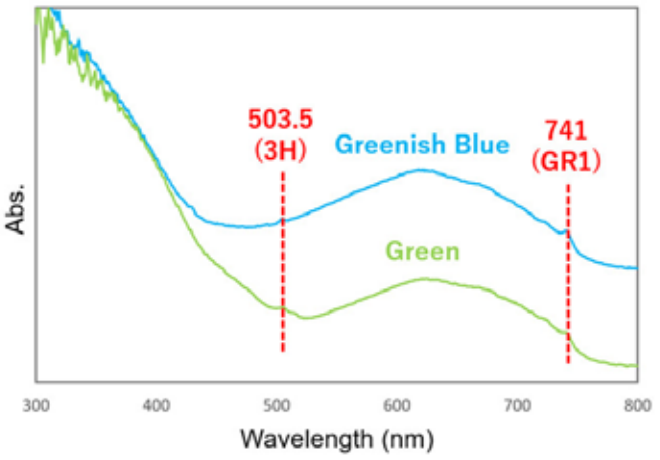

Figure 2. UV-VIS absorption spectra of the blue and greenish blue samples

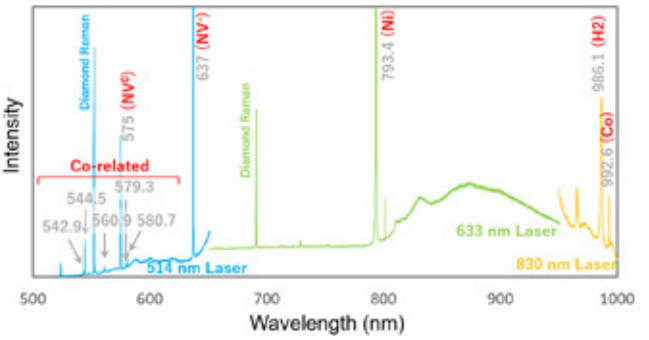

Figure 3. PL spectra of yellow samples (514, 633 and 830 nm laser excitation)

a PL spectrum, while in reddish orange samples a 741 nm (GR1) peak was observed in both UV-VIS absorption s and PL spectra. The 575 nm (NV^0), 637 nm (NV^-) and 741 nm (GR1) centers were formed by irradiation and subsequent annealing. The intensity ratio of the 575 nm (NV^0) peak to the 637 nm (NV^-) peak was in the order of pink < orangy pink < reddish orange < orange. This is the same order as the concentration of C-centres, and the concentrations may influence the colour. For two of the orange samples? There are five right?, the deep UV fluorescence image and the presence of 737 nm in the photoluminescence spectra indicate that they are CVD synthetic diamond, while all the others are HPHT synthetics due to their specific fluorescence images (Fig. 4).

Conclusion

In this study, gemmological examinations were carried out on melee-sized fancy coloured synthetic diamonds in loose form. We bought all 35 samples which were labelled as CVD synthetic diamonds, but 33 pieces of them were HPHT synthetic diamond and two of them were CVD synthetic diamonds. They had undergone multiple treatments with irradiation, annealing and HPHT treatments. If these were submitted in the form of gems set in jewellery for identification, the analysis methods would be limited and poor report may have been published. Therefore, we need to have full knowledge of characteristics of all type synthetic diamond made with the different methods and treated in the different ways so that error-free reports on the identification are published.

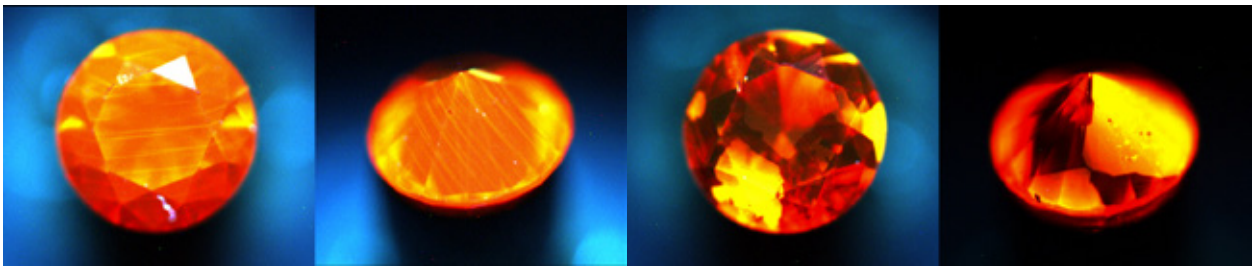

Figure 4. Step-flow structure specific to CVD synthetics (left) and sector zoning structure specific to HPHT synthetics (right)

References:

- Eaton-Magaña, S., Hardman, M. F., Odake, S., 2024. Laboratory-Grown Diamonds: An Update on Identification and Products Evaluated at GIA. Gems & Gemology, 60(2), 146-167
- Hainschwang T and Notari F., 2011. HIH : Multi-treated HPHT-grown synthetic diamonds showing some characteristics of natural diamonds. GGTL Laboratories Gemmological Newsletter 1, Sept

Nitrogen aggregates in yellow HPHT and CVD synthetic diamonds.

Yuri Shelementyev[1], Galina Kriulina[2], Olga Yarapova[1], Viktor Vins[3], and Alexander Stolyarevich[1]

[1] Gemmological Center of Moscow State University, Moscow, Russia,

[2] Department of Mineralogy, Moscow State University, Moscow, Russia,

[3] VELMAN Ltd., 43 Russkaya Str., 630058 Novosibirsk, Russia

email: yuri@gem-center.ru

The identification of natural and synthetic diamonds is an important gemmological task. Structural impurities in diamonds play a critical role in this task because they characterize the diamond growth and post-growth conditions, which differ between natural and synthetic diamonds. Optical centers in yellow diamonds partially overlap with those in colorless diamonds but also exhibit distinct differences. In recent years, there has been a growing number of synthetic yellow diamonds on the market, many of which are irradiated and annealed to alter their color. As a result, gemmological laboratories face challenges in the identification of yellow diamonds.

We studied synthetic yellow diamonds of both HPHT and CVD origin using a combination of spectral methods. Since 2023, the N3 center (415 nm) - previously considered an indicator of natural diamonds - has been observed in synthetic diamonds. In natural diamonds, the N3 center can be detected in both absorption and photoluminescence (PL) spectra, whereas in synthetic diamonds, its peak is weaker and observable only in PL spectra. Beginning in 2024, the N3 center has become common in synthetic yellow diamonds submitted by clients, with a more distinct peak in HPHT samples (Fig. 1a) and a weaker peak in CVD samples (Fig. 2). In natural diamonds, the N3 center arises from nitrogen aggregation during prolonged geological processes, while in synthetic diamonds, it can form during post-growth treatments (Vins *et al*., 2021).

In addition to the N3 center, a prominent PL series with zero-phonon lines (ZPLs) at 523.6 nm and 626.3 nm was detected in all HPHT yellow diamonds (Fig. 1a). These optical centers form in type Ib diamonds after irradiation and annealing (Dobrinets *et al*., 2013). The 580 nm center is attributed to Ni-related defects (Yelisseyev and Kanda, 2007).

FTIR spectroscopy revealed that the HPHT yellow diamonds are type Ia, with nitrogen detected in the 1100–1300 cm^{-1} range. One sample exhibited a platelet-related peak at 1364 cm^{-1}, a feature typically associated with natural post-growth annealing. Two synthetic yellow CVD diamonds (1.03 ct, cushion-cut) submitted by clients showed weak nitrogen-related peaks at 1250–1380 cm^{-1} and hydrogen-related peaks at 3107 cm^{-1} in FTIR spectra. Their PL spectra displayed weak N3 and H3 centers, along with a $[Si\text{-}V]^{-1}$ doublet at 736,6/736,9 nm (Fig. 2).

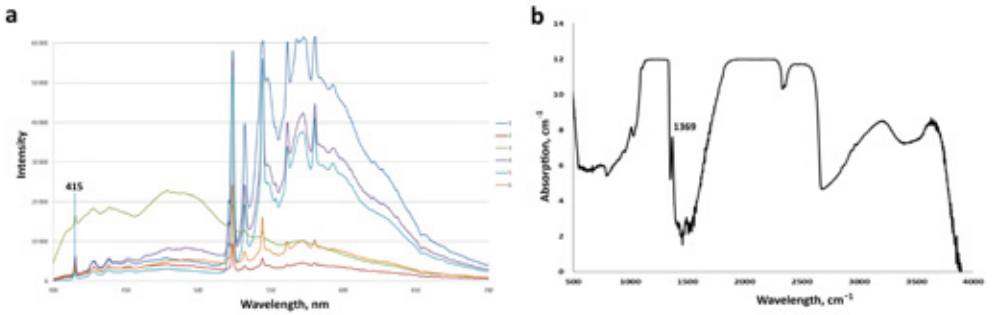

Fig. 1. a – PL spectra of 6 yellow synthetic HPHT diamonds, recorded at liquid nitrogen temperature. Excitation 365 nm. b – FTIR spectrum of yellow HPHT synthetic diamond with B2 (platelets) peak.

Experimental Stage

To investigate nitrogen aggregation mechanisms, we conducted post-growth experiments on three CVD diamond plates (0.15 ct, 0.12 ct, and 0.65 ct) and one HPHT diamond plate (6×6×1 mm, 0.86 ct). The samples were electron-irradiated (3 MeV) and subsequently annealed at 1750–1800°C.

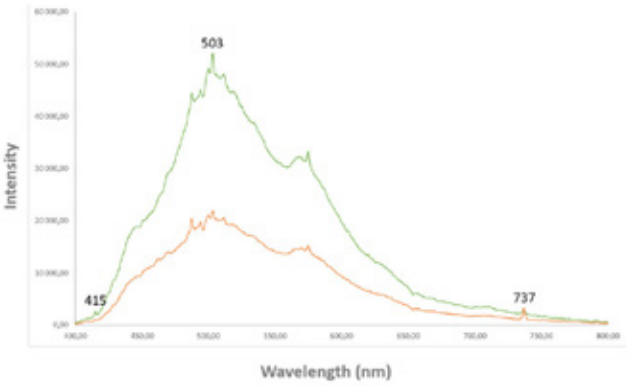

Fig. 2. PL spectra of two yellow CVD diamonds recorded at liquid nitrogen temperature with excitation 365 nm. There are peaks at 415 nm, 503 nm, 575 nm, and 737 nm.

Spectral characterization was performed before and after each stage. After irradiation, vacancies or GR1 centers (741 nm) appeared in the spectra. Following annealing, the N3 center emerged in CVD plates in PL spectra recorded at liquid nitrogen temperature. In annealed CVD plates, apart from 415 nm, additional 503 nm, 575 nm, and 737 nm peaks appear in Pl spectra recorded at liquid nitrogen temperature (Fig. 3a). Same peaks are recorded at polished CVD diamonds (see Fig. 2). In the annealed HPHT plate we did not observe the N3 center in PL spectra (Fig. 3 b) but see the H3 center (503 nm) that appeared after annealing. In the FTIR spectrum of the annealed HPHT plate there are A and C centers recorded as well as weak B2 (platelets) peaks. Probably further annealing is required for this sample in order to induce N3 center.

Our experiments confirm that the N3 center forms in synthetic diamonds after irradiation and annealing. The proposed mechanism involves:
1. As grown stage: Single nitrogen atoms are present (more abundant in HPHT, less in CVD diamonds).
2. Irradiation: Generates vacancies in the diamond lattice.
3. Annealing: Facilitates the formation of H3 aggregates, a fraction of which evolve into N3 aggregates.

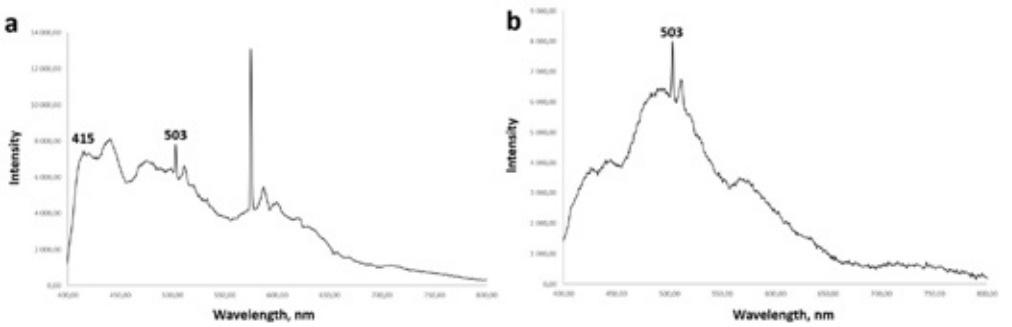

Fig. 3. PL spectra of synthetic CVD (a) and HPHT diamond (b) plates after irradiation and annealing.

References:

- Vins V., Yelisseyev A., Terentyev S., Nosukhin S. (2021). Specifics of high-temperature annealing of brown CVD single crystal diamonds at graphite-stable and diamond-stable conditions. Diamond and Related Materials. Vol. 118.
- Dobrinets I.A., Vins V.G., Zaitsev A.M. (2013) HPHT-Treated Diamonds: Diamonds Forever. Springer, Heidelberg, Germany.
- Yelisseyev A. P. and Kanda H. (2007) Optical centers related to 3D transitional metals in diamond. New Diam. Front. Carbon Technol. 17(3), 127-178.

Acknowledgments:

Authors are grateful to Vladimir Sadovoy, Diaton company, for providing HPHT synthetic diamond plate and for irradiation/annealing experiments.

Diamonds from Than Lwin River near Mong Hsu, Myanmar

Hui Ying Loke[1], Lee Cheang Hao Timothy[2], Htay Nyunt[3], Tin Nyunt Thet[4], Sellou Linda[2], Thye Sun Tay[1]

[1] Far East Gem Research Institute Pte Ltd, Singapore; huiying@gem.com.sg

[2] Department of Chemistry, Faculty of Science, National University of Singapore, Singapore; chmsll@nus.edu.sg

[3] Myanmar Geosciences Society, Yangon, Myanmar; nyunthtaygeol@gmail.com

[4] Department of Geological Survey and Mineral Exploration, Ministry of Natural Resources and Environmental Conservation, Nay Pyi Daw, Myanmar; thettinnyunt@gmail.com

Introduction

Sixteen rough diamonds were acquired in 2023 by co-author TTS from a gem dealer linked to Mong Hsu, Shan State, Myanmar. While diamonds have been reported in Myanmar, most are from limited alluvial deposits. Discoveries include Kyeindaw (1959), Mohaung near Momeik (1989), and tin mining areas in Kyaukmedaung (1981) and Myatsawnyinaung near Taungoo, both within the Mergui Group. (Griffin *et al*. ,2001; Win et al, 2001; Kyaw Thu & Khin Zaw, 2017). In 1985, 3,000 alluvial diamonds, including a 10.3-carat stone, were recovered from Theindaw mine near Myeik. Between 1995–1998, small quantities of diamonds were found during gold panning along the Than Lwin River near towns including Tangyan, Pangsang, and Mong Hsu (21°51'22"N, 98°32'36"E) (Personal communication: Nyunt Htay & Ma Gjam). The sixteen diamonds used in this study originate from this locality. As noted by Griffin *et al*. (1998), Win *et al*. (2001), and Nyunt Htay (2012), Myanmar's diamonds are largely alluvial, with no confirmed primary sources to date.

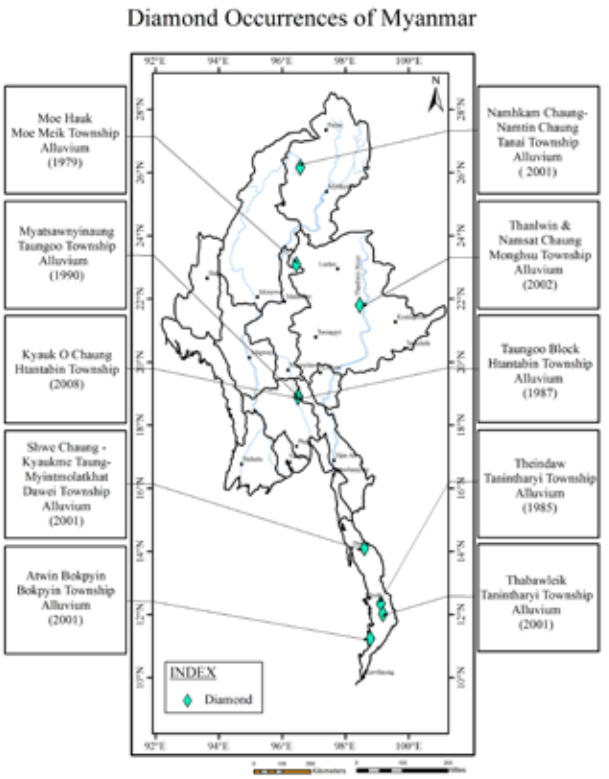

Materials and Methods

Sixteen rough diamonds ranging from 0.18 to 1.02 carats (Fig. 2) exhibited various crystal habits, including octahedral, trisoctahedral, tetrahexahedral, macle, and rhombic dodecahedral forms. Surface and internal features were examined using a GIA binocular microscope and long-wave ultraviolet (LWUV) fluorescence. Raman spectra were collected with a Renishaw inVia™ confocal Raman microscope (532 nm, spectral range from 100 to 2000cm^{-1}), while FTIR analysis was performed using a JASCO FT/IR-4X spectrometer (absorbance range 400–4000 cm^{-1}). These methods assessed structural integrity, surface alteration, and defect-related features.

Fig. 1. Various location of diamond deposits discovered in Myanmar over the years including the recent finding along Than Lwin river near Mong Hsu Township (map prepared by Thet Tin Nyunt, 2025)

Samples & Results

Microscopic Observations

Microscopic analysis revealed a variety of surface and internal features across the specimens. Notable observations included dark crystal inclusions, green and brown surface spots, percussion marks indicative of mechanical stress, hexagonal etch pits, trigons, and lamellar growth zoning. Green spots were especially prominent on some samples and suggested exposure to radioactive environments. Percussion marks implied histories of plastic deformation and mechanical impact.

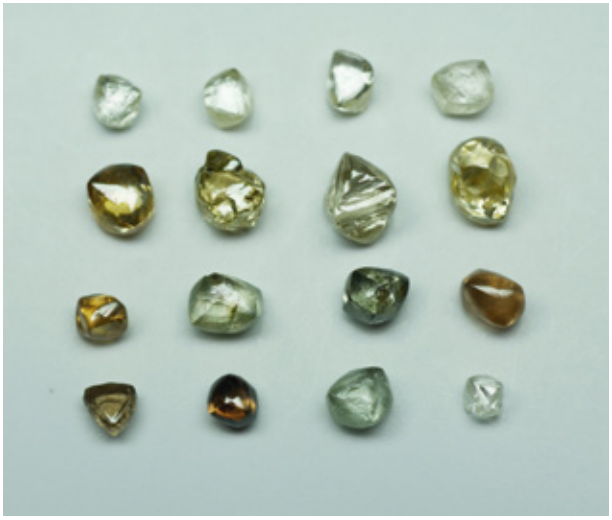

Figure 2. Sixteen pieces of rough diamonds from Mong Hsu, Myanmar with size range from 0.18 ct to 1.02 cts, with total weight 7.86 carats. (Photo by Tay T.S.)

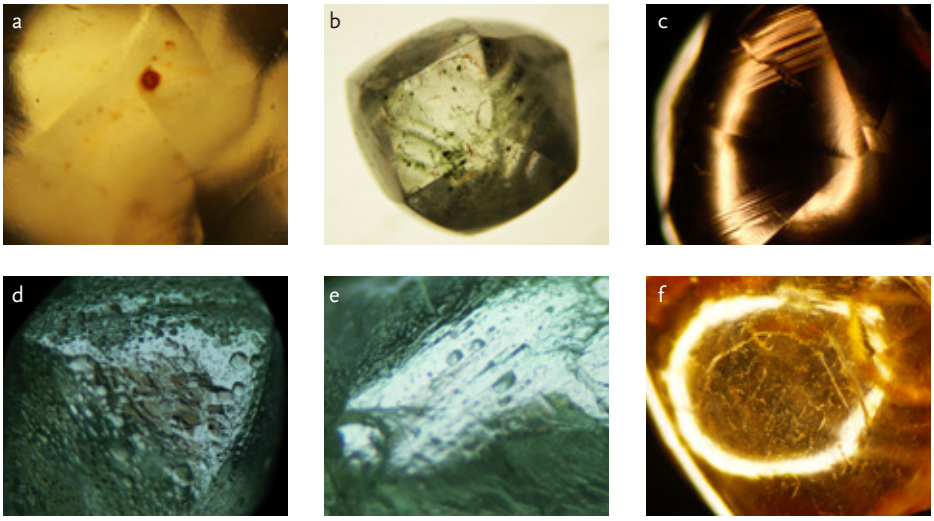

Fig. 3. Surface features of the 16 samples: (a) brown radiation spot (20x); (b) green radiation spots (20x); (c) lamellae growth marks (10x); (d) hexagonal growth marks (10x); (e) Etch marks (10x); (f) percussion marks (10x) (Microphotography by TTS).

Raman Spectroscopy

Raman spectroscopy revealed a dominant diamond peak at 1331 cm^{-1} across all specimens, confirming preservation of the crystalline diamond structure. Secondary peaks between 1442–1449 cm^{-1} were detected in several specimens, attributed to disordered carbon associated with surface-reaching inclusions or stress-altered regions. Additional features at 381 cm^{-1} and 1216 cm^{-1} (Fig. 4) observed near green surface spots suggest radiation-induced defects, while a 1419 cm^{-1} peak, found in diamonds with brown spots and percussion marks, reflects plastic deformation. Low-frequency peaks around 154 cm^{-1} (Fig. 5) were also recorded in some samples, indicating localized lattice stress or vibrational modes activated near inclusion zones (Pasteris & Wopenka, 1991; Nasdala *et al*., 2004; Zaitsev, 2001; Fischer *et al*., 2009; Smith & Dent, 2010).

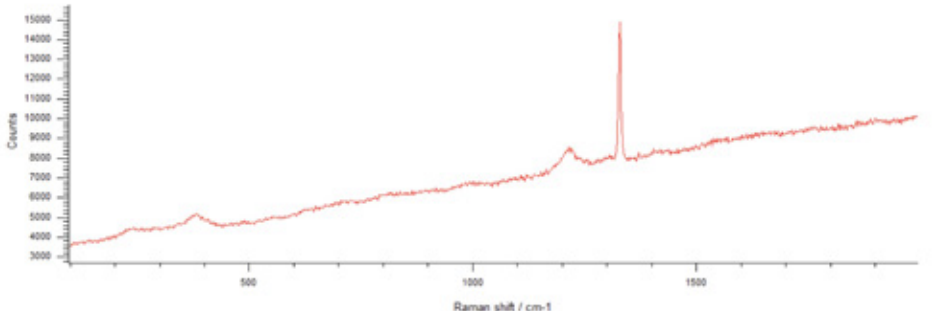

Fig. 4. Raman shift spectrum for specimen no. 11 showing peaks at 381 cm^{-1}, 1216 cm^{-1}, 1331 cm^{-1}

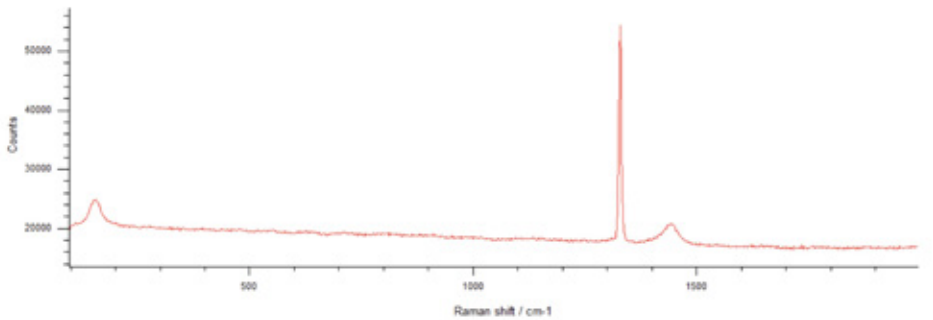

Fig. 5. Raman shift spectrum for specimen no. 6 showing peaks at 154 cm^{-1}, 1331 cm^{-1}, 1442 cm^{-1}

FTIR

FTIR spectroscopy confirmed that all diamond specimens are Type IaAB, characterized by absorption features at ~1004–1013 cm^{-1} and 1170–1370 cm^{-1}, corresponding to A-aggregated and B-aggregated nitrogen defects. Additional absorptions near 3106–3215 cm^{-1} indicate the presence of hydrogen-related defects. These results are consistent with prolonged high-temperature mantle residence, allowing nitrogen aggregation into stable forms, and suggest possible interaction with mantle fluids during or after formation (Boyd *et al*., 1994; Woods, 1986).

Ultraviolet Light

Under long-wave UV light, most specimens exhibited weak to moderate fluorescence ranging from bluish white to chalky green, while almost all were inert under short-wave UV. Stronger fluorescence, as seen in samples 6, 7, and 9, may relate to nitrogen-related defects or localized structural distortion (Zaitsev, 2001). Specimens with green or brown radiation spots frequently displayed moderate blue fluorescence. Inert samples, including specimen 16, may reflect low nitrogen concentrations or absence of optical defects (Boyd *et al*., 1994). These observations support the natural origin and defect diversity among the Mong Hsu diamonds.

Discussion

Microscopy revealed features such as percussion marks, radiation spots, and resorption patterns. Under long-wave UV light, most diamonds fluoresced faint to moderate blue. Raman spectroscopy confirmed a stable diamond lattice (1331 cm^{-1}) with additional peaks (1442–1449, 1419, 381, 1216 cm^{-1}) indicating disordered carbon, plastic deformation, and radiation-related defects (Pasteris & Wopenka, 1991; Zaitsev, 2001). FTIR analysis identified all specimens as Type IaAB, showing A- and B-aggregated nitrogen and hydrogen-related defects (Boyd *et al*., 1994; Woods, 1986), supporting a natural mantle origin with complex post-growth histories. A summary of results is given in Table 1 below.

Sample no.	Weight (Carats)	Colour	Shape	Surface Features/ Inclusions	UV	Raman cm^{-1}	FTIR Wave-length cm^{-1}	Diamond Type
01	0.295	Very light greenish yellow	Octahedral	Semi-transparent; Curved percussion marks on surface	LW – Faint blue SW – inert (very faint orangy yellow)	1331	482, 1010, 1175, 1286, 1364, 3106, 3200	IaAB
02	0.294	Light yellow	Octahedral	Semi-transparent; Resorbed surface with curved per-cussion marks	LW – faint yellow SW – inert	1331	482, 1007, 1278, 1372, 2850, 2918, 3106, 3200	IaAB
03	0.349	Light yellow	Tris-octahedron	Transparent; Re-sorbed surface	LW – very faint yellow SW – inert	1331	481, 1007, 1172, 1284, 1367, 3106, 3195	IaAB
04	0.396	Light yellow	Tetra-hexahedron	Semi-transparent; Frosty surface; Brown radiation spots	LW – moderate bluish white SW – inert	1331	488, 1010, 1176, 1224, 1363, 3106, 3201	IaAB
05	0.613	Yellow-ish brown	Rhombo-dodecahedral	Transparent; Re-sorbed surface with curved per-cussion marks; Brown stains along growth zones	LW – faint yellowish green SW – inert	1331, 1419	485, 1013, 1177, 1287, 1363, 3192	IaAB
06	0.792	Yellow	Irregular/ Twinning	Transparent; Graining; Black included crystal	LW – strong yellowish-blue SW – inert	154, 1331, 1442	477, 1009, 1175, 1280, 1362, 3106, 3200	IaAB
07	1.018	Greenish yellow	Irregular	Transparent; Brown & green radiation spot inclusion; Re-sorbed surface with curved and rhombic percus-sion marks	LW – strong blue SW – inert	1331	480, 1009, 1171, 1281, 1362, 3107, 3215	IaAB
08	0.931	Brownish Yellow	Irregular	Semi-transparent; Black included crystals; Resorbed surface; Cube-shaped growth marks	LW – moderate yellowish blue SW – inert	156, 1331, 1449	488, 1010, 1174, 1280, 1362, 3106, 3203	IaAB
09	0.299	Yellow-ish Brown	Irregular	Transparent; Brown radiation spots; Resorbed surface;	LW – strong yellowish brown SW – inert	156, 1331, 1445	478, 1008, 1177, 1276, 1362, 3106, 3200	IaAB
10	0.636	Green	Irregular	Semi-transparent; Green radiation spots; Curved percussion marks; Shield-shaped growth marks	LW – moderate blue SW – inert	156, 1331, 1447	498, 1010, 1174, 1281, 1327, 1363, 3107, 3208	IaAB
11	0.525	Green	Dodecahedral	Transparent; Green radiation spots; Brown staining along fractures; Curved and rhom-bic percussion marks	LW – moderate blue SW – inert	381, 1216, 1331	1008, 1173, 1278, 1367, 3107, 3207	IaAB
12	0.473	Brown	Irregular	Semi-transparent; Curved percussion Marks; Resorbed surface	LW – moderate yellowish blue SW – inert	154, 1331, 1447	481, 1009, 1177, 1288, 1331, 1359, 3204	IaAB
13	0.234	Brown	Macle	Transparent; Re-sorbed surface; Rhombic percus-sion marks	LW – very faint blue SW – inert	1331, 1419	475, 1004, 1174, 1280, 1362, 3107, 3182	IaAB
14	0.287	Brown	Tetra-hexahedron	Transparent; Shield-shape; Resorbed surface and lamellae	LW – inert SW – inert	1331	474, 1006, 1185, 1280, 1362, 3186	IaAB
15	0.552	Green	Irregular	Semi-transparent; Hexagonal surface etch marks; Green radiation spots (also in fissures)	LW – moderate blue SW – inert	1331	480, 1010, 1183, 1288, 1362, 3106, 3208	IaAB
16	0.179	Colour-less	Octahedral	Transparent; Octa-hedron growth marks	LW – inert SW - inert	1331	482, 1010, 1180, 1282, 1371, 3107, 3192	IaAB

Conclusions

The rough diamond specimens show evidence of natural radiation exposure, plastic deformation, and surface stress features, as revealed by microscopy, UV fluorescence, Raman, and FTIR spectroscopy. It is likely to be due to exposure to alpha radiation and regional metamorphism in the alluvial deposits. Radiation defects may be further confirmed with UV-Vis spectroscopy. Despite localized defects, the primary diamond lattice remains intact. These findings reflect a complex post-growth history involving deep mantle conditions, transport-related stress, and surface alteration. Further advanced spectroscopic studies such as photoluminescence and cathodoluminescence could refine the understanding of these processes. The study of inclusions after polishing, may also potentially be useful in studying the origins of diamonds in the future, however, it may only remain as a useful information rather than giving definitive conclusions of a diamond's origin (Smith et al, 2022).

References:

- T. T. Win, R.M. Davies, W.L. Griffin, P. Wathanakul, D.H. French, "Distribution and characteristics of diamonds from Myanmar" *Journal of Asian Earth Sciences*, 19 (2001) 563-577.
- Griffin, W.L., Win, T.T., Davies, R., Wathanakul, P., Andrew, A. and Metcalfe, I, and Cartigny P., "Diamonds from Myanmar and Thailand: Characteristics and Possible Origins", *Economic geology, 96* (2001) pp. 159-170.
- Kyaw Thu & Khin Zaw, (2017) *Gem Deposits of Myanmar*. In Barber, A.J., Khin Zaw, and Crow, M.J. (Eds.)., Myanmar: Geology, Resources and Tectonics. Geological Society of London, Memoir, Vol. 48, the Geological Society of London, London, 497-529.
- Mitchell, A., "Geological belts, plate boundaries and mineral deposits in Myanmar", (2018) Chapter 17, Alluvial diamonds in Myanmar, 478-481.
- Yang M.S., "*Diamond from Hunan province, China*." Ph.D. thesis
- Nyunt T. T, "Petrology and economic geology of Theindaw area, Tanintharyi Township." (2002), Master of Research thesis, Department of Geology, University of Yangon, Myanmar, 45pp.
- Nyunt Htay & Party (1986) Diamond exploration project in Theindaw area, Tanintharyi Division. Unpublished DGSE Report.
- Pasteris, J. D., & Wopenka, B. (1991). Raman spectra of graphite as indicators of degree of metamorphism. *The Canadian Mineralogist*, 29(1), 1–9.
- Nasdala, L., Smith, D. C., Kaindl, R., & Ziemann, M. A. (2004). Raman spectroscopy: Analytical perspectives in mineralogical research. *European Journal of Mineralogy*, 16(5), 767–784.
- Zaitsev, A. M. (2001). *Optical Properties of Diamond: A Data Handbook*. Springer-Verlag.
- Fischer, A. J., Spitzer, M. B., Studna, A. A., & Emanuel, M. A. (2009). Plastic deformation and brown color in natural diamonds. *Journal of Applied Physics*, 66(6), 2436–2440.
- Smith, E., & Dent, G. (2010). *Modern Raman Spectroscopy: A Practical Approach*. John Wiley & Sons.
- Boyd, S. R., Kiflawi, I., & Woods, G. S. (1994). The relationship between infrared absorption and the A defect concentration in diamond. *Philosophical Magazine B*, 69(6), 1149–1153.
- Woods, G. S. (1986). Infrared absorption of hydrogen-containing diamonds. *Philosophical Magazine B*, 53(5), 507–522.
- Evan M. Smith, Karen V. Smit, and Steven B. Shirey (2022). Methods and Challenges of Establishing the Geographic Origin of Diamonds. *Gems & Gemology*, Fall 2022, Vol. 58, No. 3

Acknowledgement

The author TTS wishes to thank Ma Gjam and Ko Aung Naing for supplying the diamond specimens from Mong Hsu and for their kind guidance. Sincere appreciation is also extended to Dr Mya Mya Khin, Scientific Manager, Department of Chemistry, National University of Singapore, for her expert support with the Raman spectrometer.

Morphologies and Surface Features of Diamond Samples from Southern Thailand

Somruedee Sakkaravej[1], Thanapong Lhuaamporn[2], Pantaree Lomthong[1], Wilawan Atichat[2] and Pornsawat Wathanakul[1]*

[1] Department of Earth Sciences, Faculty of Science, Kasetsart University, Bangkok, Thailand

[2] Gem and Jewelry Institute of Thailand (GIT)

* pwathanakul2@gmail.com

Introduction

In 1955, the first report on Thai diamond was made by Dr. Payome Aranyakanon, a renowned tin exploration geologist of Thailand Department of Mineral Resources. He visited a tin mine on Phuket Island and picked a shiny grain, later identified as diamond, from a tin-tailing pile. However, stories told by villagers revealing diamonds in southern Thailand provinces have been found since about a century. These so-called headless diamonds were surprisingly found in very much younger geological terranes (cf. most of the world diamond deposits) of Southeast Asia, such as in Myanmar, Indonesia (Kalimantan) and Thailand, with no old cratons, and no report of kimberlite/lamproite pipe occurrences in the vicinities. Studies of diamond samples from Myanmar and Thailand were also published (Griffin *et al*., 2001; Win *et al*., 2001; Wathanakul *et al*., 2005). As for southern Thailand, diamonds have been collected by tin-mine workers and sold to the wealthy locals for several decades, actually since the tin mining and dredging started. The diamond samples collected for this study were mainly bought and collected time to time from the miners and villagers around Phuket, Phang Nga areas (Figure 1).

Diamond Samples

More than a hundred samples of diamond from southern Thailand were collected. Thirty-five samples were selected for being representative for this study, including fifteen new diamond samples collected from the locals off the Phuket coast. The samples were primarily studied for their colours, types, morphologies, and surface features. Examples of diamond colours as well as their morphologies are shown in Figure 2.

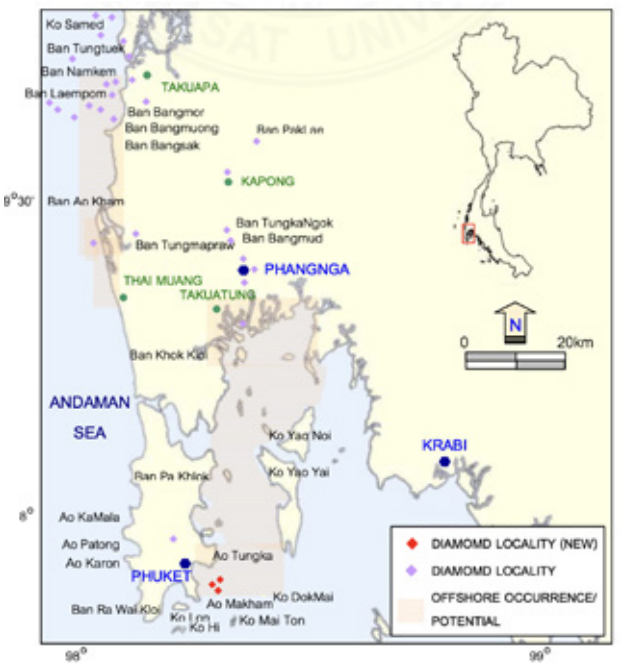

Figure 1. Diamond localities from southern Thailand, samples collected from both around Phuket and Phang Nga areas

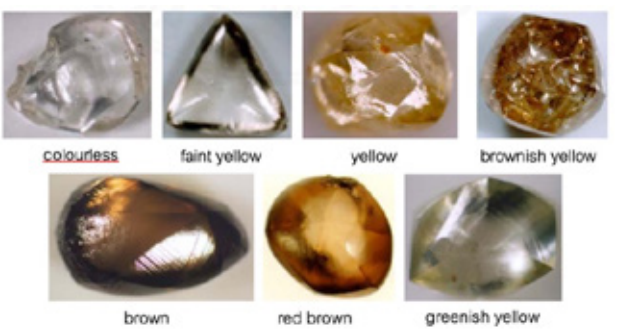

Figure 2. Representative samples, showing Thai diamond colours

Thai Diamond Types

FTIR and UV-Vis spectroscopies reveal Thai diamond types are mainly IaAB, moderate amount of IaA, and lesser IaB, and very few of type Ib. One out of fifty samples is type IIb.

Morphologies & Surface Features

Diamond samples were inspected for their morphologies and surface features using a stereo microscope, some selected samples were carefully studied using SEM and a cathodoluminoscope (CL). The results show that morphologies mainly include resorbed tetrahexahedroids (THH), a few rounded dodecahedrons, multiple twins, octahedrons and macles. Thai diamonds show about six characteristic patterns of CL images (Figure 3), which show entirely yellow or blue, yellow/blue oscillation, a yellow centre and a blue rim, a blue core with a yellow rim, and blue with yellow patches/sectors. Radiation spots are often present in Thai diamond samples.

Their surface features show straight lamination lines, shield-shaped lamination, cross-hatched lamination, hillocks, trigons, pits, radiation brown spots, percussion scars and ruts (Figure 4). Those features reveal the diamond crystals experienced high resorption of corrosive magma, which also commonly causes a glossy surface.

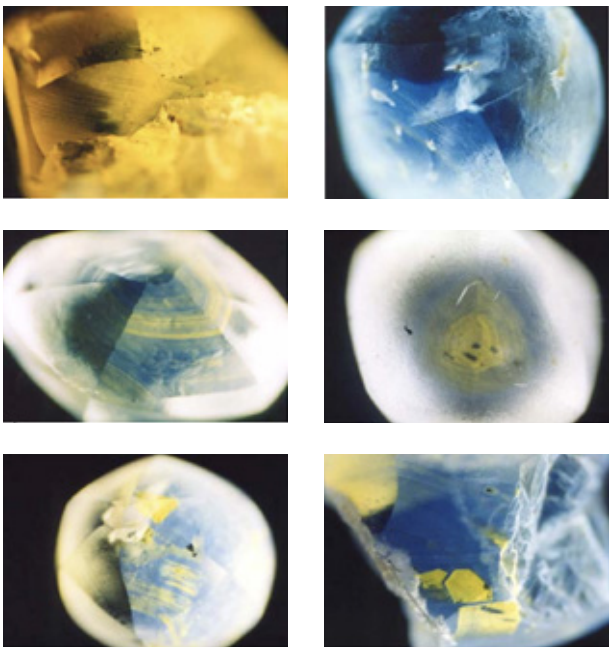

Figure 3. Examples of CL images of diamond samples, southern Thailand

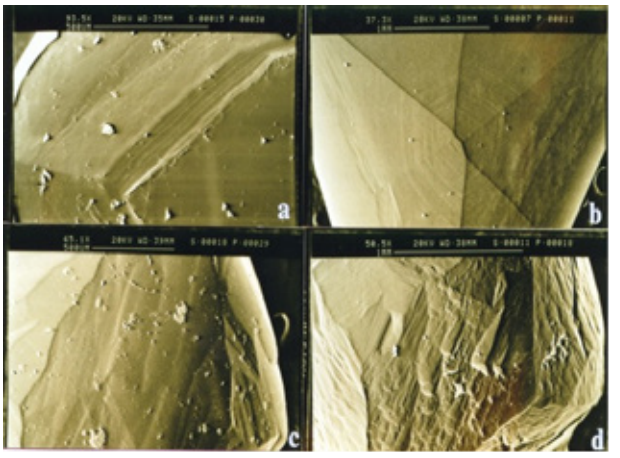

Figure 4. Examples of Thai diamonds with surface features under SEM showing (a) lamination lines, (b) shield-shaped laminae, (c) resorption etching and (d) hillock surfaces

Concluding Remarks

Thai diamonds have been found for about a century in southern Thailand. Their morphologies include mainly resorbed tetrahexahedroids (THH), but also rounded dodecahedrons, multiple twins, octahedrons and macles. Their surface features show straight laminae, shield-shaped lamination, cross-hatched lamination, pits, percussion scars and ruts. They are highly resorbed with glossy lustre suggesting more affinity with corrosive magma, i.e., related to lamproite or another minette rock type, more than to kimberlite (e.g., Kaminsky *et al*., 2000). More details on their inclusions and possible geological source region need further research.

References:

- Aranyakanon, P., 1955. Diamond discovery in Phang Nga and Phuket provinces, Thailand. Survey Report No. 1, Department of Mineral Resources, pp. 35-36 (in Thai).
- Griffin, WL., Win, TT., Davies, R., Wathanakul, P., Andrew, A., Metcalfe, I., Cartigny, P., 2001. Diamonds from Myanmar and Thailand: Characteristics and Possible Origins. Economic Geology, Vol. 96, 2001, pp. 159-170.
- Kaminsky, FV., Sablukov, SM., Sablukova, LI., Shpanov, V., 2000. Diamondiferous Minette: A new type of Diamondiferous Rocks. Izvestiya, Earth Science Section, Russian Academy of Natural Sciences. Special Issue No. 4. Moscow, Russia, pages 85-94.
- Win, TT., Davies, RM., Griffin, WL., Wathanakul, P., French, DH., 2001. Distribution and characteristics of diamonds from Myanmar. J Asian Earth Sci, Vol 19: 5, pages 563-577.
- Wathanakul, P. *et al*., 2002. Characteristics and possible origin of diamonds from southern Thailand. Final report submitted to Thailand Research Fund. 195 p (in Thai).

Acknowledgements

Anonymous villagers of Phang Nga and Phuket townships helped share samples from their collections as well as provide the history about Thai diamonds. The research was primarily supported by Thailand Research Fund. Mineral & Gem Science Research Lab, KU and GIT are thanked for instrumentation facilities.

International Gemmological Conference

Athens, Greece
October 2025

www.igc-gemmology.org